EMERGING INFECTIOUS DISEASES®

U.S. CENTERS FOR DISEASE CONTROL AND PREVENTION

Measles and Other Respiratory Infections

November 2026

Edgar Degas, *Les Choristes*, 1876–1877. Pastel over monotype. 27.1 cm × 32.3 cm (10.67 in × 12.7 in). Image © Musée d'Orsay, Paris, France. Dist. RMN-Grand Palais/Patrice Schmidt.

Pages 1777–1936

EMERGING INFECTIOUS DISEASES

A Peer-Reviewed Journal Tracking and Analyzing Disease Trends

EDITOR IN CHIEF
Matthew J. Kuehnert

ASSOCIATE EDITORS

Charles Ben Beard
United States
Ermias Belay
United States
David M. Bell
United States
Sharon Bloom
United States
Richard Bradbury
Australia
Corrie Brown
United States
Gerardo Chowell
United States
Adam Cohen
United States
Ben Cowling
Hong Kong, China
Jan Felix Drexler
Germany
Paul V. Effler
Australia
David O. Freedman
United States
Shawn Lockhart
United States
Alexandre Macedo de Oliveira
United States
Nina Marano
United States
Martin I. Meltzer
United States
J. Glenn Morris, Jr.
United States
Stephen M. Ostroff
United States
Christopher D. Paddock
United States
John Papp
United States
Clyde Partin
United States
Johann D.D. Pitout
Canada
Ann Powers
United States
David Safronetz
Canada
Frederic E. Shaw
United States
David Swayne
United States
Neil M. Vora
United States
David H. Walker
United States
J. Scott Weese
Canada

Books and Media Editor
Nkuchia M. M'ikanatha
United States

Associate Editors are also members of our Editorial Board.

EDITORIAL BOARD

Sridhar V. Basavaraju
United States
Martin Beer
Germany
Isaac Benowitz
United States
Martin J. Blaser
United States
Andrea Boggild
Canada
Adrianus C.M. Boon
United States
Christopher Braden
United States
Catherine M. Brown
United States
Charles H. Calisher
United States
Arturo Casadevall
United States
Kenneth G. Castro
United States
Michel Drancourt
France
Christian Drosten
Germany
Anthony Fiore
United States
Isaac Chun-Hai Fung
United States
Kathleen Gensheimer
United States
Rachel Gorwitz
United States
Patricia M. Griffin
United States
Duane J. Gubler
Singapore
Stephen Hadler
United States
David L. Heymann
United Kingdom
Barbara Javor
United States
Keith Klugman
United States
Ajit P. Limaye
United States
John S. Mackenzie
Australia
Joel M. Montgomery
United States
Patrick K. Moonan
United States
David Morens
United States
Kristy O. Murray
United States
Patrice Nordmann
Switzerland
Norbert Nowotny
Austria and United Arab Emirates
David A. Pegues
United States
Philip M. Polgreen
United States
Didier Raoult
France
Mario Raviglione
Italy and France
David Relman
United States
Pierre E. Rollin
United States
Sarah G.H. Sapp
United States
William Schaffner
United States
Tom Schwan
United States
Wun-Ju Shieh
Taiwan
Rosemary Soave
United States
Kathrine R. Tan
United States
Phillip Tarr
United States
Kenneth L. Tyler
United States

Managing Editor
Angela Blackwell (acting), United States

Editor in Chief Emeritus
D. Peter Drotman, United States

Managing Editor Emeriti
Byron Breedlove, United States
Polyxeni Potter, United States

Founding Editor in Chief
Joseph E. McDade, United States

STAFF

Technical Writer-Editors
Shannon O'Connor, Team Lead; Dana Dolan, Amy J. Guinn, Jill Russell, Jude Rutledge, Cheryl Salerno, Bryce Simons, Amanda Smith, Susan Zunino

Production, Graphics, and Information Technology Staff
Reginald Tucker, Team Lead; William Hale, Tae Kim, Barbara Segal

Communications/Social Media
Candice Hoffmann, Team Lead; Patricia A. Carrington-Adkins, Heidi Floyd Argumedo

Journal Administrators
J. McLean Boggess, Claudia Johnson

Editorial Assistant
Nell Stultz

Emerging Infectious Diseases is published monthly by the Centers for Disease Control and Prevention, 1600 Clifton Rd NE, Mailstop H16-2, Atlanta, GA 30329-4018, United States. Telephone 404-639-1960; email eideditor@cdc.gov

The conclusions, findings, and opinions expressed by authors contributing to this journal do not necessarily reflect the official position of the U.S. Department of Health and Human Services, the Public Health Service, the Centers for Disease Control and Prevention, or the authors' affiliated institutions. Use of trade names is for identification only and does not imply endorsement by any of the groups named above. All material published in *Emerging Infectious Diseases* is in the public domain and may be used and reprinted without special permission; proper citation, however, is required.

EMERGING INFECTIOUS DISEASES is a registered service mark of the U.S. Department of Health and Human Services (HHS).

EMERGING INFECTIOUS DISEASES®

Measles and Other Respiratory Infections **November 2026**

On the Cover

Edgar Degas (1834–1917), *Les Choristes*, 1877. Pastel on monotype. 32 cm × 27 cm (10.6 in × 12.6 in). Image © Musée d'Orsay, Paris, France. Dist. RMN-Grand Palais/ Patrice Schmidt.

About the Cover p. 1932

Perspective

The Impermanence of Public Health Gains—Lessons Learned from Measles Resurgence, Bangladesh, 2026
S. Bhuiya et al. **1777**

Synopses

Importation-Driven Measles Resurgence and the Fragility of Elimination, Japan, 2024–2026
K. Yuji et al. **1785**

Subacute Sclerosing Panencephalitis after Measles Outbreaks, the Philippines, 2007–2022
M.P. Palisoc et al. **1793**

Predictors and Patterns of Metastatic *Candidozyma auris* Infection, Spain, 2016–2024
P. Suarez-Urquiza et al. **1798**

Research

Medscape EDUCATION ACTIVITY

Reducing Antibiotic Drug Use Effects on *Clostridioides difficile* Colonization in Nursing Home Residents
This model reveals that lowering use of antibiotic drugs results in lower *C. difficile* colonization rates.
M. Reeves et al. **1807**

Global Genomic Surveillance of Middle East Respiratory Syndrome Coronavirus
J.R. Otieno et al. **1816**

Emergence of Novel Macrolide-Resistant *Mycoplasma pneumoniae* Sequence Type 3 Subclades in Children after COVID-19 Pandemic, Taiwan
Y.-C. Hsieh et al. **1827**

Microbial Etiology of Postoperative Spinal Fusion Infections and Factors Associated with Gram-Negative Infections, United States, 2021–2022
M. Lindstrom et al. **1838**

Invasive Enterovirus and Parechovirus Infections in Adults, Alberta, Canada, 2023–2025
J.N. Kanji et al. **1846**

Five-Biomarker Definition for Hypervirulent *Klebsiella pneumoniae* Bloodstream Infection and Abscess Complications, Japan, 2022–2024
N. Watanabe et al. **1855**

Dispatches

Pediatric Deaths during Measles Outbreak, Jerusalem, Israel, 2025–2026
Z. Mor et al. **1865**

Serologic Assessment of Public Health Action Needed for Trachoma, Coastal Ecuador, 2021–2024
E. Kamau et al. **1870**

EMERGING INFECTIOUS DISEASES®
November 2026

Middle East Respiratory Syndrome Coronavirus in Camels, Kazakhstan, 2025
A. Kydyrmanov et al. **1907**

Alignment-Free Tool for Assemblies and Reads in Genomic Surveillance of Tuberculosis
P. Ruiz-Rodriguez and M. Coscollá **1913**

Research Letters

Serologic Testing for Middle East Respiratory Syndrome Coronavirus and SARS-CoV-2 Cross-Reactive Immune Responses, the Netherlands
M.R. te Marvelde et al. **1874**

Differentiating Avian and Seasonal Influenza Viruses in Wastewater by Digital PCR
V. Paracchini et al. **1879**

***Dirofilaria asiatica* Infection and Asymptomatic Microfilaremia, Sri Lanka, 2025**
D. Mataraarachchi et al. **1885**

Persistent Microfilaremia Caused by *Dirofilaria asiatica* Infection in 2-year-old Child, Sri Lanka, 2024
U. Atapattu et al. **1890**

Fatal *Rickettsia parkeri* Rickettsiosis in Immunocompromised Pediatric Patient, Georgia, USA, 2025
S. Bellman et al. **1893**

Transmission Dynamics of Dengue Virus, Ceará State, Brazil, 2010–2025
S.T.S. de Lima et al. **1897**

Post–COVID-19 Expansion of *Streptococcus pyogenes* Lineages Causing Toxic Shock Syndrome, Japan, 2023–2024
T. Ikebe et al. **1902**

Evidence of Exposure to Highly Pathogenic Avian Influenza H5 Viruses in East Greenland Polar Bears
K.J. Buhler et al. **1919**

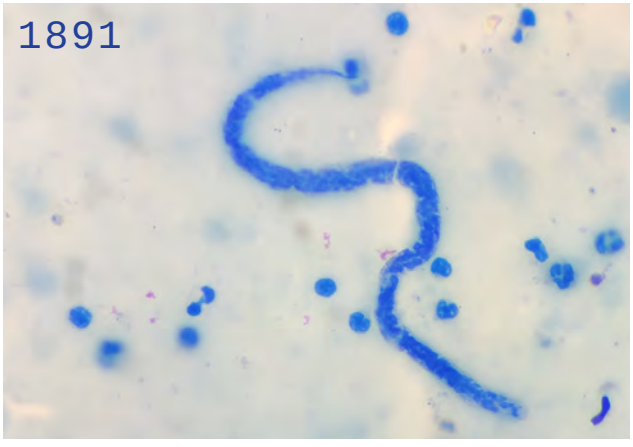

Systemic *Spiroplasma turonicum* Infection Manifested as Knee Arthritis, France, 2025
M. Vassallo et al. **1922**

Sulfamethoxazole–Resistant Nocardiosis in Renal Transplant Recipient, India
S.R. Kordcal et al. **1924**

Community Transmission of Pneumonic Plague, Fenoarivobe, Madagascar, 2022
L. Randrianasolo et al. **1928**

About the Cover

Choral Voices, Communal Vulnerability
T. Chorba **1932**

Online Report

Nationwide Surveillance and Control Measures during Large Measles Outbreak, Bangladesh, 2026
M.F. Rabbi et al.
https://wwwnc.cdc.gov/eid/article/32/11/26-0996_article

The Impermanence of Public Health Gains—Lessons Learned from Measles Resurgence, Bangladesh, 2026

Saju Bhuiya, Tanzir Ahmed Shuvo, Md. Zakiul Hassan, Mohammad Abdul Aleem, Gazi Md. Salahuddin Mamun, A.F.M. Zakaria, Mahmudur Rahman, Fahmida Chowdhury

The global resurgence of measles is a major public health concern. After the success of its Expanded Programme on Immunization, Bangladesh experienced a measles resurgence in 2026. The country faced major setbacks after measles vaccination coverage declined because of political instability, discontent among field-level staff, change in procurement policy, COVID-19–related service disruptions, and delayed supplementary immunization campaigns. During March 15–September 13, 2026, Bangladesh reported 170,638 suspected and 20,006 confirmed measles cases, including 919 deaths among suspected and 100 deaths among laboratory-confirmed cases. The outbreak disproportionately affected unvaccinated and underimmunized children. Political turmoil during 2024–2025 disrupted vaccine procurement, delayed mass vaccination campaigns, weakened the health workforce, and compromised financial and logistic continuity. Simultaneously, disruptions in vitamin A supplementation and worsening child malnutrition amplified disease severity. To prevent future resurgence, immunization programs must be depoliticized, supported by buffer vaccine stocks, strengthened through microlevel surveillance, and integrated with nutrition and primary healthcare services.

Measles is an extremely contagious viral disease; each primary case generates an average of 12–18 secondary infections (*1*). Although global measles cases declined by 71% from 2000 to 2024, the World Health Organization (WHO) reported 395,521 cases in 2024 and 254,384 in 2025; by the end of April 2026, global case counts had reached 86,503 (*1*,*2*). Like other countries, Bangladesh's measles outbreak during early 2026 served as a clear reminder that public health achievements are never permanent; they are dynamic states of equilibrium that require constant maintenance, political or structural stability, and resource security.

Bangladesh was praised as a global exemplar of the Expanded Programme on Immunization (EPI) for decades; its successful vaccination coverage increased from 2% in the late 1970s to near-universal levels by the 2010s (*3*,*4*). Measles-containing vaccine (MCV) 1 coverage increased from 74% in 2000 to 94% in 2016, and MCV2, a routine second MCV dose introduced in 2012, reached 93% in 2016 (*5*). Bangladesh achieved its regional rubella control goal in 2018 and subsequently targeted measles and rubella elimination by 2020 (*6*). However, the COVID-19 pandemic and the early 2026 measles outbreak have challenged that narrative, revealing underlying weaknesses in Bangladesh's health system. The 2026 measles outbreak was not merely a biological phenomenon driven by a highly contagious virus, it was a systems-sensitive emergency that exposed the intersection of vaccination disruption resulting from political upheaval (Appendix Table, https://wwwnc.cdc.gov/EID/article/32/11/26-1019-App1.pdf), nutritional neglect, disruption of regular vaccine procurement, perceived adverse effects of COVID-19 vaccination, widespread misconceptions, and the long-term disruption of routine immunization services in the aftermath of the COVID-19 pandemic (*7*–*9*).

Previous publications have documented the early measles resurgence, immunization gaps, vaccination disruptions, and health-system pressures in Bangladesh (*7*,*10*–*12*). Building on the evidence in those publications, this perspective provides an integrated analysis of the epidemiologic, demographic,

Author affiliations: icddr,b, Dhaka, Bangladesh (S. Bhuiya, T.A. Shuvo, M.Z. Hassan, M.A. Aleem, G.M.S. Mamun, F. Chowdhury); Shahjalal University of Science and Technology, Sylhet, Bangladesh (A.F.M. Zakaria); The Eastern Mediterranean Public Health Network, Dhaka (M. Rahman)

DOI: https://doi.org/10.3201/eid3211.261019

nutritional, socioeconomic, political, and health-system factors that might have contributed to the magnitude and severity of the outbreak, while drawing lessons for strengthening measles prevention, preparedness, and response in Bangladesh and similar settings.

Summary of the 2026 Measles Outbreak in Bangladesh

The measles outbreak came to the attention of the government and other health agencies on March 15, 2026, and by September 13, 2026, Bangladesh reported 170,638 suspected and 20,006 confirmed cases and reported 919 deaths among suspected and 100 deaths among laboratory-confirmed cases (*13*). Case-fatality rates were 0.54% among suspected and 0.50% among confirmed cases (*13*). Case definitions were described previously (*14*).

Genomic analysis of 55 measles virus whole-genome sequences showed that all virus samples belonged to the B3 subclade (*15*). Phylogenetically, the Bangladesh viruses were closely related to B3 viruses reported from other countries (including Bangladesh), supporting circulation of a globally recognized lineage rather than emergence of a distinct vaccine-escape strain (*16*,*17*). Four amino acid changes were identified within antigenic regions of the haemagglutinin protein; however, several of those changes were previously reported in measles viruses from other settings (*15*). Those amino acid changes alone do not establish reduced vaccine susceptibility, and further immunologic and functional studies are required to determine their potential effect on antibody recognition. Overall, the genomic findings provided no evidence of a novel measles lineage or genetic evolution sufficient to explain the current resurgence through vaccine escape.

The 2026 measles outbreak in Bangladesh is characterized by its clinical severity and its extensive geographic spread; all 64 districts in the country are affected (*18*). By May 3, 2026, the Directorate General of Health Services (DGHS) and WHO identified Bangladesh's capital city, Dhaka, as the primary epicenter, and noted that cases were concentrated in overcrowded informal settlements (*13*,*18*). The spatial concentration of the 2026 outbreak in Dhaka's informal settlements (slums) highlights gaps in urban health governance (*19*).

During this outbreak, hospitals, particularly the Infectious Diseases Hospital (IDH) in Mohakhali, Dhaka, were overwhelmed by a concentration of hypoxic, malnourished, and severely ill children, and in March 2026 the crude in-hospital mortality rate was 4.7% (*20*). That high mortality rate, concentrated in tertiary referral hospitals, suggests potential gaps in identifying and treating measles in secondary and primary healthcare centers. Moreover, our data only reflect hospitalized patients, and the burden among persons who did not seek healthcare at the community level remains unknown (*14*).

Potential Factors Contributing to the Bangladesh Measles Outbreak

Political Upheaval and the Disruption of Routine Immunization Activity, 2024–2025

Bangladesh's routine immunization program provided 2 doses of measles–rubella vaccine free of charge through the EPI. The first dose is administered to infants at 9 months of age and the second at 15 months (*5*). Vaccination is available at all government hospitals, upazila (subdistrict) health complexes, dedicated public clinics, and participating private maternal centers. However, the political instability in Bangladesh during 2024 and 2025 (Appendix Table) disrupted routine immunization and was associated with the 2026 measles outbreak.

A student-led uprising in 2024 and the subsequent political transition from the prior administration disrupted administrative continuity and had a consequential effect on public health administrative and leadership during the interim caretaker government's transitional rule (*3*,*4*,*10*). That period of institutional reorganization unintentionally disrupted routine decision-making channels and interrupted operational continuity within the Ministry of Health and Family Welfare (MoHFW). Consequently, systematic EPI oversight was disrupted, delaying scheduled nationwide vaccination campaigns. Before administrative stability was fully restored, the cumulative oversight gaps allowed the cohort of immunologically naive children to expand, ultimately transforming a localized coverage deficit into a widespread nationwide outbreak.

For years, Bangladesh procured vaccines through UNICEF (https://www.unicef.org) with major support from Gavi (https://www.gavi.org) and government cofinancing. After the 2024 political transition, the interim government shifted to an open tender system in 2025, causing procurement delays, nationwide vaccine shortages, disruption in routine immunization, and cancellation of the measles vaccine campaign (*21*). That shift in measles vaccine procurement from UNICEF to open tender system contributed to nationwide vaccine stockouts. Those stockouts, in turn, extended the population immunity gap

by expanding the cohort of immunologically naive children 6–9 months of age, thereby fueling the rapid resurgence of measles (*21*).

Nevertheless, the newly appointed Health Minister, Sardar Mohammed Sakhawat Husain, reportedly told in the Jatiya Sangsad (Bangladesh's national parliament) that the political turmoil over the previous 2 years had disrupted vaccine procurement and caused failures in routine national vaccination campaigns (*4*). Thus, the 2026 outbreak might not have been a failure of medical technology but rather a failure of the health system function, amplified by prolonged disruptions in immunization services and program oversight.

Accumulation of Unvaccinated Children and Disrupted Follow-up Immunization Campaigns

One of the primary drivers of the 2026 outbreak was the accumulation of susceptible children. The follow-up measles and rubella vaccination campaign, a door-to-door campaign generally conducted every 4 years as a catch-up strategy, is intended to reach children missed by fixed-site services, particularly those in hard-to-reach, mobile, poor, and urban-slum populations (*10*). The last follow-up campaign took place in 2020; the next was scheduled for 2024 (*3*,*11*). However, the political instability in 2024, combined with widespread health worker strikes and funding uncertainties, led to the indefinite postponement of that critical immunization safety net (*3*,*10*,*11*,*22*). That administrative failure resulted in a substantial cohort of zero-dose (i.e., unvaccinated) children, creating a critical immunity gap within the pediatric population (*10*). UNICEF assessments during the outbreak found that 72% of cases were among zero-dose children, and another 16% were among partially vaccinated children (*11*). Another report showed that by 2025, Bangladesh had ≈5 million children who were not fully immunized, including 70,000 who had received no doses and >400,000 who were underimmunized (*20*). That demographic vulnerability resulted directly from disruptions in routine immunization and the failure to implement catch-up mechanisms that could identify and reach unimmunized children.

In addition, neither national nor international organizations highlighted that critical immunization gap on any platform or in the media, and no red flag was raised by the EPI before 2026. That institutional silence stemmed from a combination of data-tracking failures and bureaucratic distractions after the 2024 political transition. Specifically, routine EPI surveillance relied on underestimated population denominators, which obscured the true magnitude of the decline in vaccination coverage (*23*).

Furthermore, the surveillance system lacked automated risk-linked thresholds to trigger early warnings. The transition from UNICEF prefinancing to an open tender procurement system diverted leadership attention toward logistic restructuring rather than epidemiologic risk assessment. Consequently, international agencies favored private diplomatic dialogue over public reporting. Those organizations might have exercised diplomatic caution and avoided public platform alerts to maintain working relationships with the sensitive postrevolutionary interim administration, inadvertently keeping the gap out of public and media view and leaving the widening immunologic vulnerability unaddressed until the 2026 outbreak.

Longitudinal Erosion of Vaccine Coverage during 2014–2024

The 2026 crisis was associated with a documented, multiyear decline in vaccination coverage that exacerbated the outbreak. Although crude national figures often remained above the 90% vaccine threshold, a closer analysis of valid coverage vaccines administered at the correct age and interval revealed a more precarious immunologic reality (*24*). National coverage metrics use aggregate data that frequently mask localized pockets of underimmunization, an epidemiologic vulnerability known as the fallacy of the average (*25*). When unvaccinated populations cluster geographically, such as in densely populated urban slums or remote rural subdistricts in hard-to-reach areas, effective local herd immunity falls far below the critical threshold required to prevent transmission (*25*). In Bangladesh, that structural error was compounded by denominator errors that omitted millions of children from official targets, allowing highly vulnerable, localized cohorts to expand unnoticed until they achieved the critical mass necessary to fuel an explosive nationwide resurgence of measles (*23*). Moreover, WHO immunization data suggest that the overall vaccination coverage decreased during and after the COVID-19 pandemic (*26*). Vaccination coverage further declined in 2025 (Figure), whereas concurrent adverse conditions contributed to progression toward the outbreak.

Administrative data indicated a sharp decline in MCV coverage in 2020 (Figure). In addition, MCV1 coverage fell from 98% to 92% by 2025, while MCV2 coverage decreased from 96% to 91% in the same period (Figure). The 2023 Coverage Evaluation Survey reported full vaccination coverage of 86.1%

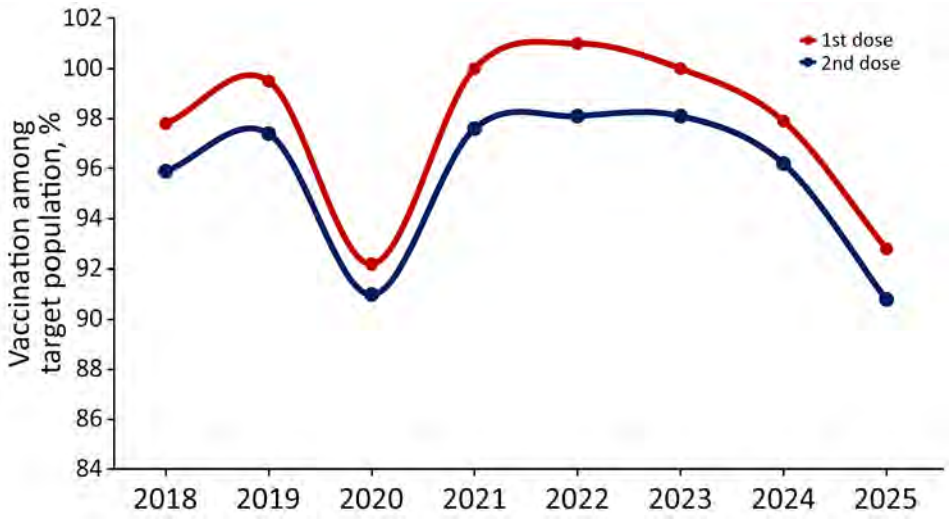

Figure. National measles-containing vaccination coverage trend among the eligible target population in study of lessons learned from measles resurgence, Bangladesh, 2026. Graph shows administrative vaccination data for children >9 months of age during 2018–2025. First measles-containing vaccine dose is recommended at 9 months of age and second dose at >15 months of age. Administrative data based on reported doses administered and estimated target population previously available in Directorate General of Health Services dashboard (https://dashboard.dghs.gov.bd).

nationally and that urban areas lagged behind rural regions (83.8% vs. 88.8%) (*24*). Although that difference was modest, aggregate estimates might mask pockets of lower coverage in densely populated urban slum areas. For example, the 2019 EPI Evaluation Survey reported only 75% valid vaccination coverage by 12 months of age among children in Dhaka slum areas, whereas overall Dhaka district coverage was 86.8%, illustrating how aggregate estimates can mask substantially lower coverage in specific urban populations (*25*,*27*). Such pockets of underimmunized populations enable rapid spread of measles in densely populated urban settings. In several countries, including Bangladesh, measles vaccination coverage decreased during and after the COVID-19 pandemic (*26*).

Healthcare System Preparedness and Clinical Case Management

By March 2026, Bangladesh's health system was under severe pressure, and by August 15, 2026, a total of 123,494 suspected measles patients were admitted to hospitals (*13*). The Infectious Diseases Hospital in Dhaka, originally a 100-bed facility, experienced severe overcrowding and limited intensive care capacity (*28*). The DGHS and WHO identified Dhaka as the primary outbreak epicenter, where a total of 62,286 suspected and 10,505 confirmed cases and 62 deaths had occurred by August 15, 2026; cases were mainly concentrated in overcrowded informal settlements (*13*,*18*). Moreover, another study showed that hospital bed occupancy generally exceeded 164%–175% in 2025, further limiting Bangladesh's ability to manage seasonal surges (*29*).

UNICEF and partners' assessments identified several critical facility-level failures, including staffing shortages, nosocomial transmission, and logistical supply gaps (*11*,*28*). The government's response, which included launching an emergency vaccination campaign for 1.2 million children in 18 high-burden districts on April 5, 2026, was a necessary tactical measure that highlighted the reactive nature of the health system (*11*,*18*). The outbreak also exposed critical systemic failures extending far beyond simple vaccination gaps, particularly in isolation capacity, infection prevention and control, and clinical case management. Despite DGHS and WHO directives for 4-day case isolation and extended precautions for immunocompromised patients, hospital overcrowding and weak referral systems drove nosocomial amplification and sustained transmission (*11*,*19*).

Furthermore, political instability in 2024 led to the reassignment of key personnel and persistent vacancies in senior EPI leadership positions (*30*), weakening program planning and implementation. Repeated healthcare worker strikes further disrupted routine immunization services (*31*).

Legacy of COVID-19–Era Global and Regional Immunization Disruption

The 2026 outbreak in Bangladesh is an extreme manifestation of the global resurgence of measles and the backsliding of immunization progress due to the COVID-19 pandemic (*8*,*9*). Moreover, 81% of cases were in children <5 years of age, highlighting the potential consequences of immunization disruptions during the COVID-19 pandemic (*13*). Worldwide data showed reduced measles vaccination during the pandemic (*8*,*26*). Pandemic-related disruptions to local immunization programs and rising vaccine hesitancy after the pandemic exacerbated this outbreak in Bangladesh (*32*). Similar results were reported in

studies conducted in India and Pakistan (*8*,*33*,*34*). The measles outbreak in Bangladesh is a reminder that vaccine gaps do not simply disappear when a pandemic ends; rather, those gaps could accumulate.

Drivers of High Rates of Illness and Death

The high rates of illness and death during the 2026 measles outbreak likely resulted from interacting epidemiologic, nutritional, socioeconomic, and health system vulnerabilities. Collectively, those vulnerabilities created a reinforcing pathway from high transmission and susceptibility to delayed care, severe complications, and excess mortality. We describe the vulnerabilities further in the following sections.

Disruption in Vitamin A Supplementation

The severity of the 2026 measles cases was exacerbated by a parallel decline in nutritional interventions in Bangladesh. In 2025, disruptions to the national Vitamin A Plus campaign meant that only 1 of the 2 scheduled annual dosing rounds were completed (*11*). Vitamin A is crucial for reducing measles-related death; without it, children are more likely to experience severe complications (*33*,*35*). Hospitals also reported that the children admitted during the outbreak were malnourished and had weight-for-height percentages far below standard (*33*). According to 1 study, malnutrition acts as a powerful epidemiologic multiplier that accelerates measles transmission and severity (*36*). The MoHFW decision in April 2026 to prioritize available vitamin A stocks specifically for children with measles was a necessary but late-stage response to a problem that should have been addressed through preventive supplementation in 2025 (*11*).

Demographic Vulnerability and Transmission Shift

A deeply concerning trend observed during this outbreak was the high percentage of infections among infants <9 months of age (*19*). Historically, maternal antibodies protected infants against measles, but only through the first 6 months after birth, leaving many infants 6–9 months of age vulnerable to measles infection before they receive the first vaccine dose (*37*). As population immunity levels dropped below the 95% threshold required for herd protection, those unprotected cohorts became the primary victims of intense community transmission (*7*,*35*). In some hospitals, such as Rajshahi Medical College, up to 57% of confirmed cases involved infants <9 months of age (*38*). That pattern suggests that reduced vaccination coverage weakened the protective effect of population immunity, increasing infants' exposure to measles virus. Moreover, hyperdense informal urban settlements formed localized micropockets of underimmunization, driven by high population mobility and a systemic deficit in routine surveillance tracking.

In Dhaka, cases clustered heavily in informal settlements such as Demra, Kamrangirchar, and Korail slums (*19*). Those areas are characterized by high population density, limited visibility to health services, and environmental stressors (*7*,*19*,*20*,*33*). Dhaka division also reported the highest cumulative burden, with >62,286 suspected cases, highlighting how static immunization delivery models can fail to maintain herd immunity among transient populations during an outbreak and how current urban health infrastructure might be insufficient to meet the public health needs of a rapidly urbanizing population during a crisis (*13*,*18*,*19*). To resolve that operational mismatch, static healthcare delivery should be complemented by an agile, mobile vaccination framework. Flexible, microtargeted teams operating during nonstandard hours at transit hubs and markets could reach highly transient populations more effectively.

Suboptimal Economic Condition

The 2026 measles surge imposed substantial economic hardship, and affected families spent an average of BDT 16,000 (Bangladeshi taka) on treatment and related costs, alongside income losses from prolonged caregiving (*39*). Among affected households, 89% borrowed money and 61% drew from their savings, highlighting the outbreak's potential to cause economic loss and vulnerability (*39*). Those costs highlight the risk for catastrophic and impoverishing healthcare expenditure (*39*). The economic burden of measles also could worsen health outcomes by delaying care-seeking and limiting access to essential treatment, nutrition, and supportive care.

Strategies for Resilient Immunization Systems

The 2026 measles outbreak in Bangladesh is a tragic case-study in the failure of acceptable national averages. To prevent a recurrence, the following lessons could be integrated into future public health strategies.

Tracking National Aggregate Coverage

Routine monitoring of national and subnational (district-level, urban, rural slum, and hard-to-reach areas) vaccination coverage is essential for identifying immunity gaps before they translate into outbreaks. Coverage data should be reviewed regularly according to age, geographic area, and relevant population characteristics to identify underimmunized populations. Timely identification of declining coverage

would enable health authorities to target catch-up vaccination programs.

Reducing Vaccine Misconceptions

Vaccine misconceptions could be reduced by disseminating accurate information through trustworthy media; professionals, such as physicians, vaccinologists, and teachers; and mass awareness campaigns (*29*,*32*). Moreover, a legal framework could help curb antivaccine activities and misinformation.

Depoliticizing Public Health Logistics

The delay of the 2024 mass follow-up vaccination campaign because of political unrest was the single most avoidable cause of the 2026 surge in deaths (*3*,*4*). To address that delay, immunization programs must be treated as essential state functions with autonomous funding and procurement mechanisms protected from political transitions. Creating a national vaccine stock would provide a cushion during national crises (*7*,*11*).

Integrating Syndemic Management

A syndemic approach requires addressing measles alongside the interacting health, social, and political conditions that amplify its impact (*40*). The 2026 crisis reflected a synergy between viral transmission and malnutrition, including vitamin A deficiency (*11*). Therefore, outbreak control should integrate vaccination with nutritional support, early identification and management of complications, and strengthened routine child health services. Follow-up vaccination should be incorporated into routine immunization activities rather than as an episodic emergency response (*7*,*20*).

Developing Urban-Specific Immunization Strategies

Urban informal settlements can contain localized clusters of underimmunized children because of population mobility, overcrowding, socioeconomic disadvantage, and limited access to routine health services (*41*). We describe that pattern as the slum cluster phenomenon, referring to the concentration of susceptible or incompletely vaccinated children within densely populated informal settlements, which can enable sustained measles transmission after virus introduction (*41*,*42*). Immunization strategies in those settings should complement routine facility-based services through targeted outreach, mobile vaccination, and follow-up of children who have missed recommended doses (*41*). Urban areas like Dhaka require specialized mobile vaccination teams that operate according to the schedules and movement patterns of informal settlement residents, rather than administrative convenience (*7*,*41*).

Linking Surveillance to Rapid Public Health Response

The 2026 outbreak was underway by December 2025, yet the emergency measles vaccination campaign was not launched until April 2026 (*3*,*11*,*18*), highlighting the need to link early warning with timely public health action. Routine surveillance of measles cases, hospital admissions, vaccination coverage, and other relevant indicators should be linked to predefined thresholds that trigger rapid epidemiologic assessment and, when warranted, activation of response teams and targeted vaccination activities (*19*,*20*). Other countries with similar healthcare settings also could adopt such initiatives.

Conclusions

The 2026 measles resurgence in Bangladesh was not adequately explained by a single national coverage trend or by COVID-19 disruption alone. The outbreak was largely driven by accumulated immunity gaps resulting from disruptions in routine immunization, declining vaccination coverage, vaccine supply constraints, lack of health system preparedness, and missed supplementary immunization opportunities. Those vulnerabilities enabled sustained transmission, particularly among young and undervaccinated children, and were further amplified by population mobility and weaknesses in timely surveillance and response. Preventing future outbreaks requires sustained and equitable coverage of at least 95% with both measles-containing vaccine doses, reliable vaccine supply, and systematic identification and follow-up of missed-dose and zero-dose children. Maintaining adequate vaccine stocks, strengthening hospital infection prevention and clinical preparedness, and addressing vaccine misinformation should be integral to a resilient measles elimination program.

In summary, the 2026 measles outbreak in Bangladesh demonstrates that strong historical performance does not ensure future protection; maintaining it requires constant vigilance, adaptive governance, and equitable healthcare delivery. The ≈803 lives lost in 2026 must serve as the impetus for a fundamental shift in how immunization is governed, funded, and delivered in an increasingly politically unstable world.

Acknowledgments

We thank Homayra Rahman Shoshi for her valuable contribution to the linguistic editing of this manuscript.

icddr,b is grateful to the governments of Bangladesh and Canada for providing core/unrestricted support. S.B., T.A.S., M.Z.H., G.S.M., M.A.A., and F.C. are supported by icddr,b; A.F.M.Z. is supported by Department of Anthropology, Shahjalal University of Science and Technology, Sylhet, Bangladesh; and M.R. is supported by The Eastern Mediterranean Public Health Network (EMPHNET), Dhaka, Bangladesh.

During the preparation of this work, we used Grammarly AI (https://www.grammarly.com) to assist with grammar checking and language refinement. After using that tool, we thoroughly reviewed and edited the content, as needed, and take full responsibility for the final content of the publication.

Athor contributions: S.B. conceptualized the analysis and developed the original draft. S.B., T.A.S., M.Z.H., G.S.M., M.A.A., A.F.M.Z., M.R., and F.C. critically reviewed, revised, and approved the final draft.

About the Author

Mr. Bhuiya is a public health researcher in the Infectious Diseases Division at icddr,b, Dhaka, Bangladesh. His research interests focus on infectious disease surveillance, particularly respiratory viruses, antimicrobial resistance, and emerging infections.

References

1. Do LAH, Mulholland K. Measles 2025. N Engl J Med. 2025;393:2447–58. https://doi.org/10.1056/NEJMra2504516
2. Venkatesan P. Global resurgence in measles. Lancet Microbe. 2026;7:101347. https://doi.org/10.1016/j.lanmic.2026.101347
3. Sumon S. Bangladesh faces deadly measles outbreak after delayed vaccination drive. Arab News. 2026 Apr 13 [cited 2026 May 10]. https://www.arabnews.com/node/2639761/world
4. Ellis-Peterson H. Bangladesh launches measles vaccination drive as child death toll passes 100. The Guardian. 2026 Apr 7 [cited 2026 May 10]. https://www.theguardian.com/world/2026/apr/07/bangladesh-measles-vaccination-drive-child-death-toll
5. Khanal S, Bohara R, Chacko S, Sharifuzzaman M, Shamsuzzaman M, Goodson JL, et al. Progress toward measles elimination—Bangladesh, 2000–2016. MMWR Morb Mortal Wkly Rep. 2017;66:753–7. https://doi.org/10.15585/mmwr.mm6628a3
6. World Health Organization. Achieving measles and rubella elimination [cited 2026 May 11]. https://www.who.int/bangladesh/activities/achieving-measles-and-rubella-elimination
7. Lateef S. Measles: 38 children dead in Bangladesh outbreak. BMJ. 2026;393:s654. https://doi.org/10.1136/bmj.s654
8. Basu S, Ashok G, Debroy R, Ramaiah S, Livingstone P, Anbarasu A. Impact of the COVID-19 pandemic on routine vaccine landscape: a global perspective. Hum Vaccin Immunother. 2023;19:2199656. https://doi.org/10.1080/21645515.2023.2199656
9. Hossen MT, Alam MSB, Islam MS, Montomoli E, Clemens R, Costa Clemens SA, et al. Impact of the COVID-19 pandemic on the routine immunization system in Bangladesh. PLoS One. 2025;20:e0334503. https://doi.org/10.1371/journal.pone.0334503
10. Raqib R, Rahman M. Measles is resurging in Bangladesh—but this outbreak was entirely preventable. BMJ. 2026;393:s819. https://doi.org/10.1136/bmj.s819
11. United Nations Children's Fund Bangladesh. Measles outbreak situation report no 1. 2026 Apr 8. [cited 2026 May 11]. https://www.unicef.org/media/179846/file/Bangladesh-Humanitarian-Situation-Report-No.1 (Measles-Outbreak)-8-April-2026.pdf
12. Hassan MZ, Islam MA, Mahmood AS, Shoshi HR, Bari MTIA, Rahman M, et al. Measles resurgence in Bangladesh: a preventable crisis in a transitioning immunisation system. Lancet Reg Health Southeast Asia. 2026 Jun 4 [Epub ahead of print]. https://doi.org/10.1016/j.lansea.2026.100787
13. Directorate General of Health Services. Measles press release [in Bengali]. 2026 Sep 13 [cited 2026 Sep 14]. https://dghs.gov.bd/pages/press-releases
14. Rabbi MF, Muztahid P, Mahdi FA. Nationwide surveillance and control measures during large measles outbreak, Bangladesh, 2026. Emerg Infect Dis. 2026; 32:e1–6. https://doi.org/10.3201/eid3211.260996.
15. icddr,b. No proof of genetic changes in measles viruses in Bangladesh capable of reducing vaccine protection. 2026 Aug 1 [cited 2026 Sep 1]. https://www.icddrb.org/press-releases/no-proof-of-genetic-changes-in-measles-viruses-in-bangladesh-capable-of-reducing-vaccine-protection-02-08-2026
16. Bucris E, Zuckerman NS, Levin T, Kanaaneh Y, Erster O, Indenbaum V, et al.; National Measles Working Group; National Measles Working Group. Genomic and epidemiologic insights into ongoing measles outbreak, Israel, 2025–2026. Emerg Infect Dis. 2026;32:1678–82. https://doi.org/10.3201/eid3209.260625
17. Choudhury SD, Khan MA, Amin E, Abedin J, Munro S, Kaczmarek M, et al. Molecular detection and genetic diversity of measles and parainfluenza viruses circulating in humans in Bangladesh: a cross-sectional study. Health Sci Rep. 2026;9:e71832. https://doi.org/10.1002/hsr2.71832
18. World Health Organization. Nationwide response mobilized to contain measles outbreak in Bangladesh. 2026 Apr 15 [cited 2026 May 10]. https://www.who.int/southeastasia/news/detail/15-04-2026-response-measlesBN
19. World Health Organization. Disease outbreak news: measles—Bangladesh [cited 2026 Jun 5]. https://www.who.int/emergencies/disease-outbreak-news/item/2026-DON598
20. Jamil S, Asif U, Mohammadnezhad M. Unusual measles mortality in Bangladesh signals an immunisation emergency. Lancet. 2026;407:1596–7. https://doi.org/10.1016/S0140-6736(26)00687-2
21. Rahman A. Measles explodes in Bangladesh after vaccination breakdown, killing hundreds of children. Science. 2026 Apr 30 [cited 2026 May 22]. https://www.science.org/content/article/measles-explodes-bangladesh-after-vaccination-breakdown-killing-hundreds-children
22. Al Jazeera. Suspected measles outbreak kills nearly 100 children in Bangladesh. 2026 Apr 6 [cited 2026 May 25]. https://www.aljazeera.com/news/2026/4/5/ suspected-measles-outbreak-kills-nearly-100-children-in-bangladesh
23. Moral S. Measles outbreak: millions of children left out of vaccination target. Prothom Alo. 2026 Jul 12. [cited 2026 Jul 15]. https://en.prothomalo.com/bangladesh/wphrk3dqc8

24. Expanded Programme on Immunization. Routine EPI coverage evaluation survey 2023 [cited 2026 Jun 5]. https://www.sdg.gov.bd/uploads/indicator-data/EPI%20CES%202023%20-%20First%2028%20pages.pdf
25. Mhatre SL, Schryer-Roy AM. The fallacy of coverage: uncovering disparities to improve immunization rates through evidence. Results from the Canadian International Immunization Initiative Phase 2—operational research grants. BMC Int Health Hum Rights. 2009;9:S1. https://doi.org/10.1186/1472-698X-9-S1-S1
26. World Health Organization. Measles vaccination coverage [cited 2026 Jun 15]. https://immunizationdata.who.int/global/wiise-detail-page/measles-vaccination-coverage
27. Expanded Programme on Immunization. Coverage evaluation survey 2019 EPI Bangladesh [cited 2026 Jun 17]. https://objectstorage.ap-dcc-gazipur-1.oraclecloud15.com/n/axvjbnqprylg/b/V2Ministry/o/office-dghs/2024/12/05944887099b432e8ad22cfed808ef74.pdf
28. BEACON. Request for information (RFI): measles outbreak reported to overwhelm hospitals amid vaccine shortage in Dhaka and other areas of Bangladesh. RFI on case numbers, diagnostic information, clinical data, and other relevant details; 2026 Mar 29 [cited 2026 May 15]. https://beacon-bio.org/en/report/?reportid=a2f7e51f-5d4c-4441-9902-44ddb77fa6bc&eventid=e1186ca5-57eb-4db1-8676-26480828e29c
29. Bhuiya S, Chowdhury F, Islam MA, Shuvo TA, Aleem MA, Basher AK, et al. A strategic blueprint for strengthening respiratory syncytial virus prevention among under-five children in low- and middle-income countries: Bangladesh as a model for new immunisation approaches. J Glob Health. 2026;16:03013. https://doi.org/10.7189/jogh.16.03013
30. Lotus AS. bdnews24.com. Measles surges amid 'patchwork' response as experts' advice ignored, coordination falters. 2026 May 4 [cited 2026 Sep 23]. https://bdnews24.com/health/e80adc990d4a
31. Adhikary TS. Healthcare workers' demo disrupts vaccination, medical services. The Daily Star. 2025 Dec 2 [cited 2026 May 22]. https://www.thedailystar.net/news/bangladesh/news/healthcare-workers-demo-disrupts-vaccination-medical-services-4049291
32. Larson HJ, Gakidou E, Murray CJL. The vaccine-hesitant moment. N Engl J Med. 2022;387:58–65. https://doi.org/10.1056/NEJMra2106441
33. Koster FT, Curlin GC, Aziz KM, Haque A. Synergistic impact of measles and diarrhoea on nutrition and mortality in Bangladesh. Bull World Health Organ. 1981;59:901–8.
34. Summan A, Nandi A, Shet A, Laxminarayan R. The effect of the COVID-19 pandemic on routine childhood immunization coverage and timeliness in India: retrospective analysis of the National Family Health Survey of 2019–2021 data. Lancet Reg Health Southeast Asia. 2023;8:100099. https://doi.org/10.1016/j.lansea.2022.100099
35. Jashim SU. Vaccine gaps and malnutrition fuel child deaths in measles outbreak. Jago News 24. 2026 Mar 30 [cited 2026 Jun 12]. https://www.jagonews24.com/en/national/news/91285
36. Amodan BO, Ssendikwanawa E, Namayanja J, Opio BR, Biroma G, Morukileng J, et al. Epidemiological investigation of measles outbreak in a refugee settlement in Lamwo District, Uganda. Pan Afr Med J. 2025;51:13. https://doi.org/10.11604/pamj.supp.2025.51.1.47672
37. Tiley KS, Ten Hulscher-van Overbeek H, Basnet S, van Binnendijk R, Clarke E, Cose S, et al. The waning of maternal measles antibodies: a multi-country maternal-infant seroprevalence study. J Infect. 2025;91:106531. https://doi.org/10.1016/j.jinf.2025.106531
38. BEACON. Follow-up on measles outbreak in Bangladesh: 674 cases and 38 child deaths reported, with 70% in infants below vaccination age. 2026 Apr 1 [cited 2026 May 15]. https://beaconbio.org/en/report/?reportid=41a6f8f7-917e-4f50-aeed-bc98a52149bf&eventid=e1186ca5-57eb-4db1-8676-26480828e29c
39. United Nations Office for the Coordination of Humanitarian Affairs Reliefweb. Nearly 9 in 10 families borrow to meet measles treatment costs: BDRCS-IFRC assessment finds. 2026 Aug 6 [cited 2026 Aug 15]. https://reliefweb.int/report/bangladesh/nearly-9-10-families-borrow-meet-measles-treatment-costs-bdrcs-ifrc-assessment-finds
40. Singer M, Clair S. Syndemics and public health: reconceptualizing disease in bio-social context. Med Anthropol Q. 2003;17:423–41. https://doi.org/10.1525/maq.2003.17.4.423
41. Crocker-Buque T, Mindra G, Duncan R, Mounier-Jack S. Immunization, urbanization and slums—a systematic review of factors and interventions. BMC Public Health. 2017;17:556. https://doi.org/10.1186/s12889-017-4473-7
42. Horng L, Kakoly NS, Abedin J, Luby SP. Effect of household relocation on child vaccination and health service utilisation in Dhaka, Bangladesh: a cross-sectional community survey. BMJ Open. 2019;9:e026176. https://doi.org/10.1136/bmjopen-2018-026176

Address for correspondence: Saju Bhuiya, Infectious Diseases Division, icddr,b, 68 Shaheed Tajuddin Ahmed Sarani, Mohakhali, Dhaka 1212, Bangladesh; email: saju.bhuiya@icddrb.org

Importation-Driven Measles Resurgence and the Fragility of Elimination, Japan, 2024–2026

Koichiro Yuji, Wakako Yuji, Eisuke Adachi

As measles elimination unravels across the Americas, Europe, and the Western Pacific, Japan is experiencing a resurgence of measles; the World Health Organization had verified elimination of measles in Japan in 2015. By epidemiologic week 20 of 2026, a total of 498 cases had been reported, exceeding every full-year total since 2020. Median case-patient age has fallen to 26 years, shifting the burden from a generation who received single-dose measles vaccinations to younger cohorts caught between successive vaccination-policy transitions. Among case-patients with a documented 2-dose vaccination history, more than half experienced modified measles, an attenuated, easily missed illness that delays diagnosis and isolation. As mass gatherings concentrate global travel, Japan has become a sentinel for the fragility of measles elimination, including in countries that consider elimination status secure. Surveillance shows importation-driven resurgence; the shift in genotype profile from D8 to B3 predominance back to D8 enabled tracking of source countries.

In November 2025, the World Health Organization (WHO) Region of the Americas lost its regional elimination status after endemic measles transmission was reestablished in Canada, which had maintained elimination since 1998 (*1*). Transmission has since accelerated: by epidemiologic week 28 of 2026, the region had reported 47,459 confirmed cases and 44 deaths, >3 times the 2025 total and the highest count since 2004 (*2*). The Pan American Health Organization (PAHO) Regional Verification Commission, which reviews all countries in the region annually, will consider the 2026 reports, including that of the United States, in November 2026 (*1*,*3*). By September 10, 2026, the United States had recorded 3,294 confirmed cases, its largest annual total since elimination was declared in 2000; of the cases, 95% were outbreak-associated and 95% occurred in unvaccinated persons or those of unknown status (*4*,*5*). The percentage internationally imported has fallen to ≈10%, signaling a shift toward sustained domestic transmission (*3*).

The erosion of measles elimination status is not confined to the Americas. The WHO European Region recorded 127,350 measles cases in 2024, double the 2023 total and the highest in >25 years (*6*); on the basis of that resurgence, WHO announced in January 2026 that 6 countries, including the United Kingdom, had lost their elimination status. The age structure for those cases is instructive: among cases reported in Europe during January–June 2026, half (51%) were among those ≥15 years of age, and 15% of those with known vaccination status had received 1 dose (*7*).

Japan's own region is a cautionary backdrop. Measles in the WHO Western Pacific Region rose 743% during 2022–2024; Mongolia and Cambodia, the first middle-income countries there to eliminate measles, later lost that status to importation-related outbreaks (*8*,*9*). Japan, where elimination was verified in 2015 (*10*), had recorded more cases by mid-2026 than in any full year since 2020. We argue that Japan is a sentinel for an elimination framework under growing strain, with lessons extending well beyond the Western Pacific to every country whose elimination status now rests on fragile foundations.

A Rapid, Geographically Dispersed Resurgence

This report draws on Japan's mandatory national surveillance data. By epidemiologic week 20 of 2026, a total of 498 cases had been notified through Japan's National Epidemiologic Surveillance of Infectious Diseases, already exceeding every full-year total since 2020 (Figures 1, 2). The lowest years, 2020–2022, had 6–10 cases annually, coinciding with stringent COVID-19 control measures and the near-cessation of international travel, so they do not

Author affiliations: The Institute of Medical Science, The University of Tokyo, Tokyo, Japan (K. Yuji, E. Adachi); Kitasato Institute Hospital, Tokyo (K. Yuji, W. Yuji, E. Adachi)

DOI: https://doi.org/10.3201/eid3211.261187

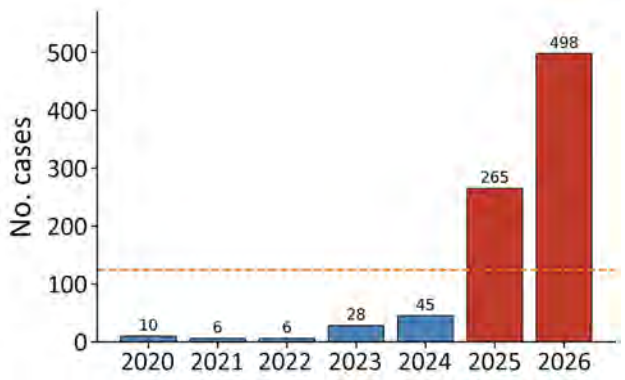

Figure 1. Annual reported cases of measles, Japan, 2020–2026. Red bars denote provisional totals not yet finalized for 2025 and all 2026 data for epidemiologic weeks 1–20. Blue bars represent finalized annual counts for 2020–2024. Dashed line marks an incidence of 1 confirmed case/1 million population/year (≈124 cases/year for Japan), a World Health Organization surveillance performance indicator for monitoring progress toward and maintenance of elimination rather than a criterion for verification, which rests on multiple lines of evidence (*11*).

represent a normal baseline. Measured instead against the prepandemic period, 2025 and 2026 still mark a clear departure from the postelimination norm (*12*). Weekly counts in 2026 were 28–39 cases across weeks 11–14; they peaked at 62–71 in weeks 15–17 and fell to 17–23 in weeks 18–20, a decline the national report attributes partly to reduced holiday-period reporting (*13*) (Figure 2).

We derived detailed epidemiologic, genotype, and clinical data from the national featured report for the first 20 weeks of 2026 (498 cases; data as of May 20, 2026), the most granular dataset available at the time of writing. Cases were identified in 27 of

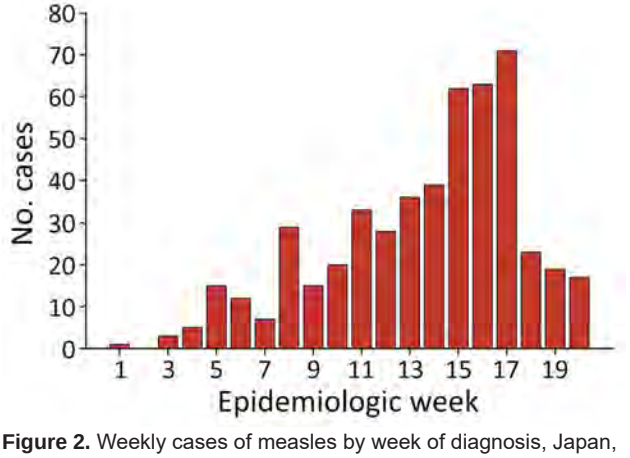

Figure 2. Weekly cases of measles by week of diagnosis, Japan, 2026. Provisional data for epidemiologic weeks 1–20, through May 20, 2026, are shown. Counts rose from week 11, peaked in week 17, and fell in weeks 18–20; the decline might reflect reduced reporting over an extended holiday period. Because reports accrue over subsequent weeks, counts for the most recent weeks are provisional and will rise.

47 prefectures, indicating multiple concurrent transmission chains rather than 1 localized outbreak. The amplifying potential of even 1 importation is illustrated by an imported case reported in March 2024 that seeded a superspreading event, including secondary transmission to fellow passengers on the same flight, with the highest transmissibility concentrated in the first generation of spread before self-isolation and public-health awareness curtailed further transmission (*14*). That episode shows how 1 importation can ignite a rapidly amplifying cluster despite nominally high population vaccination, a dynamic that recurs wherever susceptibility is unevenly distributed.

Importation Sources and Genotype Succession

The resurgence of measles in Japan is importation-driven; genotype profiles are linked closely enough to the source countries to function as a molecular record of travel patterns. In 2023, importations from Indonesia and India predominated; genotype D8 accounted for 88% of typed cases (*15*). In 2025, Vietnam became the leading source of imported infection, accounting for ≈83% of cases with an overseas-acquired source; genotype B3 surged to 87% (*16*). By 2026, Indonesia had reemerged as the leading overseas source. Genotype information was available for 341 (69%) of the 498 cases reported through week 20; among those, genotype D8, one of the 2 genotypes (with B3) responsible for most measles transmission globally in the study period, accounted for 61% and B3 for 39% of cases, reversing the ratio seen earlier in the resurgence (*13*). The geography of those cases fits an importation-anchored process. Five prefectures accounted for just over half of all modified measles cases during 2016–2025, yet incidence in neighboring prefectures was uncorrelated in every period examined; cases clustered around metropolitan gateways rather than diffusing across adjacent prefectures. The leading prefectures also moved eastward between resurgence years, from Osaka and Kanagawa in 2019 to Kanagawa and Ibaraki in 2025, over the same period in which the dominant genotype and source countries changed (*16*). That shifting genotype profile—D8 predominance in 2023, a shift to B3 predominance by 2025, and a reversal to D8 predominance in 2026—mirrors the shifting epidemiology of the Asia-Pacific source countries on which Japan's importation risk depends and underscores that domestic case counts are inseparable from the regional control situation.

Interpreting those data against the formal definition of elimination requires caution. WHO criteria defined reestablishment of endemic transmission as

uninterrupted circulation of the same measles virus genotype and lineage for ≥12 months; elimination is verified only after 36 months of interrupted transmission (*11*). Our analysis is limited to genotype-level frequencies and cannot resolve named strains or lineages. The standard 450-nt window of the nucleoprotein gene is not sufficiently discriminating to separate endemic from imported virus within a genotype; whole-genome sequencing, particularly of the noncoding region between the matrix and fusion genes, carries the phylogenetic information needed to distinguish sustained domestic chains from repeated importations (*17*). Because 31% of cases are ungenotyped, the apparent absence of a single sustained lineage is provisional. We emphasize this fact because genotype-frequency data alone can neither establish nor exclude loss of elimination.

Adult Susceptibility and the Legacy of Vaccination-Policy Transitions

The measles resurgence is concentrated in young adults, although not the same adults as in 2019. Among the 498 cases reported in Japan through week 20 of 2026, median patient age was 26 (range 0–65) years (*13*). Age-specific incidence locates that shift (Figure 3): it peaked at 30–34 years in 2019 but at 20–24 years in 2026, two 5-year bands lower; combined incidence at 30–39 years fell to about 80% of its 2019 value (*12*,*13*,*18*). That shift traces back to Japan's national immunization program.

Measles vaccine entered Japan's routine immunization program in October 1978, administered as a single dose to young children (*20*,*21*). The schedule remained single-dose for >25 years. A structural change came in 1994, when an amendment to the Immunization Act ended mandatory vaccination, shifting measles immunization from a compulsory to a recommended basis (*22*). Persons born from 1978 until the routine 2-dose schedule began in 2006 (i.e., for persons 21–48 years of age in 2026) were offered a single routine dose for part of that period on a noncompulsory basis. A single dose confers seroconversion in ≈93% of recipients, so most of that population is protected, and susceptible persons are a small fraction of it.

The 2-dose measles–rubella schedule was introduced in 2006, prompted by WHO Western Pacific Region's 2005 resolution to eliminate measles; the first dose was given to children 12–24 months of age and the second before elementary school entry (*12*,*23*). A nationwide resurgence in 2007–2008 among teenagers with a single dose exposed the gap that the new schedule could not close for those past school-entry age (*23*,*24*). Japan responded with a 5-year catch-up supplementary immunization activity during April 2008–March 2013, offering a second dose to adolescents in the first year of junior high school and the final year of high school (*23*,*24*). By reaching adolescents of specific ages at that time, the campaign created a set of transitional cohorts: persons born during 1995–2005 received their first dose under the single-dose regime and their second, if at all, through a time-limited campaign or the opening years of the 2-dose schedule.

Read against that history, the 2 resurgences implicate different cohorts. The adults infected in 2019 were born predominantly in the late 1980s; they were vaccinated under the single-dose schedule and

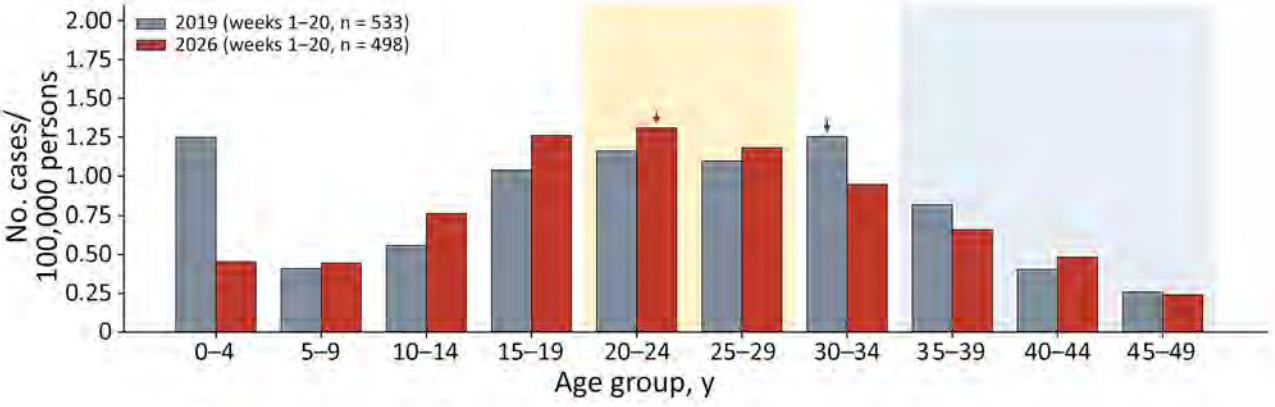

Figure 3. Measles cases by age group reported in epidemiologic weeks 1–20 of 2019 and 2026, Japan. Age-specific incidence in weeks 1–20 of 2019 (n = 533) and 2026 (n = 498) were calculated from national case counts and population estimates for the corresponding year. Shading indicates 2 cohorts defined by vaccination policy. Yellow shading indicates the age groups of the transitional cohorts, born ≈1995–2005, who received a second dose of measles vaccine, if they did so, through the time-limited 2008–2013 campaign or the opening years of the 2-dose schedule. Light blue shading indicates the single-dose cohort, born ≈1978–1990, who were offered 1 routine dose and were not eligible for the second dose through the campaign. Black arrow indicates peak age group in 2019; red arrow indicates peak age group in 2026. Source: Japan Institute for Health Security Infectious Disease Weekly Report (*13*,*19*,*36*).

already too old for the 2008–2013 catch-up. That single-dose generation was, in the 2019 resurgence, the decisive susceptible population. By 2026, both the median case-patient age and the peak of age-specific incidence fell within the transitional cohorts, born in 1995–2005, whose second dose came through a time-limited campaign or the opening years of the 2-dose schedule, if at all (Figure 3). The immunity gap has not closed so much as moved from a generation offered 1 dose to younger cohorts whose 2 doses were given inconsistently with few opportunities for natural boosting in a country where measles no longer circulates; that distinction is supported by evidence that, in a setting in which measles was eliminated, measles antibodies wane after vaccination but not after infection (*25*). We attached no point estimate to the susceptible population because coverage data cannot distinguish between primary-vaccine failure, waning immunity, and unrecorded catch-up doses (*16*).

Compounding the weakness in the historical structure, contemporary routine coverage has begun to slip. First-dose measles–rubella coverage was 95.4% in fiscal year 2022 (Japan's fiscal year runs April–March); in fiscal year 2024, first-dose coverage was 92.7% and second-dose coverage 91.0%, both below the 95% level associated with interrupting transmission (*15*,*26*). A cohort-structured susceptibility and an eroding contemporary coverage were therefore acting in combination to increase risk for infection and spread. We observed a comparable combination underlying the contemporaneous loss of regional measles elimination in the Americas, where PAHO has assessed the regional public-health risk as very high because of declining coverage and increases in susceptible populations (*2*); the parallel underscores a wider pattern.

Diagnostic Challenge of Modified Measles in Vaccinated Adults

A clinically consequential feature of measles resurgence is the appearance of infection in vaccinated adults. That observation is not evidence that vaccine failure is becoming more common; in the United States, the breakthrough fraction has remained stable at ≈8%–12% of reported cases, and the 2025 resurgence occurred overwhelmingly among unvaccinated persons or those with no documented vaccination (*5*,*27*). What such settings share is not a rising rate of vaccine failure but pockets of susceptibility within populations whose aggregate coverage appears adequate, differing in how those pockets are defined: by community in the United States, by birth cohort in Japan, and, in Israel's outbreak of ≈3,200 cases traced to a single importation, by childhood nonvaccination (median age 5.6 years, 83% unvaccinated) (*28*). Among the 159 cases in 2026 with 2 documented doses (158 of them in patients ≥6 years of age), 89 (56%) experienced modified measles, an attenuated illness characterized by a subtle rash, minimal or absent fever, and frequently absent Koplik spots (*13*,*29*); that proportion applies to documented 2-dose recipients only, because vaccination status was unknown for 41% of case-patients ≥6 years of age. In adults, the manifestation is easily mistaken for a nonspecific viral exanthem or a drug reaction, particularly because clinicians in elimination settings might not consider measles in a vaccinated patient at all. Clinical suspicion is lowest in the population in which such infection occurs.

Characterizing the transmission risk for modified measles accurately is important because both overstatement and understatement carry costs. In a systematic review of postelimination settings, index case-patients with secondary vaccination failure produced few secondary infections among their contacts; secondary attack rates were 0%–6.25%, and the estimated effective reproduction number for onward transmission from such cases was 0.063. Onward transmission from such cases is therefore substantially less efficient than from a case in an unvaccinated person, but it does occur, and clusters have been documented under conditions of close and prolonged contact (*30*). The principal hazard posed by modified measles is therefore diagnostic rather than directly epidemiologic: because its attenuated manifestation delays recognition, isolation, and contact tracing, more transmissible infections could seed in susceptible contacts. In the largest United States series, comprising 4,056 cases during 2001–2022, breakthrough infections accounted for 475 (12%) of cases, were milder, and arose predominantly from secondary rather than primary vaccine failure (*27*). Vaccinated adults will increasingly be included in case series wherever elimination is under pressure.

The practical implications for clinicians are concrete. Physicians evaluating an adult with febrile rash should elicit a vaccination and travel history, keep measles on the differential even in 2-dose recipients, and conduct both IgM serology and reverse transcription PCR, because IgM could be transiently negative early in modified measles. Of importance, the mildness of the index case does not diminish the public health stakes. Each unrecognized case can transmit to those at greatest risk: infants too young to be vaccinated, pregnant persons, and immunocompromised

persons. Historically, ≈30% of reported cases have experienced complications; the risk for complications is highest in children <5 years of age and in adults (*31*). Measles also induces immune amnesia, depleting immune memory for years after infection (*32*). A milder index case is not benign.

Uncertainty of Low-Transmission Estimates for Japan

A caveat specific to the Japan context bears directly on how the reassuringly low transmission estimates for secondary vaccination failure should be read. Two distinct susceptible groups must be separated. The first comprises fully (2-dose) vaccinated adults who nonetheless develop breakthrough infection as modified measles; for those, the low transmission estimates derived from secondary vaccination failure apply, and the dominant hazard is diagnostic delay rather than efficient onward spread. The second, larger group comprises adults whose birth cohorts were never offered a routine 2-dose schedule or who were offered a second dose only through time-limited catch-up campaigns of incomplete uptake; vaccine failure here occurs not in the immunological sense but by a structural absence of a second dose across whole birth cohorts. Conflating the two would understate the transmission potential of the resurgence because the parameters that reassure for the first group do not describe the second.

That distinction also qualifies how the secondary vaccination failure estimates themselves should be generalized. Those estimates derive overwhelmingly from highly 2-dose–vaccinated populations, in which the rare breakthrough case is surrounded by immune contacts, and onward transmission is correspondingly contained. The containment observed in such settings is a property not only of the index case-patient's attenuated infectiousness but also of the surrounding immune environment. Where that environment is itself partially susceptible, as it is where Japan's transitional cohorts are concentrated, the same low per-case transmission probability can nonetheless seed longer chains because a larger fraction of contacts are themselves at risk. Low-transmission parameters measured in 2-dose populations may therefore not extrapolate to a setting in which the susceptible fraction is generational. That conclusion does not imply that modified measles is highly transmissible; it cautions against importing reassurance from populations whose immune structure differs from Japan's. The same caution applies wherever pockets of susceptibility persist within an otherwise highly vaccinated population, whether defined by birth cohort, by community, or, as in much of Europe, where half of cases are now in adolescents and adults, by incomplete 2-dose rollout.

Mass Gatherings

The timing of this resurgence magnifies its stakes. The 2026 FIFA World Cup, held June 11–July 19 across the United States, Canada, and Mexico, brought millions of travelers into 3 host nations that were simultaneously experiencing active resurgences and maintaining coverage below the 95% threshold (*1*). Measles has a well-documented history of transmission at mass gatherings, where large numbers of persons from areas of differing immunity mix in crowded, often indoor settings. During the 1991 International Special Olympics, measles spread to 16 persons across 7 US states, including spectators exposed by airborne transmission in a domed stadium; 9 additional cases resulted from onward transmission (*33*). The episode demonstrated that 1 infectious person in a large enclosed venue can transmit measles across substantial distances and subsequently across state and national boundaries.

Sporting events involving youth have repeatedly served as foci. At a 2007 international youth sporting event, the index case-patient was a 12-year-old participant from Japan infected with genotype D5 measles; contact tracing across 8 US states identified 7 cases, 71% of whom were in unvaccinated persons (*34*). Given that measles has a basic reproduction number of 12–18, among the highest of any human pathogen (*31*), a single importation into a mass gathering can ignite rapid and geographically dispersed spread before public health authorities are aware that transmission has begun.

The measles risk associated with the 2026 World Cup has been recognized mainly from the perspective of the host region (*35*). Japan's experience adds a complementary view: that of a participating Asia-Pacific nation that is simultaneously a major source of outbound travelers and a recipient of importation-linked cases. Japan is thus embedded in a bidirectional risk network rather than positioned only as a potential importer or exporter. The 20th Asian Games in Aichi–Nagoya, Japan, during September–October 2026, shortly after the World Cup, leaves the Western Pacific region facing its own overlapping mass-gathering season. Because travel medicine frames measles as a borderless threat in which every nonimmune traveler is a potential carrier and vector (*36*), defending elimination becomes a shared transnational responsibility that no single country can discharge alone.

Implications for Surveillance and Response

Japan's measles resurgence points to 4 priorities that generalize to other elimination-era settings. First, catch-up vaccination should follow the gap as it moves toward the cohorts born between the end of the single-dose regime and the maturation of the 2-dose schedule; Japan's 2008–2013 adolescent program showed that coverage in a defined age band can be raised within a finite period. Second, pretravel vaccination checks should be integrated into routine travel-medicine practice, given that importation drives nearly every domestic chain. Third, second-dose coverage should be restored to ≥95% in every prefecture. Fourth, surveillance data on vaccination status, genotype, and transmission chains should be completed and standardized; the large percentages of missing data limit the resolution at which transmission can be understood. Because the disease burden concentrates in gateway prefectures rather than spreading contiguously, strengthening awareness and laboratory confirmation in those prefectures is likely to yield more than uniform national measures.

Beyond those immediate measures, the resolution of transmission chains in future outbreaks would benefit from analytic approaches that aggregate surveillance cannot provide. Generation-dependent modeling and transmission-network analysis, which have been applied to previous measles outbreaks in Japan, offer a route to reconstructing who-infected-whom structure and to distinguishing sustained endemic transmission from repeated independent importations; those distinctions are central to the formal assessment of elimination status. Pairing such methods with systematic genomic sequencing would replace genotype-frequency snapshots of the kind reported here with lineage-resolved chains, materially strengthening the evidentiary basis for elimination decisions.

Our analysis relied on aggregate routine surveillance, which may underconfirm modified measles, given its diagnostic difficulty. Vaccination status was unknown for 41% of eligible 2026 cases, genotype data covered 69% of cases, and place of infection was unknown for 18% of cases. Transmission chains could not be resolved from aggregate data, and no phylogenetic analysis was available, so the genomic findings reported here are descriptive genotype frequencies rather than resolved lineages. We calculated incidence (Figure 3) from aggregate case counts and population denominators, not individual vaccination histories; we determined incidence by age but could not establish differential susceptibility by vaccination status, for which serosurveillance would be required. Finally, 2025 and 2026 case counts are provisional and subject to retrospective revision. Those limitations argue for, rather than against, the strengthening of surveillance that we recommend.

Conclusions

Japan's measles resurgence is a sentinel signal. A nation with historically high vaccination coverage, robust surveillance, and verified elimination is losing ground, and it is doing so through mechanisms that are not unique to Japan: cohorts left between successive vaccination-policy transitions, eroding contemporary coverage, importation pressure, and underrecognized infection in vaccinated adults. What differs among settings is the structure of susceptibility rather than the fact of exposure; Japan's gap is cohort-structured and policy-derived, whereas recent transmission in North America has been concentrated in undervaccinated communities. That distinction matters, because it determines whether catch-up should be targeted by birth cohort or by community; the underlying dynamic of accumulated susceptibility meeting sustained importation pressure is shared. As elimination falters across the Americas and Europe and mass gatherings concentrate global travel, the lesson is that elimination is reversible everywhere, including in settings that consider it secure. Yet, as PAHO has emphasized, status that is lost can also be regained through coordinated immunization and surveillance. The reversibility cuts both ways. Defending measles elimination depends as much on clinical vigilance, keeping measles on the differential in vaccinated adults and confirming it by laboratory testing, as on population-level coverage, and it depends on recognizing that in an interconnected world the susceptibility of one country is the concern of all.

This study used routinely collected, deidentified national surveillance data; ethics approval was not required under the Ethical Guidelines for Medical and Biological Research Involving Human Subjects (MEXT/MHLW/METI, 2021). The work was conducted in accordance with the Declaration of Helsinki. All data are publicly available from the Japan Institute for Health Security Infectious Disease Weekly Report (https://id-info.jihs.go.jp), NIID Infectious Agents Surveillance Report, and the Ministry of Health, Labour and Welfare. No new sequences or primary data were generated.

This work was supported by a Health and Labour Sciences Research grant from the Ministry of Health, Labour and Welfare of Japan, to E.A. (grant no. 25HA2002).

K.Y. reports institutional support from Tokyu Land Corporation and consultation fees from Seoritsu Biotech, both outside the submitted work.

A large language model (Claude; Anthropic, https://www.anthropic.com) was used for language editing and to assist in writing the code to plot the figures from author-supplied data; the figures are data plots, not an AI-generated image. AI was not used to generate, interpret, or analyze the underlying surveillance data or to draw scientific conclusions. The authors verified all figures and content against primary sources and take full responsibility for the work, consistent with International Committee of Medical Journal Editors and World Association of Medical Editors recommendations.

Author contributions: K.Y. conceived the work, curated and analyzed data, and drafted the manuscript. W.Y. contributed to data curation and methodology and revised the manuscript. E.A. contributed validation and critical revision. All authors approved the final manuscript.

About the Author

Dr. Yuji is a project associate professor at the Institute of Medical Science, The University of Tokyo. His research interests include vaccinology, clinical laboratory medicine, and medical informatics, with a focus on the control of vaccine-preventable diseases.

References

1. Pan American Health Organization. PAHO calls for regional action as the Americas lose measles elimination status. 2025 Nov 10 [cited 2026 Jun 20]. https://www.paho.org/en/news/10-11-2025-paho-calls-regional-action-americas-lose-measles-elimination-status
2. Pan American Health Organization. Epidemiological alert: measles in the Americas Region. 2026 Aug 7 [cited 2026 Aug 15]. https://www.paho.org/en/documents/epidemiological-alert-measles-americas-region-7-august-2026
3. Pan American Health Organization. Update on the review of measles elimination status. 2026 Mar 2 [cited 2026 Jun 24]. https://www.paho.org/en/news/2-3-2026-update-review-measles-elimination-status
4. Mathis AD, Raines K, Filardo TD, Wiley N, Leung J, Rota PA, et al. Measles update—United States, January 1–April 17, 2025. MMWR Morb Mortal Wkly Rep. 2025;74:232–8. https://doi.org/10.15585/mmwr.mm7414a1
5. Centers for Disease Control and Prevention. Measles cases and outbreaks. 2026 [cited 2026 Sep 15]. https://www.cdc.gov/measles/data-research/index.html
6. World Health Organization Regional Office for Europe. European Region reports highest number of measles cases in more than 25 years—UNICEF, WHO/Europe. 2025 Mar 13 [cited 2026 Jun 24]. https://www.who.int/europe/news/item/13-03-2025-european-region-reports-highest-number-of-measles-cases-in-more-than-25-years---unicef--who-europe
7. European Centre for Disease Prevention and Control. Measles and rubella monthly report, July 2025–June 2026. 2026 [cited 2026 Aug 15]. https://measles-rubella-monthly.ecdc.europa.eu
8. World Health Organization Regional Office for the Western Pacific. Measles cases surge in the Western Pacific Region. 2024 [cited 2026 Jun 20]. https://www.who.int/westernpacific/health-topics/measles
9. Hagan J, Dashpagma O, Vichit O, Chham S, Demberelsuren S, Grabovac V, et al. Challenges for sustaining measles elimination: post-verification large-scale import-related measles outbreaks in Mongolia and Cambodia, resulting in the loss of measles elimination status. Vaccines (Basel). 2024;12:821. https://doi.org/10.3390/vaccines12070821
10. World Health Organization Regional Office for the Western Pacific. Brunei Darussalam, Cambodia, Japan verified as achieving measles elimination. 2015 Mar 27 [cited 2026 Jun 20]. https://www.who.int/westernpacific/news/item/27-03-2015-brunei-darussalam-cambodia-japan-verified-as-achieving-measles-elimination
11. World Health Organization. Framework for verifying elimination of measles and rubella. Wkly Epidemiol Rec. 2013;88:89–99.
12. Japan Institute for Health Security. Measles in Japan, as of February 2020. Infect Agents Surveill Rep. 2020;41:53–55.
13. Japan Institute for Health Security, National Institute of Infectious Diseases. Measles, epidemiological weeks 1–20, 2026. 2026 May 20 [cited 2026 Aug 15]. https://id-info.jihs.go.jp/en/surveillance/idwr/featured/2026/20/index.html
14. Amemiya Y, Kobayashi T, Nishiura H. Post-pandemic outbreak of measles seen in Japan, 2024. J Infect Public Health. 2025;18:102887. https://doi.org/10.1016/j.jiph.2025.102887
15. National Institute of Infectious Diseases. Risk assessment for measles—Japan, March 2024. 2024 Feb 22 [cited 2026 Jun 20]. https://h-crisis.niph.go.jp/wp-content/uploads/2025/03/measles_ra_2024_1_eng.pdf
16. Japan Institute for Health Security. Epidemiology of measles in Japan, 2025 (epidemiological weeks 1–19) [in Japanese]. Infect Agents Surveill Rep. 2025;46:134–5.
17. Penedos AR, Myers R, Hadef B, Aladin F, Brown KE. Assessment of the utility of whole genome sequencing of measles virus in the characterisation of outbreaks. PLoS One. 2015;10:e0143081. https://doi.org/10.1371/journal.pone.0143081
18. Japan Institute for Health Security, National Institute of Infectious Diseases. Cumulative measles cases by week, 2013–2019 (week 1–20). 2019 May 22 [cited 2026 Sep 15]. https://id-info.jihs.go.jp/surveillance/idwr/diseases/measles/graph/2019/meas19-20.pdf
19. Japan Institute for Health Security, National Institute of Infectious Diseases. Cumulative measles cases by week, 2019–2026 (week 1–20) (based on diagnosis week as of May 20, 2026). 2026 [cited 2026 Aug 15]. https://id-info.jihs.go.jp/surveillance/idwr/diseases/measles/graph/2026/meas26-20.pdf
20. Nakayama T. Vaccine chronicle in Japan. J Infect Chemother. 2013;19:787–98. https://doi.org/10.1007/s10156-013-0641-6
21. Nakatani H, Sano T, Iuchi T. Development of vaccination policy in Japan: current issues and policy directions. Jpn J Infect Dis. 2002;55:101–11. https://doi.org/10.7883/yoken.JJID.2002.101
22. Saitoh A, Okabe N. Current issues with the immunization program in Japan: can we fill the "vaccine gap"? Vaccine. 2012;30:4752–6. https://doi.org/10.1016/j.vaccine.2012.04.026

23. National Institute of Infectious Diseases. Measles in Japan as at July 2021. Infect Agents Surveill Rep. 2021;42:177–9.
24. Sunagawa T, Kobayashi Y, Takashima Y, Kamiya H, Shimada T, Nakashima K, et al. Using regular high-quality serosurveys to identify and close national immunity gaps—measles and rubella elimination in Japan. Vaccines (Basel). 2024;12:939. https://doi.org/10.3390/vaccines12080939
25. Bolotin S, Osman S, Hughes SL, Ariyarajah A, Tricco AC, Khan S, et al. In elimination settings, measles antibodies wane after vaccination but not after infection: a systematic review and meta-analysis. J Infect Dis. 2022;226:1127–39. https://doi.org/10.1093/infdis/jiac039
26. Ministry of Health, Labour and Welfare. Number of people receiving routine vaccinations. 2025 [cited 2026 Jun 20]. https://www.mhlw.go.jp/topics/bcg/other/5.html
27. Leung J, Munir NA, Mathis AD, Filardo TD, Rota PA, Sugerman DE, et al. The effects of vaccination status and age on clinical characteristics and severity of measles cases in the United States in the postelimination era, 2001–2022. Clin Infect Dis. 2025;80:663–72. https://doi.org/10.1093/cid/ciae470
28. Bucris E, Zuckerman NS, Levin T, Kanaaneh Y, Erster O, Indenbaum V, et al.; National Measles Working Group. Genomic and epidemiologic insights into ongoing measles outbreak, Israel, 2025–2026. Emerg Infect Dis. 2026;32:1678–82. https://doi.org/10.3201/eid3209.260625
29. Kobayashi A, Shimada T, Tanaka-Taya K, Kanai M, Okuno H, Kinoshita M, et al. Epidemiology of a workplace measles outbreak dominated by modified measles cases at Kansai international airport, Japan, during August–September 2016. Vaccine. 2020;38:4996–5001. https://doi.org/10.1016/j.vaccine.2020.05.067
30. Tranter I, Smoll N, Lau CL, Williams DL, Neucom D, Barnekow D, et al. Onward virus transmission after measles secondary vaccination failure. Emerg Infect Dis. 2024;30:1747–54. https://doi.org/10.3201/eid3009.240150
31. Kondamudi NP, Tobin EH, Waymack JR. Measles. In: StatPearls. Treasure Island (FL): StatPearls Publishing; 2026.
32. Mina MJ, Metcalf CJE, de Swart RL, Osterhaus ADME, Grenfell BT. Long-term measles-induced immunomodulation increases overall childhood infectious disease mortality. Science. 2015;348:694–9. https://doi.org/10.1126/science.aaa3662
33. Ehresmann KR, Hedberg CW, Grimm MB, Norton CA, MacDonald KL, Osterholm MT. An outbreak of measles at an international sporting event with airborne transmission in a domed stadium. J Infect Dis. 1995;171:679–83. https://doi.org/10.1093/infdis/171.3.679
34. Chen TH, Kutty P, Lowe LE, Hunt EA, Blostein J, Espinoza R, et al. Measles outbreak associated with an international youth sporting event in the United States, 2007. Pediatr Infect Dis J. 2010;29:794–800. https://doi.org/10.1097/INF.0b013e3181dbaacf
35. Mirofsky M, Nachón MN, Durán MV, Savia A, Zunino S, Rosas A, et al. Measles in the Americas: emerging risk ahead of the 2026 World Cup. Medicina (B Aires). 2026;86:562–3.
36. McGuinness SL, Lau CL, Leder K. Measles without borders: how can travel medicine help limit global resurgence? J Travel Med. 2025;32:taaf056. https://doi.org/10.1093/jtm/taaf056

Address for correspondence: Koichiro Yuji, Project Division of International Healthcare Innovation Research, The Institute of Medical Science, The University of Tokyo, 4-6-1 Shirokanedai, Minato-ku, Tokyo 108-8639, Japan; email: yuji-tky@umin.ac.jp

EID Podcast

Emerging Infectious Diseases Cover Art

Byron Breedlove, managing editor emeritus of the journal, elaborates on aesthetic considerations and historical factors, as well as the complexities of obtaining artwork for Emerging Infectious Diseases.

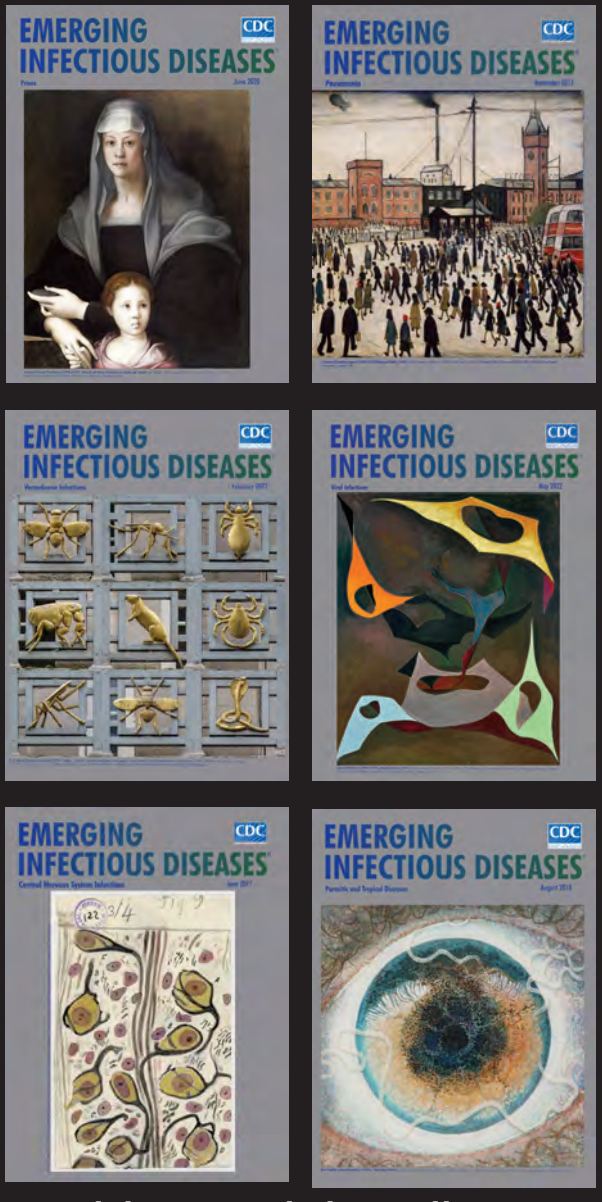

Visit our website to listen:

https://www2c.cdc.gov/podcasts/player.asp?f=8646224

EMERGING INFECTIOUS DISEASES

Subacute Sclerosing Panencephalitis after Measles Outbreaks, the Philippines, 2007–2022

Maela P. Palisoc, Maridel S. Ramones, Roland Dominic G. Jamora

Subacute sclerosing panencephalitis (SSPE) is a delayed, almost uniformly fatal complication of measles. The Philippines had measles outbreaks in 2010–2011, 2013, and 2018–2019; the last was the largest in the World Health Organization Western Pacific Region. Published SSPE data from the Philippines end in 2015. We reviewed all 20 children admitted with SSPE to a tertiary pediatric hospital in Quezon City during 2007–2022 and estimated year of measles infection. Median patient age was 6.2 years at hospital admission and 0.7 years at reported measles illness. Five (25.0%) of 20 admissions occurred in 2022, and estimated infection dates placed 4 patients within the 2018–2019 outbreak; all were admitted during 2020–2022. Given the multiyear latency of SSPE, additional cases might emerge over coming years. Reported measles history could not be established in one quarter of patients. Strengthened measles surveillance and sustained 2-dose vaccination coverage are needed.

Subacute sclerosing panencephalitis (SSPE) is a progressive neurodegenerative disorder caused by persistent central nervous system infection with a defective, hypermutant measles virus. It typically follows measles acquired in early childhood after a latency of years and is almost always fatal (*1*,*2*). Because SSPE follows measles by years rather than weeks, the neurologic consequences of an outbreak do not become visible until long after the outbreak has ended.

Measles vaccination was introduced in the Philippines in 1983; the first routine dose is scheduled at 9 months of age (*3*). Nationwide immunization campaigns in 1998 and 2004 were followed by historically low measles incidence in 2006 (*3*). First-dose measles-containing vaccine coverage later declined from 92% in 2004–2007 to 80% in 2015–2016 and 64% in 2021 (*4*). Reported measles cases rose sharply during a 2018–2019 outbreak, from 2,428 in 2017 to 48,525 in 2019, the largest outbreak in the World Health Organization Western Pacific Region during that period (*5*).

Published data on SSPE in the Philippines are limited; the largest local series described children seen at a single tertiary hospital during 2005–2015 (*6*). No published series from the Philippines spans the period during which children infected in the 2018–2019 outbreak would be expected to demonstrate symptoms of SSPE. We describe children admitted with SSPE to a tertiary government pediatric hospital over 16 years and examine the distribution of their estimated years of measles infection against the national outbreak record.

Methods

Design and Setting

We retrospectively reviewed the records of all children admitted to National Children's Hospital, a tertiary government pediatric hospital in Quezon City, the Philippines, with a final diagnosis of SSPE during January 1, 2007–December 31, 2022. All such patients were enumerated. The 2007 start date reflects the period from which complete institutional records and corresponding registry data were available.

Case Definition

We modified the case definition from Dyken's criteria (*1*). We defined a case as a clinical diagnosis of SSPE by the attending pediatric neurologist on the basis of progressive neurologic deterioration

Author affiliations: National Children's Hospital, Quezon City, the Philippines (M.P. Palisoc, M.S. Ramones); College of Medicine, San Beda University, Manila, the Philippines (M.P. Palisoc); College of Medicine and Philippine General Hospital, University of the Philippines Manila, Manila (R.D.G. Jamora)

DOI: https://doi.org/10.3201/eid3211.261395

with qualitatively positive measles antibody in cerebrospinal fluid (CSF), serum, or both. We excluded children with bacterial, tuberculous, or viral meningitis and children with intracranial masses. Because quantitative measles antibody titers, CSF globulin fractionation, brain biopsy, and uniform electroencephalography were unavailable, we could not apply the full Dyken criteria; we classified cases as clinically diagnosed SSPE with varying levels of supportive evidence.

Variables

Age at reported measles infection and reported measles history came from parental or guardian recall recorded at admission; measles history was recorded as reported, absent, or unknown. Vaccination status was likewise based on parent or guardian report recorded at admission and was not consistently verified against immunization records.

Estimation of Year of Reported Measles Infection

For each patient, we calculated the interval between measles infection and development of SSPE as age at hospital admission minus age at measles infection. We obtained the estimated calendar year of measles infection by subtracting that interval from the year of admission. We then compared estimated infection years with the recorded periods of national measles outbreak activity.

For the 14 children with a parent- or guardian-reported history of measles, we calculated the interval between reported measles illness and hospital admission. We excluded 3 children with a reported measles-to-admission interval of <1 year from the interval analysis, because such a short interval is atypical for SSPE and the timing of the reported measles illness could not be independently verified. A very short interval can also reflect acute measles encephalitis (within 14 days of rash onset) or acute disseminated encephalomyelitis (within weeks), rather than SSPE, which follows a latency of years (*1*).

Statistical Analysis

We summarized categorical variables as frequencies and percentages and summarized continuous variables as medians with interquartile ranges. We did not group patients by admission year for comparison, because the multiyear interval between infection and admission makes such grouping uninterpretable. Analyses used Stata 16.1 (StataCorp LLC, https://www.stata.com) and Microsoft Excel (https://www.microsoft.com). The protocol was approved by the National Children's Hospital Institutional Review Board (approval no. NCH-IRB 2023–12-NCT) using unlinked, deidentified data.

Results

Twenty children admitted during January 1, 2007–December 31, 2022, met the case definition. Cases were unevenly distributed across the study period (Figure 1, panel A). Eight (40.0%) of the 20 admissions occurred in the final 3 years of the series, and 5 (25.0%) admissions occurred in 2022 alone.

Four patients had an estimated measles infection year of 2018 or 2019, corresponding to the national outbreak period (Figure 1, panel B); all 4 had a reported

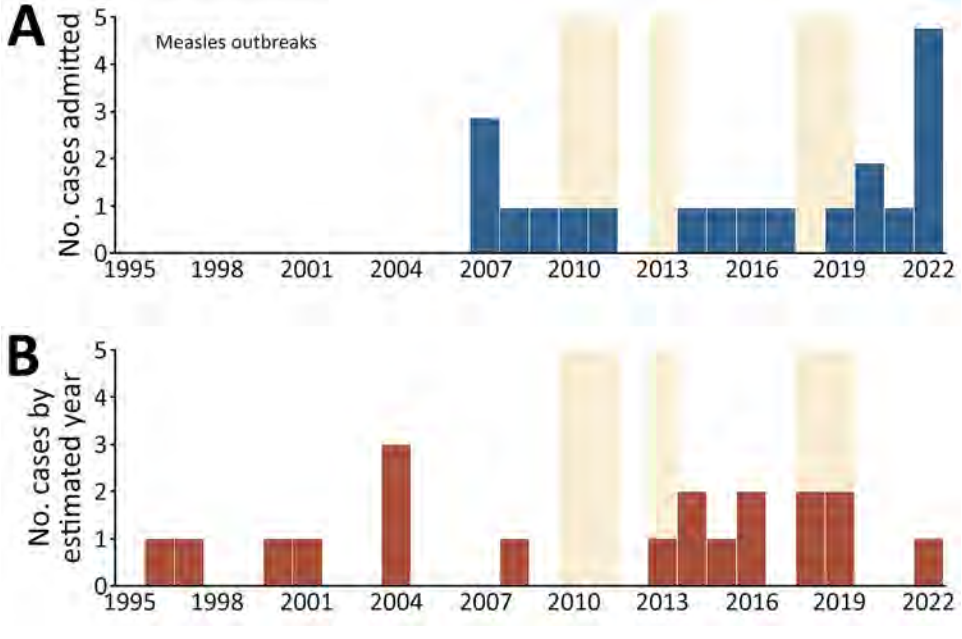

Figure. Hospital admissions for subacute sclerosing panencephalitis (SSPE) in study of SSPE after measles outbreaks, Philippines, 2007–2022. A) SSPE admissions by year (blue); B) the same cases by estimated year of measles infection (maroon). Ivory bands mark periods of reported nationwide measles outbreaks (2010–2011, 2013, 2018–2019). For 1 patient, no recorded age at measles infection was available; that patient is not represented in panel B.

Table. Demographic and clinical characteristics of 20 children with subacute sclerosing panencephalitis in study of subacute sclerosing panencephalitis after measles outbreaks, National Children's Hospital, the Philippines, 2007–2022*

Characteristic	No. patients, N = 20
Sex	
M	14 (70.0)
F	6 (30.0)
Median age at admission, y (IQR)	6.2 (3.8–8.4)
Median age at reported measles illness, y, n = 19 (IQR)	0.7 (0.4–2.0)
Median duration of symptoms before admission, d (IQR)	82 (30–128)
Median length of stay, d (IQR)	10 (6–14)
Nutritional status	
No stunting, no wasting	12 (60.0)
Wasted, not stunted	5 (25.0)
Concurrent stunting and wasting	2 (10.0)
Stunted, not wasted	1 (5.0)
No comorbidity	17 (85.0)
Tuberculosis	2 (10.0)
Bilateral cryptorchidism	1 (5.0)
Reported measles history	
Present	15 (75.0)
Unknown	4 (20.0)
Absent	1 (5.0)
Vaccination	
Measles vaccine only	11 (55.0)
Measles and MMR	6 (30.0)
None	3 (15.0)
Stage at admission†	
Stage 1	3 (15.0)
Stage 2	12 (60.0)
Stage 3	5 (25.0)
Stage 4	0

*Values are no. (%) except as indicated. IQR, interquartile range; MMR, measles, mumps, and rubella.
†Clinical stage follows the conventional description of SSPE: stage 1, behavioral and cognitive decline; stage 2, myoclonus and seizures; stage 3, extrapyramidal signs and progressive unresponsiveness; stage 4, coma or vegetative state (*1*,*2*).

measles history and positive CSF antibody, and all were admitted during 2020–2022 with intervals of 2.1–3.5 years since measles infection. For 3 patients, the estimated infection year was 2004; estimated infection year for 1 patient was 2013. Most patients with an estimable year (14 of 19) were infected outside recognized outbreak periods, consistent with continued transmission between outbreaks.

SSPE was suspected at time of admission in 9 (45.0%) patients. The remainder were admitted under other working diagnoses: probable intracranial mass in 4 (20.0%) patients, meningitis in 3 (15.0%) patients, encephalitis in 2 (10.0%) patients, and 1 (5.0%) each of acute rheumatic fever and traumatic brain injury. At discharge, 18 (90.0%) patients carried a diagnosis of SSPE and 2 (10.0%) patients probable SSPE.

Of the 20 patients, 14 (70.0%) patients were male and 6 (30.0%) were female. The median age was 6.2 years at admission and 0.7 years at reported measles illness; 10 of the 19 patients with an estimable age were infected before the age of 9 months. Eight children had stunting or wasting, and 3 had comorbidities. A reported measles history was present in 15 (75.0%), unknown in 4 (20.0%), and absent in 1 (5.0%). Seventeen (85.0%) patients had received ≥1 measles-containing vaccine; 11 (55.0%) patients had received a single dose only. Twelve (60.0%) patients were admitted in stage 2 and 5 (25.0%) were admitted in stage 3 (Table; Appendix Table, https://wwwnc.cdc.gov/EID/article/32/11/26-1395-App1.pdf). Among the 14 children with a reported measles history, the median interval from measles to hospital admission was 5.8 (interquartile range 3.5–8.9) years.

Among the 20 children, 5 had progressive neurologic deterioration, tested positive for measles antibody in CSF, and had characteristic electroencephalography; 12 had progressive deterioration and antibody-positive CSF without electroencephalography; and 3 had progressive deterioration with antibody-positive serum only. Measles antibody testing of CSF was performed in 17 patients and was positive in all 17; serum antibody was tested in 13 and positive in all 13. Both were tested in 10 patients; 3 patients had serum testing alone. Electroencephalography was performed in 5 patients (25.0%); all showed patterns consistent with SSPE (*7*).

Discussion

In this 16-year series, cases of SSPE clustered in recent years: 40% of admissions occurred in the last 3 years of the study period (2020–2022) and one quarter occurred in 2022 alone; 4 children had an estimated measles

infection during the 2018–2019 outbreak. Because SSPE follows measles after a latency of years, those observations most likely represent the leading edge of a postoutbreak wave; additional cases might emerge over the coming years. For public health, the priority is heightened measles surveillance, early recognition of SSPE in children infected during recent outbreaks, and restoration of high 2-dose vaccination coverage.

The short intervals between measles infection and SSPE (2.1–3.5 years) seen in the 4 outbreak-associated cases do not indicate shortening latency: a child infected in 2018 cannot show an interval beyond 4 years in a series closing in 2022, so recent cases are truncated by the observation window. First-dose coverage fell to 64% by 2021, enlarging the susceptible pool beyond the 2018–2019 cohort. A comparable postoutbreak resurgence of SSPE has been reported from the United Kingdom (*8*).

A reported measles history was absent or unknown in a quarter of children; in those children, diagnosis rested on progressive neurodegeneration and presence of measles antibody in CSF or serum. Absence of a reported measles history is often used to argue against SSPE, yet such reasoning would have delayed or missed diagnosis in 5 of those 20 children. Measles antibody testing of CSF is therefore warranted in any child with progressive neurodegeneration and myoclonus, regardless of reported history.

Although 85% of children had received a measles-containing vaccine, that does not implicate vaccination: SSPE follows wild-type measles, not the vaccine (*1*,*2*). Ten of 19 patients were infected before 9 months, the age of the first scheduled measles-containing vaccine dose in the Philippines (*3*) and an age group at particularly high risk for SSPE (*1*,*2*), and most had received only 1 dose. Those findings support earlier and more complete 2-dose coverage and supplementary immunization during outbreaks.

The profile (male predominance, diagnostic delay of weeks to months) was broadly comparable with an earlier Philippines series (*6*); undernutrition and social disadvantage, noted locally (*9*), might limit timely vaccination and thereby raise measles and SSPE risk. SSPE cases in the Philippines currently cannot be staged against international criteria because quantitative antibody titers, CSF globulin fractionation, and consistent electroencephalography and neuroimaging are unavailable, a diagnostic-capacity gap worth closing in a country with recurrent measles outbreaks.

The first limitation of this study is that, as a single-center retrospective review of 20 patients, it might not represent SSPE nationally, and no population denominator was available, so counts cannot be expressed as rates. Second, measles history, age at infection, and vaccination status were based on guardian recall and could not be verified; the infection-to-SSPE interval is therefore estimated and could not be determined in one quarter of children. Measles antibody was reported only qualitatively, and 3 children were diagnosed using serum antibody without CSF confirmation, although the temporal findings were unchanged when restricted to the 17 with CSF confirmation. Finally, molecular confirmation and genotyping, which require tissue, were not performed, and outcome after discharge was not available.

In conclusion, measles antibody testing of CSF should be considered in any child with progressive neurodegeneration and myoclonus, irrespective of the reported measles history. Additional SSPE cases temporally associated with the 2018–2019 outbreak might continue to occur over the remainder of the 2020s. National surveillance for SSPE should be strengthened accordingly. Laboratory capacity should be developed for quantitative measles antibody titration in serum and CSF and for CSF globulin fractionation, so that Philippine cases can be characterized against international diagnostic criteria. Prospective studies capturing outcome and survival in children from the Philippines with SSPE are needed, as is evaluation of supportive and disease-modifying treatment in this population, building on the limited local experience with intravenous immunoglobulin (*10*). Efforts to restore and sustain 2-dose measles vaccination coverage, including supplementary immunization activities during outbreaks, remain the only means of preventing disease. Where postmortem or biopsy tissue is available, molecular confirmation of measles RNA and genotyping to link cases to circulating strains would strengthen future SSPE surveillance.

Acknowledgments

We thank Tereynz Paul D. Mendoza for statistical analysis.

M.P.P. conceived the study, designed and performed the analysis, and drafted the manuscript. M.S.R. acquired the data and verified the references and source data. R.D.G.J. reviewed the manuscript critically for important intellectual content. All authors approved the final version and agree to be accountable for all aspects of the work.

The authors used Claude (Anthropic, https://www.anthropic.com) in preparing this manuscript. The tool assisted with verification of statistical calculations from data extracted by the authors, generation of the figure,

and drafting and revision of the manuscript text. All source data were collected by the authors. All analyses were checked against the source data, all references were verified by the authors against the statements they support, and all content was reviewed and approved by the authors, who take full responsibility for the accuracy and integrity of the work.

About the Author

Dr. Palisoc is a pediatric neurologist in the Section of Pediatric Neurology, National Children's Hospital, Quezon City, and Associate Professor II at the Neuroscience Department, College of Medicine, San Beda University, Manila. Her research interests include pediatric epilepsy, neuroinfectious disease, and medical education.

References

1. Garg RK, Mahadevan A, Malhotra HS, Rizvi I, Kumar N, Uniyal R. Subacute sclerosing panencephalitis. Rev Med Virol. 2019;29:e2058. https://doi.org/10.1002/rmv.2058
2. Jafri SK, Kumar R, Ibrahim SH. Subacute sclerosing panencephalitis—current perspectives. Pediatric Health Med Ther. 2018;9:67–71. https://doi.org/10.2147/PHMT.S126293
3. Takashima Y, Schluter WW, Mariano KM, Diorditsa S, de Quiroz Castro M, Ou AC, et al.; Centers for Disease Control and Prevention (CDC). Progress toward measles elimination—Philippines, 1998–2014. MMWR Morb Mortal Wkly Rep. 2015;64:357–62.
4. World Health Organization. UNICEF. WHO/UNICEF estimates of national immunization coverage: Philippines, 2025 revision [cited 2026 Jul 23]. https://worldhealthorg.shinyapps.io/wuenic-trends
5. Domai FM, Agrupis KA, Han SM, Sayo AR, Ramirez JS, Nepomuceno R, et al. Measles outbreak in the Philippines: epidemiological and clinical characteristics of hospitalized children, 2016–2019. Lancet Reg Health West Pac. 2022;19:100334. https://doi.org/10.1016/j.lanwpc.2021.100334
6. Rabanes AC, Cruz-Urbi CM. Demographic, clinical, imaging, and EEG characteristics of subacute sclerosing panencephalitis. Eur J Paediatr Neurol. 2017;21:2–45. https://doi.org/10.1016/j.ejpn.2017.04.944
7. Ali S, Kumar H, Ullah S, Haq MAU, Gul NG, Kumar J. Electroencephalography patterns of subacute sclerosing panencephalitis. Cureus. 2021;13:e15728.
8. Lam T, Ranjan R, Newark K, Surana S, Bhangu N, Lazenbury A, et al. A recent surge of fulminant and early onset subacute sclerosing panencephalitis (SSPE) in the United Kingdom: an emergence in a time of measles. Eur J Paediatr Neurol. 2021;34:43–9. https://doi.org/10.1016/j.ejpn.2021.07.006
9. Pipo-Deveza JR, Kusuhara K, Silao CLT, Lukban MB, Salonga AM, Sanchez BC, et al. Analysis of MxA, IL-4, and IRF-1 genes in Filipino patients with subacute sclerosing panencephalitis. Neuropediatrics. 2006;37:222–8. https://doi.org/10.1055/s-2006-924724
10. Lukban MB, Chua-Macrohon BC, Salonga AM. The use of intravenous immunoglobulin in subacute sclerosing panencephalitis: a retrospective cohort study. Acta Med Philipp. 2013;47:46–50. https://doi.org/10.47895/amp.v47i1.2020

Address for correspondence: Maela P. Palisoc, Neuroscience Department, College of Medicine, San Beda University, 638 Mendiola St, San Miguel, Manila 1005, Philippines; email: mppalisoc@sanbeda.edu.ph

Predictors and Patterns of Metastatic *Candidozyma auris* Infection, Spain, 2016–2024

Pedro Suarez-Urquiza,[1] Alba Ruiz-Gaitán,[1] Eva Calabuig, María Tasias, Víctor García Bustos, Ignacio Moreno, María Ángeles Ferre, Ana María Moret, Juan Frasquet, Patricio Favier, Javier Pemán, Maria Jesus Castaño-Aroca, Paula Muñoz Brell, Mónica Gordon, Maria Dolores Gomez-Ruiz, Miguel Salavert-Lleti

Metastatic infection after *Candidozyma auris* candidemia remains poorly characterized. We retrospectively studied patients with *C. auris* candidemia at a tertiary hospital in Spain during 2016–2024. Of 108 patients, 24 (22.2%) experienced metastatic infections; endocarditis was most frequent (7.4%), followed by osteoarticular infection, meningitis, and hepatosplenic infection (3.7% each). In multivariable Fine–Gray regression, a cardiac device or prosthetic valve was independently associated with metastatic infection (subdistribution hazard ratio [HR] 2.89 [95% CI 1.21–6.91]), although that association was attenuated in a sensitivity analysis restricted to echocardiographed patients. Persistent candidemia showed a higher, nonsignificant risk for metastatic infection in the day-5 landmark analysis (subdistribution HR 2.67 [95% CI 0.86–8.32]). Metastatic infection was associated with increased deaths in time-dependent analyses at 60 days (adjusted HR 2.21 [95% CI 1.04–4.67]) and 90 days (adjusted HR 2.26 [95% CI 1.09–4.67]). Our findings support echocardiography in patients with intracardiac devices.

Invasive candidiasis, in particular candidemia, is a significant infectious threat, especially among patients in intensive care units (ICUs). It represents between 15%–30% of infections in these units and, despite improvements in diagnosis and treatment, the mortality rate associated remain high, 30%–60% in most series (*1*,*2*). In that context, metastatic complication, in which infection spreads through the bloodstream to other organs, plays a key role. The most common manifestations include endophthalmitis, osteomyelitis, hepatosplenic abscesses, meningitis, and endocarditis (*3*). Depending on underlying clinical conditions and the screening protocols used, 4%–50% of candidemia cases develop metastatic involvement (*4*–*7*), which is frequently associated with increased risk for death and prolonged hospitalization (*8*).

Candidozyma auris (formerly *Candida auris*) (*9*) is an emerging, often multidrug-resistant yeast often associated with nosocomial outbreaks worldwide (*10*,*11*). It can colonize patients and healthcare environments. Since its identification in Japan in 2009 (*12*), *C. auris* has been reported on all continents except Antarctica and is often associated with high mortality rates. Most research to date has focused on its antifungal resistance patterns, outbreak dynamics, and infection control measures (*11*). However, its ability to cause metastatic complications, such as ocular involvement, endocarditis, osteomyelitis, or hepatosplenic candidiasis, is poorly characterized. Available evidence is largely confined to isolated case reports and small series, in which endocarditis in recipients of left ventricular assist devices and central nervous system infection associated with neurosurgical devices predominate (*13*–*23*). A few cohort studies have reported secondary organ involvement in 7.7%–27% of patients with *C. auris* candidemia, but they rarely

Author affiliations: Hospital Universitari i Politècnic La Fe, Valencia, Spain (P. Suarez-Urquiza, A. Ruiz-Gaitán, E. Calabuig, M. Tasias, V. García Bustos, I. Moreno, M.Á. Ferre, A.M. Moret, J. Frasquet, P. Favier, J. Pemán, M.J. Castaño-Aroca, P. Muñoz Brell, M. Gordon, M.D. Gomez-Ruiz, M. Salavert-Lletí); Instituto de Investigación Sanitaria La Fe, Valencia (P. Suarez-Urquiza, A. Ruiz-Gaitán, E. Calabuig, M. Tasias, V. García Bustos, J. Frasquet, P. Favier, J. Pemán, P. Muñoz Brell, M. Gordon, M.D. Gomez-Ruiz, M. Salavert-Lletí); Universitat de València, Valencia (E. Calabuig)

DOI: https://doi.org/10.3201/eid3211.260984

[1]These authors contributed equally to this work and are co–first authors.

specify the spectrum of complications, their predictors, or their outcomes (*18*–*20*,*22*). Further investigation is essential to clarify its clinical spectrum and the burden of secondary organ-specific infections. In this study, we aimed to characterize clinical and microbiological features of patients with metastatic *C. auris* infection after candidemia and to identify factors associated with metastatic involvement.

Methods

Study Design and Setting

We conducted this retrospective observational study at the Hospital Universitari i Politècnic La Fe, a 900-bed tertiary institution in Valencia, Spain, during May 2016–December 2024. *C. auris* was first detected in the institution in May 2016 during a hospital outbreak, and it has remained endemic since then, affecting both ICU and non-ICU patients (*24*).

Patient Selection and Definitions

We identified all episodes of *Candidozyma auris* candidemia occurring in adult patients (≥18 years of age) during the study period through the laboratory information system. We then manually reviewed the electronic medical records of the corresponding patients to collect demographic, clinical, microbiological, treatment, and outcome data.

We classified patients according to the presence or absence of metastatic infection, defined as compatible clinical manifestations together with either microbiological confirmation from a normally sterile site, radiologic findings consistent with metastatic infection, or histopathologic evidence. In addition, the presumed source of candidemia had to be unknown or anatomically distinct from the metastatic site. We defined persistent candidemia as the recovery of *C. auris* from ≥1 blood culture obtained on or after day 5 after the index positive blood culture. We considered the date of the index blood culture day 0.

Microbiology

We identified *C. auris* isolates using classical microbiological phenotypic methods combined with matrix-assisted laser desorption/ionization-time of flight (MALDI-TOF) mass spectrometry (Bruker, https://www.bruker.com). We conducted antifungal susceptibility testing using the commercial microdilution method Sensititre YeastOne (Thermo Fisher Scientific, https://www.thermofisher.com) and interpreted results in accordance with the tentative breakpoints for *C. auris* established by the US Centers for Disease Control and Prevention (*25*), because the Clinical and Laboratory Standards Institute has not defined species-specific clinical breakpoints.

Statistical Analysis

We compared patients with metastatic *C. auris* infection after candidemia to those with confirmed candidemia without evidence of dissemination, to assess clinical outcomes and potential associated factors. We analyzed categorical variables using χ^2 test or Fisher exact test and continuous variables using unpaired *t*-test or Mann-Whitney-Wilcoxon test, as appropriate.

For the competing-risk analysis, follow-up began on the date of the index positive blood culture. The event of interest was the diagnosis of metastatic infection; we considered death before the diagnosis of metastatic infection a competing event. We followed patients who remained alive without documented metastatic infection through their last documented hospital contact. We estimated cumulative incidence functions accounting for death as a competing event. We developed a multivariable Fine–Gray regression model; we included variables with $p<0.1$ in bivariable analysis, together with variables considered clinically relevant, to estimate subdistribution hazard ratios (HRs) and 95% CI. To assess potential diagnostic bias related to echocardiography, we performed a sensitivity analysis restricted to patients who underwent echocardiographic evaluation. To address immortal time bias in the assessment of candidemia persistence, we performed a landmark analysis restricted to patients who survived beyond day 5 after the index blood culture. To further evaluate the association between metastatic infection and mortality, we performed a cause-specific Cox regression analysis for 30-day, 60-day, and 90-day all-cause mortality recorded for all patients from electronic and regional health records irrespective of hospital discharge, treating metastatic infection as a time-dependent exposure. Patients contributed person-time to the non–metastatic infection group until diagnosis and to the metastatic infection group thereafter. We included age and Charlson Comorbidity Index score in an adjusted model. We performed statistical analysis using R version 4.5.0 (The R Project for Statistical Computing, https://www.r-project.org); we considered $p<0.05$ statistically significant.

Results

We included a total of 108 patients with *C. auris* candidemia. Among them, 24 (22.2%) experienced metastatic infection. Forty-four (40.7%) patients died without metastatic complications; we treated their deaths as competing events. Forty (37.0%) patients remained

alive without documented metastatic infection; follow-up for those patients ended at their last available hospital discharge date. The median age was 60.6 (interquartile range [IQR] 48.9–72.0) years, and 78 (72.2%) were admitted to the ICU.

No patient experienced >1 metastatic complication. The most frequent metastatic complication was endocarditis, observed in 8 (7.4%) patients, followed by osteoarticular infection (4 [3.7%]), meningitis (4 [3.7%]), and hepatosplenic infection (4 [3.7%]). Chorioretinitis was documented in 1 (0.9%) patient. Three (2.8%) additional patients experienced other late-onset complications such as aneurysm sac infection and subcutaneous abscess. Among the 24 patients with metastatic infections, the diagnosis was supported by imaging findings in 18 (75.0%) patients, microbiological confirmation from the metastatic site in 19 (79.2%) patients, and histopathologic evidence in 4 (16.7%) patients; those diagnostic modalities were not mutually exclusive. Most (84 [77.8%]) patients showed no evidence of metastatic involvement beyond the initial bloodstream infection.

Risk Factors for Complications

In bivariable analysis, patients who had metastatic infections were older (median age 68.9 [IQR 54.4–75.5] vs. 59.7 [IQR 43.9–70.7] years; p = 0.065) and had a longer duration of candidemia (median 6 [IQR 1–38] vs. 1 [IQR 1–5] days; p = 0.034) than those without metastatic complications. A cardiac device or prosthetic valve was significantly more frequent in patients with metastatic infection than in those without (54.2% vs. 26.2%; p = 0.020). Among patients with cardiac devices or prosthetic valves, prosthetic heart valves were the most frequent subtype in both groups, those with metastatic infection and those without (6/13 [46.2%] vs. 12/22 [54.5%]), followed by permanent pacemakers or implantable cardioverter-defibrillators (5/13 [38.5%] vs. 10/22 [45.5%]). Left ventricular assist devices were present in 2/13 (15.4%) patients with metastatic infections and in none of the patients without. The distribution of device subtypes did not differ significantly between groups (p = 0.266). Echocardiography was performed significantly more frequently in patients with complications (87.5% vs. 63.1%; p = 0.026). The frequency of fundoscopic examination did not differ significantly between patients with and without metastatic infections (83.3% vs. 64.3%; p = 0.087).

We reviewed the initial management of candidemia. We found no significant differences in early central venous catheter removal (58.3% vs. 52.4%; p = 0.777), initiation of antifungal therapy within 48 hours (75.0% vs. 85.7%; p = 0.352), or resolution of the infectious focus within 48 hours (12.5% vs. 19%; p = 0.557). Initial antifungal treatment consisted predominantly of echinocandin monotherapy, administered to 62.5% of patients with and 78.6% of those without metastatic infections. Amphotericin B monotherapy was used in 8.3% of patients with and 1.2% of those without metastatic infections. No patients with metastatic infections received isavuconazole monotherapy; 1.2% of patients without metastatic infections received it. Initial combination antifungal therapy was administered to 29.2% of patients with metastatic infections and 19.0% of those without (p = 0.432). The most frequent combinations were an echinocandin plus isavuconazole (16.7% vs. 8.3%) and an echinocandin plus amphotericin B (12.5% vs. 10.7%). We observed no statistically significant differences in initial antifungal therapy between groups or in patients with concurrent or underlying conditions or baseline risk factors (Table 1).

We performed multivariable Fine–Gray competing risks analysis with death as a competing event; the presence of a cardiac device or prosthetic valve was the only factor independently associated with the development of metastatic complications (subdistribution HR [sHR] 2.89 [95% CI 1.21–6.91]; p = 0.017). Age, previous candidemia, and recent surgery were not independently associated with metastatic infection (Table 2). In a sensitivity analysis restricted to patients who underwent echocardiography, the presence of a cardiac device or prosthetic valve was associated with metastatic infection in the unadjusted Fine–Gray model (sHR 2.32 [95% CI 1.01–5.33]; p = 0.046). After adjustment for age, previous candidemia, and recent surgery, the estimated association remained elevated but was not statistically significant (sHR 2.15 [95% CI 0.90–5.15]; p = 0.085).

In the landmark analysis performed including only patients alive at day 5 (n = 97), persistent candidemia at day 5 was associated with a higher risk for metastatic complications, although that association was not statistically significant (sHR 2.67 [95% CI 0.86–8.32]; p = 0.091). The presence of a cardiac device or prosthetic valve remained an independent predictor (sHR 4.04 [95% CI 1.19–13.7]; p = 0.025) (Table 3).

Patient Outcomes

Crude mortality rate at 30 days after *C. auris* candidemia was 34.3%; at 60 days, 40.7%; and at 90 days, 46.3%. We found no significant differences between patients with and without metastatic complications; 30-day rates were 20.8% vs. 38.1% (p = 0.184); 60-day: 33.3% vs. 42.9% (p = 0.547); 90-day: 41.7% vs. 47.6% (p = 0.777). In cause-specific Cox regression analy-

ses, metastatic infection, treated as a time-dependent exposure, was not significantly associated with 30-day mortality after adjustment for age and Charlson Comorbidity Index (adjusted HR [aHR] 1.75 [95% CI 0.58–5.29]; p = 0.323). However, metastatic infection was independently associated with higher risk for death at 60 days (aHR 2.21 [95% CI 1.04–4.67]; p = 0.038) and 90 days (aHR 2.26 [95% CI 1.09–4.67]; p = 0.028) (Table 4). In addition, patients with metastatic complications required significantly prolonged antifungal therapy (median 43 [IQR [4.0–72.2] days vs. 23 [IQR 15.0–32.2] days; p<0.001) and longer hospital stays, although the difference was not statistically significant (median 47 [IQR 16.0–66.0] days vs. 22.5 [IQR 15.2–29.8] days; p = 0.052). At the time of diagnosis of metastatic complications, 12.5% of patients

Table 1. Baseline characteristics of patients with *Candidozyma auris* candidemia in study of metastatic *C. auris* infection, Spain, 2016–2024*

Variable	Total, n = 108	Metastatic infection absent, n = 84	Metastatic infection present, n = 24	p value
Median age, y (IQR)	60.6 (48.9-72.0)	59.7 (43.9–70.7)	68.9 (54.4–75.5)	0.065
Charlson Comorbidity Index, median (IQR)	5 (3–7.2)	5 (2.8–7.2)	5.5 (3–7.2)	0.465
Sex				0.757
M	76 (70.4)	58 (69)	18 (75)	
F	32 (29.6)	26 (31)	6 (25)	
Surgery in the past 30 d	44 (40.7)	30 (35.7)	14 (58.3)	0.080
Previous therapy				
Broad-spectrum antibiotics	100 (92.6)	80 (95.2)	20 (83.3)	0.071
Previous antifungal treatment	30 (27.8)	25 (29.8)	5 (20.8)	0.547
Corticosteroid therapy	21 (19.4)	14 (16.7)	7 (29.2)	0.284
Other immunosuppressive therapy	18 (16.7)	14 (16.7)	4 (16.7)	Referent
Risk factors				
Persistent candidemia	34 (31.5)	23 (27.4)	11 (45.8)	0.142
Median duration of candidemia, d (IQR)	1 (1–8)	1 (1–5)	6 (1–38)	0.034
Central venous catheter	93 (86.1)	72 (85.7)	21 (87.5)	Referent
Previous multisite colonization	81 (75)	64 (76.2)	17 (70.8)	0.789
Parenteral nutrition	68 (63)	53 (63.1)	15 (62.5)	Referent
Invasive mechanical ventilation	52 (48.1)	37 (44)	15 (62.5)	0.173
Cardiac device/prosthetic valve	35 (32.4)	22 (26.2)	13 (54.2)	0.020
Prosthetic heart valve	18 (51.4)	12 (54.5)	6 (46.2)	
PPM/ICD	15 (42.9)	10 (45.5)	5 (38.5)	
Left ventricular assist device	2 (5.7)	0 (0)	2 (15.4)	
Solid organ transplant	6 (5.6)	3 (3.6)	3 (12.5)	0.122
Severe sepsis	24 (22.2)	19 (22.6)	5 (20.8)	Referent
Osteoarticular prosthesis	15 (13.9)	11 (13.1)	4 (16.7)	0.739
Hemodialysis	15 (13.9)	11 (13.1)	4 (16.7)	0.739
Previous candidemia	10 (9.3)	6 (7.1)	4 (16.7)	0.224
Profound neutropenia, <500 cells/μL	7 (6.5)	4 (4.8)	3 (12.5)	0.182
Concomitant bacteremia	6 (5.6)	6 (7.1)	0 (0)	Referent
Admission department				
Surgical intensive care unit	57 (52.8)	47 (56)	10 (41.7)	0.460
Medical intensive care unit	21 (19.4)	15 (17.9)	6 (25)	
Other	30 (27.8)	22 (26.2)	8 (33.3)	
Management approach to candidemia				
Catheter removed within 48 h	58 (53.7)	44 (52.4)	14 (58.3)	0.777
Non-catheter focus resolution within 48 h	19 (17.6)	16 (19)	3 (12.5)	0.557
Cardiac echocardiography performed	74 (68.5)	53 (63.1)	21 (87.5)	0.026
Fundoscopic examination performed	74 (68.5)	54 (64.3)	20 (83.3)	0.087
Initial antifungal therapy				
Antifungal therapy within 48 h	90 (83.3)	72 (85.7)	18 (75)	0.352
Echinocandin monotherapy	81 (75)	66 (78.6)	15 (62.5)	0.181
Amphotericin B monotherapy	3 (2.8)	1 (1.2)	2 (8.3)	0.123
Isavuconazole monotherapy	1 (0.9)	1 (1.2)	0 (0)	Referent
Initial dual antifungal therapy	23 (21.3)	16 (19)	7 (29.2)	0.432
Echinocandin + isavuconazole	11 (10.2)	7 (8.3)	4 (16.7)	0.258
Echinocandin + amphotericin B	12 (11.1)	9 (10.7)	3 (12.5)	0.727
Outcome				
Median duration of antifungal therapy, d (IQR)	26.5 (15–35.2)	23 (15.0–32.2)	43 (4.0–72.2)	<0.001
Median length of hospital stay after candidemia, d (IQR)	23 (15.5–42.5)	22.5 (15.2–29.8)	47 (16.0–66.0)	0.052
Deaths within 30 d	37 (34.3)	32 (38.1)	5 (20.8)	0.184
Deaths within 60 d	44 (40.7)	36 (42.9)	8 (33.3)	0.547
Deaths within 90 d	50 (46.3)	40 (47.6)	10 (41.7)	0.777

*Values are no. (%) except as indicated. ICD, implantable cardioverter-defibrillators; IQR, interquartile range Q1–Q3; PPM, permanent pacemakers.

Table 2. Multivariable Fine–Gray competing risks regression analysis of factors associated with metastatic infection in patients with *Candidozyma auris* candidemia, Spain, 2016–2024*

Variable	sHR (95% CI)	p value
Previous candidemia	1.61 (0.54–4.79)	0.412
Age, per year	1.02 (0.99–1.05)	0.241
Recent surgery	0.79 (0.33–1.90)	0.603
Cardiac device/prosthetic valve	2.89 (1.21–6.91)	0.017

*sHR, subdistribution hazard ratio.

were receiving combination antifungal therapy including amphotericin B.

Susceptibility Profiles of Cases and Controls

Overall, echinocandins demonstrated MIC values within the susceptible range according to the tentative breakpoints proposed by the US Centers for Disease Control and Prevention. For anidulafungin, MIC_{50} (MIC at which 50% of the isolates are inhibited) was 0.125 mg/L; MIC_{90} (MIC at which 90% of the isolates are inhibited) was 0.25 mg/L. For caspofungin, MIC_{50} was 0.06 mg/L and MIC_{90} was 0.25 mg/L. For micafungin, MIC_{50} was 0.06 mg/L and MIC_{90} 0.125 mg/L. All isolates were susceptible to amphotericin B; MIC_{50} was 0.5 mg/L and MIC_{90} was 1 mg/L. In contrast, all isolates were resistant to fluconazole (MIC $\geq$256 mg/L). Voriconazole MICs were consistently $\geq$2 mg/L across all isolates. We observed no significant differences in MIC values between groups (Table 5).

Discussion

We identified metastatic complications in ≈25% of patients with *C. auris* candidemia; endocarditis was the predominant clinical manifestation. Those findings underscore the propensity of *C. auris* to cause invasive device-associated infections. The presence of intracardiac devices or prosthetic valves was strongly associated with metastatic dissemination in our primary analysis. In the sensitivity analysis restricted to patients who underwent echocardiography, the association remained similar in magnitude but was no longer statistically significant after adjustment. Although prolonged candidemia was associated with dissemination in bivariable analysis, it did not reach independent significance after accounting for competing risks. Crude mortality proportions did not differ significantly between groups, but time-dependent analyses identified an association between metastatic infection and increased mortality at 60 and 90 days. Metastatic infection was also associated with prolonged antifungal treatment; hospital stay was longer among patients with metastatic infection, but the difference was not statistically significant. We observed no clear differences between groups with respect to initial antifungal strategies or antifungal susceptibility profiles, including MIC patterns.

Table 3. Landmark analysis of factors associated with metastatic infection in patients with *Candidozyma auris* candidemia, Spain, 2016–2024*

Variable	sHR (95% CI)	p value
Persistent candidemia at day 5	2.67 (0.86–8.32)	0.091
Age, per year	1.02 (0.98–1.06)	0.413
Previous candidemia	1.37 (0.31–6.13)	0.688
Cardiac device/prosthetic valve	4.04 (1.19–13.7)	0.025
Recent surgery	0.99 (0.32–3.07)	0.943

*Analysis restricted to patients surviving beyond day 5 (n = 97). Death was retained as a competing event. sHR, subdistribution hazard ratio.

Few published studies have described the incidence of metastatic complications after *C. auris* candidemia. In a multicenter study (*20*), metastatic infection was identified in 13 (8.02%) of 162 patients; endocarditis was the most common complication, consistent with our findings. Another study (*19*) reported metastatic infection in 10 (27.02%) of 37 cases, a proportion comparable to that observed in our cohort; however, neither the spectrum of complications nor associated outcomes were specified. Lower rates of metastatic infection were previously described (*18*,*22*); as in our cohort, a substantial proportion of patients in those studies received combination antifungal therapy. Beyond those cohorts, published experience is confined to isolated case reports and small series, dominated by endocarditis in recipients of left ventricular assist devices (*15*,*17*) and by central nervous system infection associated with external ventricular drains or intracranial pressure monitors (*14*,*21*,*23*); osteoarticular involvement is described only occasionally (*13*,*16*). That device-associated pattern mirrors the one observed in our cohort, although it may also reflect publication bias toward severe or device-related manifestations. Interpretation of the available literature is further limited by considerable heterogeneity in study design, diagnostic strategies, and outcome reporting, which hinders reliable comparisons and underscores the value of cohort-based analyses such as our investigation.

The incidence of metastatic infection in our study (22.2%) is situated within the broad range previously reported for metastatic complications in candidemia, estimated at 4%–50% (*4*–*7*,*26*). Our findings are consistent with higher rates described in critically ill and younger patient populations. The CandidICU multicenter study in France identified $\geq$1 secondary focus of infection in 21.8% of screened ICU patients with candidemia (*26*), whereas a separate study in children and young adults reported disseminated disease in 25% of evaluated episodes (*6*). A notable finding of our study is the high incidence of endocarditis (7.4%), which exceeded that

Table 4. Cause-specific hazard of all-cause death associated with metastatic infection in patients with *Candidozyma auris* candidemia, Spain, 2016–2024*

Model and variable	HR (95% CI)	p value
30 d		
Metastatic infection, unadjusted	2.01 (0.70–5.76)	0.196
Metastatic infection, adjusted	1.75 (0.58–5.29)	0.323
Age, per year	1.02 (0.99–1.04)	0.295
Charlson Comorbidity Index, per point	1.02 (0.91–1.14)	0.782
60 d		
Metastatic infection, unadjusted	2.45 (1.15–5.20)	0.020
Metastatic infection, adjusted	2.21 (1.04–4.67)	0.038
Age, per year	1.02 (0.99–1.04)	0.181
Charlson Comorbidity Index, per point	1.06 (0.98–1.14)	0.172
90 d		
Metastatic infection, unadjusted	2.38 (1.15–4.94)	0.020
Metastatic infection, adjusted	2.26 (1.09–4.67)	0.028
Age, per year	1.01 (0.99–1.03)	0.300
Charlson Comorbidity Index, per point	1.06 (0.97–1.14)	0.191

*Adjusted models included age (per year) and the Charlson Comorbidity Index (per point). Patients were followed until death or at the end of the corresponding follow-up horizon. HR, hazard ratio using cause-specific Cox proportional hazards models for all-cause death (n = 108).

reported in other previously published cohorts; that difference could be attributable to the greater prevalence of intracardiac devices and prosthetic valves in our population and the strong association of cardiac devices with metastatic infection in our cohort. Such an association is biologically plausible, given the well-recognized ability of *C. auris* to form biofilms on abiotic surfaces, which enables persistence and infection of intracardiac devices (*27*). Prosthetic heart valves were the most frequent type of cardiac foreign material in both groups, whereas left ventricular assist devices were observed only among patients with metastatic infection. However, the small number of patients within each device subtype precludes reliable subtype-specific inference. Similarly, one study (*7*) reported an overall endocarditis incidence of 0.5%, increasing to 3.6% among patients who underwent echocardiography evaluation; of note, 1 of 4 patients with endocarditis had a prosthetic valve. Another study (*28*) reported overall endocarditis incidence of 2.5% among patients with candidemia and identified preexisting valvular heart disease as an independent risk factor, further supporting the contribution of structural cardiac abnormalities to the development of *Candida* endocarditis. In addition, several case series have described *C. auris* candidemia in patients with left ventricular assist devices, frequently documenting valvular or device-associated vegetations, consistent with the pattern observed in our cohort (*15*,*17*). Those observations are further reinforced by data from our center in transplant populations, where a particularly high risk for *C. auris* infection has been identified among cardiac transplant recipients (*29*).

In our cohort, ocular involvement occurred in 0.9% of patients, a substantially lower proportion than that reported in studies of *Candida* spp. candidemia that identified ocular complications in 10%–16% of systematically screened patients (*7*,*30*,*31*). That finding also differs from one in which panophthalmitis was the most frequently reported complication after *C. auris* candidemia (*18*).

Although candidemia duration was associated with metastatic dissemination in bivariable analysis (p = 0.034), it was not confirmed as an independent predictor in the multivariable Fine–Gray model. A landmark analysis restricted to day-5 survivors, performed to avoid immortal time bias inherent to the definition of persistence, showed a higher but not statistically significant risk for metastatic dissemination with persistent candidemia (sHR 2.67 [95% CI 0.86–8.32]; p = 0.091), consistent with previous reports in

Table 5. Antifungal susceptibility of *Candidozyma auris* isolates from patients with and without metastatic infection, Spain, 2016–2024*

		Metastatic infection absent		Metastatic infection present	
Antifungal drug	p value	MIC_{50}, mg/L	MIC_{90}, mg/L	MIC_{50}, mg/L	MIC_{90}, mg/L
Amphotericin B	0.521	0.5	1	0.5	1
Fluconazole	0.949	256	256	256	256
Itraconazole	0.440	0.25	0.5	0.125	0.5
Voriconazole	0.501	2	4	2	4
Caspofungin	0.416	0.06	0.125	0.06	0.25
Anidulafungin	0.192	0.125	0.25	0.125	0.25
Micafungin	0.853	0.06	0.125	0.06	0.125
Posaconazole	0.528	0.06	0.25	0.125	0.25
Isavuconazole	0.280	0.25	0.5	0.25	2

*MIC_{50}, MIC inhibiting 50% of *C. auris* isolates; MIC_{90}, MIC inhibiting 90% of *C. auris* isolates.

young adults (*6*) and in ICU settings (*26*) but likely underpowered given the sample size.

In crude comparisons, the risk for death did not differ between patients with and without metastatic infection and was lower among those with metastatic infection at day 30. The apparent paradox reflects the fact that patients must survive long enough for dissemination to be diagnosed. When we modeled infection as a time-dependent exposure, the direction of the association reversed; we observed that cause-specific hazard of death was almost twice as high at 60 and 90 days than at day 30. Our findings are therefore consistent with those published previously (*20*) that identified disseminated disease after *C. auris* candidemia as an independent predictor of death. Patients with metastatic disease in our cohort also required significantly longer antifungal therapy (43 vs. 23 days) and longer hospitalization, although the difference was not statistically significant (47 vs. 22.5 days), consistent with previous studies showing that complicated candidemia frequently requires prolonged treatment courses and additional therapeutic interventions (*7*,*26*).

Our study cohort provided detailed clinical and microbiological information on the range of metastatic complications after *C. auris* candidemia in a hospital where the pathogen has remained endemic since its emergence in 2016. The relatively large size of the cohort and the extended period of data collection enabled us to estimate the frequency of metastatic involvement and identify factors associated with its development. In contrast to previous reports, which have largely been limited to case reports or small case series (*13*–*17*,*21*,*23*), our study provided cohort-based estimates of metastatic dissemination.

The retrospective, single-center design might limit the generalizability of our findings, particularly across settings with differing patient populations, diagnostic approaches, or antifungal stewardship strategies. Furthermore, metastatic involvement might have been underestimated; blood cultures have limited sensitivity, and advanced imaging, or invasive diagnostic procedures were not performed systematically. Echocardiography was performed more frequently in patients with metastatic infection, raising the possibility of diagnostic ascertainment bias. Although the association between cardiac devices and metastatic infection remained similar in magnitude in the sensitivity analysis restricted to patients who underwent echocardiography, it was no longer statistically significant after adjustment. Therefore, residual detection bias cannot be excluded. Finally, the relatively small number of patients with metastatic infection limited statistical power and the precision of the effect estimates, particularly in the multivariable and landmark analyses. We recommend caution in interpreting the associations we observed; they should not be considered definitive evidence of causality.

Our findings expand the body of knowledge of *C. auris* candidemia, showing that metastatic complications are not uncommon and most frequently involve the cardiovascular system, especially the heart. The association with intracardiac devices and the trend toward higher risk with persistent candidemia observed in the landmark analysis suggest that dissemination may be driven by both device-related and fungemia-related factors. Those results underscore the need for heightened clinical vigilance and targeted cardiac assessment in at-risk patients.

Although it remains uncertain whether metastatic complications occur more frequently in *C. auris* candidemia than in infections caused by other yeast species, the proportion observed in our cohort was notable. That finding supports the potential value of systematic colonization screening in healthcare settings where *C. auris* has been identified, particularly because previous studies suggest that colonization is associated with an increased risk for subsequent invasive infection (*32*).

Future studies should compare the risk for and spectrum of metastatic complications of *C. auris* candidemia with those observed in other yeast infections. Such comparative analyses are essential to determine whether *C. auris* candidemia itself constitutes an independent risk factor for dissemination, beyond host-related and device-related predictors. Multicenter prospective studies with systematic screening for deep-seated foci will establish the relative contributions of pathogen-specific versus host-related factors in the pathogenesis of *C. auris* dissemination.

As of September 2026, international guidelines recommend fundoscopy after candidemia in selected patients, particularly those experiencing ocular symptoms, persistent fungemia, immunosuppression, or an inability to report visual disturbances. Similarly, echocardiography is advised in patients with suspected endocarditis (e.g., new cardiac murmur or embolic phenomena), persistent candidemia, underlying valvular disease, or the presence of cardiac implantable devices (*33*–*35*), although further research is needed to determine the optimal timing for echocardiographic assessment after candidemia diagnosis. Our findings support this risk-based approach and highlight the importance of echocardiographic evaluation, particularly in patients with prosthetic valves or intracardiac devices; those subgroups exhibited the highest risk for metastatic complications.

Instituto de Salud Carlos III (ISCIII), co-funded by the European Union, provided funding (nos. PI23/00826, JR21/00061, and CM24/00167). P.S.-U. has received honoraria for lectures at educational events sponsored by Diasorin. P.F. has received consulting fees from bioMérieux Argentina.

The authors used ChatGPT (GPT-5.5; OpenAI, https://openai.com) exclusively for English-language editing and grammatical revision of this manuscript. All scientific content, data, analyses, and conclusions are solely the responsibility of the authors.

About the Authors

Dr. Suárez-Urquiza is a clinical microbiologist at Hospital Universitari i Politècnic La Fe, Valencia, Spain. His primary research interests include invasive fungal infections, with a focus on *Candida* bloodstream infections and *Candidozyma auris* at an endemic center. Dr. Ruiz-Gaitán is a physician and specialist in clinical microbiology with an extensive research trajectory in medical mycology at Hospital Universitari i Politècnic La Fe. Her work focuses on *Candidozyma auris* and other emerging fungal pathogens.

References

1. Kutlu M, Sayın-Kutlu S, Alp-Çavuş S, Öztürk ŞB, Taşbakan M, Özhak B, et al. Mortality-associated factors of candidemia: a multi-center prospective cohort in Turkey. Eur J Clin Microbiol Infect Dis. 2022;41:597–607. https://doi.org/10.1007/s10096-021-04394-0
2. Paiva JA, Pereira JM, Tabah A, Mikstacki A, de Carvalho FB, Koulenti D, et al. Characteristics and risk factors for 28-day mortality of hospital acquired fungemias in ICUs: data from the EUROBACT study. Crit Care. 2016;20:53. https://doi.org/10.1186/s13054-016-1229-1
3. Barantsevich N, Barantsevich E. Diagnosis and treatment of invasive candidiasis. Antibiotics (Basel). 2022;11:718. https://doi.org/10.3390/antibiotics11060718
4. Clancy CJ, Nguyen MH. Non-culture diagnostics for invasive candidiasis: promise and unintended consequences. J Fungi (Basel). 2018;4:27. https://doi.org/10.3390/jof4010027
5. Murphy CR, Teoh Z, Whitehurst D, Brammer C, Perkins K, Paulsen G, et al. Disseminated disease after candidemia in children and young adults: epidemiology, diagnostic evaluation and risk factors. Pediatr Infect Dis J. 2024;43:328–32. https://doi.org/10.1097/INF.0000000000004212
6. Whitehurst D, Murphy CR, Teoh Z, Brammer CN, Perkins K, Paulsen GC, et al. 1702. Disseminated candidiasis after candidemia: epidemiology, diagnostic evaluation, and risk factors. Open Forum Infect Dis. 2023;10:ofad500.1535. https://doi.org/10.1093/ofid/ofad500.1535
7. Shin SU, Yu YH, Kim SS, Oh TH, Kim SE, Kim UJ, et al. Clinical characteristics and risk factors for complications of candidaemia in adults: focus on endophthalmitis, endocarditis, and osteoarticular infections. Int J Infect Dis. 2020;93:126–32. https://doi.org/10.1016/j.ijid.2020.01.049
8. Anaissie EJ, Rex JH, Uzun O, Vartivarian S. Predictors of adverse outcome in cancer patients with candidemia. Am J Med. 1998;104:238–45. https://doi.org/10.1016/S0002-9343(98)00030-8
9. Liu F, Hu ZD, Zhao XM, Zhao WN, Feng ZX, Yurkov A, et al. Phylogenomic analysis of the *Candida auris–Candida haemuli* clade and related taxa in the *Metschnikowiaceae,* and proposal of thirteen new genera, fifty-five new combinations and nine new species. Persoonia. 2024;52:22–43. https://doi.org/10.3767/persoonia.2024.52.02
10. Garcia-Bustos V, Cabanero-Navalon MD, Ruiz-Saurí A, Ruiz-Gaitán AC, Salavert M, Tormo MÁ, et al. What do we know about *Candida auris*? State of the art, knowledge gaps, and future directions. Microorganisms. 2021;9:2177. https://doi.org/10.3390/microorganisms9102177
11. Du H, Bing J, Hu T, Ennis CL, Nobile CJ, Huang G. *Candida auris*: epidemiology, biology, antifungal resistance, and virulence. PLoS Pathog. 2020;16:e1008921. https://doi.org/10.1371/journal.ppat.1008921
12. Satoh K, Makimura K, Hasumi Y, Nishiyama Y, Uchida K, Yamaguchi H. *Candida auris* sp. nov., a novel ascomycetous yeast isolated from the external ear canal of an inpatient in a Japanese hospital. Microbiol Immunol. 2009;53:41–4. https://doi.org/10.1111/j.1348-0421.2008.00083.x
13. Jenkins LB, Christian RL, Karaman BA, Ghannoum MA, Dousa KM. Bad to the bone: *Candida (Candidozyma) auris* vertebral osteomyelitis treated with combination antifungal therapy followed by a novel long-acting echinocandin. ASM Case Rep. 2025;1:e00114-25. https://doi.org/10.1128/asmcr.00114-25
14. Jelkin GL, Heineman AL, Beckett HT, Goddard CM, Ngwenya LB. Intracranial *Candida auris* infection: a case report and scoping review. World Neurosurg. 2026;206:124775. https://doi.org/10.1016/j.wneu.2025.124775
15. Kerai A, Doshi S, Laleker A, Majumdar A. Fungal foe and mechanical hearts: a retrospective case series on *Candida auris* bloodstream infection with left ventricular assist devices. Open Forum Infect Dis. 2024;11:ofae286. https://doi.org/10.1093/ofid/ofae286
16. Rodriguez L, Grabosky LB, Cypen J. *Candida auris* candidemia, septic arthritis, and vertebral osteomyelitis requiring dual antifungal therapy: a case report. Infection. 2026;54:527–32. https://doi.org/10.1007/s15010-025-02643-4
17. Stack MA, Ostrosky-Zeichner L, Hasbun R, Park SO, Babic J, Kapadia M. Rezafungin for suppressive therapy of *Candida auris* in a patient with a left ventricular assist device (LVAD). IDCases. 2025;40:e02232. https://doi.org/10.1016/j.idcr.2025.e02232
18. Mulet Bayona JV, Tormo Palop N, Salvador García C, Guna Serrano MDR, Gimeno Cardona C. *Candida auris* from colonisation to candidemia: a four-year study. Mycoses. 2023;66:882–90. https://doi.org/10.1111/myc.13626
19. Sayeed MA, Farooqi J, Jabeen K, Mahmood SF. Comparison of risk factors and outcomes of *Candida auris* candidemia with non-*Candida auris* candidemia: a retrospective study from Pakistan. Med Mycol. 2020;58:721–9. https://doi.org/10.1093/mmy/myz112
20. Erdem H, Şakir-Yildirim S, Ankarali H, Batirel A, Kul G, Fidan G, et al. Managing *Candida auris* fungemias: the results of a prospective and international study. Antimicrob Agents Chemother. 2025;69:e0035825. https://doi.org/10.1128/aac.00358-25
21. Mirhendi H, Charsizadeh A, Aboutalebian S, Mohammadpour M, Nikmanesh B, de Groot T, et al. South Asian (clade I) *Candida auris* meningitis in a paediatric patient in Iran with a review of the literature. Mycoses. 2022;65:134–9. https://doi.org/10.1111/myc.13396

22. Morales-López SE, Parra-Giraldo CM, Ceballos-Garzón A, Martínez HP, Rodríguez GJ, Álvarez-Moreno CA, et al. Invasive infections with multidrug-resistant yeast *Candida auris*, Colombia. Emerg Infect Dis. 2017;23:162–4. https://doi.org/10.3201/eid2301.161497
23. Khatamzas E, Madder H, Jeffery K. Neurosurgical device-associated infections due to *Candida auris*—three cases from a single tertiary center. J Infect. 2019;78:409–21. https://doi.org/10.1016/j.jinf.2019.02.004
24. Ruiz-Gaitán A, Martínez H, Moret AM, Calabuig E, Tasias M, Alastruey-Izquierdo A, et al. Detection and treatment of *Candida auris* in an outbreak situation: risk factors for developing colonization and candidemia by this new species in critically ill patients. Expert Rev Anti Infect Ther. 2019;17:295–305. https://doi.org/10.1080/14787210.2019.1592675
25. Centers for Disease Control and Prevention. Antifungal susceptibility testing for *C. auris*. 2024 [cited 2026 Jul 28]. https://www.cdc.gov/candida-auris/hcp/laboratories/antifungal-susceptibility-testing.html.
26. Reizine F, Henry J, Desmedt L, Camus C, Coirier V, Arrive F, et al. Screening, prevalence, and risk factors for secondary localization during candidemia in intensive care unit patients: the French CandidICU multicenter study. Crit Care. 2025;29:281. https://doi.org/10.1186/s13054-025-05527-z
27. Bing J, Guan Z, Zheng T, Zhang Z, Fan S, Ennis CL, et al. Clinical isolates of *Candida auris* with enhanced adherence and biofilm formation due to genomic amplification of ALS4. PLoS Pathog. 2023;19:e1011239. https://doi.org/10.1371/journal.ppat.1011239
28. Foong KS, Sung A, Burnham JP, Kronen R, Lian Q, Salazar Zetina A, et al. Risk factors predicting *Candida* infective endocarditis in patients with candidemia. Med Mycol. 2020;58:593–9. https://doi.org/10.1093/mmy/myz104
29. López-Vilella R, Ruiz Gaitán AC, Gimeno Costa JR, Marqués-Sulé E, Vicente Guillén R, Pemán García J, et al. *Candida auris* and heart transplantation. Preoperative attitude. OBM Transplant. 2019;3:1–10. https://doi.org/10.21926/obm.transplant.1901053
30. Sakai D, Matsumiya W, Kusuhara S, Nakamura M. Factors associated with the development of ocular candidiasis and ocular prognosis with echinocandin therapy for candidemia. J Ophthalmic Inflamm Infect. 2021;11:17. https://doi.org/10.1186/s12348-021-00248-0
31. Lehman A, Tessier KM, Sattarova V, Montezuma SR, Kline S, Erayil SE. Do patients with candidemia need an ophthalmologic examination? Open Forum Infect Dis. 2024;11:ofae663. https://doi.org/10.1093/ofid/ofae663
32. Suárez-Urquiza P, Pemán J, Gordon M, Favier P, Muñoz-Brell P, López-Hontangas JL, et al. Predicting fungemia in the ICU: unveiling the value of weekly fungal surveillance and yeast colonisation monitoring. J Fungi (Basel). 2024;10:674. https://doi.org/10.3390/jof10100674
33. Cornely OA, Sprute R, Bassetti M, Chen SCA, Groll AH, Kurzai O, et al. Global guideline for the diagnosis and management of candidiasis: an initiative of the ECMM in cooperation with ISHAM and ASM. Lancet Infect Dis. 2025; 25:e280–93. https://doi.org/10.1016/S1473-3099(24)00749-7
34. Cornely OA, Bassetti M, Calandra T, Garbino J, Kullberg BJ, Lortholary O, et al.; ESCMID Fungal Infection Study Group. ESCMID guideline for the diagnosis and management of *Candida* diseases 2012: non-neutropenic adult patients. Clin Microbiol Infect. 2012;18(Suppl 7):19–37. https://doi.org/10.1111/1469-0691.12039
35. Pappas PG, Kauffman CA, Andes DR, Clancy CJ, Marr KA, Ostrosky-Zeichner L, et al. Clinical practice guideline for the management of candidiasis: 2016 update by the Infectious Diseases Society of America. Clin Infect Dis. 2016;62:e1–50. https://doi.org/10.1093/cid/civ933

Address for correspondence: Alba Ruiz-Gaitán, Severe Infection Research Group, Health Research Institute La Fe, Hospital Universitari i Politècnic La Fe, Avinguda de Fernando Abril Martorell 106, 46026 Valencia, Spain; email: albacruiz@gmail.com

Reducing Antibiotic Drug Use Effects on *Clostridioides difficile* Colonization in Nursing Home Residents[1]

Majerle Reeves,[2] Mihnea R. Mangalea,[2] Camden D. Gowler, Prabasaj Paul,[3] Hannah Wolford, Joseph D. Lutgring, Sujan C. Reddy, Alison Laufer Halpin, L. Clifford McDonald, Rachel B. Slayton

Medscape CME Activity

In support of improving patient care, this activity has been planned and implemented by Medscape, LLC and Emerging Infectious Diseases. Medscape, LLC is jointly accredited with commendation by the Accreditation Council for Continuing Medical Education (ACCME), the Accreditation Council for Pharmacy Education (ACPE), and the American Nurses Credentialing Center (ANCC), to provide continuing education for the healthcare team.

Medscape, LLC designates this Journal-based CME activity for a maximum of 1.00 ***AMA PRA Category 1 Credit(s)™***. Physicians should claim only the credit commensurate with the extent of their participation in the activity.

Successful completion of this CME activity, which includes participation in the evaluation component, enables the participant to earn up to 1.0 MOC points in the American Board of Internal Medicine's (ABIM) Maintenance of Certification (MOC) program. Participants will earn MOC points equivalent to the amount of CME credits claimed for the activity. It is the CME activity provider's responsibility to submit participant completion information to ACCME for the purpose of granting ABIM MOC credit.

All other clinicians completing this activity will be issued a certificate of participation. To participate in this journal CME activity: (1) review the learning objectives and author disclosures; (2) study the education content; (3) take the post-test with a 75% minimum passing score and complete the evaluation at http://www.medscape.org/journal/eid; and (4) view/print certificate. For CME questions, see page 1936.

NOTE: It is the policy of Medscape Education to avoid the mention of brand names or specific manufacturers in accredited educational activities. However, trade and manufacturer names in this activity are provided in an effort to provide clarity. The use of brand or manufacturer names should not be viewed as an endorsement by Medscape of any specific product or manufacturer.

Release date: October 26, 2026; Expiration date: October 26, 2027

Learning Objectives

Upon completion of this activity, participants will be able to:

- Distinguish and compare risk factors for *Clostridioides difficile* colonization among nursing home residents in the current study
- Evaluate the relationship between antibiotic use and *C. difficile* infection in the current study
- Identify the impact of reducing antibiotics on the risk for *C. difficile* colonization in the current study

CME Editor

Bryce Simons, MPH, Technical Writer/Editor, Emerging Infectious Diseases. *Disclosure: Bryce Simons, MPH, has no relevant financial relationships.*

CME Author

Charles P. Vega, MD, Health Sciences Clinical Professor of Family Medicine, University of California, Irvine School of Medicine, Irvine, California, USA. *Charles P. Vega, MD, has the following relevant financial relationships: consultant or advisor for Boehringer Ingelheim; Exact Sciences; GlaxoSmithKline.*

Authors

Majerle Reeves, PhD; Mihnea R. Mangalea, PhD; Camden D. Gowler, PhD; Prabasaj Paul, PhD; Hannah Wolford, MSPH; Joseph D. Lutgring, MD; Sujan C. Reddy, MD; Alison Laufer Halpin, PhD; L. Clifford McDonald, MD; Rachel B. Slayton, PhD.

Antibiotic drug–mediated changes in the human gut microbiota affect *Clostridioides difficile* colonization. We created a compartmental model of *C. difficile* colonization in nursing home residents to improve understanding of how the gut microbiota mediates the transmission process. When analyzing *C. difficile* colonization as a function of the daily percentage of the nursing home resident population on antibiotic drugs, the model displayed increases in *C. difficile* colonization as antibiotic drug use increased. Reducing the daily percentage of the nursing home resident population receiving antibiotic drugs from 8% to 6.6% could halve endemic colonization. In sensitivity analyses, increases in the time to recover microbiota diversity, duration of colonization, daily percentage of the nursing home resident population on antibiotic drugs, and susceptibility to *C. difficile* in the low-diversity microbiota population had the largest effect on endemic colonization. Our model demonstrates that reductions in antibiotic drug use yield reductions in *C. difficile* colonization.

Clostridioides difficile poses a serious threat to persons within healthcare systems, especially nursing home residents and long-term acute care patients (*1*). Both direct and indirect factors contribute to *C. difficile* colonization risk (Figure 1). Antibiotic drug use can disrupt the gut microbiome and lead to a decrease in microbial diversity and subsequent loss of protection against pathogens (*2*,*3*). Previous studies have demonstrated how antibiotic drug use and duration (*4*,*5*), in addition to gut microbiome status (*3*), affect a person's risk for colonization and infection by *C. difficile* (*6*).

One meta-analysis found that antibiotic drug use within 3 months of the study period was not significantly associated with *C. difficile* colonization, although several studies within the analysis found that prior hospitalization, within 6 months of the study period, was associated with increased colonization risk (*7*). Those results suggest 2 possible explanations: collinearity between hospitalization and antibiotic drug use widened the CIs for antibiotic drug use and reduced statistical significance, or antibiotic drug use increased colonization risk only when accompanied by elevated *C. difficile* exposure at the facility level (*7*).

Person-level links between antibiotic drug use and C. *difficile* colonization and infection cannot quantify the population-level consequences of antibiotic drug-induced microbiota disruption and the drivers of transmission within a facility or population (*2*–*5*). Together, those factors highlight the difficulty of disentangling the direct and indirect effects of antibiotic drug use on population level effects versus exposure to *C. difficile* in a person, underscoring the need to explicitly account for microbiome disruption. Consolidating that information to elucidate C. *difficile* transmission and the potential effects of public health interventions remain a challenge that mathematical models are well-suited to address (*8*). We built a model of antibiotic drug use, microbiota dynamics, and *C. difficile* transmission to estimate the magnitude of those indirect effects and to quantify the population-level colonization effect attributable to microbiome-mediated transmission.

Methods

Model Design

We developed a compartmental model (*9*) of *C. difficile* colonization in nursing home residents in which microbiome status affects the transmission process (Figure 2). For microbiome status, we classified the population into high and low ecologic diversity microbiota groups, or α diversity, which quantifies bacterial species' relative abundance in a microbial community and is a commonly reported metric of microbial community diversity, especially in studies associating colonization (*6*,*10*) or antibiotic drug use (*11*–*14*; P. Ferretti, unpub. data, https://doi.org/10.7554/eLife.90111.1) with the microbiome. The rate of transition from the high to low microbiota diversity group is proportional to the daily percentage of the nursing home resident population on antibiotic drugs. This structure reflects the well-established observation that low microbiota diversity is a risk factor for *C. difficile* colonization (*15*). Within each high and low α diversity group, we further stratified the population as either uncolonized or colonized with *C. difficile*.

Transmission dynamics followed a susceptible-infectious-susceptible framework. The low microbiota diversity groups are more susceptible to *C. difficile* colonization and are more infectious if colonized with *C. difficile*. The *C. difficile*–colonized, low-diversity microbiota group takes more time to recover microbiota diversity than the uncolonized counterparts.

Author affiliations: Centers for Disease Control and Prevention, Atlanta, Georgia, USA (M. Reeves, M.R. Mangalea, C.D. Gowler, P. Paul, H. Wolford, J.D. Lutgring, S.C. Reddy, A.L. Halpin, L.C. McDonald, R.B. Slayton); US Public Health Service, Rockville, Maryland, USA (A.L. Halpin, R.B. Slayton)

DOI: https://doi.org/10.3201/eid3211.260743

[1]Preliminary results from this study were presented at the SHEA Spring conference; April 12–14, 2023; Seattle, Washington, USA.

[2]These first authors contributed equally to this article.

[3]Current affiliation: Robert Koch Institute, Berlin, Germany

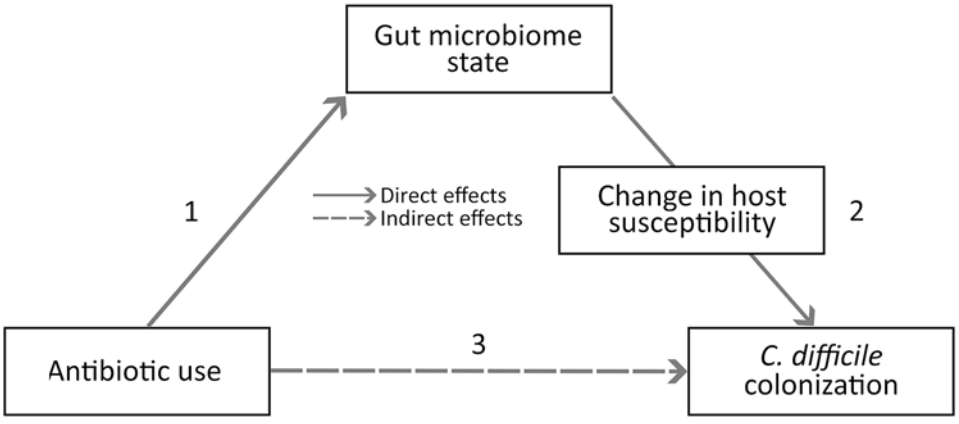

Figure 1. Diagram showing the relationships between antibiotic drug use, gut microbiome state, and *Clostridioides difficile* transmission in study of antibiotic drug use effects on the microbiome state and endemic *C. difficile* colonization and transmission in nursing homes. Increasing antibiotic drug use could lead to higher *C. difficile* transmission through indirect effects, fully mediated by gut microbiota. The negative direct effects of antibiotic drugs on gut microbiota are related to changes in the gut microbiome state that influence host susceptibility to C. *difficile*, leading to an overall indirect effect of antibiotic drugs on C. *difficile* colonization.

The *C. difficile*–colonized, high-diversity microbiome group can spontaneously decolonize, but the *C. difficile*–colonized, low-diversity microbiota group cannot. We chose this framework to reflect how well C. *difficile* has evolved to survive in the gut (Table; Appendix, Figure 1, http://wwwnc.cdc.gov/EID/article/32/11/26-0743-App1.pdf).

Both increased susceptibility and infectivity increase the colonization rate, which is the force of infection in the model. Although increases in susceptibility and infectivity because of low microbiota diversity are supported by several studies (*6*,*20*,*21*), their magnitude is unknown and therefore assumed. Increased susceptibility increases the colonization rate in the uncolonized, low-diversity microbiota group, reflecting reduced colonization resistance to C. *difficile* when fewer resource-competing microorganisms are present in the gut. Increased infectivity increases the colonization rate in both the uncolonized, high-diversity microbiota group and uncolonized, low-diversity microbiota groups. This effect is akin to the *C. difficile*–colonized, low-diversity microbiota group shedding more *C. difficile* spores, either from a higher *C. difficile* bacterial load relative to competing microorganisms or higher transmissibility because of symptomatic infection in a portion of the population. We set a modest increase in infectivity for the *C. difficile*–colonized, low-diversity microbiota group well below the 15–30-fold greater infectiousness that previous transmission models attribute to symptomatic infection over asymptomatic colonization (*21*). Because we were modeling colonization dynamics rather than symptomatic *C. difficile* infection, and because susceptibility is mechanistically established, we assume susceptibility

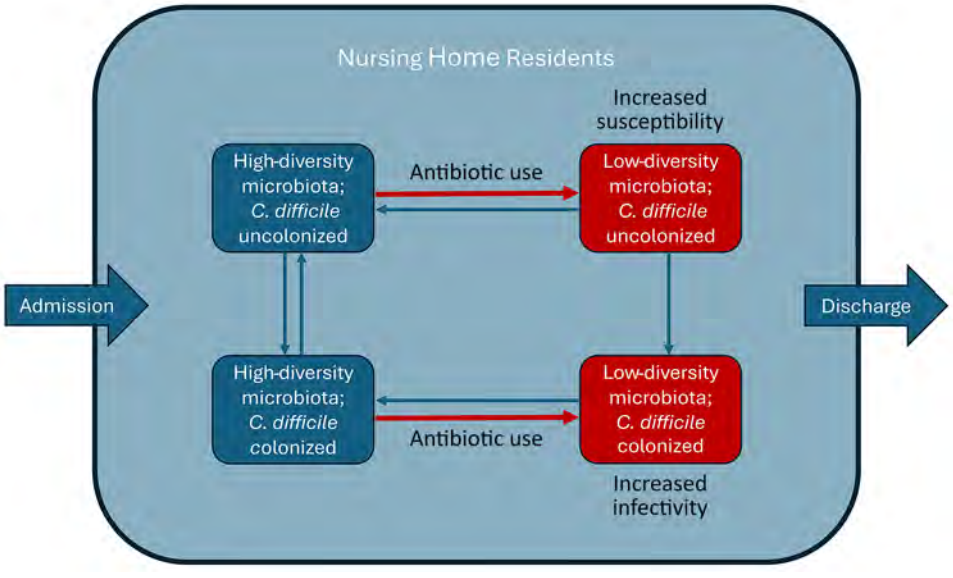

Figure 2. Simplified diagram of a compartmental model in study of indirect effects of antibiotic drug use on the microbiome state and the implications for endemic *Clostridioides difficile* colonization and transmission in nursing homes. Each box represents states nursing home residents can fall under. Each arrow denotes transitions between different states (states of high and low microbiota diversity and uncolonized and colonized with *C. difficile*). The size of the population in the high and low microbiota states is a function of the daily percentage of the nursing home resident population on antibiotic drugs.

Table. Full parameter table for compartmental model of *Clostridioides difficile* colonization transmission in nursing home residents*

Description	Variable or parameter notation	Modeled value range	Sources
Initial and newly admitted proportion of population with low-diversity microbiota	b_L	0–0.5	(*6*,*10*)
Total population size	*N*	50–200	Assumed
Proportion of *C. difficile*–colonized newly admitted nursing home residents	μ	0–0.02	Assumed
Transmission rate	β	NA	Fitted value
Relative increase in *C. difficile* infectivity because of low diversity microbiota	θ	1–2.5	Assumed
Relative increase in susceptibility to colonization with *C. difficile* for low-diversity microbiota group	ω	1–5	Assumed
Spontaneous *C. difficile* decolonization indicator for low-diversity microbiota group	η	0	Assumed
Antibiotic drug-induced transition rate from high to low diversity microbiota	α†	0.0014–0.07	Estimated
Daily nursing home resident population receiving antibiotic drugs, %	*abx*	2–14	(*16*,*17*)
High to low microbiota diversity after starting antibiotic drugs, d	ψ	2–15	(*13*)
Microbiota diversity recovery rate from low to high for *C. difficile* uncolonized group	δ‡	0.0215–0.065	Estimated
Daily nursing home resident population not on antibiotic drugs, %	1 – *abx*	86–98	(*16*,*17*)
Recovery from low to high microbiota diversity when discontinuing antibiotic drugs, days	r_d	15–40	(*13*)
Duration of *C. difficile* colonization, d	1/γ	24–90	(*15*,*18*)
Multiplier of microbiota diversity recovery for the *C. difficile* colonized group	ϕ	0.75–1	Assumed
Average length of nursing home stay, d	1/ζ	25–406	(*19*)

*NA, not applicable.
†α = (daily percentage of the nursing home resident population on antibiotic drugs) × (1/days to go from high to low diversity upon starting antibiotic drugs).
‡δ = (daily percentage of the nursing home resident population not on antibiotic drugs) × (1/days to recover from low to high diversity upon discontinuing antibiotic drugs).

has a larger effect on the colonization rate than infectivity in the low-diversity microbiota groups.

Microbiota-Mediated Indirect Effects

We first investigated microbiota-mediated indirect effects of antibiotic drug use (Figure 1). We used literature-informed parameter ranges to account for and analyze how the microbiota mediates the effect of antibiotic drug use on colonization risk in the nursing home population (Table). In our model, the low α diversity group could have higher susceptibility and infectivity and no spontaneous decolonization. We included parameter values for a comparator model in which the microbiome has no effect on *C. difficile* colonization (Appendix Table 1).

Model Equilibria Dynamics

Using our model, we analyzed the equilibrium (i.e., endemic) dynamics, and all results reveal the equilibrium colonization prevalence (Appendix). We calculated the endemic colonization prevalence in response to varying the daily percentage of the nursing home resident population on antibiotic drugs. We assumed the baseline daily percentage of the nursing home resident population receiving antibiotic drugs to be 8% (*17*) and the percentage colonized at equilibrium to be

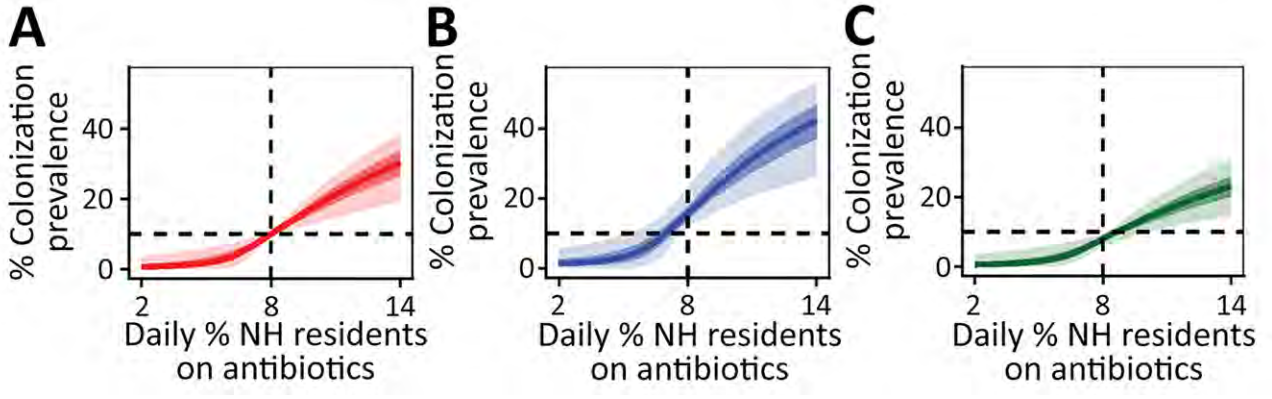

Figure 3. Model results from study of the indirect effects of antibiotic drug use on the microbiome state and the implications for endemic *Clostridioides difficile* colonization and transmission in nursing homes. A) Total population; B) low microbiota diversity group; C) high microbiota diversity group. Dashed horizontal lines represent endemic *C. difficile* colonization at 10% total colonization prevalence when daily population-level antibiotic drug use is 8% (dashed vertical lines). The darker and lighter shaded regions show the central 50% and 95% simulation intervals, and the darkest solid lines depict median values. NH, nursing home.

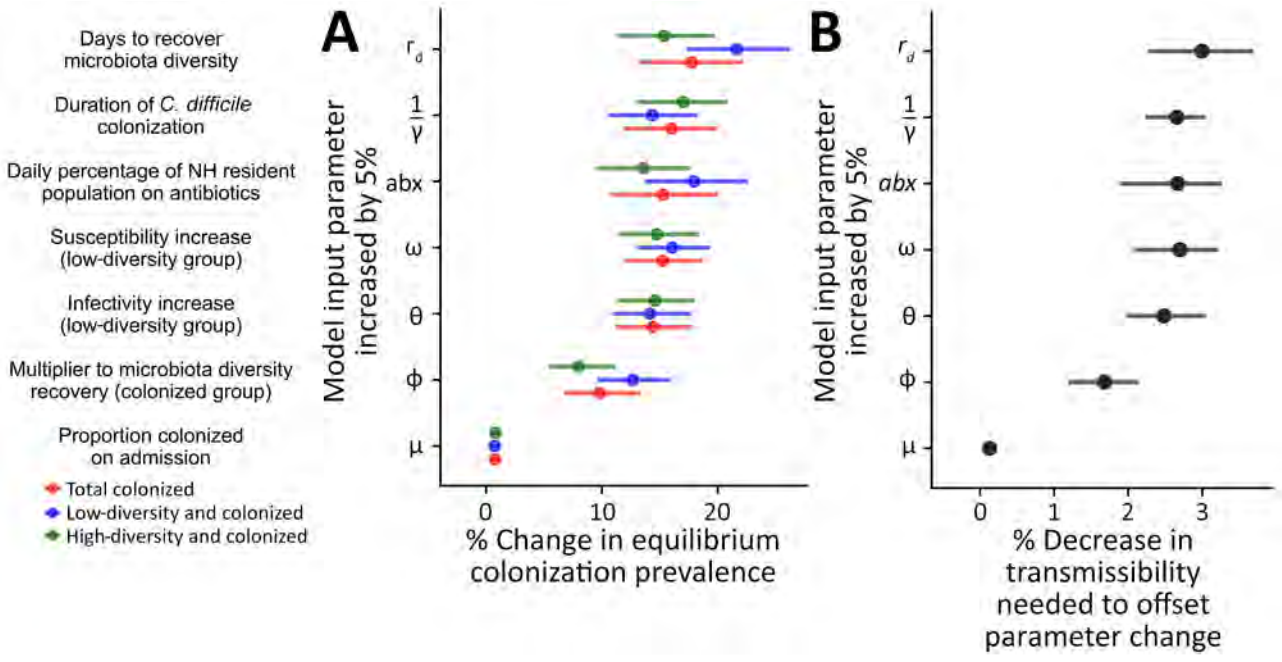

Figure 4. Results from study of the indirect effects of antibiotic drug use on the microbiome state and the implications for endemic *Clostridioides difficile* colonization and transmission in nursing homes. A) Changes in colonization prevalence; B) and the percentage decrease in transmissibility required to return the population to its original *C. difficile* colonization prevalence after a perturbation. Points show the medians, and error bars mark the central 50% distribution of estimated values.

10% (22). We varied the daily percentage of the nursing home resident population receiving antibiotic drugs from 2% to 14% and calculated the proportion colonized with C. *difficile* at equilibrium. That range denotes a symmetric 75% decrease and increase in the daily percentage of the nursing home resident population receiving antibiotic drugs; we chose this range as reasonable because total elimination of antibiotic drugs is not feasible. The daily percentage of the nursing home resident population receiving antibiotic drugs affects movement from high to low microbiota diversity and from low to high microbiota diversity. The bidirectional effect of antibiotic drug use creates a nonlinear relationship between antibiotic drug use and the proportion of the population with low-diversity microbiota. Because of the wide ranges for many of the model parameters (Table), we fit 500 scenarios to capture the potential variation in endemic C. *difficile* colonization and report the median, 50%, and 95% simulation intervals for the 500 model scenarios (Appendix).

Parameter Effects and Uncertainty

Our compartmental model substantially simplifies *C. difficile* colonization, microbiota diversity, and antibiotic drug use. We chose a simple model because of limited data on pathogen natural history and within host ecologic interactions. We aim to use mathematical modeling to help inform future data collection efforts. With an eye toward applied public health study design, we used the uncertainty in model parameters to evaluate their contribution to model outputs.

We increased individual model parameters and calculated the increase in endemic colonization prevalence and the reduction in transmission rate required to offset the difference between the baseline and new colonization prevalence. This reduction in the transmissibility parameter represents efforts to disrupt transmission, such as hand hygiene with soap and water, contact precautions, or related infection prevention and control interventions. We fit 500 scenarios to capture the potential variation and report the median value and the 50% distribution of estimated values (Appendix).

Results

C. difficile Comparative Equilibrium Colonization Prevalence

In our model, increasing the daily percentage of the nursing home resident population on antibiotic drugs generated higher endemic colonization prevalence; decreasing the daily percentage of the nursing home resident population on antibiotic drugs reduced endemic colonization prevalence. When looking at endemic colonization prevalence by microbiota

diversity status, the proportion of each group colonized as a function of antibiotic drug use increased at a faster rate in the low-diversity microbiota group compared with the high-diversity microbiota group (Figure 3; Appendix Figure 2). The model predicts that a reduction of 17.5% to the daily percentage of the resident population receiving antibiotic drugs, from 8% to 6.6%, would halve median colonization prevalence to 5% (95% CI 2.1%–8.0%).

Quantifying Parameter Uncertainty

In the sensitivity analysis, we sampled from parameter ranges as defined by the literature (Table). Uniformly sampled parameters (Appendix Figure 3) revealed some weak correlations (Appendix Figure 4). To gauge the effect of each parameter, we individually increased parameters and calculated endemic C. *difficile* colonization. Many parameters had considerable effects on median C. *difficile* colonization prevalence (Figure 4, panel A). For example, increasing the daily percentage of the nursing home resident population receiving antibiotic drugs by 5% in the model led to a median 15.3% increase in colonization prevalence in the simulated nursing home (Figure 4, panel A). Although the uncertainty around the estimated change in colonization prevalence is substantial (interquartile range [IQR] 10.8%–20.0%) (Figure 4, panel A), the change corresponds to a roughly 2–4-fold increase in the percent of residents colonized per percentage increase in the daily percentage of the nursing home resident population receiving antibiotic drugs.

Microbiome State and Transmissibility

Parameters in the model tying the microbiome state and transmissibility (i.e., relative increases in infectivity or susceptibility because of low-diversity microbiota) had both high effect and wide uncertainty estimates (infectivity, median 14.4%, IQR 11.2%–17.8%; susceptibility, median 15.3%, IQR 11.9%–18.7%) (Figure 4, panel A). Parameters linking *C. difficile* colonization and microbiome state also had both high effect and wide uncertainty estimates. Increasing the microbiota diversity recovery time had the largest effect (median 17.7%, IQR 13.2%–22.2%), followed by the duration of colonization (median 16.0%, IQR 11.9%–19.9%) (Figure 4, panel A). In addition, parameters associated with low-diversity microbiota, such as the daily percentage of the nursing home population receiving antibiotic drugs (median 15.3%, IQR 10.8%–20.0%) and the multiplier to microbiota diversity recovery for the colonized group (median 9.8%, IQR 6.8%–13.3%) had large effects on colonization prevalence with wide uncertainty, largely following the transmissibility parameter set patterns (Figure 4, panel A).

We next quantified the percent reduction in the transmission rate parameter required to restore the original *C. difficile* colonization prevalence after the model input parameters increased by 5%. The same parameters affected in the sensitivity analysis revealed a similar qualitative pattern when individually evaluated (Figure 4, panel B). For instance, increasing antibiotic drug use overall by 5% would require a median 2.7% (IQR 1.9%–3.3%) reduction in transmissibility (e.g., increased contact precautions) to offset the parameter change and return the population to its original, lower colonization prevalence. The rankings and relative magnitude of each parameter were comparable to colonization results (Figure 4, panel A). The central 50% of estimates for most parameters also exhibited considerable uncertainty for the required decrease in transmissibility (Figure 4, panel B).

Discussion

Our modeling study demonstrates that the host microbiota diversity is critical in *C. difficile* colonization prevalence at the population level. In our model, colonization prevalence increased in response to increased antibiotic drug use, and those nonlinear increases are driven by the nonlinear relationship between antibiotic drug use and the proportion of the population with low-diversity microbiota. That effect is compounded because susceptibility and infectivity are linked to that proportion. Because the microbiome mediates the relationship, low-diversity microbiota represents a modifiable risk factor for *C. difficile* colonization, much like antibiotic drug use (*4*,*23*,*24*), but one that can be directly targeted. Our results therefore highlight the potential for microbiome-targeted therapeutics and pathogen reduction approaches to restore or strengthen *C. difficile* colonization resistance (*25*). Mechanistically, such interventions could decrease the nonlinearity between antibiotic drug use and the proportion of the population with low-diversity microbiota or reduce the effect of low-diversity microbiota on colonization risk.

The construction of our mathematical model of *C. difficile* transmission would be impossible without data from laboratory experiments and population-based observational studies on antibiotic drug use, host microbiota diversity, and *C. difficile* colonization. Through consolidating this data, our model reveals that the effects of the microbiome state can create dramatic changes. The model predicts that reducing antibiotic drug use by <20% could halve endemic colonization. Such a reduction could be achieved by

reducing unnecessary antibiotic drug use or shortening the duration of antibiotic drug courses when appropriate. Because antibiotic drug stewardship interventions have been shown to reduce antibiotic drug use in US long-term care facilities (*26*), reductions in the daily percentage of the nursing home resident population on antibiotic drugs could be feasible.

Incorporating the microbiome state might be necessary to accurately predict changes in pathogen colonization prevalence because of interventions such as antibiotic stewardship programs and pathogen reduction efforts (*27*). Accounting for those microbiota-mediated indirect effects, and reducing uncertainty in associated parameters, is increasingly necessary as new microbiome-targeted therapies emerge. That accounting is especially relevant when antibiotic drug use is unavoidable. Restoring microbiota diversity after necessary antibiotic drug treatment is a critical mechanism to leverage for reducing the susceptibility and infectivity that drives *C. difficile* transmission. Microbiome-based pathogen reduction interventions (e.g., fecal microbiota products and live biotherapeutic products) promote changes in microbial growth and work by reducing susceptibility (i.e., increasing colonization resistance) or selectively decolonizing body sites in the host to reduce infectivity and onward transmission (*25*). Our model provides a framework for evaluating the possible population-level effect of such interventions depending on which pathways they interrupt (e.g., duration of colonization, infectivity, microbiota diversity recovery), helping prioritize the treatments with the greatest potential to reduce colonization.

The first limitation of our study is that we did not distinguish between symptomatic *C. difficile* infection and asymptomatic colonization. Persons with symptomatic infection might have differences in infectivity, microbiota diversity recovery rate, duration of colonization, and antibiotic drug use compared with persons with asymptomatic colonization. Second, we have made assumptions about the relationships between low-diversity microbiota groups and increases in colonization susceptibility and infectivity. Although those mechanisms for increases are supported by literature (*6*,*20*,*21*), the chosen values are not directly supported by literature. We have chosen small ranges to avoid overstating the effect of antibiotic drugs on model outcomes. Third, we chose α diversity as our microbiota metric because of its ubiquity in the literature and generalizability across the nursing home population. Other measures of the microbiome might have higher predictive value (*28*) for colonization but require more individualized patient-level data. Fourth, we assumed a single linear relationship between antibiotic drug use over time in the nursing home population and disruption of the host microbiota. That relationship is likely nonlinear and dependent on drug dose, duration, or type (*29*–*33*). Previous work has linked specific antibiotic drugs to increased colonization risk (*23*,*34*), but accurately assessing the proportion of the population at an average nursing home receiving antibiotic drugs and the microbiome response remains challenging because of a lack of data. In addition, other medications might have adverse effects on the gut microbiota and affect *C. difficile* colonization risk (*35*). Fifth, we did not validate the modeled relationship between population-level antibiotic drug use and *C. difficile* colonization prevalence against empirical data (Figure 3). That limitation reflects a lack of paired data regarding antibiotic drug use and *C. difficile* colonization prevalence at different levels of antibiotic drug use. Our results should therefore be interpreted as model-based projections rather than empirically fitted results. Closing that gap is a key priority for future work; measuring prevalence of *C. difficile* colonization when antibiotic drug use is low could validate our findings (Figure 3) that small changes in antibiotic drug use can lead to large changes in colonization prevalence. Confirming that finding with empirical data would considerably strengthen the case for targeted stewardship interventions. Finally, we did not make distinction between competing *C. difficile* strains (e.g., nontoxigenic and toxigenic), which might yield different disease outcomes.

We built a mathematical model that elucidates the relationship between antibiotic drug use, gut microbiota diversity, and *C. difficile* colonization. To clarify the relationship between antibiotic drug use and colonization, we also quantified the relative effect of individual model parameters on *C. difficile* colonization burden. Two findings carry direct public health relevance. First, the relationship between population-level antibiotic drug use and colonization prevalence is nonlinear: our model predicts that, as antibiotic drug use approaches zero, there are larger effects on reduction in population-level colonization prevalence. Such a reduction suggests even small increases in stewardship initiatives could have large effects, especially in scenarios where antibiotic drugs use is already low. Second, because gut microbiota composition mediates that relationship, microbiota-targeting interventions that restore diversity offer a complementary mechanism for reducing colonization prevalence in situations where antibiotic drug use is unavoidable. Achieving

those goals will require data collection of relevant epidemiologic data to validate our findings. Our results can help prioritize data collection, together with future modeling, to better characterize the cascading population-level effects of both microbiome-based pathogen reduction and antibiotic drug stewardship.

P.P.'s spouse is employed by Pfizer Inc. J.D.L. had institutional support provided for travel to the Society for Healthcare Epidemiology of America Spring meeting and to the Clinical and Laboratory Standards Institute antibiotic susceptibility testing subcommittee meetings.

Author contributions: conceptualization, C.D.G. and M.R.M.; formal analysis, C.D.G., M.R., and M.R.M.; original draft, C.D.G., M.R., and M.R.M.; result interpretation, all authors; draft review and editing, all authors; study supervision, P.P., R.B.S., and A.L.H.

About the Author

Dr. Reeves is an applied mathematician in the Division of Healthcare Quality Promotion, National Center for Emerging and Zoonotic Infectious Diseases, Centers for Disease Control and Prevention. Her research interests include mathematical modeling, machine learning, and applications in public health. Dr. Mangalea is a microbial ecologist and bioinformatician in the Division of Healthcare Quality Promotion, National Center for Emerging and Zoonotic Infectious Diseases, Centers for Disease Control and Prevention. His research interests include metagenomic analysis of microbiomes and antibiotic resistance profiles.

References

1. McKinnell JA, Singh RD, Miller LG, Kleinman K, Gussin G, He J, et al. The SHIELD Orange County project: multidrug-resistant organism prevalence in 21 nursing homes and long-term acute care facilities in southern California. Clin Infect Dis. 2019;69:1566–73. https://doi.org/10.1093/cid/ciz119
2. Woelfel S, Silva MS, Stecher B. Intestinal colonization resistance in the context of environmental, host, and microbial determinants. Cell Host Microbe. 2024;32:820–36. https://doi.org/10.1016/j.chom.2024.05.002
3. Seekatz AM, Safdar N, Khanna S. The role of the gut microbiome in colonization resistance and recurrent *Clostridioides difficile* infection. Therap Adv Gastroenterol. 2022;15:17562848221134396. https://doi.org/10.1177/17562848221134396
4. Brown KA, Langford B, Schwartz KL, Diong C, Garber G, Daneman N. Antibiotic prescribing choices and their comparative *C. difficile* infection risks: a longitudinal case-cohort study. Clin Infect Dis. 2021;72:836–44. https://doi.org/10.1093/cid/ciaa124
5. Stevens V, Dumyati G, Fine LS, Fisher SG, van Wijngaarden E. Cumulative antibiotic exposures over time and the risk of *Clostridium difficile* infection. Clin Infect Dis. 2011;53:42–8. https://doi.org/10.1093/cid/cir301
6. van Werkhoven CH, Ducher A, Berkell M, Mysara M, Lammens C, Torre-Cisneros J, et al.; ANTICIPATE Study Group. Incidence and predictive biomarkers of *Clostridioides difficile* infection in hospitalized patients receiving broad-spectrum antibiotics. Nat Commun. 2021;12:2240. https://doi.org/10.1038/s41467-021-22269-y
7. Anjewierden S, Han Z, Brown AM, Donskey CJ, Deshpande A. Risk factors for *Clostridioides difficile* colonization among hospitalized adults: a meta-analysis and systematic review. Infect Control Hosp Epidemiol. 2021;42:565–72. https://doi.org/10.1017/ice.2020.1236
8. Smith DR, Temime L, Opatowski L. Microbiome-pathogen interactions drive epidemiological dynamics of antibiotic resistance: a modeling study applied to nosocomial pathogen control. eLife. 2021;10:e68764. https://doi.org/10.7554/eLife.68764
9. Tolles J, Luong T. Modeling epidemics with compartmental models. JAMA. 2020;323:2515–6. https://doi.org/10.1001/jama.2020.8420
10. Berkell M, Mysara M, Xavier BB, van Werkhoven CH, Monsieurs P, Lammens C, et al.; ANTICIPATE study group. Microbiota-based markers predictive of development of *Clostridioides difficile* infection. Nat Commun. 2021;12:2241. https://doi.org/10.1038/s41467-021-22302-0
11. Burdet C, Nguyen TT, Duval X, Ferreira S, Andremont A, Guedj J, et al.; DAV132-CL-1002 Study Group. Impact of antibiotic gut exposure on the temporal changes in microbiome diversity. Antimicrob Agents Chemother. 2019;63:e00820–19. https://doi.org/10.1128/AAC.00820-19
12. Burdet C, Sayah-Jeanne S, Nguyen TT, Hugon P, Sablier-Gallis F, Saint-Lu N, et al. Antibiotic-induced dysbiosis predicts mortality in an animal model of *Clostridium difficile* infection. Antimicrob Agents Chemother. 2018;62:e00925–18. https://doi.org/10.1128/AAC.00925-18
13. Anthony WE, Wang B, Sukhum KV, D'Souza AW, Hink T, Cass C, et al. Acute and persistent effects of commonly used antibiotics on the gut microbiome and resistome in healthy adults. Cell Rep. 2022;39:110649. https://doi.org/10.1016/j.celrep.2022.110649
14. Martinez E, Taminiau B, Rodriguez C, Daube G. Gut microbiota composition associated with *Clostridioides difficile* colonization and infection. Pathogens. 2022;11:781. https://doi.org/10.3390/pathogens11070781
15. Crobach MJT, Vernon JJ, Loo VG, Kong LY, Péchiné S, Wilcox MH, et al. Understanding *Clostridium difficile* colonization. Clin Microbiol Rev. 2018;31:e00021–17. https://doi.org/10.1128/CMR.00021-17
16. Magill SS, O'Leary E, Ray SM, Kainer MA, Evans C, Bamberg WM, et al.; Emerging infections program hospital prevalence survey team. Assessment of the appropriateness of antimicrobial use in US hospitals. JAMA Netw Open. 2021;4:e212007. https://doi.org/10.1001/jamanetworkopen.2021.2007
17. Thompson ND, Stone ND, Brown CJ, Penna AR, Eure TR, Bamberg WM, et al. Antimicrobial use in a cohort of US nursing homes, 2017. JAMA. 2021;325:1286–95. https://doi.org/10.1001/jama.2021.2900
18. Donskey CJ, Kundrapu S, Deshpande A. Colonization versus carriage of *Clostridium difficile*. Infect Dis Clin North Am. 2015;29:13–28. https://doi.org/10.1016/j.idc.2014.11.001
19. Morris SE, Zipfel CM, Peer K, Madewell ZJ, Brenner S, Garg S, et al. Modeling the impacts of antiviral prophylaxis strategies in mitigating seasonal influenza outbreaks in nursing homes. Clin Infect Dis. 2024;78:1336–44. https://doi.org/10.1093/cid/ciad764

20. Buffie CG, Bucci V, Stein RR, McKenney PT, Ling L, Gobourne A, et al. Precision microbiome reconstitution restores bile acid mediated resistance to *Clostridium difficile*. Nature. 2015;517:205–8. https://doi.org/10.1038/nature13828
21. Lanzas C, Jara M, Tucker R, Curtis S; CDC Modeling Infectious Diseases in Healthcare Program (MinD). A review of epidemiological models of *Clostridioides difficile* transmission and control (2009–2021). Anaerobe. 2022;74:102541. https://doi.org/10.1016/j.anaerobe.2022.102541
22. Baron SW, Ostrowsky BE, Nori P, Drory DY, Levi MH, Szymczak WA, et al. Screening of *Clostridioides difficile* carriers in an urban academic medical center: understanding implications of disease. Infect Control Hosp Epidemiol. 2020;41:149–53. https://doi.org/10.1017/ice.2019.309
23. Dubberke ER, Reske KA, Seiler S, Hink T, Kwon JH, Burnham CA. Risk factors for acquisition and loss of *Clostridium difficile* colonization in hospitalized patients. Antimicrob Agents Chemother. 2015;59:4533–43. https://doi.org/10.1128/AAC.00642-15
24. McDonald LC, Gerding DN, Johnson S, Bakken JS, Carroll KC, Coffin SE, et al. Clinical practice guidelines for *Clostridium difficile* infection in adults and children: 2017 update by the Infectious Diseases Society of America (IDSA) and Society for Healthcare Epidemiology of America (SHEA). Clin Infect Dis. 2018;66:987–94. https://doi.org/10.1093/cid/ciy149
25. Mangalea MR, Halpin AL, Haile M, Elkins CA, McDonald LC. Decolonization and pathogen reduction approaches to prevent antimicrobial resistance and healthcare-associated infections. Emerg Infect Dis. 2024;30:1069–76. https://doi.org/10.3201/eid3006.231338
26. Katz MJ, Tamma PD, Cosgrove SE, Miller MA, Dullabh P, Rowe TA, et al. Implementation of an antibiotic stewardship program in long-term care facilities across the US. JAMA Netw Open. 2022;5:e220181. https://doi.org/10.1001/jamanetworkopen.2022.0181
27. Wolford H, Khan MA, Paul P, Toth DJA, Octaria R, Healy JM, et al. Projected impact of a pathogen reduction intervention on carbapenem-resistant Enterobacterales bloodstream infections and deaths in the United States. Infect Control Hosp Epidemiol. 2026;47:1–7. https://doi.org/10.1017/ice.2025.10335
28. Fishbein SR, Robinson JI, Hink T, Reske KA, Newcomer EP, Burnham CD, et al. Multi-omics investigation of *Clostridioides difficile*-colonized patients reveals pathogen and commensal correlates of *C. difficile* pathogenesis. eLife. 2022;11:e72801. https://doi.org/10.7554/eLife.72801
29. Shaw LP, Bassam H, Barnes CP, Walker AS, Klein N, Balloux F. Modelling microbiome recovery after antibiotics using a stability landscape framework. ISME J. 2019;13:1845–56. https://doi.org/10.1038/s41396-019-0392-1
30. Lekang K, Shekhar S, Berild D, Petersen FC, Winther-Larsen HC. Effects of different amoxicillin treatment durations on microbiome diversity and composition in the gut. PLoS One. 2022;17:e0275737. https://doi.org/10.1371/journal.pone.0275737
31. Leo S, Lazarevic V, von Dach E, Kaiser L, Prendki V, Schrenzel J, et al. Effects of antibiotic duration on the intestinal microbiota and resistome: the PIRATE RESISTANCE project, a cohort study nested within a randomized trial. EBioMedicine. 2021;71:103566. https://doi.org/10.1016/j.ebiom.2021.103566
32. Rashid MU, Zaura E, Buijs MJ, Keijser BJ, Crielaard W, Nord CE, et al. Determining the long-term effect of antibiotic administration on the human normal intestinal microbiota using culture and pyrosequencing methods. Clin Infect Dis. 2015;60(Suppl 2):S77–84. https://doi.org/10.1093/cid/civ137
33. Zaura E, Brandt BW, Teixeira de Mattos MJ, Buijs MJ, Caspers MP, Rashid MU, et al. Same exposure but two radically different responses to antibiotics: resilience of the salivary microbiome versus long-term microbial shifts in feces. MBio. 2015;6:e01693–15. https://doi.org/10.1128/mBio.01693-15
34. Solbach P, Chhatwal P, Woltemate S, Tacconelli E, Buhl M, Autenrieth IB, et al. Microbiota-associated risk factors for *Clostridioides difficile* acquisition in hospitalized patients: a prospective, multicentric study. Clin Infect Dis. 2021;73:e2625–34. https://doi.org/10.1093/cid/ciaa871
35. Maier L, Pruteanu M, Kuhn M, Zeller G, Telzerow A, Anderson EE, et al. Extensive impact of non-antibiotic drugs on human gut bacteria. Nature. 2018;555:623–8. https://doi.org/10.1038/nature25979

Address for correspondence: Majerle Reeves, Centers for Disease Control and Prevention, 1600 Clifton Rd NE, Mailstop H16-B, Atlanta, GA 30329-4018, USA; email: utg7@cdc.gov

Global Genomic Surveillance of Middle East Respiratory Syndrome Coronavirus

James Richard Otieno, Ahmed Mohammed Albarraq, Francis Amirtharaj Selvaraj, Amna Omair Al Mehairi, Esam Ibraheem Azhar, Christopher Ruis, Hasan Zackaria Ali Ishaq, Asma Abi Mohamed Shah, Zelalem Tadesse, Qiu Yu, Ihab El Masry, Hala Abou El Naja, Belinda L. Herring, Amal Barakat, Maria Van Kerkhove, Sophie von Dobschuetz, Lorenzo Subissi

Middle East respiratory syndrome coronavirus (MERS-CoV) is a persistent zoonotic and epidemic threat. We analyzed 807 publicly available human- and camel-derived MERS-CoV genomes collected during 2012–2024 to assess global genomic surveillance. Most sequences originated from Saudi Arabia and the United Arab Emirates. Major gaps in surveillance persist across Africa and South and Central Asia despite large camel populations, active trade, and evidence of viral circulation. Phylogenetic analysis confirmed predominance of clade B in the Arabian Peninsula and clade C in East Africa, consistent with regional patterns. We identified uneven sampling, incomplete metadata, and long delays between sample collection and public sequence submission, often spanning years. Those limitations reduce the value of genomic data for timely situational awareness. Integrating genomic with population and trade data supports timelier, more representative, and coordinated One Health surveillance for MERS-CoV but reveals major blind spots.

Middle East respiratory syndrome coronavirus (MERS-CoV) was first detected in humans in 2012 (*1*). Saudi Arabia has recorded 84% of the 2,617 laboratory-confirmed human cases reported to the World Health Organization (WHO) as of May 2025 (*2*). Although limited human-to-human transmission has been documented within healthcare settings and in communities, most human infections are linked directly or indirectly to contact with infected dromedary camels, the main animal reservoir (*3*). In camels, infection is usually asymptomatic or mild (*4*), whereas infected humans can suffer severe respiratory illness and a crude case-fatality ratio of ≈37% (*5*). More than a decade after its discovery, MERS-CoV remains a public health concern because of its epidemic and pandemic potential, severe clinical outcomes, and the absence of licensed vaccines or therapeutics (*6*).

MERS-CoV belongs to the *Merbecovirus* subgenus within the genus *Betacoronavirus*, which also includes severe acute respiratory syndrome coronavirus (SARS-CoV), which caused the SARS epidemic in 2002–2003, and SARS-CoV-2, responsible for the COVID-19 pandemic (*7*). Three major clades within the MERS-CoV phylogeny have been identified, clades A, B and C, which differ in their geographic distribution and ecology. Differences in the clades phenotypic properties are still being investigated (*8*). Understanding MERS-CoV genetic diversity therefore remains necessary for situational awareness, interpretation of transmission patterns, and future preparedness planning (*9*,*10*).

Genomic epidemiology has become a critical component of pathogen surveillance, enabling the description of pathogen diversity, the contextualization of outbreaks, and identifying changes in circulating lineages over time (*11*). However, the utility of genomic surveillance depends not only on the existence of and access to sequence data but also on

Author affiliations: World Health Organization, Geneva, Switzerland (J.R. Otieno, M. Van Kerkhove, S. von Dobschuetz, L. Subissi); Public Health Authority, Riyadh, Saudi Arabia (A.M. Albarraq); PureLab, Sheikh Khalifa Medical City, Abu Dhabi, United Arab Emirates (F.A. Selvaraj, A.O. Al Mehairi); Khalifa University, Abu Dhabi (F.A. Selvaraj); King Fahd Medical Research Center and Department of Medical Laboratory Sciences, King Abdulaziz University, Jeddah, Saudi Arabia (E.I. Azhar); University of Cambridge, Cambridge, UK (C. Ruis); Abu Dhabi Agriculture and Food Safety Authority, Abu Dhabi (H.Z.A. Ishaq, A.A.M. Shah); Food and Agriculture Organization of the United Nations, Rome, Italy (Z. Tadesse, Q. Yu, I. El Masry); World Health Organization, Cairo, Egypt (H.A. El Naja, A. Barakat); World Health Organization, Manila, the Philippines (B.L. Herring)

DOI: https://doi.org/10.3201/eid3211.260668

how representative, timely, and well annotated those data are. Recent reviews have documented major MERS-CoV surveillance and research gaps, such as incomplete virologic and serologic evidence in dromedary populations from Africa and South and Central Asia, uneven genomic characterization, and regional differences in research priorities (*12*–*14*). MERS-CoV sequence availability remains uneven across regions, and the extent to which currently available public genomic data support global situational awareness remains unclear.

MERS-CoV exhibits distinct epidemiologic patterns across regions. In Africa, clade C predominates in dromedary camels, yet we could not find evidence of officially reported autochthonous human cases despite serologic evidence of infection among occupationally exposed humans in some settings (*15*). Recent systematic reviews similarly highlight limited and uneven virologic and genomic evidence from camel populations in Africa (*12*,*13*). In the Arabian Peninsula, clade B predominates and is associated with high infection rates in dromedary camels and repeated spillover into humans, alongside occasional human-to-human transmission. Transmission intensity might vary seasonally, with increased spillover risk after the camel calving season, when maternally derived immunity in young camels declines and susceptibility increases (*16*). Although the reasons underlying those regional differences are not fully resolved, ex vivo studies suggest biological differences between clades, including variation in replication efficiency and host cell entry, that might contribute to their distinct epidemiologic patterns (*17*). Of note, recent detection of clade B sequences in camels from Africa suggests possible geographic expansion and underscores the importance of representative genomic surveillance (*18*,*19*).

We evaluated the current landscape of publicly available MERS-CoV genomic data as a surveillance resource. Rather than reconstructing the full evolutionary history of MERS-CoV, we assessed whether existing genomic data support timely and representative situational awareness. Specifically, we assessed sequence availability by country, host, and year; examined the completeness and operational usefulness of accompanying metadata; analyzed turnaround time between sample collection and public sequence submission; and contextualized genomic sampling against camel population size and reported camel trade flows. Our findings highlight practical gaps that might limit genomic risk assessment and suggest priorities for strengthening One Health surveillance.

Methods

Dataset Curation

On August 18, 2026, we retrieved all MERS-CoV sequences from GenBank by using the following taxonomy identifier query: (txid1335626[Organism:exp] OR txid1298362[Organism:exp] OR txid1306931[Organism:exp]) (Appendix 1, http://wwwnc.cdc.gov/EID/article/32/11/26-0668-App1.xlsx) (*20*). We restricted analyses to human- and camel-derived sequences because these hosts represent the main epidemiologic interface for zoonotic transmission. To improve dataset reliability and comparability, we excluded sequences containing >10% ambiguous bases or <15,000 nucleotides, ≈50% of the reference genome length (30,119 bp) (National Center for Biotechnology Information RefSeq [https://www.ncbi.nlm.nih.gov/refseq] identification no. NC_019843.3). We supplemented missing or incomplete metadata, including geographic origin, host species, and collection dates, where possible through cross-referencing with published literature and public reports. We used the resulting curated dataset for all downstream analyses.

To support standardized genomic classification and quality assessment, we also developed a MERS-CoV Nextclade community dataset on the basis of the curated reference genome and clade framework used in this study (https://nextstrain.org/community/jrotieno/mers_cov). This resource is intended to enable more consistent clade assignment and interpretation across MERS-CoV genomic analyses.

Sequence Alignments and Phylogenetic Analysis

We conducted multiple sequence alignment of the MERS-CoV genome sequences at the nucleotide level by using MAFFT version 7.526 with default parameters (*21*). We undertook manual inspection and editing of the alignments on AliView version 1.30 to ensure robust and accurate alignment of the dataset (*22*). We reconstructed phylogenetic trees by using IQ-TREE version 3.1.3 and by using the best-fit nucleotide substitution model (general time reversible plus empirical base frequencies plus invariable sites plus discrete gamma model with 4 rate categories) identified by using ModelFinder on the basis of the Bayesian information criterion (*23*,*24*). We used ultrafast bootstrap analysis (1,000 replicates) to assess branch support (*25*), and visualized trees in FigTree version 1.4.4 (https://tree.bio.ed.ac.uk/software/figtree).

We verified MERS-CoV clade assignments through comparison with reference sequences and analysis of tree topology. To validate clade assignment accuracy, we considered additional metadata, including geographic origin and host species.

Because this study evaluated public genomic data as a surveillance resource, our phylogenetic analyses contextualized known MERS-CoV clades across regions, hosts, and time rather than inferring detailed transmission histories or evolutionary rates. To summarize genetic diversity within clades, we calculated the mean and median pairwise distances by using the *dist.dna* function (model = raw) from the ape package in R version 4.6.1 (The R Project for Statistical Computing, https://www.r-project.org), applying pairwise deletion to handle missing data.

Turnaround Time Analysis

To evaluate timeliness of public genomic data sharing, we calculated turnaround time (TAT) as the interval between sample collection and public sequence submission dates. We excluded sequences lacking complete collection or submission date metadata. We summarized TAT primarily by using median values to reduce the influence of extreme outliers and stratified results by WHO region, host, and year when possible. Because rapid sequence availability is central to public health value of genomic surveillance, we treated TAT as an operational indicator of surveillance performance rather than a virologic characteristic.

Camel Population and Movement Data

To contextualize genomic sampling in relation to camel populations, trade patterns, and sequence sampling density, we used camel population and trade data from the Food and Agriculture Organization of the United Nations statistics database (FAOSTAT, https://www.fao.org/faostat). FAOSTAT reports aggregate camel populations without distinguishing between dromedary and Bactrian camels. We used data as broad contextual indicators of camel-associated surveillance coverage and not as species-specific estimates of dromedary reservoir size.

To align with the temporal coverage of the MERS-CoV sequence data, we restricted analyses to 2013–2024 for camel population and trade metrics. Camel data from 2025 were unavailable, and 2012 was excluded from some summary analyses because only 6 genomic sequences were available from that year.

We calculated annual camel sequence sampling density per 1 million camels and estimated country-level sampling density by using the median camel population over the study period. Those metrics were defined as:

$$\text{Sampling density per year (per 1 million camels} = \frac{\text{no. camel sequences for year}}{\text{camel population for year}} \times 1 \text{ million}$$

$$\text{Country sampling density (per 1 million camels)} = \frac{\text{country total camel sequences}}{\text{country median camel population}} \times 1 \text{ million}$$

We visualized live camel trade flows to identify settings where genomic surveillance might be limited relative to the scale and connectivity of animal movement networks. Those analyses were intended to provide ecologic and operational context for surveillance interpretation, rather than to directly infer viral movement through trade.

Results

Geographic Concentration of MERS-CoV Genomic Data

We identified 1,738 MERS-CoV sequence records. After restricting the dataset to human- and camel-derived sequences and applying predefined length, ambiguity, and metadata curation criteria, we retained 807 sequences for analysis. Sequences represented 18 countries across 6 WHO regions, and collection dates spanned 2012–2025 (Appendix 1). The dataset comprised 449 (55.6%) camel-derived sequences and 358 (44.4%) human-derived sequences. Most sequences belonged to clade B (89.3%; n = 721 sequences, 356 human, 365 camel), whereas clade C accounted for 83 genomes (10.3%, all camel) and clade A for 3 genomes (0.4%, 2 human, 1 camel).

Of the 807 genomes, 52.5% originated from Saudi Arabia, making it by far the largest contributor to the public MERS-CoV sequence record (Figure 1). Together, Saudi Arabia and the United Arab Emirates (UAE) accounted for 75.0% of all genomes analyzed. Saudi Arabia contributed both camel- and human-derived sequences from many years, whereas the UAE dataset was concentrated during 2013–2017 and was predominantly camel-derived. The remaining countries contributed ≤5% of all genomes individually, highlighting the narrow geographic basis of the current public evidence base (*15*,*26*–*30*).

Regionally, the WHO Eastern Mediterranean Region (EMR) (including Morocco, Tunisia, Libya, Egypt, Sudan, Djibouti, and Somalia) contributed 681 (84.4%) genomes to the public dataset. However, the WHO African Region (AFR) contributed only 67 (8.3%) genomes, indicating substantial underrepresentation of key transmission settings in the global

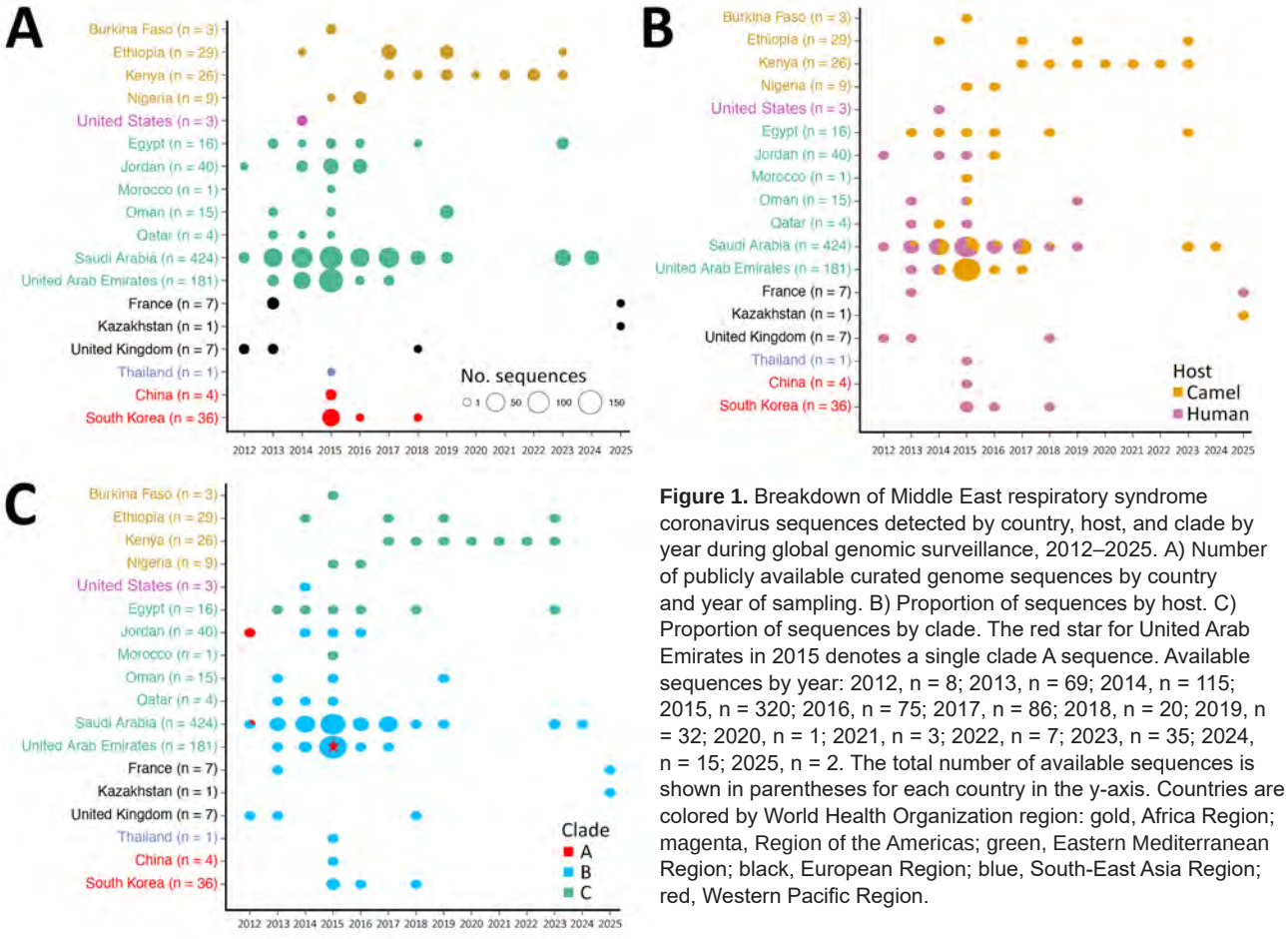

Figure 1. Breakdown of Middle East respiratory syndrome coronavirus sequences detected by country, host, and clade by year during global genomic surveillance, 2012–2025. A) Number of publicly available curated genome sequences by country and year of sampling. B) Proportion of sequences by host. C) Proportion of sequences by clade. The red star for United Arab Emirates in 2015 denotes a single clade A sequence. Available sequences by year: 2012, n = 8; 2013, n = 69; 2014, n = 115; 2015, n = 320; 2016, n = 75; 2017, n = 86; 2018, n = 20; 2019, n = 32; 2020, n = 1; 2021, n = 3; 2022, n = 7; 2023, n = 35; 2024, n = 15; 2025, n = 2. The total number of available sequences is shown in parentheses for each country in the y-axis. Countries are colored by World Health Organization region: gold, Africa Region; magenta, Region of the Americas; green, Eastern Mediterranean Region; black, European Region; blue, South-East Asia Region; red, Western Pacific Region.

genomic dataset. Sequences were also available from the WHO European region (n = 15, from France, the United Kingdom, and Kazakhstan) and the Region of the Americas (n = 3, from the United States). The human sequences from those 2 regions were mainly associated with travel-related MERS-CoV cases exposed in the Arabian Peninsula and rare, limited onward human-to-human transmission (*31*,*32*). The Kazakhstan sequence was obtained from a resident camel and characterized as clade B. We used WHO regional groupings to summarize surveillance contributions and operational patterns, not to imply biologically homogeneous evolutionary units.

TAT is a key determinant of the operational value of genomic surveillance (*33*). Across the global MERS-CoV dataset, TAT varied markedly by region and time (Appendix 2 Figure, http://wwwnc.cdc.gov/EID/article/32/11/26-0668-App1.pdf). Early submissions, particularly in 2013–2014, had shorter delays, whereas more recent submissions often reflected substantially longer lags, in some cases exceeding 5 years. Overall, median TAT increased over time, with wide variability between countries and submission periods. Our results indicate that MERS-CoV sequences might not be available in time to support real-time situational awareness, outbreak interpretation, or timely assessment of changes in circulating viral diversity.

MERS-CoV Clades Phylogenetic Structure, Geographic Distribution, and Host Associations

MERS coronaviruses exhibit distinct evolutionary and epidemiologic characteristics by clade and host (Figures 2–4). Clade C (n = 78) viruses are characterized by long branch lengths (Figure 2) and a median pairwise nucleotide distance of 159 nucleotide bases (mean 152 bases, SD ± 0.80), consistent with their genetic divergence within camel populations sampled in both WHO EMR and AFR (Figures 3, 4). Whereas clade A had too few genomic sequences (n = 3) to generate a meaningful estimate, clade B (n = 716) had a median pairwise distance of 57 bases (mean 68 bases, SD ± 0.06).

In publicly available genomic data, in EMR, clade B has replaced clade A, with the last clade A sequence from the region collected from a camel in 2015 (*34*).

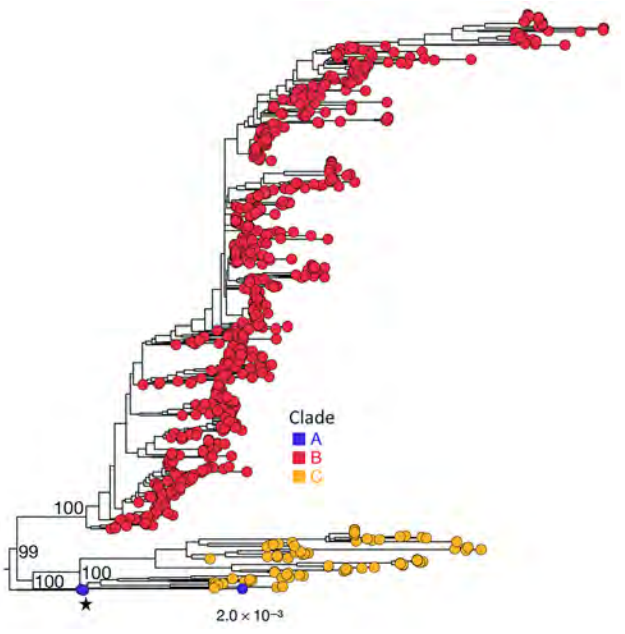

Figure 2. Maximum-likelihood phylogenetic tree highlighting the primary Middle East respiratory syndrome coronavirus clades described during global genomic surveillance, 2012–2025. The tree is rooted on a clade A sequence from GenBank (accession no. KC776174.1), indicated by the black star. The branches are colored by clade. Bootstrap values are shown for major nodes.

Although clade B MERS-CoV sequences have historically been restricted to the Arabian Peninsula, recent genomic surveillance has documented the introduction of clade B sequences into the continent of Africa, specifically identified in dromedary camels from Egypt (*19*). As clade B continues to diversify (Figure 5, panel A), those viruses have been characterized into multiple lineages (*35*–*37*). Apart from a single travel-related human sequence collected in December 2025, the most recent human clade B sequences date back to January 2024, underscoring the need to monitor geographic distribution and lineage composition in exposed camel and human populations.

Clade C has been identified in WHO AFR (Kenya, Burkina Faso, Ethiopia, and Nigeria) and EMR (Egypt and Morocco), with all the sequences coming from continental Africa (*29*,*38*,*39*). The clade C phylogenetic tree (Figure 5, panel B) demonstrates temporal and geographic clustering, especially among sequences from Ethiopia and Kenya, including recent clusters from Kenya during 2022–2023, compatible with ongoing circulation and diversification in parts of East Africa. Sequences from Egypt were found across multiple sampling years and included a recent 2023 camel-associated cluster, whereas sequences from Nigeria formed a geographically distinct but temporally limited cluster during 2015–2016 (*19*). Sparse and uneven sampling limits wider regional interpretation. To date, clade C has been associated with human infections only indirectly (*15*); however, underreporting cannot be ruled out (*17*).

Surveillance Gaps and Implications for MERS-CoV Transmission

Among 47 countries with available camel population data (Figure 6), 27 had median populations >100,000 animals and 9 had median populations >1 million animals. Because FAOSTAT does not distinguish dromedary from Bactrian camels, those figures represent aggregate camel populations and should be interpreted as contextual indicators rather than direct estimates of the distribution of the MERS-CoV dromedary reservoir. Camel-derived MERS-CoV genomes were available from 12 countries, but only 10 (37.0%) of the 27 countries with median camel populations of >100,000 animals were represented. That comparison indicates gaps in genomic surveillance relative to camel populations and recognizes that the denominator is not species-specific.

We calculated a contextual sampling-density metric as the number of genomes per 1 million camels, stratified by country and year (Figure 7). The data demonstrated disparities in sampling efforts; genomic sequences per 1 million camels were a median of 353 for Saudi Arabia, 334 for UAE, 103 for Egypt, 20 for Ethiopia, 10 for Qatar, and 7 for Kenya. No formal minimum sampling density is established according to our literature review; nevertheless, those

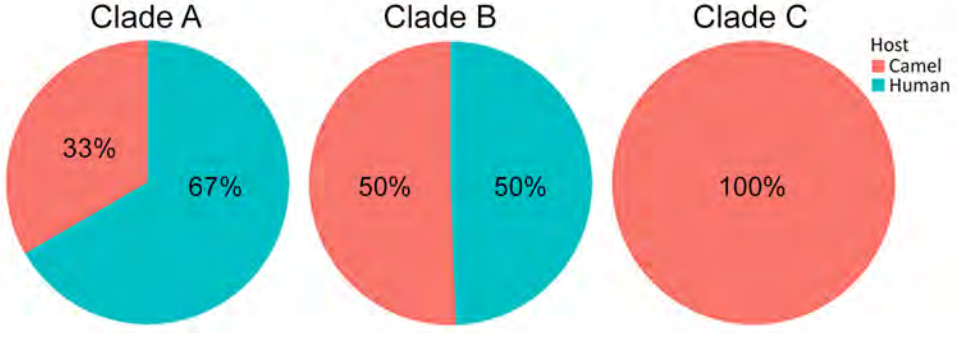

Figure 3. Percentages of clades A, B, and C Middle East respiratory syndrome coronavirus sequences, by host species, described during global genomic surveillance, 2012–2025.

findings demonstrate substantial heterogeneity and support more consistent, geographically representative camel surveillance.

Live camel trade might create opportunities for cross-border virus movement, but currently available trade and genomic data are insufficient to quantify that relationship directly. Nevertheless, the scale and complexity of camel trade flows highlight surveillance blind spots in several highly connected settings (Figure 8). We observed substantial trade activity among countries in EMR and between parts of Africa and the Arabian Peninsula, although genomic data remained absent or outdated for several countries participating in those networks. Those findings support stronger surveillance at transit, market, and other animal-human interface settings. Of note, trade flows are not evidence of MERS-CoV infection, infected-animal movement, or viral circulation; they are presented only as contextual indicators of animal-movement connectivity. Australia is a useful example because its large feral dromedary population might not be fully represented in conventional livestock statistics (*40*). The small Australia-directed flows shown (Figure 8), 5 camels in 2015 and 1 in 2021, indicate animal movement only and should not be interpreted as evidence of MERS-CoV infection or circulation in Australia.

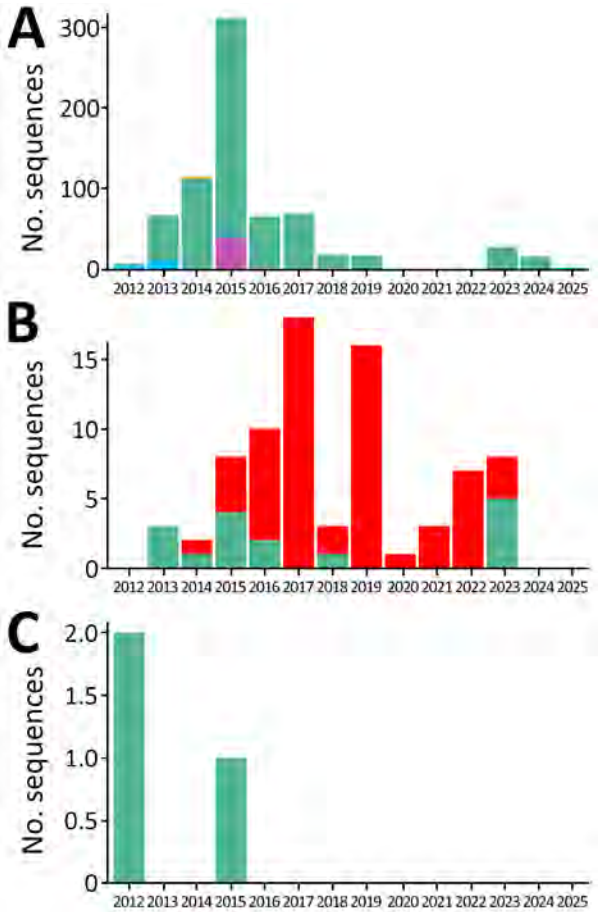

Figure 4. Temporal and regional distribution of Middle East respiratory syndrome coronavirus sequences for each clade described during global genomic surveillance, 2012–2025. A) Clade B, n = 721; B) clade C, n = 83; C) clade A, n = 3. Bar colors indicate World Health Organization region: gold, Africa Region (AFR); magenta, Region of the Americas (AMR); green, Eastern Mediterranean Region (EMR); black, European Region (EUR); blue, South-East Asia Region (SEAR); red, Western Pacific Region (WPR).

Discussion

We evaluated the extent to which publicly available genomic data support global situational awareness for MERS-CoV. More than a decade after MERS-CoV was first identified, the public genomic record remains highly concentrated in a small number of countries, with major gaps in representativeness, metadata completeness, and timeliness. Those limitations constrain not only comparative phylogenetic interpretation but also the practical use of genomics for surveillance, risk assessment, and operational decision-making across both human and animal health systems.

Available genomic data show that clade B dominates among publicly available human and camel genomes from the Arabian Peninsula, whereas clade C remains largely represented by camel-derived genomes from Africa. Those findings are consistent with previous reports and support marked regional phylogenetic structure. However, the limited and uneven availability of genomes, particularly from settings in Africa and South and Central Asia, means that crucial components of viral diversity might remain unsampled. Recent MERS-CoV clade B genomes detected in camels originating from Egypt and Kazakhstan underscore the importance of geographically representative genomic surveillance and generation of full-length genome sequences for timely risk assessment (*18*,*19*). Although the current data identify surveillance gaps and broad phylogenetic structure, they do not enable definitive conclusions about global evolutionary dynamics.

Our findings complement recent reviews of MERS-CoV epidemiology, camel infection, genomic features, and regional research priorities (*12*,*13*). Whereas previous studies primarily synthesized epidemiologic or genomic evidence, our study evaluates the public genomic record as an operational surveillance resource by quantifying geographic representation, metadata completeness, submission delays, and coverage relative to camel populations and trade

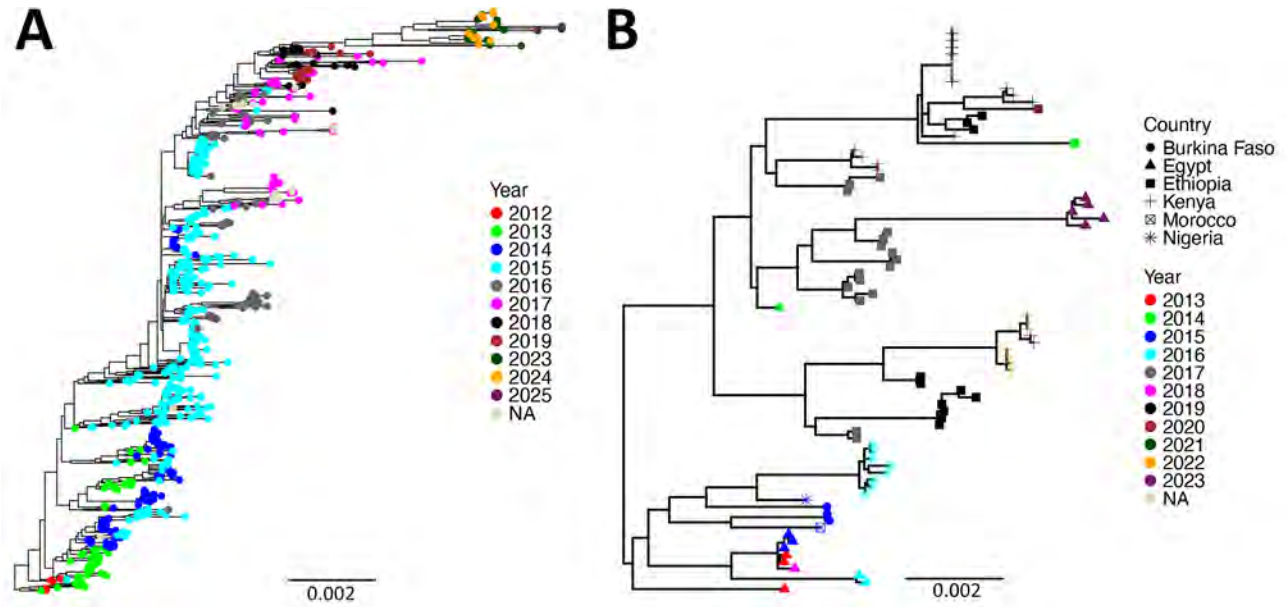

Figure 5. Maximum-likelihood phylogenetic trees of Middle East respiratory syndrome coronavirus described during global genomic surveillance, 2012–2025. A) Clade B sequences. The tips are colored by the year of sample collection. B) Clade C sequences. The tip-shape represents the country of isolation, and the color represents the year of sample collection. Scale bars indicate nucleotide substitutions per site.

networks. We observed large disparities in camel genomic sampling density across countries with substantial camel populations. Median sequence density was far higher in Saudi Arabia and UAE than in Kenya or Ethiopia, whereas several countries with large camel populations lacked publicly available genomic data. Those disparities likely reflect targeted studies, differences in laboratory capacity, funding, and data-sharing practices. Our findings support context-appropriate reporting standards for camel genomic surveillance and the need for clearer denominator data.

The integration of camel population and trade data provides an operational perspective on where genomic surveillance might be most incomplete. Although our analyses do not directly demonstrate trade-mediated viral movement, they show that several countries participating in major trade networks have limited, outdated, or no public genomic data. That gap is particularly relevant for routes linking endemic areas and high-contact animal movement corridors. Better integration of genomic, epidemiologic, and animal movement data would improve

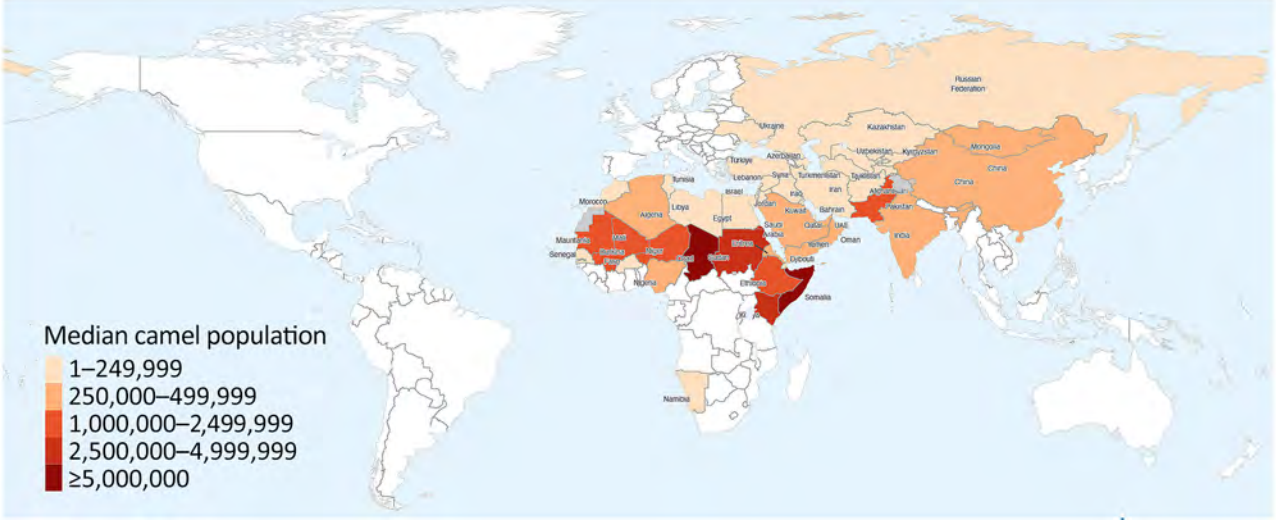

Figure 6. Median camel populations by country described during global genomic surveillance, 2012–2025. Map courtesy of the World Health Organization.

interpretation of cross-border risk and help prioritize surveillance in high-connectivity settings.

A contribution of note is the analysis of TAT from sample collection to public sequence submission. Although sequence availability is often used as a proxy for surveillance effort, timeliness is equally critical for public health utility. Many MERS-CoV genomes are shared only after substantial delays, often years after collection, limiting their utility for timely risk assessment or outbreak interpretation. Those delays likely reflect differences in surveillance design, sequencing workflows, publication timelines, and data-sharing practices. For MERS-CoV, improving TAT might be crucial, as well as increasing the absolute number of publicly available genomes, and particularly relevant for a zoonotic pathogen with sporadic spillover and fragmented surveillance.

The main challenge for MERS-CoV genomics is ensuring that sequence data are representative, timely, and interpretable enough to support public health action. Strengthening routine genomic surveillance in camels and humans, improving metadata completeness, and reducing delays in public data sharing would increase the operational value of MERS-CoV genomics.

Whole-genome sequencing should be applied strategically rather than universally. Targeted sequencing might be sufficient when the objective is a defined diagnostic, antiviral resistance, or vaccine-relevant genomic region. However, representative full or near-complete genomes provide broader surveillance value by supporting clade and lineage assignment, detecting unexpected genetic changes, assessing recombination, placing sequences in an evolutionary context, and investigating unusual epidemiologic events. A tiered approach combining routine diagnostic testing with representative whole-genome sequencing through national or regional reference laboratories would be appropriate.

Existing global initiatives, such as the WHO Coronavirus Network, provide a platform for strengthening laboratory and analytical capacity, enabling data sharing, and promoting harmonized approaches to genomic surveillance (*41*). However, network representation and national sequencing capacity remain uneven across regions with substantial camel populations or epidemiologic relevance to MERS-CoV. In countries where national sequencing capacity is limited, referral of selected positive specimens to regional reference laboratories could enable representative and timely whole-genome sequencing. The institutional, logistic, and policy factors influencing national participation or specimen referral warrant further investigation.

The first limitation of this study is that the available public genomic dataset is affected by substantial temporal and geographic bias, with more than 75% of genomes originating from Saudi Arabia, the UAE, and neighboring countries in the Arabian Peninsula. Of consequence, the analyses should not be interpreted as a complete description of global MERS-CoV evolutionary dynamics, but rather as an assessment of the current public genomic evidence base and resulting surveillance gaps.

Second, crucial metadata fields were missing for a proportion of sequences, including collection dates, host information, and subnational geographic detail.

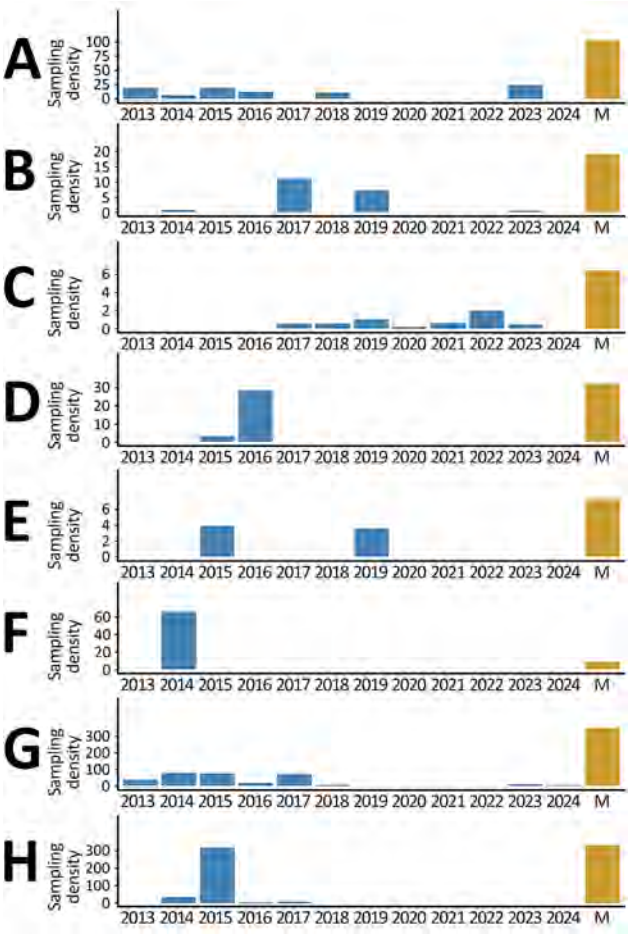

Figure 7. Middle East respiratory syndrome coronavirus sequence sampling density (sequences/1 million camels) by country and year described during global genomic surveillance, 2012–2025. A) Egypt; B) Ethiopia; C) Kenya; D) Nigeria; E) Oman; F) Qatar; G) Saudi Arabia; H) United Arab Emirates. The median sampling density per country is shown by the golden-brown bar to the right. y-axes differ among countries. The Food and Agriculture Organization of the United Nations statistics database does not distinguish dromedary from Bactrian camels; data are therefore presented as contextual indicators of camel-associated surveillance coverage and should not be interpreted as species-specific estimates of dromedary reservoir coverage.

Figure 8. Live camel exports between countries described during global genomic surveillance, 2013–2024. The arrow tail represents the source country and the arrowhead represents destination country. The color of the arrow represents the number of camel exports. Trade flows are contextual indicators of animal movement connectivity and do not provide evidence of Middle East respiratory syndrome coronavirus infection, infected-animal movement, viral introduction, or viral circulation. The Australia-directed flows represent 6 animals in total, 5 in 2015 and 1 in 2021, and should be interpreted accordingly. Map provided by the World Health Organization Health Emergencies Programme using data from the Food and Agriculture Organization of the United Nations statistics database.

Those gaps reduced the number of genomes included in some analyses, particularly TAT, and limited more detailed interpretation of local evolutionary patterns.

Third, camel population and trade data were derived from FAOSTAT and reflect officially collected data only. FAOSTAT does not distinguish dromedary from Bactrian camels and might misrepresent camel populations relevant to MERS-CoV surveillance. Trade statistics might also miss informal or undocumented animal movements and contain no information on infection status. Of consequence, camel population, sampling density, and trade comparisons should be interpreted as contextual indicators rather than precise estimates of dromedary-reservoir surveillance coverage or direct evidence of viral movement. Australia provides an additional example because its large feral dromedary population might not be fully captured by conventional livestock statistics (*40*).

Finally, because this study was designed to evaluate the utility of genomic data for surveillance, we did not perform additional phylogeographic, recombination, or phenotypic analyses. Recombination is a major driver of coronavirus evolution with potential implications for lineage-specific phenotypes and has been explored extensively in previous studies (*37*,*42*–*45*). Such analyses remain a necessary avenue for future work as more representative and timely genomic data become available.

This study reveals that publicly available MERS-CoV genomic data provide a necessary but incomplete foundation for global surveillance. The major constraints include limited sequence generation, uneven representativeness, incomplete metadata, and prolonged delays in public data sharing. By evaluating sequence coverage, TAT, and surveillance context alongside camel population and trade indicators, we identify practical gaps that currently limit the public health utility of MERS-CoV genomics. Strengthening representative sampling, improving the timeliness of sequence sharing, and embedding genomic surveillance within a coordinated One Health framework would enhance the value of those data for risk assessment, preparedness, and response. Improving camel population and trade datasets should also be prioritized. Achieving a One Health framework will require sustained coordination across human, animal, and environmental health sectors, including collaboration among WHO, the Food and Agriculture Organization of the United Nations, the World Organisation for Animal Health, and regional surveillance networks. Such efforts are essential for developing more integrated, timely, and actionable genomic surveillance systems for MERS-CoV and future zoonotic threats.

Acknowledgments

We thank the dedicated professionals involved in clinical care, laboratory diagnosis, and genomic sequencing, whose continuous efforts make it possible to achieve accurate differential diagnoses and generate high-quality data. We also acknowledge the contributions of national public health institutions and surveillance programmes that support the collection, curation, and sharing of genomic and epidemiological data used in this study.

Author contributions: J.R.O., S.v.D., and L.S. conceived the study. J.R.O. and L.S. wrote the first draft. A.A.M.S., F.A.S., A.O.A.M., E.I.A., C.R., H.Z.A.I., A.M.A., Z.T., Q.Y., I.E.M., H.A.E.N., A.B., S.v.D., and M.V.K. reviewed the first draft. All authors reviewed the manuscript and accepted the final version.

About the Author

Dr. Otieno is a researcher with the World Health Organization focused on infectious disease epidemiology, with expertise in zoonotic pathogens and genomic surveillance. His work centers on integrating molecular data with epidemiological and ecological indicators to better understand transmission dynamics and inform public health responses.

References

1. Zaki AM, van Boheemen S, Bestebroer TM, Osterhaus ADME, Fouchier RAM. Isolation of a novel coronavirus from a man with pneumonia in Saudi Arabia. N Engl J Med. 2012;367:1814–20. https://doi.org/10.1056/NEJMoa1211721
2. World Health Organization, European Region Office. MERS outbreaks [cited 2025 Oct 6]. https://www.emro.who.int/health-topics/mers-cov/mers-outbreaks.html
3. Reusken CBEM, Haagmans BL, Müller MA, Gutierrez C, Godeke GJ, Meyer B, et al. Middle East respiratory syndrome coronavirus neutralising serum antibodies in dromedary camels: a comparative serological study. Lancet Infect Dis. 2013;13:859–66. https://doi.org/10.1016/S1473-3099(13)70164-6
4. Adney DR, van Doremalen N, Brown VR, Bushmaker T, Scott D, de Wit E, et al. Replication and shedding of MERS-CoV in upper respiratory tract of inoculated dromedary camels. Emerg Infect Dis. 2014;20:1999–2005. https://doi.org/10.3201/eid2012.141280
5. World Health Organization. Middle East respiratory syndrome. Global summary and assessment of risk. 2022 [cited 2026 Aug 18]. https://www.who.int/publications/i/item/B09692
6. World Health Organization, Food and Agriculture Organization of the United Nations, and World Organisation for Animal Health. Research gaps and needs on Middle East respiratory syndrome coronavirus (MERS-CoV) and other emerging zoonotic coronaviruses: report of the Quadripartite technical meeting, Riyadh, Saudi Arabia, 27–29 November 2023. 2025 [cited 2026 Aug 18]. https://www.who.int/publications/i/item/9789240105812
7. Schoch CL, Ciufo S, Domrachev M, Hotton CL, Kannan S, Khovanskaya R, et al. NCBI taxonomy: a comprehensive update on curation, resources and tools. Database (Oxford). 2020;2020:baaa062. https://doi.org/10.1093/database/baaa062
8. Memish ZA, Perlman S, Van Kerkhove MD, Zumla A. Middle East respiratory syndrome. Lancet. 2020;395:1063–77. https://doi.org/10.1016/S0140-6736(19)33221-0
9. Hilgenfeld R, Peiris M. From SARS to MERS: 10 years of research on highly pathogenic human coronaviruses. Antiviral Res. 2013;100:286–95. https://doi.org/10.1016/j.antiviral.2013.08.015
10. de Wit E, van Doremalen N, Falzarano D, Munster VJ. SARS and MERS: recent insights into emerging coronaviruses. Nat Rev Microbiol. 2016;14:523–34. https://doi.org/10.1038/nrmicro.2016.81
11. Kraemer MUG, Hill V, Ruis C, Dellicour S, Bajaj S, McCrone JT, et al.; COVID-19 Genomics UK (COG-UK) Consortium. Spatiotemporal invasion dynamics of SARS-CoV-2 lineage B.1.1.7 emergence. Science. 2021;373:889–95. https://doi.org/10.1126/science.abj0113
12. Gaddafi MS, Lawal H, Musawa IA, Garba B, Goni MD, Jolayemi KO, et al. Serological and virological evidence of MERS-CoV infection among dromedary camels in Africa: a systematic review and meta-analysis. Vet Res Commun. 2026;50:167. https://doi.org/10.1007/s11259-026-11095-6
13. Ogoti B, Riitho V, Wildemann J, Mutono N, Mureithi M, Oyugi J, et al. Epidemiology and genomic features of MERS coronavirus in Africa: a systematic and meta-analysis review. Int J Infect Dis. 2026;165:108456. https://doi.org/10.1016/j.ijid.2026.108456
14. Lambrou AS, South E, Midgley CM, Harrington C, Wang L, Cubeñas C, et al. Update on the epidemiology of Middle East respiratory syndrome coronavirus—worldwide, 2017–2023. MMWR Morb Mortal Wkly Rep. 2025;74:313–20. https://doi.org/10.15585/mmwr.mm7419a1
15. Munyua PM, Ngere I, Hunsperger E, Kochi A, Amoth P, Mwasi L, et al. Low-level Middle East respiratory syndrome coronavirus among camel handlers, Kenya, 2019. Emerg Infect Dis. 2021;27:1201–5. https://doi.org/10.3201/eid2704.204458
16. Dudas G, Carvalho LM, Rambaut A, Bedford T. MERS-CoV spillover at the camel-human interface. eLife. 2018;7:e31257. https://doi.org/10.7554/eLife.31257
17. Zhou Z, Hui KPY, So RTY, Lv H, Perera RAPM, Chu DKW, et al. Phenotypic and genetic characterization of MERS coronaviruses from Africa to understand their zoonotic potential. Proc Natl Acad Sci U S A. 2021;118:e2103984118. https://doi.org/10.1073/pnas.2103984118
18. Global Early Warning System for Health Threats, World Health Organisation. GLEWS+ risk assessment of the introduction, spread, and zoonotic spillover of MERS-CoV clade B in camel populations of the Nile basin and across Africa [cited 2026 Aug 18]. https://www.who.int/publications/m/item/risk-assessment-of-the-introduction--spread--and-zoonotic-spillover-of-mers-cov-clade-b-in-camel-populations-of-the-nile-basin-and-across-africa
19. Gomaa M, Edwards KM, Wang R, El Taweel A, Moatasim Y, Kutkat O, et al. Local and introduced lineages drive MERS-CoV recombination in Egyptian camels. J Virol. 2025;99:e0064125. https://doi.org/10.1128/jvi.00641-25
20. Sayers EW, Bolton EE, Brister JR, Canese K, Chan J, Comeau DC, et al. Database resources of the national center for biotechnology information. Nucleic Acids Res. 2022;50(D1):D20–6. https://doi.org/10.1093/nar/gkab1112

21. Katoh K, Standley DM. MAFFT multiple sequence alignment software version 7: improvements in performance and usability. Mol Biol Evol. 2013;30:772–80. https://doi.org/10.1093/molbev/mst010
22. Larsson A. AliView: a fast and lightweight alignment viewer and editor for large datasets. Bioinformatics. 2014;30:3276–8. https://doi.org/10.1093/bioinformatics/btu531
23. Minh BQ, Schmidt HA, Chernomor O, Schrempf D, Woodhams MD, von Haeseler A, et al. IQ-TREE 2: new models and efficient methods for phylogenetic inference in the genomic era. Mol Biol Evol. 2020;37:1530–4. https://doi.org/10.1093/molbev/msaa015
24. Kalyaanamoorthy S, Minh BQ, Wong TKF, von Haeseler A, Jermiin LS. ModelFinder: fast model selection for accurate phylogenetic estimates. Nat Methods. 2017;14:587–9. https://doi.org/10.1038/nmeth.4285
25. Hoang DT, Chernomor O, von Haeseler A, Minh BQ, Vinh LS. UFBoot2: Improving the ultrafast bootstrap approximation. Mol Biol Evol. 2018;35:518–22. https://doi.org/10.1093/molbev/msx281
26. Gikonyo S, Kimani T, Matere J, Kimutai J, Kiambi SG, Bitek AO, et al. Mapping potential amplification and transmission hotspots for MERS-CoV, Kenya. EcoHealth. 2018;15:372–87. https://doi.org/10.1007/s10393-018-1317-6
27. Kiambi S, Corman VM, Sitawa R, Githinji J, Ngoci J, Ozomata AS, et al. Detection of distinct MERS-coronavirus strains in dromedary camels from Kenya, 2017. Emerg Microbes Infect. 2018;7:195. https://doi.org/10.1038/s41426-018-0193-z
28. Karani A, Ngere I, Ombok C, Singh D, Jaoko W, Njenga MK, et al. Low prevalence of Middle East respiratory syndrome coronavirus infection in camel-exposed patients presenting with respiratory symptoms in Northern Kenya. Am J Trop Med Hyg. 2025;113:537–42. https://doi.org/10.4269/ajtmh.25-0098
29. Ngere I, Hunsperger EA, Tong S, Oyugi J, Jaoko W, Harcourt JL, et al. Outbreak of Middle East respiratory syndrome coronavirus in camels and probable spillover infection to humans in Kenya. Viruses. 2022;14:1743. https://doi.org/10.3390/v14081743
30. Abroug F, Slim A, Ouanes-Besbes L, Hadj Kacem M-A, Dachraoui F, Ouanes I, et al.; World Health Organization Global Outbreak Alert and Response Network Middle East Respiratory Syndrome Coronavirus International Investigation Team. Family cluster of Middle East respiratory syndrome coronavirus infections, Tunisia, 2013. Emerg Infect Dis. 2014;20:1527–30. https://doi.org/10.3201/eid2009.140378
31. Mailles A, Blanckaert K, Chaud P, van der Werf S, Lina B, Caro V, et al.; The investigation team Collective. First cases of Middle East respiratory syndrome coronavirus (MERS-CoV) infections in France, investigations and implications for the prevention of human-to-human transmission, France, May 2013. Euro Surveill. 2013;18:20502. https://doi.org/10.2807/ese.18.24.20502-en
32. Bialek SR, Allen D, Alvarado-Ramy F, Arthur R, Balajee A, Bell D, et al.; Centers for Disease Control and Prevention. First confirmed cases of Middle East respiratory syndrome coronavirus (MERS-CoV) infection in the United States, updated information on the epidemiology of MERS-CoV infection, and guidance for the public, clinicians, and public health authorities—May 2014. MMWR Morb Mortal Wkly Rep. 2014;63:431–6.
33. Han AX, Toporowski A, Sacks JA, Perkins MD, Briand S, van Kerkhove M, et al. SARS-CoV-2 diagnostic testing rates determine the sensitivity of genomic surveillance programs. Nat Genet. 2023;55:26–33. https://doi.org/10.1038/s41588-022-01267-w
34. Lau SKP, Wernery R, Wong EYM, Joseph S, Tsang AKL, Patteril NAG, et al. Polyphyletic origin of MERS coronaviruses and isolation of a novel clade A strain from dromedary camels in the United Arab Emirates. Emerg Microbes Infect. 2016;5:e128. https://doi.org/10.1038/emi.2016.129
35. Cotten M, Watson SJ, Zumla AI, Makhdoom HQ, Palser AL, Ong SH, et al. Spread, circulation, and evolution of the Middle East respiratory syndrome coronavirus. MBio. 2014;5:e01062–13. https://doi.org/10.1128/mBio.01062-13
36. Sabir JSM, Lam TT-Y, Ahmed MMM, Li L, Shen Y, Abo-Aba SEM, et al. Co-circulation of three camel coronavirus species and recombination of MERS-CoVs in Saudi Arabia. Science. 2016;351:81–4. https://doi.org/10.1126/science.aac8608
37. Hassan AM, Mühlemann B, Al-Subhi TL, Rodon J, El-Kafrawy SA, Memish Z, et al. Ongoing evolution of Middle East respiratory syndrome coronavirus, Saudi Arabia, 2023–2024. Emerg Infect Dis. 2025;31:57–65. https://doi.org/10.3201/eid3101.241030
38. Chu DKW, Hui KPY, Perera RAPM, Miguel E, Niemeyer D, Zhao J, et al. MERS coronaviruses from camels in Africa exhibit region-dependent genetic diversity. Proc Natl Acad Sci U S A. 2018;115:3144–9. https://doi.org/10.1073/pnas.1718769115
39. Chu DKW, Poon LLM, Gomaa MM, Shehata MM, Perera RAPM, Abu Zeid D, et al. MERS coronaviruses in dromedary camels, Egypt. Emerg Infect Dis. 2014;20:1049–53. https://doi.org/10.3201/eid2006.140299
40. Crameri G, Durr PA, Barr J, Yu M, Graham K, Williams OJ, et al. Absence of MERS-CoV antibodies in feral camels in Australia: implications for the pathogen's origin and spread. One Health. 2015;1:76–82. https://doi.org/10.1016/j.onehlt.2015.10.003
41. World Health Organization WHO Coronavirus Network (CoViNet) [cited 2026 Aug 18]. https://www.who.int/groups/who-coronavirus-network
42. Gomaa M, Edwards KM, Wang R, El Taweel A, Moatasim Y, Kutkat O, et al. Local and introduced lineages drive MERS-CoV recombination in Egyptian camels. J Virol. 2025;99:e0064125. https://doi.org/10.1128/jvi.00641-25
43. So RTY, Hui KPY, Ho JCW, Lau KKM, Zhou Z, Chan MCW, et al. The impact of clade B lineage 5 MERS coronaviruses spike mutations from 2015 to 2023 on virus entry and replication competence. PLoS Pathog. 2026;22:e1013336. https://doi.org/10.1371/journal.ppat.1013336
44. Tolentino JE, Lytras S, Ito J, Sato K. Recombination analysis on the receptor switching event of MERS-CoV and its close relatives: implications for the emergence of MERS-CoV. Virol J. 2024;21:84. https://doi.org/10.1186/s12985-024-02358-2
45. Schroeder S, Mache C, Kleine-Weber H, Corman VM, Muth D, Richter A, et al. Functional comparison of MERS-coronavirus lineages reveals increased replicative fitness of the recombinant lineage 5. Nat Commun. 2021;12:5324. https://doi.org/10.1038/s41467-021-25519-1

Address for correspondence: Lorenzo Subissi, Health Emergency Preparedness and Response Programme, World Health Organization, Avenue Appia 20, CH-1211 Geneva 27, Switzerland; email: subissil@who.int

Emergence of Novel Macrolide-Resistant *Mycoplasma pneumoniae* Sequence Type 3 Subclades in Children after COVID-19 Pandemic, Taiwan

Yu-Chia Hsieh, Chen-Ching Lin, Jia-Wen Wu, Yi-Hsuan Liu, Yi-Jiun Pan, Tzu-Ya Lo, Shian-Sen Shie, Huey-Ling You, Chong-Wei Huang, Yi-Chuan Huang, Tzu-Ching Huang, Yu-Xin She, Yin-Cheng Chen,[1] Shiao-Wen Li[1]

Post–COVID-19 pandemic *Mycoplasma pneumoniae* resurgences have occurred globally and have been particularly severe in Taiwan. We conducted a multicenter study to assess *M. pneumoniae* trends in children. Compared with the 2019 peak, 2024 data revealed a doubling of incidence (546/100,000 population), a 2.2-fold increase in intensive care unit admissions (10.9/100,000 population), and a 13.7-fold surge in central nervous system complications (6.1/100,000 population). In a 2023–2024 prospective cohort (n = 226), intensive care unit admission risk factors were neutrophils >7,000/μL (adjusted odds ratio [aOR] 6.2 [95% CI 1.3–29.9]), platelets >400 × 103/μL (aOR 12.5 [95% CI 2.7–57.9]), pleural effusion (aOR 9.7 [95% CI 1.6–58.1]), and central nervous system involvement (aOR 27.9 [95% CI 4.1–188.3]). Phylogenetic analysis of 698 genomes demonstrated that 4 emerging subclades replaced pre–COVID-19 lineages by mid-2024; 1 subclade was associated with severe outcomes, highlighting evolving resistant, neurotropic lineages and calling for enhanced surveillance.

After the height of the COVID-19 pandemic, *Mycoplasma pneumoniae* respiratory infections did not reemerge as quickly as influenza or respiratory syncytial virus did, likely because of the pathogen's long incubation period, long periodicity, and slow growth rate (*1*). *M. pneumoniae* activity increased markedly in mid-2023, leading to unprecedented epidemics and varying disease severity across multiple countries worldwide. In parts of Europe and the United States, where macrolide resistance remains <10%, an increase in severe pediatric cases has been reported in Spain, England, and Texas (USA), but not in the Netherlands, Norway, or Denmark (*2*–*5*). France and Switzerland documented high rates of intensive care unit (ICU) admissions among adults (*6*,*7*). In contrast, a highly publicized outbreak in China was notable for an exceptionally high macrolide resistance rate (90%–100%) and a substantial burden of severe disease, primarily affecting children (*8*). Although prolonged fever is frequently reported in macrolide-resistant *M. pneumoniae* infections, an increased risk for complications or ICU admission compared with macrolide-sensitive strains has not been consistently demonstrated (*9*,*10*). Nevertheless, *M. pneumoniae* is increasingly associated with severe clinical manifestations, irrespective of macrolide resistance, although the role of genetic evolution in that trend remains unclear. Timely diagnosis and initiation of appropriate therapy are crucial to reducing disease duration and preventing progression to severe illness requiring intensive care (*7*).

Author affiliations: Chang Gung Children's Hospital, Chang Gung Memorial Hospital, Chang Gung University, College of Medicine, Taoyuan, Taiwan (Y.-C. Hsieh, J.-W. Wu, Y.-H. Liu, T.-Y. Lo); School of Medicine, National Yang Ming Chiao Tung University, Taipei, Taiwan (C.-C. Lin, Y.-C. Chen); School of Medicine, College of Medicine, People's Republic of China Medical University, Taichung, Taiwan (Y.-J. Pan); Chang Gung Memorial Hospital, Taoyuan (S.-S. Shie); Kaohsiung Chang Gung Memorial Hospital, Kaohsiung, Taiwan (H.-L. You); Keelung Chang Gung Memorial Hospital, Keelung, Taiwan (C.-W. Huang, Y.-C. Huang); School of Medicine, College of Medicine, National Yang Ming Chiao Tung University, Taipei (T.-C. Huang); College of Science Department of Life Sciences, National University of Kaohsiung, Kaohsiung (Y.-X. She, S.-W. Li)

DOI: https://doi.org/10.3201/eid3211.260439

[1]These senior authors contributed equally to this article.

Taiwan has a high prevalence of macrolide-resistant *M. pneumoniae*; resistance rates reached 70% before the COVID-19 pandemic (*10*). In this multisite study, we assessed the effects of the 2023–2024 resurgence among children by comparing the incidence of hospitalization, ICU admission, and neurologic complications across 8 seasons from 2017 through 2024. We also analyzed molecular genetic changes in *M. pneumoniae* and risk factors associated with severe disease in the post–COVID-19 period to better understand pathogen dynamics and inform strategies to combat the disease.

Materials and Methods

Incidence Estimation

This study focused on 2 primary objectives. First, we used the Chang Gung Memorial Hospital (CGMH)–based laboratory surveillance system, which spans 4 branches (Linkou, Taipei, Tucheng, and Kaohsiung), representing one of the largest healthcare networks in Taiwan. The study was approved by the Research Ethics Committee of CGMH (approval no. 202102039A3). We identified positive *M. pneumoniae* cases in children (persons <18 years of age) evaluated across outpatient clinics, emergency departments, general wards, and ICUs through respiratory specimens or cerebrospinal fluid (CSF) samples submitted for clinical care. Diagnostic testing for *M. pneumoniae* across the 4 CGMH branches was clinician-driven on the basis of standardized clinical indications. Testing was routinely ordered by attending physicians for pediatric patients with compatible clinical signs and symptoms, such as acute lower respiratory tract infection, persistent fever, or suspected central nervous system (CNS) manifestations. Respiratory specimens collected during January 2017–December 2024 were tested using real-time PCR (*10*) or, starting in 2019, the BioFire Film Array Respiratory Panel (bioMérieux, https://www.biomerieux.com). For patients with suspected CNS involvement, CSF samples were tested using real-time PCR.

We used data from the National Health Insurance system to estimate the population sizes served by the 4 CGMH branches and then calculated the annual and monthly incidence of *M. pneumoniae* infection. We conducted medical chart reviews to record the diagnosis, hospitalization, ICU admission, and *M. pneumoniae*–related CNS complications, defined as neurologic syndromes occurring in association with *M. pneumoniae* infection, confirmed by PCR detection of *M. pneumoniae* in respiratory or CSF samples, and in the absence of an alternative etiology (*11*). Included manifestations were isolated encephalopathy, encephalitis, brainstem or basal ganglia encephalitis, acute disseminated encephalomyelitis, cerebellitis, Guillain–Barré syndrome, and transverse myelitis. In children demonstrating CNS complications, paired CSF and serum samples were collected on the same day. Paired CSF and serum IgG and albumin concentrations were measured using commercial ELISA kits according to the manufacturer's instructions. The CSF IgG index was calculated using the followings formula:

$$\text{CSF IgG index} = \frac{\text{CSF IgG, mg/dL} \div \text{serum IgG, g/dL}}{\text{CSF albumin, mg/dL} \div \text{serum albumin, g/dL}}$$

Patients with Risk Factors for ICU Admission

For the second primary objective, we extended a previously initiated prospective study that enrolled children <18 years of age with laboratory-confirmed *M. pneumoniae* infection at CGMH during 2023–2024 (*10*). We excluded children with chronic lung disease, genetic or metabolic disorders, neurologic disease, immunodeficiency, or cancer. Diagnosis required compatible clinical features and confirmation by PCR or culture (*10*). For clinically suspected cases, attending physicians obtained throat swab specimens and forwarded them to the CGMH–Linkou central laboratory, after written informed consent had been secured from patients or their legal guardians. We performed DNA extraction and PCR targeting the 23S rRNA gene as described previously (*10*). We performed multilocus sequence typing (MLST) using the *M. pneumoniae* PubMLST scheme and assigned sequence type (ST) according to the allelic profiles of 8 loci (Appendix 1, https://wwwnc.cdc.gov/EID/article/32/11/26-0439-App1.pdf). We recorded demographic, clinical, and laboratory variables prospectively in a standardized case-report form. We defined severe *M. pneumoniae* infection as admission to an ICU.

Isolation of *M. pneumoniae* and Determination of MICs

Oropharyngeal swab, pleural fluid, and CSF samples were collected from pediatric patients and cultured as previously described (*10*). For patients with respiratory infection, culture was performed when respiratory specimens were PCR-positive for *M. pneumoniae*. When CNS involvement occurred, CSF culture was performed only when respiratory or CSF specimens were PCR-positive for *M. pneumoniae*. During the 2023–2024 epidemic in Taiwan, a total of 113 *M. pneumoniae* isolates were

successfully obtained from 234 specimens (222 respiratory specimens, 8 CSF samples, and 4 pleural fluid samples), consisting of 103 isolates from oropharyngeal swab specimens, 7 isolates from cerebrospinal fluid, and 3 isolates from pleural fluid. MIC testing was performed as previously described (*10*).

Whole-Genome Sequencing and Bioinformatic Analysis

We performed whole-genome sequencing on the 113 clinical isolates described previously. We integrated the resulting data with 100 *M. pneumoniae* genomes sequenced in Taiwan during 2018–2020 and published in our previous study (*12*), as well as 485 publicly available global genomes spanning 1960–2024. We quality filtered and assembled raw sequencing reads, then performed separate genome alignments for P1 subtype 1 and P1 subtype 2 against M129 (GenBank accession no. NC_000912.1) and FH (RefSeq assembly accession no. GCF_001272835.1). We generated core-genome single-nucleotide polymorphism alignments using Snippy (https://github.com/tseemann/snippy), then performed phylogenetic reconstruction using Gubbins version 2.4.1 (https://nickjcroucher.github.io/gubbins) (Appendix 1). We identified clade-specific single-nucleotide polymorphisms using a 2-sided 2-proportion test implemented with the prop.test function in R version 4.2.0 (The R Project for Statistical Computing, https://www.r-project.org), applying multiple-testing correction (Appendix 1; Appendix 2, https://wwwnc.cdc.gov/EID/article/32/11/26-0439-App2.xlsx).

Statistical Analysis

We defined incidence rate per 100,000 population as the number of cases divided by estimated population for the year in Taiwan. We defined incidence rate ratio (IRR) as the ratio of incidence rate in year A to incidence rate in year B. We calculated median values and interquartile ranges (IQRs) for continuous variables and used percentages for categorical variables. We compared continuous variables using Mann-Whitney U test; we compared categorical variables using χ^2 test or Fisher exact test. We used logistic regression analysis to identify factors associated with ICU admission. We included variables with $p<0.1$ in the univariate analysis in the multivariate analysis. We considered a $p<0.05$ using a 2-tailed test statistically significant. We performed all statistical analyses using SPSS Statistics version 22.0 (IBM, https://www.ibm.com).

Results

Epidemiologic Trends and Clinical Burden of Pediatric *M. pneumoniae* Infection

M. pneumoniae cases occurred year-round; monthly positivity rates ranged from 10% to 20% on the basis of 100–200 tests. Large-scale outbreaks were observed in both 2019 and 2024; positivity rates peaked at 40%–50% during June–July. *M. pneumoniae* sometimes showed secondary peaks during January–March (Figure 1, panel A). We analyzed monthly and annual incidences of *M. pneumoniae* infection per 100,000 population by age group: 0–4 years, 5–9 years, 10–17 years, and the combined <18 years cohort. Trends in monthly incidence closely paralleled *M. pneumoniae* detection rates; the highest incidence was consistently seen in children 5–9 years of age, followed by those 0–4 years of age and 10–17 years of age, particularly during late spring and summer (Figure 1, panel B). In 2019, incidence increased markedly across all age groups; a roughly 3-fold increase was observed over 2017 and 2018 (Table 1). Although incidence declined during the COVID-19 pandemic, a substantial resurgence was noted after the pandemic. In 2024, incidence rose ≈1.5- to 2-fold in the 0–4 year (470/100,000 populations) and 5–9 year (986/100,000 populations) age groups and tripled in the 10–17 year age group (313/100,000 populations) compared with 2019 levels (Table 1).

M. pneumoniae–associated hospitalization incidence and seasonality closely mirrored overall *M. pneumoniae* incidence across all age groups (Table 1; Figure 1, panel C). We further assessed the effects of post–COVID-19 *M. pneumoniae* outbreaks by analyzing ICU admissions (Table 1; Figure 1, panel D) and neurologic complications; an increase was observed specifically in cases of CNS involvement (Table 1; Figure 1, panel E). The incidence of ICU admissions among children <18 years of age increased from 0.8/100,000 population in 2017 to 4.9/100,000 population in 2019 (incidence rate ratio [IRR] 5.8 [95% CI 1.3–26.2]; p = 0.02). Compared with 2019, ICU admission incidence further rose to 10.9/100,000 population in 2024 (IRR 2.2 [95% CI 1.1–4.5]; p = 0.03). Meanwhile, CNS complications showed a striking rise, from 0.4/100,000 population in 2019 to 6.1/100,000 population in 2024 (IRR 13.7 [95% CI 1.8–104.9]; p = 0.01). The incidence of ICU admissions and CNS complications peaked during June–July, consistent with the overall trend of *M. pneumoniae* cases. Of note, the increase in CNS complications was not observed during the 2019 outbreak.

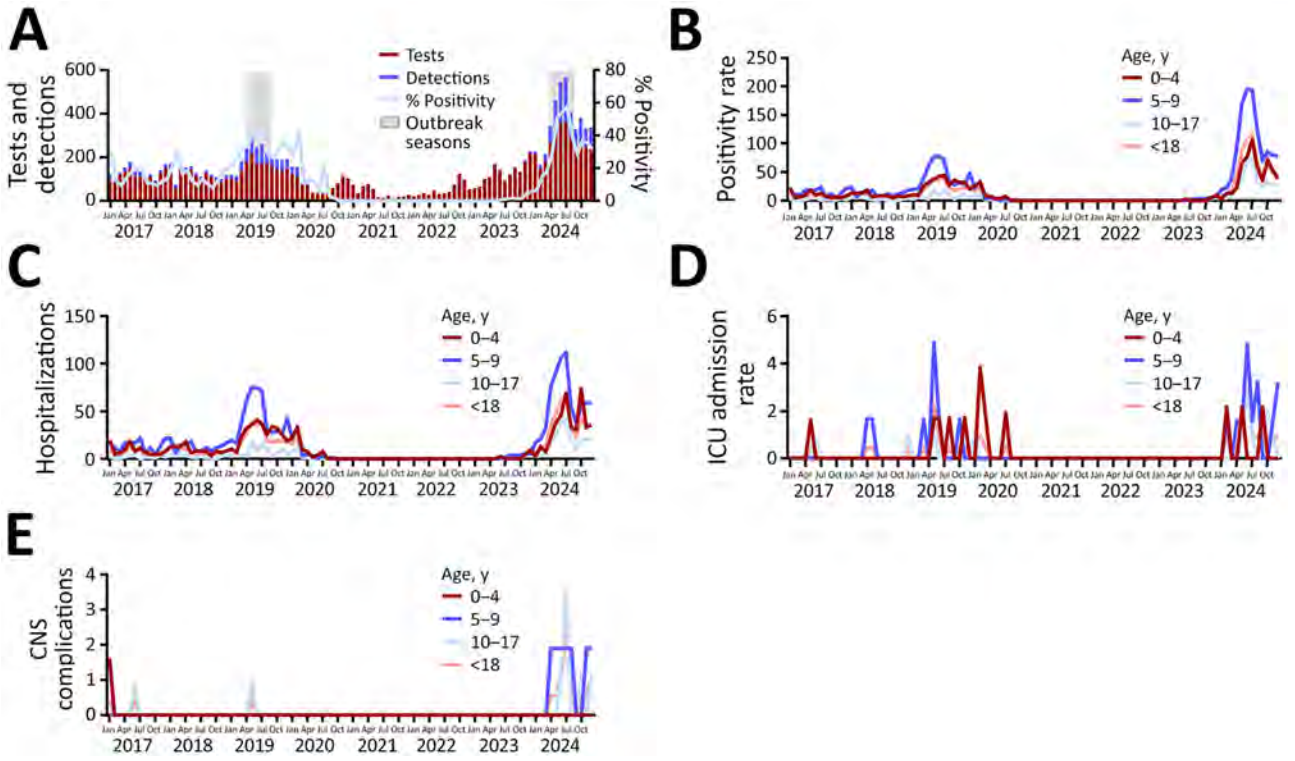

Figure 1. *Mycoplasma pneumoniae*–related incidence among persons <18 years of age in study of emergence of novel macrolide-resistant *M. pneumoniae* sequence type 3 subclades in children after COVID-19 pandemic, Taiwan, 2017–2024 (n = 2,340). A) Monthly numbers of *M. pneumoniae* tests and laboratory-confirmed cases at Chang Gung Memorial Hospital, Taoyuan, Taiwan. B–E) Monthly rates per 100,000 population by age group: B) *M. pneumoniae* positivity; C) *M. pneumoniae*–related hospitalizations; D) *M. pneumoniae*–related ICU admissions; E) *M. pneumoniae*–related CNS complications. CNS, central nervous system; ICU, intensive care unit.

The median age for patients with CNS involvement during the post–COVID-19 period was 8 (IQR 6.8–11.5) years; all patients were >5 years of age (Figure 2; Appendix 1 Table). Absence of respiratory prodrome or respiratory prodrome lasting <7 days was observed in 30.8% (4/13) of patients, whereas 69.2% (9/13) had prodrome lasting ≥7 days. The most common neurologic syndrome was encephalitis (n = 7), followed by isolated encephalopathy (n = 2), acute disseminated encephalomyelitis (n = 1), transverse myelitis (n = 1), cerebellitis (n = 1), and Guillain-Barré syndrome (n = 1). CSF testing using the BioFire Film Array Meningitis/Encephalitis Panel (bioMérieux) was negative in all 13 patients. CSF culture was performed in 10 patients, yielding *M. pneumoniae* growth in 2 patients with a prodrome of <7 days and in 5 patients with a prodrome of ≥7 days; all isolates were identified as macrolide-resistant *M. pneumoniae* ST3. CSF *M. pneumoniae* in-house PCR was positive in 1 patient (7.7% [1/13]), in whom 23S rRNA sequencing and MLST identified macrolide-resistant *M. pneumoniae* ST3, although culture was unsuccessful. All 13 patients were treated with doxycycline and corticosteroids; some also received intravenous immunoglobulin, and all had favorable outcomes.

Risk Factors for Severe Disease and Alternatives to Macrolide-Resistant *M. pneumoniae* Treatment

A total of 226 patients were prospectively enrolled during the post–COVID-19 period to investigate risk factors associated with ICU admission (Table 2). Of those, 17 patients required ICU care. Compared with non-ICU patients, those admitted to the ICU had higher neutrophil counts and platelet counts and longer hospital stays. CNS complications and pleural effusion were also more frequent among ICU patients. In multivariable analysis, neutrophil count >7,000 cells/μL (odds ratio [OR] 6.2 [95% CI 1.3–29.9]; p = 0.02), platelet count >400 × 10^3/μL (OR 12.5 [95% CI 2.7–57.9]; p = 0.001), pleural effusion (OR 9.7 [95% CI1.6–58.1]; p = 0.01), and CNS complication (OR 27.9 [95% CI 4.1–188.3]; p = 0.001) remained independently associated with ICU admission (Table 2). We tested upper respiratory tract samples from all patients using the BioFire Respiratory Panel (bioMérieux) to detect respiratory pathogens. Codetection occurred in 62 (27.4%) patients but was not associated

with increased complications. MLST and macrolide-resistance mutation analysis revealed that ST3 was the predominant circulating genotype, accounting for 207/226 (91.6%) cases. Macrolide resistance was observed in 219 (96.9%) patients, all of whom carried the A2063G mutation in the 23S rRNA gene. Neither genotype nor resistance profile was associated with clinical outcomes.

Among 219 macrolide-resistant *M. pneumoniae* strains, ST3 predominated (207 [94.5%]), followed by ST14 (10 [4.6%]), ST11 (1 [0.45%]), and ST44 (1 [0.45%]). Among 7 macrolide-susceptible *M. pneumoniae* strains, we identified ST14 (4 [57.1%]), ST2, ST3, and ST17 (each 1 [14.3%]). We determined MIC ranges, MIC_{50} (MIC at which 50% of antimicrobial is inhibited), and MIC_{90} (MIC at which 90% of antimicrobial is inhibited) values for 10 antimicrobial agents in 109 culturable macrolide-resistant isolates (Table 3). Doxycycline demonstrated the lowest MIC_{50} (<0.03 mg/L) and MIC_{90} (0.03 mg/L), and no isolates showed resistance to levofloxacin or moxifloxacin according to Clinical and Laboratory Standards Institute guidelines (*13*).

Shifts in *M. pneumoniae* Genomic Structure during Postpandemic Period

To identify the specific genomic variations associated with the postpandemic resurgence of ST3, we analyzed a total of 698 *M. pneumoniae* genomes. That dataset consisted of 100 prepandemic isolates from Taiwan (2018–2020), 113 isolates collected during the 2023–2024 outbreak, and 485 publicly available global genomes spanning 1944–2024 across 4 continents (Figure 3, panel A). Phylogenetic analysis identified 5 major clades; no novel high-level clades emerged during the post–COVID-19 resurgence. However, we observed a striking regional shift in lineage dominance. Across East Asia, ST3 (T1–2) and ST14 (T2–2) were the predominant clades during the postpandemic period. ST3 accounted for 89.4% (101/113) of postpandemic isolates in Taiwan and 81.4% (232/285) in China.

Table 1. *Mycoplasma pneumoniae*–related hospitalizations, ICU admissions, and CNS complications among children <18 years of age in study of emergence of novel macrolide-resistant *M. pneumoniae* sequence type 3 subclades in children after COVID-19 pandemic, Taiwan, 2017–2024 (n = 2,340)*

Age	Incidence per 100,000 (no. cases)								2017 vs. 2019		2019 vs. 2024	
group, y	2017	2018	2019	2020	2021	2022	2023	2024	IRR (95% CI)	p value	IRR (95% CI)	p value
M. pneumoniae incidence												
<18	87 (206)	90 (204)	284 (635)	55 (112)	0	0	12.8 (28)	546 (1,155)	3.25 (2.78–3.81)	<0.0001	1.92 (1.74–2.11)	<0.0001
0–4	117 (72)	117 (71)	348 (205)	90 (47)	0	0	14.0 (7)	470 (219)	2.99 (2.29–3.91)	<0.0001	1.4 (1.11–1.63)	0.002
5–9	173 (105)	157 (95)	535 (329)	73 (44)	0	0	21.3 (14)	986 (616)	3.09 (2.48–3.85)	<0.0001	1.84 (1.61–2.11)	<0.0001
10–17	26 (29)	36 (38)	98 (101)	23 (21)	0	0	6.8 (7)	313 (320)	3.83 (2.54–5.80)	<0.0001	3.2 (2.55–3.98)	<0.0001
M. pneumoniae–related hospitalization												
<18	82 (194)	86 (197)	268 (599)	53 (108)	0	0	12.3 (27)	348 (735)	3.26 (2.77–3.83)	<0.0001	1.30 (1.16–1.44)	<0.0001
0–4	107 (66)	115 (70)	323 (190)	86 (45)	0	0	14.0 (7)	341 (159)	3.02 (2.28–4.00)	<0.0001	1.07 (0.86–1.30)	0.6
5–9	167 (101)	154 (93)	513 (315)	71 (43)	0	0	19.8 (13)	608 (380)	3.07 (2.46–3.85)	<0.0001	1.19 (1.02–1.38)	0.03
10–17	24 (27)	32 (34)	91 (94)	22 (20)	0	0	6.8 (7)	191 (196)	3.83 (2.50–5.88)	<0.0001	2.10 (1.64–2.68)	<0.0001
M. pneumoniae–related ICU admission												
<18	0.8 (2)	1.3 (3)	4.9 (11)	2.4 (5)	0	0	0	10.9 (23)	5.8 (1.29–26.2)	0.02	2.2 (1.08–4.53)	0.03
0–4	1.6 (1)	0	8.5 (5)	7.6 (4)	0	0	0	6.4 (3)	5.25 (0.61–44.93)	0.13	0.76 (0.18–3.17)	0.7
5–9	0	3.3 (2)	8.1 (5)	0	0	0	0	19.2 (12)	ND	ND	2.36 (0.83–6.7)	0.11
10–17	0.9 (1)	0.9 (1)	1.0 (1)	1.1 (1)	0	0	0	7.8 (8)	1.1 (0.07–17.6)	0.95	8.04 (1.01–64.3)	0.05
M. pneumoniae–related CNS complications												
<18	0.8 (2)	0	0.4 (1)	0	0	0	0	6.1 (13)	0.53 (0.05–5.82)	0.6	13.7 (1.80–104.90)	0.01
0–4	1.6 (1)	0	0	0	0	0	0	0	ND	ND	ND	ND
5–9	0	0	0	0	0	0	0	11.2 (7)	ND	ND	ND	ND
10–17	0.9 (1)	0	0	0	0	0	0	5.9 (6)	1.1 (0.07–17.6)	0.95	6.03 (0.73–50.10)	0.1

*ICU, intensive care unit; IRR, incidence rate ratio; CNS, central nervous system; ND, not done.

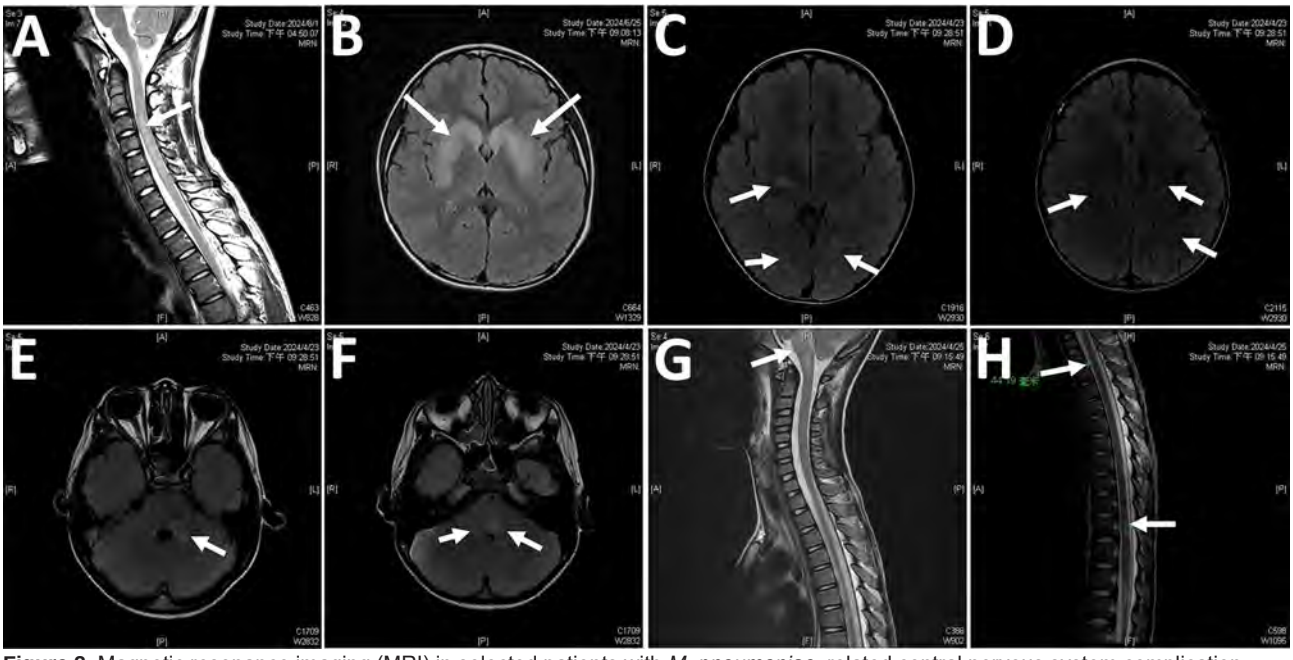

Figure 2. Magnetic resonance imaging (MRI) in selected patients with *M. pneumoniae*–related central nervous system complication in study of emergence of novel macrolide-resistant *M. pneumoniae* sequence type 3 subclades in children after COVID-19 pandemic, Taiwan, 2017–2024. A) Sagittal T2-weighted cervical spine MRI in patient 3, demonstrating a hyperintense lesion extending from C3 to C6 (arrow). B) Axial T2-FLAIR brain MRI of patient 5, showing a focal hyperintense lesion in the bilateral basal ganglia (arrows). C–F) Axial T2-FLAIR brain MRI scans of patient 10, revealing multiple hyperintense lesions involving the subcortical white matter of the bilateral parietal, temporal, and occipital lobes, as well as the midbrain, pons, and middle cerebellar peduncles, findings consistent with acute disseminated encephalomyelitis (arrows). G–H) Sagittal T2-weighted spine MRI of patient 10, indicating hyperintense lesions at the brainstem and at the T3 and T11 spinal levels (arrows).

Given that ST3 represented ≈80% of circulating strains in East Asia, we examined the phylogenetic structure within this lineage (Figure 3, panel B). Root-to-tip regression demonstrated a robust temporal signal (Pearson correlation coefficient = 0.573) (Figure 4, panel A), supporting clock-like accumulation of mutations and reliable reconstruction of evolutionary trajectories. ST3 isolates from Taiwan segregated into 5 distinct monophyletic groups that were phylogenetically separate from dominant ST3 strains from China, indicating independent regional diversification rather than simple importation.

A preexisting Taiwan lineage (subclade_pre), which accounted for 50% of prepandemic ST3 isolates (30/60), persisted into 2023 and early 2024 and accounted for 61% of ST3 cases (25/41) in the first half of the year. However, that lineage rapidly declined and was completely replaced in the second half of 2024 (Figure 4, panel B), demonstrating clear within-lineage turnover. In contrast, 4 newly emerged ST3 lineages (subclade_post_a–d) (Figure 3) progressively appeared and had largely replaced subclade_pre by mid-2024. Those postpandemic subclades accumulated 7, 14, 15, and 9 lineage-specific mutations (Appendix 2 Table 1). That clade replacement temporally coincided with the peak in *M. pneumoniae*–related hospitalizations, ICU admissions, and CNS complications, and accounted for most severe cases. Subclade_post_b underwent rapid expansion and became dominant in late 2024 (43.1% of isolates). The lineage was characterized by lineage-specific mutations in MPN_RS01335 and MPN_RS01875 (Appendix 2 Table 1). Of note, subclade_post_a exhibited significantly higher percentages of ICU admissions and CNS complications (both 37.5%) than other clades ($p = 0.015$ for ICU admissions and $p = 0.00061$ for CNS complications by the χ^2 test). That lineage was characterized by lineage-specific mutations in MPN_RS01790, MPN_RS04325, and MPN_RS02200 (Appendix 2 Table 1).

Discussion

The 2024 resurgence of *M. pneumoniae* in Taiwan was characterized by the predominance of macrolide-resistant ST3 strains, continuous genomic diversification, and a notable increase in ICU admissions and neurologic complications correlated with CNS invasion. In Denmark, where *M. pneumoniae* is a notifiable disease, surveillance data revealed post–COVID-19 incidence rates comparable to those observed in our study; 500–600 PCR-confirmed cases and 200–300

hospitalizations occurred per 100,000 children <18 years of age in 2024 (*14*). A rise in *M. pneumoniae*–associated rash and mucositis was noted, without a corresponding increase in ICU admissions (*14*). In China, the 2023 surge of *M. pneumoniae* infections involved severe disease, including dyspnea requiring bronchoalveolar lavage, necrotizing pneumonia with pulmonary thrombosis, and parapneumonic effusion in 25% of cases (*15*,*16*). Those infections were associated with the continued circulation of macrolide-resistant ST3 and ST14 strains, which clustered with isolates detected during 2019–2022 on phylogenetic analysis. ST3 demonstrated genomic enrichment in virulence, signaling, and metabolism-related genes compared with ST14, potentially explaining its greater clinical effects and predominance (*8*,*17*). Consistent with previous reports from China, Japan, and South Korea (*8*,*18*,*19*), our comparative genomic analysis demonstrated that ST3 (T1–2) remained the predominant lineage during the postpandemic resurgence in Taiwan and China, indicating its continued widespread circulation across East Asia. In adults,

Table 2. Demographic, clinical, laboratory and radiologic characteristics and risk factors for ICU admission in study of emergence of novel macrolide-resistant *Mycoplasma pneumoniae* sequence type 3 subclades in children after COVID-19 pandemic, Taiwan, 2023–2024 (n = 226)*

Characteristic	ICU admission, n = 17	Non-ICU admission, n = 209	p value	Univariate analysis		Multivariate analysis	
				OR (95% CI)	p value	OR (95% CI)	p value
Median age, y (IQR)	8.5 (7.8–12.0)	8.9 (7.2–10.6)	0.5	1.06 (0.9–1.23)	0.44	–	–
Male sex	9 (52.9)	106 (50.7)	1.0	0.92 (0.34–2.46)	0.86	–	–
Days from symptom onset to hospital admission, median (IQR)	5.0 (1.5–7.0)	6.0 (4.0–7.0)	0.3	0.89 (0.7–0.11)	0.32	–	–
Receiving effective treatment	16 (94.1)	195 (93.3)	1.0	1.15 (0.14–9.3)	0.9	–	–
Days from symptom onset to effective treatment, median (IQR)	7.0 (5.0–7.0)	7.0 (5.0–8.3)	0..3	0.86 (0.7–1.08)	0.2	–	–
Total days with fever, median (IQR)	9 (4–12)	8.0 (6.0–9.0)	0.5	1.06 (0.9–1.3)	0.5	–	–
Median hospital duration, d (IQR)	13.0 (11.5–15.5)	5.0 (1.0–8.0)	<0.001	1.71 (1.4–2.1)	<0.001	–	–
Laboratory characteristic							
Leukocytes, × 10^3 cells/μL; median (IQR)	11.7 (9.75–13.35)	7.2 (6.0–8.8)	<0.001	1.0 (1.0–1.0)	<0.001	ND	ND
Neutrophil count >7,000 cells/μL	13 (76.5)	31 (14.8)	<0.001	18.7 (5.7–61)	<0.001	6.2 (1.3–29.9)	0.02
Hemoglobin, g/dL; median (IQR)	11.7 (9.7–13.4)	12.3 (11.7–13.1)	0.15	0.77 (0.5–1.06)	0.11	–	–
Platelets, × 10^3/μL; median (IQR)	451 (265–648)	264 (212–320)	<0.001	1.0 (1.0–1.0)	<0.001	ND	ND
Platelet count >400 × 10^3/μL	11 (64.7)	19 (9.1)	<0.001	18.3 (6.1–55.1)	<0.001	12.5 (2.68–57.9)	0.001
CRP, mg/L; median (IQR)	45.7 (11–154.4)	26.6 (14.3–62.8)	0.23	1.01 (1.001–1.01)	0.01	1.002 (0.99–1.01)	0.6
AST, U/L; median (IQR)	26.0 (18.5–140.0)	28.0 (23.0–47.3)	0.49	1.001 (1.0–1.003)	0.6		
ALT, U/L; median (IQR)	24.0 (12.0–153.3)	13.0 (9.0–22.0)	0.02	1.001 (1.0–1.003)	0.3		
Codetection	3 (17.6)	59 (28.2)	0.4	0.54 (0.15–1.97)	0.4		
Macrolide resistance	17 (100)	202 (96.7)	1.0	ND	ND		
ST			0.5	ND	ND		
ST3	15 (88.2)	192 (91.9)					
ST14	2 (11.8)	12 (5.7)					
Others	0	5 (2.4)					
Chest radiography findings							
Increased infiltration	8 (47.1)	71 (34)	0.3	1.7 (0.6–4.7)	0.28		
Patchy consolidation	9 (52.9)	138 (66)	0.3	0.58 (0.2–1.57)	0.28		
Pleural effusion	5 (29.4)	14 (6.7)	0.008	5.8 (1.8–18.8)	0.003	9.96 (1.6–58.1)	0.01
CNS complication				21.4 (5.07–89.9)	<0.001	27.9 (4.1–188.3)	0.001

*Values are no. (%) except as indicated. AST, aspartate aminotransferase; ALT, alanine aminotransferase; CNS, central nervous system; CRP, Cc-reactive protein; ICU, intensive care unit; ND, not done; OR, odds ratio; ST, sequence type.

Table 3. Macrolide-resistant *Mycoplasma pneumoniae* strains and antimicrobial susceptibility to 10 agents in study of emergence of novel macrolide-resistant *M. pneumoniae* sequence type 3 subclades in children after COVID-19 pandemic*

	Macrolide-resistant *M. pneumoniae* with A2063G mutation, n = 109		
Antimicrobial agent	MIC_{50}	MIC_{90}	MIC range
Macrolide			
Erythromycin	64	128	16–256
Azithromycin	16	32	1–128
Clarithromycin	32	128	2–128
Quinolones			
Levofloxacin	0.25	0.5	0.03–0.5
Moxifloxacin	0.03	0.06	<0.03–0.06
Ciprofloxacin	0.5	1	0.06–1
Tosufloxacin	0.06	0.125	0.03–0.25
Tetracyclines			
Doxycycline	<0.03	0.03	<0.03–0.125
Minocycline	0.03	0.06	<0.03–0.125
Omadacycline	0.06	0.125	0.03–0.125

*MIC_{50}, MIC at which 50% of isolates are inhibited; MIC_{90}, MIC at which 90% of isolates are inhibited.

the frequent atypical radiological manifestation of alveolar consolidation, which contributed to delays in effective treatment, was associated with a 31.7% ICU admission rate during the 2023–2024 *M. pneumoniae* epidemic in France (*7*). Regional differences in the clinical spectrum and severity of *M. pneumoniae* infection might result from challenges in initiating appropriate treatment, especially in areas with high macrolide resistance, compounded by viral co-infections, and diminished innate immune priming because of prolonged pandemic restrictions (*2*,*8*,*20*). However, the increase in *M. pneumoniae*–related CNS complications, typically occurring in parallel with community outbreaks, has been seldom addressed after the COVID-19 pandemic and was not observed during the 2019 *M. pneumoniae* wave in Taiwan (*10*).

The pathogenic mechanisms of *M. pneumoniae* involve direct damage to the respiratory epithelium through toxic molecules including hydrogen peroxide, hydrogen sulfide, the community-acquired respiratory distress syndrome toxin (*21*), and tissue injury resulting from excessive immune response (*22*). In addition to respiratory tract infections, *M. pneumoniae* can cause extrapulmonary manifestations; encephalitis is

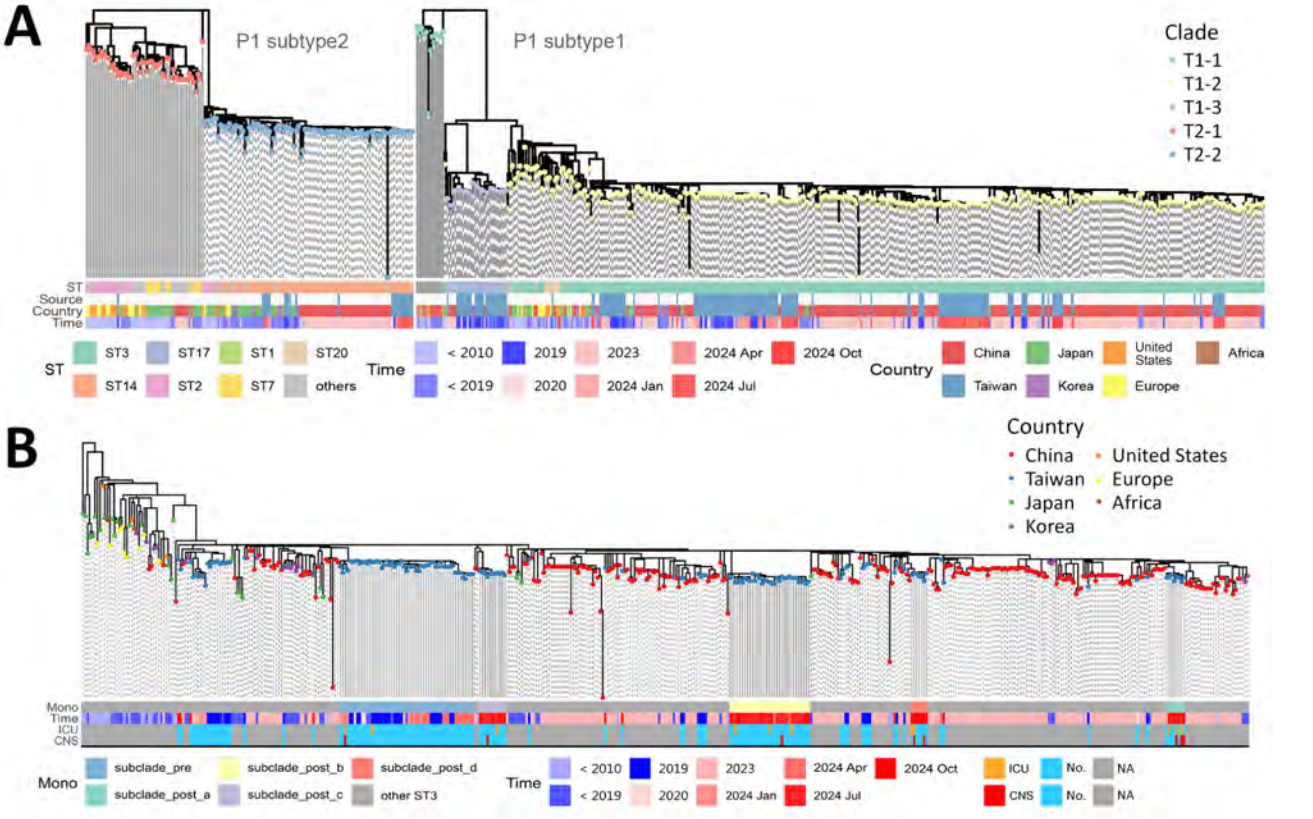

Figure 3. Phylogenomic evolution of *Mycoplasma pneumoniae* in study of emergence of novel macrolide-resistant *M. pneumoniae* ST3 subclades in children after COVID-19 pandemic, Taiwan, 2017–2024. A) Global phylogenetic tree showing evolutionary relationships among all sequenced strains. Nodes are colored by clade according to our previous study (*12*). Annotation bands indicate sequence type, data source, country, and sampling time. For 2024, isolates were grouped into quarterly intervals (January–March, April–June, July–September, and October–December) to provide greater temporal resolution during the outbreak. B) Phylogeny of ST3 strain. Nodes are colored by country, with annotation bands indicating monophyletic subclades (Mono), sampling time, ICU admission, and CNS complications. CNS, central nervous system; ICU, intensive care unit; ST, sequence type.

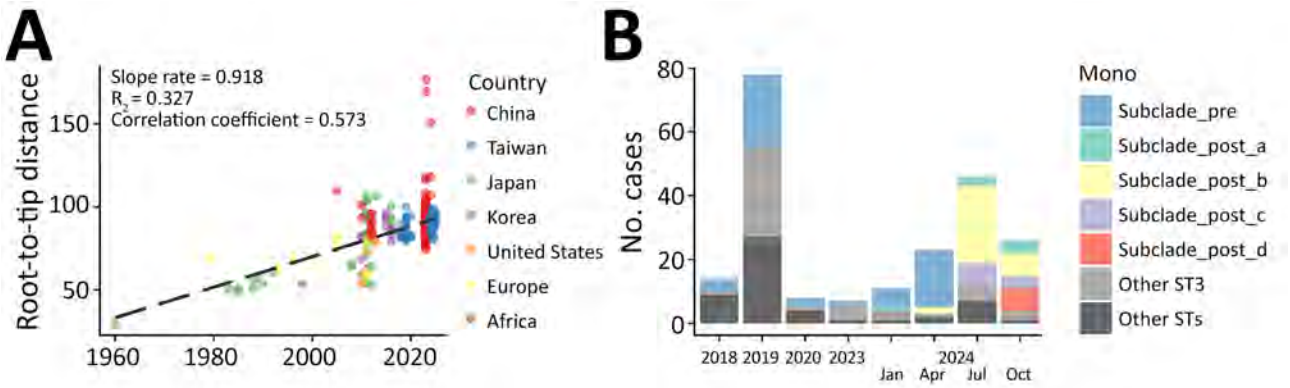

Figure 4. Temporal prevalence of *Mycoplasma pneumoniae* in study of emergence of novel macrolide-resistant *M. pneumoniae* sequence type 3 subclades in children after COVID-19 pandemic, Taiwan, 2017–2024. A) Temporal signal in ST3 genomes evaluated by linear regression of root-to-tip genetic distances against sampling year for global isolates collected during 1960–2024, indicating molecular clock consistency. B) Temporal prevalence of ST3 subclades among persons <18 years of age, Taiwan, 2018–2024. Isolates collected in 2024 are shown at quarterly intervals. ST, sequence type.

one of the most severe (*22*). *M. pneumoniae* infection has been identified in 5%–10% of pediatric encephalitis cases; up to 60% of affected patients develop long-term neurologic sequelae (*22*). *M. pneumoniae*–related encephalitis involves 2 main pathogenic mechanisms: direct CNS invasion and postinfectious immune-mediated injury (*23*). *M. pneumoniae* DNA is typically detectable in 50%–80% of CSF samples within 1 week of respiratory symptoms or in cases without prodrome (*11*,*24*). When prodrome lasts ≥7 days, *M. pneumoniae* DNA is detected in only 7%–14% of CSF samples, supporting the notion that disease at that stage is predominantly immune-mediated (*11*,*24*). Among 13 patients with CNS complications, respiratory multiplex PCR identified *M. pneumoniae* as the sole pathogen in 11 (84.6%) patients. Although CSF PCR for *M. pneumoniae* was positive only in 1 case, CSF cultures were performed in 10 patients and yielded growth in 7 (70%) patients, irrespective of prodrome duration. The discrepancy between PCR-negative and culture-positive results likely reflects low bacterial load (<400 copies/mL) (*24*). Of note, those findings reduce the likelihood of alternative infectious etiologies and suggest a neuroinvasive potential of macrolide-resistant *M. pneumoniae* ST3 strains; some cases show evidence of postinfectious immune response, as indicated by an elevated CSF IgG index. During the 2019 *M. pneumoniae* epidemic wave in Taiwan, attention focused on the use of doxycycline to manage *M. pneumoniae* infections, given the high prevalence of macrolide resistance (*10*). In the 2023–2024 wave, doxycycline was adopted as the first-line agent for most patients. The favorable outcomes observed in our patients might be attributed to the synergistic effect of doxycycline's reliable CNS penetration and the early, aggressive use of immunomodulatory therapy. The American Academy of Pediatrics considers doxycycline safe for children <8 years of age when prescribed for ≤21 days (*25*) and also recognizes the role of fluoroquinolones, which are available in intravenous formulations and achieve favorable CNS penetration, in the management of multidrug-resistant infections (*26*). In our study, macrolide-resistant isolates remained uniformly susceptible to tetracyclines and fluoroquinolones, confirming their value as essential therapeutic options for macrolide-resistant *M. pneumoniae*. In regions characterized by high rates of macrolide resistance, doxycycline, levofloxacin, and moxifloxacin might serve as preferred first-line therapeutic options.

M. pneumoniae has a reduced genome of ≈800 kb that has remained relatively stable across time and geography. Sequence variations are predominantly located in the antigenic regions of P1 and P40/P90, which together form the Nap transmembrane complex, responsible for host antibody recognition and binding to sialic acid oligosaccharides of target host cells (*27*). Our previous study demonstrated that ST3 exhibits high homologous recombination capacity and extensive genomic diversity, which might explain its global epidemiologic success despite selective pressure from widespread macrolide use (*12*). In the post–COVID-19 era in Taiwan, that lineage appears to have undergone further sustained expansion through specific adaptive changes. The lack of association between the broad ST3 genotype and clinical outcomes suggested that finer-scale genomic variations within the dominant lineage might be responsible for the observed surge in severe cases. Our genomic analysis identified lineage-specific mutations in several genes that might warrant further investigation. Subclade_post_b, which became predominant in late 2024, was characterized by mutations in MPN_

RS01335, encoding thioredoxin-disulfide reductase, and MPN_RS01875, encoding an ABC transporter permease. Of note, subclade_post_a was significantly associated with increased disease severity, accounting for disproportionately higher rates of ICU admissions and CNS complications. That lineage was characterized by mutations in MPN_RS02200, encoding a dihydrolipoamide acetyltransferase family protein; MPN_RS04325, encoding a DUF16 domain-containing protein; and MPN_RS01790, encoding an APC family permease.

The first limitation of this study is that the rise in severe cases could partly reflect the expanded scale of the total surge, and the clinical effects of the identified mutations require further functional validation. The hospital-based cohort might overrepresent severe cases and underestimate community prevalence. PCR cannot fully distinguish active infection from asymptomatic carriage; however, all patients were symptomatic and tested after physician assessment, reducing that concern. Strengths of the study include its multicenter design, comprehensive assessment of incidence and risk factors for severe disease, detailed antimicrobial susceptibility testing, and genome analysis associated with severe and neuroinvasive manifestations.

In summary, our findings indicate that *M. pneumoniae* clinical effects extend beyond self-limiting pneumonia and highlight the ongoing genomic diversification of ST3 during the postpandemic resurgence. Continued genomic surveillance is essential to monitor emerging variants and guide public health strategies and therapeutic interventions.

All data generated or analyzed in this study are available in the main article and the Appendices. Complete or draft genome assemblies were deposited in GenBank; accession numbers are listed in Appendix 2 Table 2. The code relevant to this manuscript is publicly available on GitHub (https://github.com/YinchengChen23/MP_resurgence_scripts).

This work was supported by Chang Gung Memorial Hospital in Taiwan (grant nos. CMRPG3P0081 and CMRPG3P0082) and the National Science and Technology Council in Taiwan (grant nos. 111-2314-B-182A-071-MY3 and 114-2314-B-182A-133-MY3).

During the preparation of this work, the authors used ChatGPT (https://www.chatgpt.com) to improve the readability and language of the manuscript. All content was subsequently reviewed and revised by the authors, who take full responsibility for the final version.

Y.-C.H. initiated and supervised the project. S.-W.L., C.-C.L., and Y.-C.C. were involved in conceptualizing and designing the overall work and conducted most of the bioinformatics and statistical analyses. J.-W.W., E.-W.H., Y.-J.P., T.-Y.L., S.-S.S., H.-L.Y., C.-W.H., and Y.-C.H. were involved in the investigation, collected the bacterial isolates, performed phenotypic characterization, and analyzed the results. S.-W.L., Y.-C.C., T.-C.H., and Y.-X.S. conducted data curation and visualization. S.-W.L., Y.-C.C., Y.-H.L., and Y.-C.H. wrote and revised the manuscript. All authors reviewed and approved the final version of the manuscript. All authors had full access to all data in the study and accept responsibility for the decision to submit it for publication.

About the Author

Dr. Hsieh is a professor in the department of pediatrics, Chang Gung Children's Hospital, Chang Gung Memorial Hospital, and Chang Gung University College of Medicine, Taoyuan, Taiwan. Her primary research interest is infectious diseases, particularly the pathogenesis of *Mycoplasma penumoniae* and pneumococcal disease.

References

1. Meyer Sauteur PM, Beeton ML, Pereyre S, Bébéar C, Gardette M, Hénin N, et al.; ESGMAC the ESGMAC MAPS study group. *Mycoplasma pneumoniae*: gone forever? Lancet Microbe. 2023;4:e763. https://doi.org/10.1016/S2666-5247(23)00182-9
2. Méndez-Echevarría A, Calle-Miguel L, Miralbés S, Barreiro-Pérez S, Afonso-Rodriguez O, Soler-Simón JA, et al.; Spanish Mycoplasma Study Group. Increased severity of *Mycoplasma pneumoniae* infections in Spanish children. Pediatr Infect Dis J. 2024;43:1113–9. https://doi.org/10.1097/INF.0000000000004461
3. McCarthy KN, Hatcher J, Best T, Kaliakatsos M, Hassell J, Turnbull A, et al. Increasing number of clinically severe *Mycoplasma pneumoniae* infections in children after the COVID-19 pandemic: a single-center case series. J Pediatric Infect Dis Soc. 2025;14:14. https://doi.org/10.1093/jpids/piae132
4. Danner MT, Binns HC, Nguyen K, Johnson C, Dunn J, Niles D, et al. Resurgence of pediatric *Mycoplasma pneumoniae* infections in southeast Texas, November 2023–June 2024. J Pediatric Infect Dis Soc. 2025;14:14. https://doi.org/10.1093/jpids/piae119
5. Meyer Sauteur PM, Zhang XS, Emborg HD, Sidorov S, Pereyre S, Fischer A, et al.; ESGMAC MAPS study group. Global spatiotemporal dynamics of *Mycoplasma pneumoniae* re-emergence after COVID-19 pandemic restrictions: an epidemiological and transmission modelling study. Lancet Microbe. 2025;6:101019. https://doi.org/10.1016/j.lanmic.2024.101019
6. Garzoni C, Bernasconi E, Zehnder C, Malossa SF, Merlani G, Bongiovanni M. Unexpected increase of severe *Mycoplasma pneumoniae* pneumonia in adults in southern Switzerland. Clin Microbiol Infect. 2024;30:953–4. https://doi.org/10.1016/j.cmi.2024.03.008
7. Gavaud A, Holub M, Asquier-Khati A, Faure K, Leautez-Nainville S, Le Moal G, et al.; MYCADO Study Group. *Mycoplasma pneumoniae* infection in adult

inpatients during the 2023–24 outbreak in France (MYCADO): a national, retrospective, observational study. Lancet Infect Dis. 2025;25:801–12. https://doi.org/10.1016/S1473-3099(24)00805-3
8. Li H, Li S, Yang H, Chen Z, Zhou Z. Resurgence of *Mycoplasma pneumonia* by macrolide-resistant epidemic clones in China. Lancet Microbe. 2024;5:e515. https://doi.org/10.1016/S2666-5247(23)00405-6
9. Kim K, Jung S, Kim M, Park S, Yang HJ, Lee E. Global trends in the proportion of macrolide-resistant *Mycoplasma pneumoniae* infections: a systematic review and meta-analysis. JAMA Netw Open. 2022;5:e2220949. https://doi.org/10.1001/jamanetworkopen.2022.20949
10. Hung HM, Chuang CH, Chen YY, Liao WC, Li SW, Chang IY, et al. Clonal spread of macrolide-resistant *Mycoplasma pneumoniae* sequence type-3 and type-17 with recombination on non-P1 adhesin among children in Taiwan. Clin Microbiol Infect. 2021;27:1169e1–e6.
11. Al-Zaidy SA, MacGregor D, Mahant S, Richardson SE, Bitnun A. Neurological complications of PCR-proven *M. pneumoniae* infections in children: prodromal illness duration may reflect pathogenetic mechanism. Clin Infect Dis. 2015;61:1092–8. https://doi.org/10.1093/cid/civ473
12. Hsieh YC, Li SW, Chen YY, Kuo CC, Chen YC, Chang IY, et al. Global genome diversity and recombination in *Mycoplasma pneumoniae.* Emerg Infect Dis. 2022;28:111–7. https://doi.org/10.3201/eid2801.210497
13. Clinical and Laboratory Standards Institute. Methods for antimicrobial susceptibility testing for human mycoplasmas. Supplement M43. Wayne (PA): The Institute; 2011.
14. Dungu KHS, Holm M, Hartling U, Jensen LH, Nielsen AB, Schmidt LS, et al. *Mycoplasma pneumoniae* incidence, phenotype, and severity in children and adolescents in Denmark before, during, and after the COVID-19 pandemic: a nationwide multicentre population-based cohort study. Lancet Reg Health Eur. 2024;47:101103. https://doi.org/10.1016/j.lanepe.2024.101103
15. Yu Y, Jin X, Zhang X, Shen Y. Pulmonary thrombotic complication of *Mycoplasma pneumoniae* pneumonia in Chinese children: clinical feature and risk factor analysis. Pediatr Infect Dis J. 2024;43:505–10. https://doi.org/10.1097/INF.0000000000004287
16. Zhang XB, He W, Gui YH, Lu Q, Yin Y, Zhang JH, et al. Current *Mycoplasma pneumoniae* epidemic among children in Shanghai: unusual pneumonia caused by usual pathogen. World J Pediatr. 2024;20:5–10. https://doi.org/10.1007/s12519-023-00793-9
17. Jiao W, Wang J, Li C, Wang P, Xu S, Bi J, et al. Genetic factors driving the *Mycoplasma pneumoniae* outbreak among children post-COVID-19 in China: a whole genome analysis. Lancet Reg Health West Pac. 2025;59:101578. https://doi.org/10.1016/j.lanwpc.2025.101578
18. Lee JK, Lee JH, Lee H, Ahn YM, Eun BW, Cho EY, et al. Clonal expansion of macrolide-resistant sequence type 3 *Mycoplasma pneumoniae*, South Korea. Emerg Infect Dis. 2018;24:1465–71. https://doi.org/10.3201/eid2408.180081
19. Ando M, Morozumi M, Adachi Y, Ubukata K, Iwata S. Multilocus sequence typing of *Mycoplasma pneumoniae*, Japan, 2002–2016. Emerg Infect Dis. 2018;24:1895–901. https://doi.org/10.3201/eid2410.171194
20. Rubin R. From "immunity debt" to "immunity theft"—how COVID-19 might be tied to recent respiratory disease surges. JAMA. 2024;331:378–81. https://doi.org/10.1001/jama.2023.26608
21. Kannan TR, Baseman JB. ADP-ribosylating and vacuolating cytotoxin of *Mycoplasma pneumoniae* represents unique virulence determinant among bacterial pathogens. Proc Natl Acad Sci U S A. 2006;103:6724–9. https://doi.org/10.1073/pnas.0510644103
22. Meyer Sauteur PM, Jacobs BC, Spuesens EBM, Jacobs E, Nadal D, Vink C, et al. Antibody responses to *Mycoplasma pneumoniae*: role in pathogenesis and diagnosis of encephalitis? PLoS Pathog. 2014;10:e1003983. https://doi.org/10.1371/journal.ppat.1003983
23. Bitnun A, Ford-Jones EL, Petric M, MacGregor D, Heurter H, Nelson S, et al. Acute childhood encephalitis and *Mycoplasma pneumoniae.* Clin Infect Dis. 2001;32:1674–84. https://doi.org/10.1086/320748
24. Fan G, Guo Y, Tang F, Chen M, Liao S, Wang J. Determining the clinical characteristics, treatment strategies, and prognostic factors for *Mycoplasma pneumoniae* encephalitis in children: a multicenter study in China. J Clin Neurol. 2023;19:402–9. https://doi.org/10.3988/jcn.2022.0328
25. Ravindra D, Huang G, Hallett K, Burgner DP, Gwee A, Silva MJ. Antibiotic exposure and dental health: a systematic review. Pediatrics. 2023;152:e2023061350. https://doi.org/10.1542/peds.2023-061350
26. Committee on Infectious Diseases. The use of systemic fluoroquinolones. Pediatrics. 2006;118:1287–92. https://doi.org/10.1542/peds.2006-1722
27. Vizarraga D, Kawamoto A, Matsumoto U, Illanes R, Pérez-Luque R, Martín J, et al. Immunodominant proteins P1 and P40/P90 from human pathogen *Mycoplasma pneumoniae.* Nat Commun. 2020;11:5188. https://doi.org/10.1038/s41467-020-18777-y

Address for correspondence: Shiao-Wen Li, National University of Kaohsiung, No. 700, Kaohsiung University Road, Nanzih District, Kaohsiung 811, Taiwan; email: winncesnow@gmail.com

Microbial Etiology of Postoperative Spinal Fusion Infections and Factors Associated with Gram-Negative Infections, United States, 2021–2022

Molly Lindstrom, Benjamin W. Langworthy, Jonathan N. Sembrano, Don Bambino Geno Tai

Accurate knowledge of microbial etiology is essential for optimizing spinal fusion surgical site infection (SSI) management, yet contemporary national data in the United States, particularly prevalence and factors associated with gram-negative infections, remain poorly understood. We conducted a cross-sectional analysis of US data reported to the Centers for Disease Control and Prevention National Healthcare Safety Network (2021–2022) to characterize the microbiology of spinal fusion SSI and identify factors associated with gram-negative infection. Among 7,187 cases, gram-negative organisms caused 31.5% (n = 2,265) of SSIs. Older age, female sex, higher body mass index, longer operative times, higher American Society of Anesthesiologists class, lumbar involvement, inpatient surgery, and emergent and trauma surgeries were independently associated with gram-negative infections relative to monomicrobial *Staphylococcus aureus* infections. Our findings might inform future studies focusing on high-risk cohorts as targets for expanded gram-negative prophylactic regimens. Clinicians can use risk profiles to guide empiric gram-negative antibiotic coverage in treating SSIs.

Surgical site infection (SSI) after spinal surgery occurs in ≈2% of procedures and is associated with substantial illness and healthcare utilization (*1*,*2*). Evidence suggests that the percentage of gram-negative pathogens in spinal fusion SSIs is higher than for other musculoskeletal infections (*3*). However, whether that trend persists across a large-scale national cohort remains unverified. Furthermore, the specific independent factors for gram-negative involvement among patients with spinal fusion SSIs remain poorly understood. Although institution-specific studies offer valuable insights, their findings are inherently susceptible to local surgical practices, institutional protocols, and regional healthcare epidemiology, thereby limiting their generalizability.

Our objective in this study was to characterize the contemporary national distribution of microbial etiology in spinal fusion SSI. We also aimed to identify the patient characteristics or procedural characteristics that are associated with gram-negative infection in spinal fusion SSI.

Methods

We performed a cross-sectional study of SSI episodes associated with spinal fusions in the United States reported to the Centers for Disease Control and Prevention National Healthcare Safety Network (NHSN) during January 2021–December 2022. We acquired deidentified data through a Freedom of Information Act request. Spinal fusion infection cases were reported to the NHSN voluntarily by participating hospitals and surgical centers using the criteria for surgical site infection (*4*). We selected the 2021–2022 cohort because it was the most recently completed dataset available at the time of our data request, enabling us to evaluate the most contemporary trends.

We abstracted available patient demographic and clinical characteristics from the database. Those data consisted of age, sex, body mass index (BMI), diabetes status, American Society of Anesthesiologists (ASA) physical status classification, presence of trauma before surgery, emergency status, and timing of infection relative to the index spinal fusion. Extracted surgical and procedural characteristics consisted of operative approach (anterior, posterior, or combined), wound class at the time of the index procedure, spinal

Author affiliations: University of Minnesota Medical School, Minneapolis, Minnesota, USA (M. Lindstrom, J.N. Sembrano, D.B.G. Tai); University of Minnesota School of Public Health, Minneapolis (B.W. Langworthy)

DOI: https://doi.org/10.3201/eid3211.260662

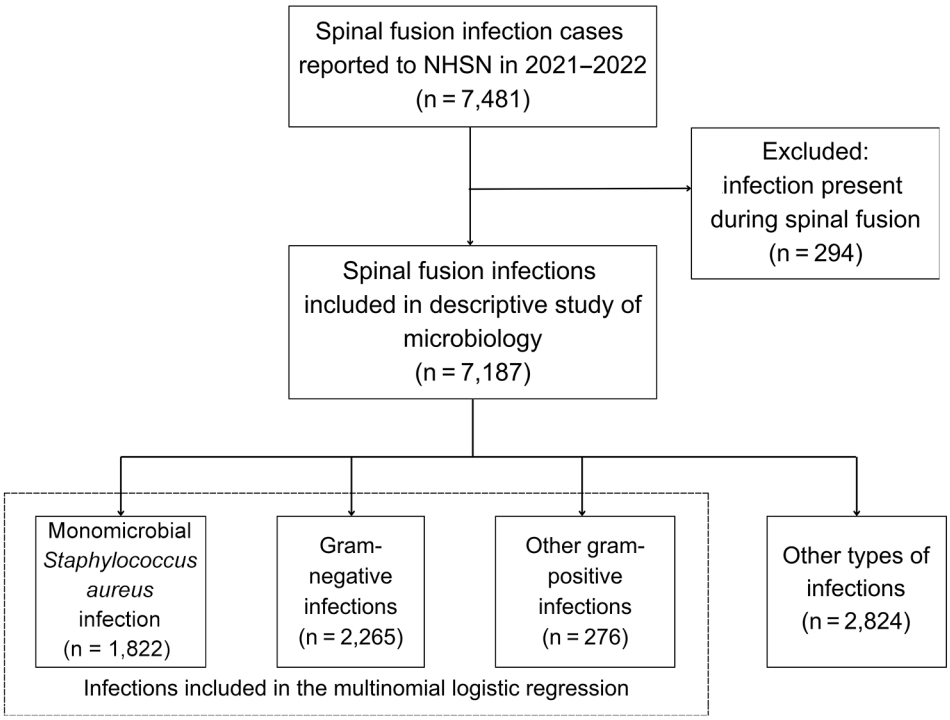

Figure. Flow diagram of postoperative surgical fusion infection cases in study of microbial etiology of postoperative spinal fusion infections and factors associated with gram-negative infections. NHSN, National Healthcare Safety Network.

level, method of wound closure (primary vs. other), procedural setting (inpatient vs. outpatient), and use of a scope or percutaneous endoscopic approach. We excluded cases in which an infection was explicitly documented as present at the time of surgery, because those cases represent a distinct clinical entity from postoperative spinal fusion SSIs.

We defined the unit of analysis (denominator) at the case level rather than at the isolate level. For patients with multiple positive cultures during a single SSI episode, we compressed duplicate bacterial species isolated from the same case and counted them only once. To analyze the independent predictors of different microbiological profiles, we categorized cases into 3 mutually exclusive, hierarchically defined analytic groups on the basis of the identified organisms. We categorized any case in which *S. aureus* was isolated as the sole microbial etiology as monomicrobial *S. aureus* infection (the reference group). The category of gram-negative infection consisted of all cases in which ≥1 gram-negative bacterial organism was isolated, regardless of whether it occurred as a monomicrobial infection or as part of a mixed/polymicrobial infection (i.e., coisolated with gram-positive organisms). Last, we categorized any case in which ≥1 gram-positive bacterial species were isolated without the presence of any gram-negative bacteria, *S. aureus*, or *Enterococcus* species as other gram-positive infection. The third cohort served as an exploratory group to approximate the profile of normal cutaneous flora. We excluded cases that did not meet the criteria for those 3 analytic categories or culture-negative cases from the multinomial regression model (Figure).

Statistical Analysis

We used frequency counts and percentages for categorical variables and used median (interquartile range [IQR]) or mean (SD) for continuous variables as appropriate. We performed a multinomial logistic regression analysis to determine the patient and procedural characteristics associated with the microbiological etiology of the infection. Our primary analysis evaluated the odds of a gram-negative infection compared with a reference group of monomicrobial *S. aureus* infection. To assess whether coinfection with other organisms influenced the observed effects, we performed a secondary analysis evaluating 2 additional cohorts within our model. The secondary analysis evaluated whether monomicrobial gram-negative and other gram-positive infections showed consistent results when compared with the same reference group. We followed that process to ensure the primary results were not driven by coinfections. The model simultaneously accounted for all patient and procedural covariates detailed above. We conducted analysis by using R version 4.3.2 (The R Project for Statistical Computing, httpw://www.r-project.org) and performed multinomial logistic regression using the multinom function in the nnet package. For multinomial logistic regression, the odds ratio (OR) can

be interpreted as the multiplicative effect on the odds of infection relative to the reference group for a one-unit increase in continuous variable, or relative to the reference category for a categorical variable.

Results

A total of 7,481 cases of spinal fusion SSI were reported to the NHSN during January 1, 2021–December 31, 2022. After excluding 294 (3.9%) cases because of the presence of infection during the initial fusion surgery, 7,187 cases remained for primary analysis. The mean patient age was 61.7 (SD 13.4) years; 54.1% were female (n = 3,889) and 45.9% (n = 3,297) were male (sex was unknown for 1 case). Most procedures were performed in an inpatient setting (n = 7,084 [98.6%]) and used a posterior surgical approach (n = 5,686 [83.7%]). The mean operative duration was 3.86 (SD 2.3) hours, and the median time from spinal fusion to infection diagnosis was 21 (IQR 14–29) days (Table 1).

Microbiology of Spinal Fusion SSI

Most cases were monomicrobial infections (n = 4,407 [61.3%]), 1,263 (17.6%) cases were polymicrobial, and the rest were culture-negative (1,517 [21.1%]). A total of 7,551 unique microorganisms were isolated among all cases reported to NHSN during the study period. Gram-positive bacteria were implicated in 53% (n = 3,813) of all cases. *Staphylococcus* spp. was the most prevalent bacterial genus, infecting 42.4% (n = 3,044) of cases. *S. aureus* was identified as the single most common pathogen, isolated in 30.6% (n = 2,200) of all cases (Table 2; Appendix Table, https://wwwnc.cdc.gov/EID/article/32/11/26-0662-App1.pdf). Gram-negative bacteria were implicated in 31.5% (n = 2,265) of cases; the most common species were *Escherichia coli* (n = 565 [7.9%]) and *Pseudomonas aeruginosa* (n = 501 [7.0%]). Fungi and mycobacterial infections were very rare; <2% of cases involved fungal organisms, and 0.1% involved mycobacteria.

Table 1. Demographics and clinical characteristics of patients with spinal fusion surgical site infections in study of microbial etiology of postoperative spinal fusion infections and factors associated with gram-negative infections, United States, 2021–2022*

Characteristic	All patients, n = 7,187
Mean age, y (SD)	61.67 (13.4)
Mean BMI (SD)	32.26 (7.8)
Sex	
M	3,297 (45.9)
F	3,889 (54.1)
Unknown	1
Outpatient	103 (1.4)
Mean duration of surgery, h (SD)	3.86 (2.3)
Approach	
Anterior	920 (13.5)
Posterior	5,686 (83.7)
Both	189 (2.8)
ASA class	
1	40 (0.6)
2	1,568 (23.1)
3	4,649 (68.4)
4	533 (7.9)
5	3 (0.04)
Diabetes	2,216 (32.6)
Wound class	
Clean	6,574 (96.8)
Clean-contaminated	135 (2.0)
Contaminated	23 (0.3)
Dirty	63 (0.9)
Spinal level	
Axis-atlas	4 (0.1)
Axis-atlas/cervical	60 (0.9)
Cervical	1,367 (20.1)
Cervical/dorsal/ dorsolumbar	300 (4.4)
Dorsal/dorsolumbar	1,299 (19.1)
Lumbar/lumbosacral	3,765 (55.4)
Trauma, yes	349 (5.1)
Closure	
Intentionally left open	65 (1.0)
Fully closed or partial	6,728 (99.0)
Timing of infection, days from procedure, median (IQR)	21 (14, 29)
Emergency	521 (7.7)
Use of scope	21 (0.3)

*Values are no. (%) except as indicated. ASA, American Society of Anesthesiologists; BMI, body mass index; IQR, interquartile range.

Table 2. Distribution of causative microorganisms in postoperative spinal infections after spinal fusion in study of microbial etiology of postoperative spinal fusion infections and factors associated with gram-negative infections, United States, 2021–2022*

Microorganism	No. (%) cases, n = 7,187
Staphylococcus species	3,044 (42.4)
Staphylococcus aureus	2,200 (30.6)
Coagulase-negative staphylococci (except *S. lugdunensis*)	824 (11.5)
S. lugdunensis	73 (1.0)
Enterococcus species	340 (4.7)
Streptococcus species, including nutritionally variant streptococci	191 (2.7)
Other commensal gram-positive bacteria (e.g., *Corynebacterium* species)	143 (2.0)
Enterobacterales	1,786 (24.9)
Escherichia coli	565 (7.9)
Proteus mirabilis	362 (5.0)
Klebsiella pneumoniae	297 (4.1)
Enterobacter cloacae complex	275 (3.8)
Serratia marcescens	255 (3.5)
Nonfermenting gram-negative bacilli	560 (7.8)
Pseudomonas aeruginosa	501 (7.0)
Other mucosal gram-negative bacilli (e.g., *Hemophilus* species)	16 (0.2)
Cutibacterium species	274 (3.8)
Other anaerobic bacteria (e.g., *Bacteroides*, *Finegoldia* species)	214 (3.0)
Fungi	139 (1.9)
Candida species	131 (1.8)
Mycobacteria	8 (0.1)
Organism not fully identified	144 (2.0)

*All organisms represent unique organisms identified in all cultures across cases. The total number of unique organisms (n = 7,512) is greater than the total number of reported cases (n = 7,187) due to the number of polymicrobial cases reported. Organism frequency is reported as the percent of organisms involved across cases. Enterobacterales category includes additional species not individually listed. Nonfermenting gram-negative bacilli include species other than *Pseudomonas aeruginosa*. Percentages do not sum to 100% because not all organisms are listed in this table.

Variables for Types of Infections

In multivariable multinomial logistic regression comparing gram-negative infections to a reference group of monomicrobial *S. aureus* infections, several independent predictors demonstrated significantly increased odds of a gram-negative etiology. Female sex was associated with 39% (95% CI 1.19–1.59) higher odds of gram-negative infection (p<0.001). Increasing age was associated with higher odds of gram-negative infection (OR 1.03 [95% CI 1.02–1.03] per year; p<0.001), representing a 3% increase in the likelihood of gram-negative involvement per additional year of age. Higher BMI was similarly associated with an increased likelihood of gram-negative infection (OR 1.03 [95% CI 1.02–1.04]; p<0.001).

Each additional hour of operative duration increased the odds of a gram-negative infection by 20% (OR 1.20 [95% CI 1.16–1.24]; p<0.001). A greater comorbidity burden was also strongly and independently associated with higher odds of a gram-negative etiology in a stepwise manner; patients classified as ASA class 4 exhibited a nearly 16-fold increase in the odds of gram-negative infection compared with those in ASA class 1 (OR 15.7 [95% CI 3.35–73.5]; p<0.001). Furthermore, surgical procedures involving the lumbar spine (OR 1.51 [95% CI 1.23–1.86]; p<0.001) and cases associated with trauma (OR 1.91 [95% CI 1.38–2.64]; p<0.001) demonstrated significantly higher odds of manifesting a gram-negative infection rather than monomicrobial *S. aureus*.

A longer duration of time between the index procedure and diagnosis was associated with significantly lower odds of a gram-negative infection (OR 0.97 [95% CI 0.96–0.97] per day; p<0.001), corresponding to a 3% reduction in odds for each additional postoperative day. Patients who underwent outpatient procedures were also 59% less likely to develop gram-negative infections than were those in the reference group (OR 0.41 [95% CI 0.18–0.96]; p = 0.041) (Table 3).

For monomicrobial gram-negative infections, female sex was also associated with higher odds (OR 1.38 [95% CI 1.19–1.59]; p<0.001). Similar to the overall gram-negative cohort, each additional year of age increased the likelihood of monomicrobial gram-negative infection by 3% (OR 1.03 [95% CI 1.02–1.04]; p<0.001). Other significantly associated factors were higher BMI and ASA class, lumbar spinal level, longer duration of surgery, inpatient surgery, surgeries for trauma, and emergency surgeries. Conversely, other gram-positive infections were associated with significantly higher odds of occurring in male patients (OR 1.39 [95% CI 1.06–1.82]; p = 0.019) and lower odds of thoracic spine involvement (OR 0.49 [95% CI 0.32–0.74]; p<0.001) or lumbar spine involvement (OR 0.44 [95% CI 0.32–0.62]; p<0.001) relative to the reference group (Table 4).

Discussion

Our study represents a large national surveillance-based analysis describing the contemporary microbial

etiology of spinal fusion SSI. Our analysis of a national patient cohort showed gram-negative organisms made up nearly one third of all patient cases and organisms identified in diagnostic cultures for spinal fusion SSI. Among gram-negative bacteria, Enterobacterales (most commonly *E. coli*), and *Pseudomonas* spp. were the predominant organisms identified. Gram-negative bacteria have been previously reported to affect 30%–54% of infections, occurring more frequently in infections involving lower spinal levels, particularly lumbar and sacral instrumentation (*5*,*6*). The percentage is much larger than that reported for other orthopedic implant infections, such as periprosthetic joint infection, where gram-negative infection made up ≈11% of cases (*7*).

Consistent with previous literature demonstrating an anatomic gradient wherein lower spinal levels carry an increased likelihood of gram-negative organism involvement in spinal fusion SSI (*8*), our analysis further delineates multiple independent patient-specific and procedural variables that increase the probability of gram-negative pathogen involvement

Table 3. Multinomial logistic regression analysis of factors associated with gram-negative spinal infections in study of microbial etiology of postoperative spinal fusion infections and factors associated with gram-negative infections, United States, 2021–2022*

Characteristic	*Staphylococcus aureus* infection, N = 1,822	Gram-negative infection, n = 2,265		
		No. infections	OR (95% CI)	p value
Mean age, y (SD)	59.4 (13.6)	64.1 (13.5)	1.03 (1.02–1.03)	<0.001
Mean BMI (SD)	31.1 (7.6)	33.4 (8.1)	1.03 (1.02–1.04)	<0.001
Unknown	123 (6.8)	112 (4.9)	–	–
Male sex	862 (47.3)	884 (39.1)	0.72 (0.63–0.84)	<0.001
Unknown	–	1	–	–
Outpatient surgery	28 (1.5)	10 (0.4)	0.41 (0.18–0.96)	0.041
Duration of surgery, h	3.59 (2.1)	4.4 (2.5)	1.20 (1.16–1.24)	<0.001
Approach				
Anterior	208 (12.2)	204 (9.5)	Referent	
Posterior	1,447 (85.2)	59 (2.7)	1.01 (0.80–1.28)	>0.9
Both	44 (2.6)	1,890 (87.8)	0.87 (0.54–1.40)	0.6
Unknown	123 (6.8)	112 (4.9)	–	–
ASA class				
1	16 (0.9)	2 (0.1)	Referent	
2	465 (27.4)	369 (17.2)	4.90 (1.06–22.6)	0.042
3	1,131 (66.6)	1,556 (72.3)	7.15 (1.56–32.8)	0.011
4	86 (5.1)	224 (10.4)	15.7 (3.35–73.5)	<0.001
Unknown	123 (6.8)	113 (5.0)	–	–
Diabetes	492 (29.0)	757 (35.2)	1.07 (0.92–1.24)	0.4
Wound class				
Clean	1,656 (97.5)	2,064 (95.9)	Referent	
Clean-contaminated	28 (1.7)	54 (2.5)	1.74 (1.06–2.86)	0.030
Contaminated	4 (0.2)	12 (0.6)	2.14 (0.65–7.07)	0.2
Dirty	11 (0.7)	23 (1.1)	1.75 (0.79–3.85)	0.2
Unknown	123 (6.8)	112 (4.9)	–	–
Spinal level				
Axis-atlas/cervical	12 (0.7)	21 (0.7)	Referent	
Cervical/dorsal/dorsolumbar	332 (19.5)	330 (14.5)	1.11 (0.77–1.62)	0.6
Dorsal/dorsolumbar	350 (20.6)	469 (21.8)	1.27 (0.99–1.63)	0.056
Lumbar/lumbosacral	916 (53.9)	1,333 (61.9)	1.51 (1.23–1.86)	<0.001
Unknown	123 (6.8)	112 (4.9)		
Trauma	87 (5.1)	139 (6.5)	1.91 (1.38–2.64)	<0.001
Closure				
Intentionally left open	14 (0.8)	21 (0.98)	Referent	
Fully closed or partial	1,684 (99.2)	2,131 (99.0)	1.08 (0.50–2.33)	0.9
Unknown	123 (6.8)	112 (4.9)		
Timing of infection, mean days from procedure (IQR)	24 (17–33)	19 (14–27)	0.97 (0.96–0.97)	<0.001
Depth of infection				
Superficial	424 (23.3)	657 (29.0)	Referent	
Deep	868 (47.6)	1,025 (45.3)	0.88 (0.74–1.05)	0.15
Organ space	530 (29.1)	583 (25.7)	0.85 (0.70–1.03)	0.1
Emergency	120 (7.1)	167 (7.8)	0.99 (0.75–1.32)	>0.9
Unknown	123 (6.8)	112 (4.9)	–	–
Use of scope	2 (0.1)	7 (0.3)	2.60 (0.51–13.4)	0.3
Unknown	123 (6.8)	112 (4.9)	–	–

*Values are no. (%) except as indicated. ORs represent the relative odds of gram-negative infection compared with the reference group of monomicrobial *Staphylococcus aureus* spinal fusion surgical site infection. ASA level 5 was removed because of insufficient numbers. Dashes indicate value was not calculated. ASA, American Society of Anesthesiologists; IQR, interquartile range; OR, odds ratio.

Table 4. Multinomial logistic regression analysis of predictors of monomicrobial gram-negative and other gram-positive spinal fusion surgical site infections compared with monomicrobial *Staphylococcus aureus* infections in study of microbial etiology of postoperative spinal fusion infections and factors associated with gram-negative infections, United States, 2021–2022*

	Monomicrobial gram-negative infections		Other gram-positive infections	
Characteristic	OR (95% CI)	p value	OR (95% CI)	p value
Age	1.03 (1.02–1.03)	<0.001	1.01 (1.00–1.02)	0.061
BMI	1.03 (1.02–1.04)	<0.001	1.02 (1.00–1.04)	0.043
Male sex	0.73 (0.63–0.84)	<0.001	1.39 (1.06–1.82)	0.019
Outpatient surgery	0.41 (0.18–0.96)	0.040	0.88 (0.29–2.65)	0.8
Duration of surgery	1.20 (1.16–1.24)	<0.001	1.06 (1.00–1.13)	0.066
Surgical approach				
Anterior	Referent		Referent	
Posterior	1.01 (0.80–1.28)	>0.9	0.98 (0.66–1.46)	>0.9
Both	0.86 (0.53-1.39)	0.5	1.31 (0.57–2.99)	0.5
ASA class				
1	Referent		Referent	
2	4.83 (1.05-22.3)	0.044	2.10 (0.27–16.5)	0.5
3	7.04 (1.53-32.3)	0.012	2.33 (0.30–18.1)	0.4
4	15.4 (3.29-72.0)	<0.001	1.96 (0.24–16.3)	0.5
Diabetes			1.20 (0.90–1.60)	0.2
Wound class				
Clean	Referent		Referent	
Clean-contaminated	1.74 (1.06–2.87)	0.029	1.13 (0.43–2.97)	0.8
Contaminated	2.21 (0.66–7.33)	0.2	0.00 (0.00-0.00)	<0.001
Dirty	1.76 (0.80–3.89)	0.2	0.00 (0.00-0.00)	<0.001
Spinal level				
Axis-atlas/cervical	Referent		Referent	
Cervical/dorsal/dorsolumbar	1.11 (0.77–1.61)	0.6	0.59 (0.32–1.08)	0.087
Dorsal/dorsolumbar	1.27 (0.99–1.63)	0.056	0.49 (0.32–0.74)	<0.001
Lumbar/lumbosacral	1.51 (1.22–1.85)	<0.001	0.44 (0.32–0.62)	<0.001
Trauma	1.91 (1.38–2.64)	<0.001	1.04 (0.57–1.89)	0.9
Closure				
Intentionally left open	Referent		Referent	
Fully closed or partial	1.07 (0.50–2.33)	0.9	2.33 (0.30–18.1)	0.4
Timing of infection, days from procedure	0.97 (0.96–0.97)	<0.001	0.99 (0.98–1.00)	0.11
Depth of infection				
Superficial	Referent		Referent	
Deep	0.88 (0.74–1.05)	0.15	0.95 (0.68–1.33)	0.8
Organ space	0.85 (0.70–1.03)	0.10	1.14 (0.79–1.66)	0.5
Emergency	0.99 (0.75–1.31)	>0.9	1.50 (0.93–2.39)	0.093
Use of scope	2.55 (0.49–13.1)	0.3	0.00 (0.00-0.00)	<0.001

*ORs represent the relative odds of monomicrobial gram-negative infections or other gram-positive infection compared with the reference group of monomicrobial *Staphylococcus aureus* spinal fusion surgical site infection. ASA level 5 was removed because of insufficient numbers. ASA, American Society of Anesthesiologists; BMI, body mass index; OR, odds ratio.

relative to monomicrobial *S. aureus* infection. Specifically, female sex, advanced age, higher BMI, prolonged operative duration, greater comorbidity burden, and emergency and trauma-related procedures were independently associated with a higher likelihood of gram-negative infection compared with infections involving monomicrobial *S. aureus*. The associations remained consistent in a secondary analysis restricted to monomicrobial gram-negative and monomicrobial *S. aureus* infections, demonstrating that the findings are not confounded by coinfecting organisms.

The precise underlying mechanisms driving the observed associations between those independent variables and gram-negative infections remain to be fully elucidated. Of note, our finding that trauma before spinal fusion independently correlates with a gram-negative etiology aligns with existing literature on fracture-related infections, which similarly demonstrate a high proportion of gram-negative infections (*9*). Those parallel clinical observations highlight a critical area for future prospective studies to investigate the specific pathophysiological pathways.

The strengths of this study include the use of a large, national dataset derived from the NHSN, encompassing thousands of spinal fusion SSI cases reported from multiple centers across the United States. This sample size exceeds that of most previously published studies, which have often been limited to single institutions or regional networks and therefore subject to potential biases because of local practice patterns, patient demographics, and institutional protocols. The multicenter nature of the dataset enhances the generalizability of our findings and provides substantially greater statistical power

to detect associations among patient characteristics, surgical factors, and microbial etiology.

The first limitation of our study is that the reporting of spinal fusion SSIs to the NHSN is voluntary, introducing the possibility of reporting bias. Because the NHSN database only records infected episodes, the lack of an uninfected control group prevents evaluation of risk factors for development of infection. The use of *S. aureus* infections as the statistical reference limits generalizability because that cohort only involves those that already have infections. Because this national registry dataset contains only standardized, registry-submitted data, we lacked access to granular clinical details, such as specific perioperative antimicrobial protocols, antibiotic susceptibility profiles, use of allografts, instrumentation, and the precise anatomic source of the cultures. Furthermore, the redaction of key geographic and institutional variables, including facility size and type, prevented their inclusion in our multinomial models, limiting our ability to assess the variables that might have been pertinent. As an example, an outbreak of spinal fusion SSIs associated with the use of bone allografts infected with *Mycobacterium tuberculosis* that was reported in 2021 might not be fully captured in our study (*10*).

Because our cohort spans 2021–2022, our findings reflect pandemic-era practice patterns and case mixes. Institutional restrictions and altered clinical priorities during this period might have altered typical patient demographics and surgical volumes. As a consequence, those transient pandemic-era modifications could limit the generalizability of our results to current, postpandemic clinical practice.

In conclusion, gram-negative infections account for nearly one third of spinal fusion SSIs and are associated with specific patient and surgical factors. The identification of independent factors related to gram-negative infections provides a practical foundation for transitioning from a universal approach to risk-stratified clinical decision-making. For researchers, specific high-risk cohorts highlight key target populations for future studies evaluating expanded gram-negative prophylactic regimens. For clinicians, using these risk profiles can guide timely, targeted empiric antimicrobial selection when spinal fusion SSIs occur, ultimately balancing optimal antimicrobial stewardship with tailored patient care.

Acknowledgment

We thank the Centers for Disease Control and Prevention staff who provided the data used in this study.

We also acknowledge research support from NIH National Institute of Allergy and Infectious Diseases (grant no. T32AI055433).

During the preparation of this work, we used ChatGPT-5 (OpenAI, https://openai.com) to check the grammar and clarity of the manuscript. After using this tool, we reviewed and edited the content as needed and take full responsibility for the content of the published article.

About the Author

Dr. Lindstrom is a first-year clinical fellow at the University of Minnesota Division of Infectious Diseases and International Medicine. Her research interests are orthopedic infectious diseases, such as periprosthetic joint infections and postoperative spine infections.

References

1. Shaw JD, Nelson SB, Simpfendorfer C, Berbari EF, Henry MW, Kleck CJ, et al. New definition for postoperative spine infection (PSI): from the workgroup of the Musculoskeletal Infection Society (MSIS) and the European Bone & Joint Infection Society (EBJIS). Spine. 2025. https://doi.org/10.1097/BRS.0000000000005604
2. Edmiston CE Jr, Leaper DJ, Chitnis AS, Holy CE, Chen BPH. Risk and economic burden of surgical site infection following spinal fusion in adults. Infect Control Hosp Epidemiol. 2023;44:88–95. https://doi.org/10.1017/ice.2022.32
3. Alfin DJ, Shilong DJ, Bot GM, Dengunu Salun W. Surgical site infection rate in spine surgery, incidence, and risk factors: a ten-year retrospective cohort review in a developing neurosurgical centre. BMC Surg. 2025;25:127. https://doi.org/10.1186/s12893-025-02846-4
4. Centers for Disease Control and Prevention. CDC/NHSN surveillance definitions for specific types of infections, 2024. In: National Healthcare Safety Network Patient Safety Component Manual [cited 2026 Jan 6]. https://www.cdc.gov/nhsn/pdfs/validation/2024/pcsmanual_2024.pdf
5. Abdul-Jabbar A, Berven SH, Hu SS, Chou D, Mummaneni PV, Takemoto S, et al. Surgical site infections in spine surgery: identification of microbiologic and surgical characteristics in 239 cases. Spine. 2013;38:E1425–31. https://doi.org/10.1097/BRS.0b013e3182a42a68
6. Shillingford JN, Laratta JL, Reddy H, Ha A, Lehman RA Jr, Lenke LG, et al. Postoperative surgical site infection after spine surgery: an update from the Scoliosis Research Society (SRS) Morbidity and Mortality Database. Spine Deform. 2018;6:634–43. https://doi.org/10.1016/j.jspd.2018.04.004
7. Tai DBG, Patel R, Abdel MP, Berbari EF, Tande AJ. Microbiology of hip and knee periprosthetic joint infections: a database study. Clin Microbiol Infect. 2022;28:255–9. https://doi.org/10.1016/j.cmi.2021.06.006
8. Long DR, Bryson-Cahn C, Pergamit R, Tavolaro C, Saigal R, Chan JD, et al. 2021 Young investigator award winner: anatomic gradients in the microbiology of spinal fusion surgical site infection and resistance to surgical antimicrobial prophylaxis. Spine. 2021;46:143–51. https://doi.org/10.1097/BRS.0000000000003603
9. Depypere M, Sliepen J, Onsea J, Debaveye Y, Govaert GAM, IJpma FFA, et al. The microbiological etiology of fracture-related infection. Front Cell Infect Microbiol. 2022;12:934485. https://doi.org/10.3389/fcimb.2022.934485

10. Wortham JM, Haddad MB, Stewart RJ, Annambhotla P, Basavaraju SV, Nabity SA, et al. Second nationwide tuberculosis outbreak caused by bone allografts containing live cells—United States, 2023. MMWR Morb Mortal Wkly Rep. 2024;72:1385–9. https://doi.org/10.15585/mmwr.mm725253a1

Address for correspondence: Don Bambino Geno Tai, University of Minnesota Division of Infectious Diseases and International Medicine, 420 Delaware St SE, Minneapolis, MN 55455, USA; email: geno@tai-md.com

EID journal

Want to stay updated on the latest news in *Emerging Infectious Diseases*? Let us connect you to the world of global health. Discover groundbreaking research studies, pictures, podcasts, and more by following us on Instagram at @eidjournal

Invasive Enterovirus and Parechovirus Infections in Adults, Alberta, Canada, 2023–2025

Jamil N. Kanji, Hong Yuan Zhou, Nathan Zelyas, Kanti Pabbaraju, Anita Wong, Kara Gill, Tarah Lynch, Graham Tipples, Nabeela Nathoo, Dima Kabbani, Adil Adatia

We conducted a retrospective, population-based laboratory surveillance study during May 2023–December 2025 in Alberta, Canada, to characterize adult invasive enterovirus and parechovirus infections and to identify groups at high risk for those infections. Of 15,621 samples tested, 162 (1.0%) were virus positive, of which 51 (31.5%) samples from 39 patients indicated invasive infections. Cerebrospinal fluid, blood, and cardiac tissue were the most frequent virus-positive specimens. The invasive enterovirus and parechovirus incidence rate was 0.37 cases/100,000 person-years; rates were higher in patients <50 versus ≥50 years of age (incidence rate ratio 8.2; p<0.001). The annual incidence rates were 0.20–0.56 cases/100,000 person-years; rates appeared higher in 2025 than in 2024 (incidence rate ratio 2.1; p = 0.11). Severe disseminated enterovirus infection occurred in 2 patients who received ocrelizumab. Continuous surveillance and ongoing optimization of enterovirus and parechovirus detection assays is essential for comprehensive public health tracking.

Enteroviruses and parechoviruses are globally circulating picornaviruses that typically cause mild or asymptomatic infections but can cause severe invasive disease in certain clinical contexts. Several nationwide studies in Denmark reported that enteroviruses are among the leading viral causes of adult meningitis, which has a favorable outcome in immunocompetent patients (*1*–*3*). Beyond meningitis, enteroviruses can cause encephalitis and meningoencephalitis (*4*), as well as myocarditis and pericarditis (commonly caused by coxsackievirus B) (*5*). Invasive enterovirus infection can also manifest a disseminated sepsis-like syndrome in immunocompromised hosts (*6*). Surveillance and cerebrospinal fluid (CSF)–based typing studies in Europe and North America have characterized coxsackievirus B5, enterovirus A71 (EV-A71), and EV-D68 as commonly identified invasive genotypes (*7*–*9*). Among echoviruses (a subset of enteroviruses), echoviruses 6, 9, 11, and 18 are commonly reported invasive types (*7*,*10*). Invasive enterovirus-type distribution likely varies according to clinical syndrome, geography, and time, which reflects the heterogeneity of observed genotypes (*11*).

Parechovirus infections are reported less frequently in adults than in neonates and infants. One study found parechovirus prevalence in adults was 0.18% (*12*). Nevertheless, adult cases of parechovirus-induced meningoencephalitis and severe systemic infections have been documented, usually in the setting of immunosuppression or critical care (*12*). That finding suggests that adult disease might be underrecognized. Parechoviruses 1, 3, 5, and 6 are the most frequently reported invasive parechovirus genotypes (*12*–*15*). Outcome data for adults with invasive parechovirus infections are limited to small series and case reports that describe outcomes ranging from recovery to fatal encephalitis in vulnerable hosts (*16*).

Being immunocompromised is commonly reported as a risk factor for invasive enterovirus or parechovirus infections in adults (*17*). Severe enterovirus infections have been described in patients who have hematologic malignancies, organ transplantation, and hypogammaglobulinemia (congenital or acquired) and in those receiving B-cell depleting therapies (*17*–*19*). Long-term follow-up studies on enterovirus infections of the central nervous system (CNS) in adults also identified immunosuppression as a predictor of poor outcomes (*20*). More recently,

Author affiliations: Alberta Precision Laboratories Public Health Laboratory, Edmonton, Alberta, Canada (J.N. Kanji, H.Y. Zhou, N. Zelyas, K. Pabbaraju, A. Wong, K. Gill, T. Lynch, G. Tipples); University of Calgary, Calgary, Alberta, Canada (J.N. Kanji, H.Y. Zhou, T. Lynch); University of Alberta, Edmonton (J.N. Kanji, N. Zelyas, G. Tipples, N. Nathoo, D. Kabbani, A. Adatia)

DOI: https://doi.org/10.3201/eid3211.260941

multiple reports have described disseminated enterovirus infections in patients who had B-cell depletion after ocrelizumab treatment for multiple sclerosis; almost all patients had documented hypogammaglobulinemia, and outcomes included recovery, residual deficits, and death (*9*,*21*–*24*).

Data on invasive enterovirus and parechovirus infections in adults are limited, particularly in immunocompromised populations. Prompted by the laboratory identification of severe disseminated enterovirus infections in ocrelizumab-treated patients, we conducted a population-based review of laboratory-confirmed invasive enterovirus and parechovirus infections among adults in Alberta, Canada, during 2023–2025.

Materials and Methods

Study Design, Data Extraction, and Chart Review

We extracted laboratory data regarding all enterovirus and parechovirus testing in adult patients conducted in Alberta, Canada, during May 1, 2023–December 31, 2025, from the provincial electronic medical records in the laboratory information system (Epic, https://www.epic.com). The Conjoint Health Research Ethics Board at the University of Calgary in Calgary, Alberta, Canada, approved this study before data collection (study identification no. REB25-2031).

We included data for adult patients (≥17 years of age at the time of specimen collection, according to the provincial health administration definition). We defined invasive infection as the detection of enterovirus or parechovirus nucleic acid by using real-time reverse transcription PCR of blood, CSF, joint fluid, or tissue biopsy samples collected from a sterile site. We did not classify detection of enteroviruses or parechoviruses in tissue samples from skin, respiratory, oral, or mucosal tissue as an invasive infection.

We extracted and tabulated data for specimens that met the inclusion criteria (samples from adult patients and invasive infection). We conducted retrospective chart reviews to collect patient information regarding disease manifestation, diagnostic evaluation, presence of underlying immunosuppressive conditions or medications, need for critical care, extracorporeal membrane oxygenation, and whether the patient survived the infection. We categorized patients as either having no recognized immunosuppression, receiving ocrelizumab, or having a recognized immunocompromising condition. We defined geographic distribution by using the second digit within the patient's postal code, which categorized the patient as residing in urban or rural postal sorting areas. We used a composite of intensive or coronary care unit admission, requirement for extracorporeal membrane oxygenation, or death attributable to enterovirus or parechovirus infection to define a critical or fatal outcome. We recorded results of genetic testing for inborn errors of immunity when those tests were requested by clinicians managing each patient.

Setting and Enteroviruses and Parechoviruses Testing

As of April 1, 2026, Alberta had a population of 5.06 million persons (https://economicdashboard.alberta.ca/dashboard/population-quarterly). Testing for enterovirus and parechovirus in Alberta is conducted centrally at the Alberta Precision Laboratories Public Health Laboratory in Calgary. Testing is performed on a wide range of specimen types by using a validated, nonquantitative, laboratory-developed multiplex real-time reverse transcription PCR that targets the 5′ nontranslated regions of both enteroviruses and parechoviruses (Appendix, https://wwwnc.cdc.gov/EID/article/32/11/26-0941-App1.pdf) (*25*).

Typing of Enterovirus Isolates

We performed enterovirus typing for specimens from all invasive cases. For patients with multiple positive specimens, we selected the specimen that had the lowest cycle threshold (Ct) value for genotyping. Genotyping included PCR amplification and Sanger sequencing of a segment of the 5′ nontranslated region (293 bp), the viral protein (VP) 4 gene (207 bp), and 5′ region of the VP2 gene (250 bp) (*26*,*27*). We performed phylogenetic analysis of 62 amino acids from the VP2 protein by using the neighbor-joining method in MEGA version 10.2.2 (https://www.megasoftware.net) (Appendix).

Statistical Analysis

We performed statistical analyses by using R Studio version 2026.08.0, build 187 (Posit Software, https://posit.co). We compared Ct values by using medians and interquartile ranges and by using the Mann-Whitney U test for nonnormal distributions.

We obtained population estimates for persons in Alberta who were ≥17 years of age from the Government of Alberta Office of Statistics and Information and stratified those data according to age and sex during 2023–2025. Only two thirds of a population year were available for estimates in 2023 because surveillance commenced in May (hence, 2023 denominator contributions were multiplied by 2/3). We used those estimates to calculate incidence rates for all invasive enterovirus and parechovirus infections, enterovirus-only infections, calendar year, age strata (17–29,

30–49, 50–64, and ≥65 years of age), and sex, as well as for critical or fatal invasive infection. We expressed all rates as per 100,000 person-years along with exact 95% Poisson CIs because of the low number of events.

The manufacturer of ocrelizumab (Hoffman-La Roche Canada, https://www.rochecanada.com) provided the number of patients who received ≥1 dose of the agent in Alberta annually during 2023–2025. We estimated the crude risk for invasive enterovirus disease and mortality rates for patients taking ocrelizumab by dividing the number of observed events by the treated patient-years (summed annual counts of active ocrelizumab-treated persons) and calculated exact 95% CIs as described. We prorated the 2023 patient count for the May–December observation period as described. We scaled the results according to treated patient-years. We assumed that invasive enterovirus disease was a patient-level outcome rather than an infusion-level outcome and that stable treatment exposure occurred within each calendar year (i.e., dosing every 6 months).

We assessed event rates between groups by calculating pairwise incidence rate ratios (IRRs) and exact 95% Poisson CIs. To evaluate rate differences according to age, we tested for consistency across all age groups (exact conditional test of homogeneity) assuming a null hypothesis of equal incidence. We compared incidences between sex, 2024 and 2025, and various age categories (Appendix).

Results

Virus Testing

Over the ≈3-year study period, a total of 15,621 samples were received for enterovirus and parechovirus testing (Table 1). Of those, 162 (1.0%) samples were positive; 51 (31.5%) met our definition of invasive infection. CSF was the most common specimen type received (40 [78.4%] samples), followed by blood (8 [15.7%] samples) and heart tissue (3 [5.9%] samples) (Appendix Table 1). Of the 51 samples positive for invasive infection, 50 were positive for enterovirus and 1 for parechovirus (Appendix).

Characteristics of Patients with Invasive Virus Infection

The 51 positive specimens were from 39 patients who were a median age of 32.5 years (range 17–72 years; interquartile range 23–35 years); 22 (56.4%) were female and 17 (43.6%) male (Table 2; Appendix Tables 2, 3). According to postal code sorting, 33 (84.6%) patients resided in urban areas and 6 (15.4%) in rural areas. Invasive cases occurred in 14 (35.9%) patients in 2023, eight (20.5%) in 2024, and 17 (43.6%) in 2025 (38 cases were caused by enterovirus; 1 was caused by parechovirus in 2024). Most (69.2%; n = 27) patients were hospitalized; median stay was 3 days. Only 2 patients required admission to a critical care setting. The most common enterovirus syndromes were aseptic meningitis (31 [79.5%] patients) and encephalitis or meningoencephalitis (6 [15.4%] patients). Two patients in the cohort died.

CSF analysis was conducted for 37 (94.9%) patients (Appendix Table 3). All patients with aseptic meningitis had CSF leukocytosis (>5 × 10^6 leukocytes/L). In 30 (76.9%) patients who underwent CNS imaging, 28 (93.3%) had no acute abnormality reported. The cases demonstrated a seasonal pattern (Figure 1) in 2023 and 2025, with peaks in the summer and early autumn; fewer cases were reported in 2024.

Incidence Rates and Comparisons

The overall incidence rate of invasive enterovirus and parechovirus infections was 0.37 (95% CI 0.27–0.51) cases/100,000 person-years (Table 3). Annual incidence rates varied from 0.20 to 0.56 cases/100,000 person-years; the highest incidence was observed in 2023 and lowest in 2024. Incidence varied significantly according to age group (overall p value was <0.001), and the highest rates were among adults 17–29 and 30–49 years of age. The incidence rate for a critical or fatal outcome was 0.02 (95% CI 0.0–0.07) cases/100,000 person-years. Analysis combining age strata demonstrated that the incidence among adults <50 years of age was 8.2-fold higher than among those ≥50 years of age (IRR 8.21 [95% CI 2.59–41.65]; p<0.001). Incidence did not differ significantly

Table 1. Numbers of specimens tested for enterovirus and parechovirus from adults with invasive infections, Alberta, Canada, 2023–2025

Specimens	No. (%) specimens/study year			Total, no. (%)
	2023	2024	2025	
No. specimens received*	3,723	5,767	6,131	15,621
Positive for virus	42 (1.1)	58 (1.0)	62 (1.0)	162 (1.0)
Positive invasive infection†	15 (35.7)	9 (15.5)	27 (43.5)	51 (31.5)
Cerebrospinal fluid samples	15 (100)	8 (88.9)	17 (63.0)	40 (78.4)
Blood samples	0	1 (11.1)	7 (25.9)	8 (15.7)
Sterile tissue samples	0	0	3 (11.1)	3 (5.9)

*All specimens received (sterile and nonsterile sites).
†No. (%) virus-positive samples. Counts reflect positive specimens; some patients contributed >1 specimen.

Table 2. Clinical characteristics of patients in study of invasive enterovirus and parechovirus infections in adults, Alberta, Canada, 2023–2025*

Characteristics	Not IC, n = 33	IC by ocrelizumab, n = 3	IC for other reasons, n = 3	Total
Median age, y (IQR)	31 (23–35)	29 (29–32)	39 (38–53)	32.5 (23–35)
Age groups, y				
17–29	14 (42.4)	2 (66.7)	0	16 (41.0)
30–49	17 (51.5)	1 (33.3)	2 (66.7)	20 (51.3)
50–64	1 (3.0)	0	0	1 (2.6)
≥65	1 (3.0)	0	1 (33.3)	2 (5.1)
Study year				
2023, May–December	14 (42.4)	0	0	14 (35.9)
2024	7 (21.2)	1 (33.3)	0	8 (20.5)
2025	12 (36.4)	2 (66.7)	3 (100)	17 (43.6)
Sex				
F	18 (54.5)	2 (66.7)	2 (66.7)	22 (56.4)
M	15 (45.5)	1 (33.3)	1 (33.3)	17 (43.6)
Geographic distribution†				
Urban postal code	29 (87.9)	1 (33.3)	3 (100)	33 (84.6)
Rural postal code	4 (12.1)	2 (66.7)	0	6 (15.4)
Enterovirus/parechovirus syndrome				
Aseptic meningitis‡	28 (84.8)	0	3 (100)	31 (79.5)
Encephalitis/meningoencephalitis	5 (15.2)	1 (33.3)	0	6 (15.4)
Disseminated infection, myocarditis	0	2 (66.7)	0	2 (5.1)
Clinical course and outcomes				
Hospitalized	21 (63.6)	3 (100)	3 (100)	27 (69.2)
Median length of stay, d (IQR) [range]	2 (2–3) [1–11]	45 (26.5–62.5) [8–80]§	4 (3.5–5.5) [3–7]	3 (2–5.5)
ICU or ECMO admission	0	2 (66.7)	0	2 (5.1)
Death	0	2 (66.7)	0	2 (5.1)
Underlying illnesses				
None	10 (30.3)	0	0	10 (25.6)
Hyperlipidemia	1 (3.0)	0	1 (33.3)	2 (5.1)
Hypothyroid	2 (6.1)	0	1 (33.3)	3 (7.7)
Inflammatory bowel disease	0	0	1 (33.3)	1 (2.6)
Irritable bowel syndrome	0	1 (33.3)		1 (2.6)
Lymphoma	0	0	1 (33.3)	1 (2.6)
Migraine	4 (12.1)	0	0	4 (10.3)
Multiple sclerosis	0	3 (100)	0	3 (7.7)
Obstructive sleep apnea	0	0	1 (33.3)	1 (2.6)
Opioid/substance use disorder	4 (12.1)	0	0	4 (10.3)
Solid organ transplant	0	0	1 (33.3)	1 (2.6)
Rheumatoid arthritis	0	1 (33.3)	0	1 (2.6)

*Values are no. (%) except as indicated. Total no. patients = 39. ADHD, attention deficit hyperactivity disorder; ECMO, extracorporeal membrane oxygenation; IC, immunocompromised; ICU, intensive care unit; IQR, interquartile range.
†Urban and rural postal code classifications were according to the second character of the Forward Sortation Area of Canada Post; numerals 1–9 were classified as urban and 0 as rural. Those categories represent postal delivery geography and do not necessarily correspond to census-based definitions of urban and rural residence (https://www.canadapost-postescanada.ca/cpc/en/support/articles/addressing-guidelines/postal-codes.page, accessed 2026 Aug 10).
‡Thirty (96.8%) of 31 patients with aseptic meningitis had cerebrospinal fluid pleocytosis (leukocyte count >5 × 10^6 cells/L).
§One of the 3 hospitalized patients in this group had 2 hospitalizations, which were counted separately.

according to sex (IRR 1.30 [95% CI 0.66–2.61]; p = 0.43). Incidence appeared to be approximately 2-fold higher in 2025 than in 2024, although that difference was not statistically significant (IRR 2.07 [95% CI 0.85–5.54]; p = 0.11).

Invasive Enterovirus Infections in Immunocompromised Patients

Six (15.4%) of 39 patients with invasive enterovirus infection were considered immunocompromised (Table 2; Appendix Table 4). The underlying causes of immunosuppression were CD20 monoclonal antibody treatment in 4 patients (3 used ocrelizumab for multiple sclerosis, and 1 used rituximab for lymphoma), organ transplantation in 1 patient, and infliximab use for Crohn's disease in 1 patient. Three of the 6 patients had aseptic meningitis, 1 had encephalitis, and 2 had disseminated infection with fulminant myocarditis. The 2 patients with myocarditis were receiving ocrelizumab, and both died (Appendix Table 4).

The numbers of patients who received ≥1 dose of ocrelizumab in Alberta during the study years were 1,778 for 2023, 1,972 for 2024, and 2,119 for 2025 (M. Davies, Hoffman-La Roche Limited, pers. comm., email, 2026 Jan 14). On the basis of those data, the estimated crude incidence rate for invasive enterovirus disease among persons receiving ocrelizumab was 56.9 (95% CI 11.7–166.2) cases/100,000 ocrelizumab-

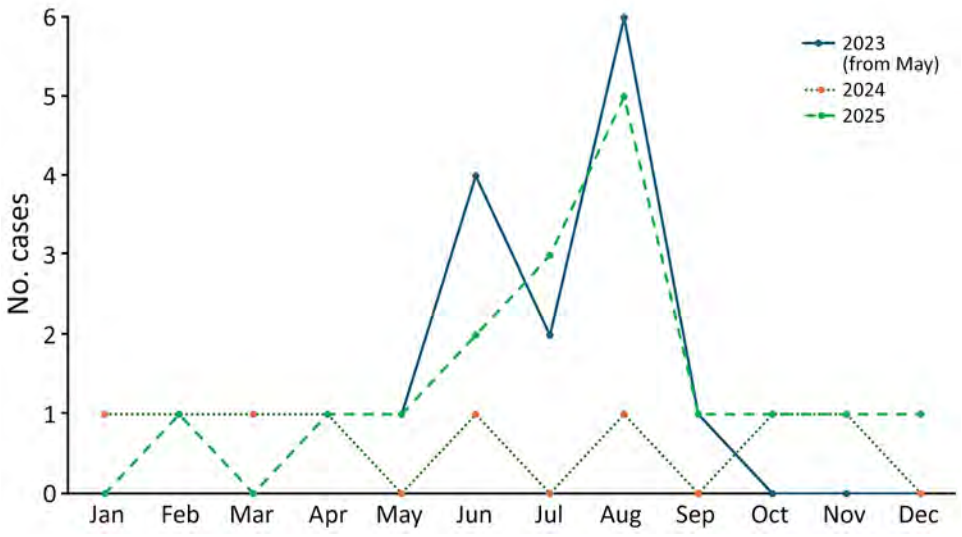

Figure 1. Seasonal variation of invasive enterovirus and parechovirus infections in adults, Alberta, Canada, 2023–2025.

treated patient-years. The crude incidence rate for death caused by invasive enterovirus disease for a person using ocrelizumab was 37.9 (95% CI 4.6–136.9) cases/100,000 ocrelizumab-treated patient-years. Denominators for other immunocompromised populations in the province were not available, preventing subgroup incidence determination.

Genotyping of Invasive Enterovirus Isolates

Invasive enteroviruses could be amplified for genotyping in 18 (46.2%) of 39 cases (Figure 2; Appendix Table 5). The most frequently identified enterovirus was echovirus 30, followed by coxsackievirus B4 and echovirus 9. Echovirus 9 and echovirus 18 were observed over multiple surveillance years (both during 2024 and 2025). Enterovirus typing was possible for samples from 4 of 6 immunocompromised patients (Appendix Table 4). Coxsackievirus B3 was identified in 2 of 6 immunocompromised patients who had sepsis and myocarditis (both receiving ocrelizumab), echovirus 9 was found in 1 patient with meningitis, and EV-A71 was found in 1 patient with meningoencephalitis. Both fatal cases involved coxsackievirus B3 that was associated with severe, fulminant myocarditis and heart failure (Appendix Table 4). We submitted all 18 sequences from this study to GenBank (accession nos. PZ914341–58) (Appendix Table 6).

We created a dendrogram to evaluate the relatedness of the typed strains, including strains that infected ocrelizumab-treated persons (Appendix Figure). Phylogenetic analysis of the VP2 regions demonstrated that clinical isolates from adult patients clustered among established reference strains without evidence of close relatedness among the sequences. Those findings indicate genetic diversity among the enteroviruses causing invasive disease in Alberta without a single clonal cluster.

Discussion

In a provincewide, laboratory-based retrospective study in Alberta, Canada, we identified 39 adults with invasive enterovirus or parechovirus infections over a 32-month period, which resulted in an overall incidence rate of 0.37 cases/100,000 person-years. Most patients were not immunosuppressed and had favorable outcomes; aseptic meningitis was the principal manifestation of infection. Deaths were only recorded among a subgroup of immunocompromised patients who received ocrelizumab, a CD20-binding B-cell depleting agent.

The incidence of invasive enterovirus infection in our cohort was higher among adults <50 years of age. Rates were 0.51–0.72 cases/100,000 person-years for persons 17–49 years of age, compared with 0.05–0.10 cases/100,000 person-years for those ≥50 years of age. That age distribution is consistent with several studies in Denmark that identified a median age of 31–33 years among adults with invasive enterovirus infection (*1*,*3*). In our analysis, incidence was ≈8-fold higher among adults <50 years than for those ≥50 years of age; however, the analysis might be limited by low case numbers in the ≥50 years of age group. Although the exact reason for the ≈8-fold difference is unclear, published studies hypothesized that older adults are protected more by accumulated type-specific and cross-reactive immunity than younger adults (*1*,*28*). In contrast, the observed incidence did not differ according to sex, suggesting that age was the more prominent variable associated with invasive infection, as previously reported (*1*,*3*). However,

2 studies identified sex as a driver of outcome; 1 of those studies reported female patients with invasive enterovirus infections were 2.3 times more likely to experience an unfavorable outcome at discharge than those who had other causes of viral meningitis (*1*,*3*).

The annual incidence of invasive enterovirus infections varied during the surveillance period. Fewer infection cases were identified in 2024 than in 2025, which is unlikely to represent an interruption in laboratory surveillance. We can confirm that laboratory surveillance was continuous throughout 2024, and the overall enterovirus and parechovirus PCR test positivity remained at 1% across study years. Although the population incidence rate of invasive enterovirus infection appeared ≈2-fold higher in 2025 (0.42 cases/100,000 person-years) than in 2024 (0.20 cases/100,000 person-years), that difference was not statistically significant (IRR 2.1; p = 0.11). Because of the small number of invasive infections, we hypothesize that the observed annual differences reflect year-to-year variation in enterovirus circulation rather than a sustained change in incidence. The 2023 rate was not directly compared (in terms of IRRs) to 2024 and 2025 because surveillance only started in May of that year.

Among patients receiving ocrelizumab in our cohort, 3 invasive enterovirus infections occurred, which caused 2 deaths. Although we reported few deaths (thus, requiring cautious interpretation), that clustering highlights a potential pharmacovigilance signal. The crude incidence rate of 56.9 cases/100,000 ocrelizumab-treated patient-years in our study is higher than reported population-based enterovirus-mediated meningitis estimates (1.8–3.6 cases/100,000 patient-years) (*1*), although differences in study populations and endpoints make direct comparisons difficult. Disseminated enterovirus infection among patients receiving ocrelizumab has been previously reported (Appendix Table 7), and numerous recent reports have also emphasized a potential safety signal (*21*,*22*,*24*). The mechanisms leading to infection have been proposed to be ocrelizumab-induced hypogammaglobulinemia that causes deficient humoral immunity and B-cell depletion that causes reduced enterovirus clearance. Two of the 3 affected patients in our study had serum IgG concentrations

Table 3. Population-estimated incidence rates and rate comparisons for invasive enterovirus and parechovirus infections in adults, Alberta, Canada, 2023–2025*

Measurements†	Incidence/100,000 PY (95% CI)‡	IRR (95% CI)‡	p value
Overall incidence rates			
Invasive enterovirus and parechovirus	0.37 (0.27–0.51)	NA	
Enterovirus only	0.36 (0.26–0.50)	NA	
Incidence rates according to age group, y			
17–29	0.72 (0.41–1.16)	NA	
30–49	0.51 (0.31–0.78)	NA	
50–64	0.05 (0.00–0.25)	NA	
≥65	0.10 (0.01–0.36)	NA	
Age-group comparisons, y§			
17–29 vs. 30–49	NA	1.42 (0.69–2.89)	0.30
<50 vs. ≥50	NA	8.21 (2.59–41.65)	<0.001
Annual incidence rates¶			
May–December 2023	0.56 (0.31–0.95)	NA	
2024	0.20 (0.09–0.40)	NA	
2025	0.42 (0.25–0.68)	NA	
Annual comparison			
2025 vs. 2024	NA	2.07 (0.85–5.54)	0.11
Sex-stratified incidence rates#			
F	0.42 (0.26–0.64)	NA	
M	0.33 (0.19–0.52)	NA	
Sex comparison			
F vs. M	NA	1.30 (0.66–2.61)	0.43
Critical or fatal outcome incidence rate**			
ICU/CCU admission, ECMO support, or death attributed to invasive virus infection	0.02 (0.00–0.07)	NA	

*CCU, cardiac care unit; ECMO, extracorporeal membrane oxygenation; ICU, intensive care unit; IRR, incidence rate ratio; NA, not applicable; PY, person-years.
†Unless otherwise indicated, rates were calculated for the entire study (May 2023–December 2025) and represent invasive enterovirus and parechovirus infections. Rates were calculated by using population estimates obtained from the Alberta Population Table, Government of Alberta, Office of Statistics and Information (https://goa-osi-dashboards.azurewebsites.net/Reports).
‡Exact Poisson 95% CI was calculated.
§The overall comparison of incidence rates across all 4 age groups was statistically significant (exact conditional test of homogeneity; p<0.001).
¶Because the surveillance period in this study began in May 2023, the annualized 2023 incidence disproportionately represents months of expected seasonal enterovirus circulation and should not be directly compared with complete calendar years.
#Reported in the patient's charts at the time PCR was used to detect enterovirus and parechovirus.
**Includes all patients infected with invasive enterovirus or parechovirus (n = 39).

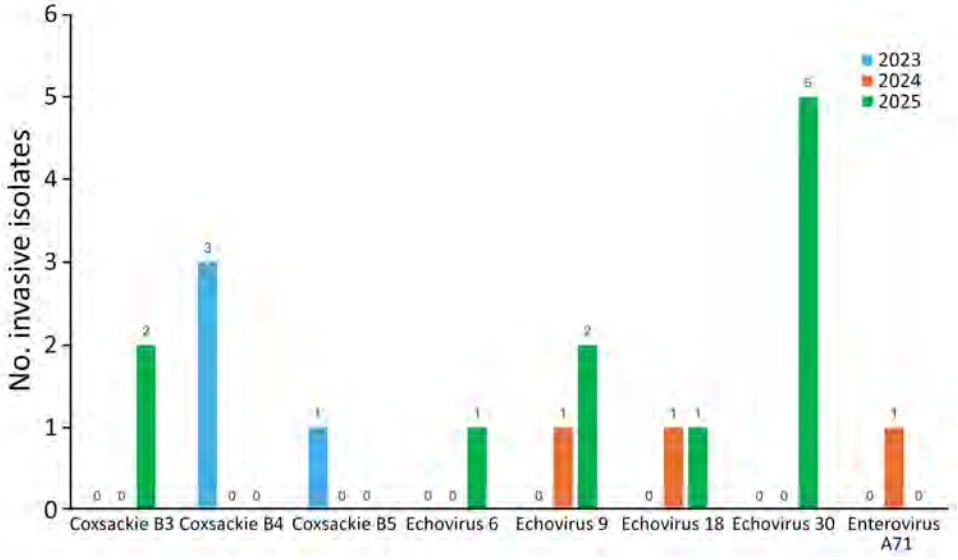

Figure 2. Genotyping of invasive enterovirus isolates in study of invasive enterovirus and parechovirus infections in adults, Alberta, Canada, 2023–2025. Of 39 unique patients with invasive virus infections, PCR amplification and genotyping were performed on samples from 4 of 14 patients in 2023, three of 8 patients in 2024, and 11 of 17 patients in 2025.

above the commonly cited 4 g/L threshold for immunoglobulin replacement and had no history of recurrent infections (*29*). Clinician-ordered testing for inborn errors of immunity was performed for only 2 ocrelizumab-treated patients; 1 of those patients had a *TNFRSF13B* C104R gene variant, which increases susceptibility to antibody deficiency (*30*). However, because the remaining patients in this cohort (including other immunocompromised patients) were not tested, the potential contribution of underlying genetic susceptibilities to severe enterovirus disease could not be assessed. Further study will be needed to determine clinical predictors of susceptibility in this group of patients.

Our genotyping results suggest that multiple enterovirus types (e.g., coxsackievirus B viruses, various echoviruses, and EV-A71) circulated during the study period. The frequent detection of echovirus 9 and echovirus 30 is consistent with previous reports identifying those as common virus types that contribute to adult aseptic meningitis (*31*). The seasonal distribution of cases mirrors that of established enterovirus circulation patterns in North America, which peak during late spring through early autumn (*32*).

Our findings highlight critical diagnostic considerations pertaining to enterovirus infection diagnoses. Neuroimaging showed no obvious abnormality in 28 (93.3%) of 30 patients who were imaged, consistent with previous studies of virus-induced or aseptic meningitis in which leptomeningeal enhancement is variably present (*1*,*33*). Many available multiplex respiratory panels combine enterovirus and rhinovirus targets. Although those panels can provide early indicators of enterovirus disease, distinction from rhinovirus is required, and the presence of enterovirus in respiratory samples alone cannot establish invasive, disseminated disease (*34*). Furthermore, the enterovirus load within the CNS is typically low (*35*). Low-level smoldering enterovirus loads in immunocompromised patients who have potential meningoencephalitis have been described (*36*). Thus, in immunocompromised patients who have delayed or atypical manifestations of infection, testing additional specimens, such as blood, other sterile sites, or tissue (e.g., myocardial biopsy), should be considered to enhance the diagnostic yield (*37*,*38*).

The principal strength of this study is the centralized testing of enterovirus from different specimen types; thus, we captured all positive samples accurately during the study period. The first limitation of our study is that the genotyping of enterovirus isolates was only available for 18 (46.2%) of 39 isolates because of low virus loads. Our sequencing assay does not reliably amplify virus sequences when the Ct is >34 cycles. Second, because a retrospective laboratory-based study relies on clinician-directed testing, we were more likely to capture more severe infections. Patients with milder cases might not have sought care or undergone diagnostic testing. Finally, the risk estimates for ocrelizumab-treated patients should be interpreted with caution because of the small number of events and reliance on aggregate measures of drug treatment exposure. Further study will be critical to help refine those estimates.

In conclusion, invasive adult enterovirus and parechovirus infections are uncommon in Alberta and manifest most often as self-limited aseptic meningitis among adults <50 years of age. Severe infections that required care in an intensive care unit or had a poor outcome were rare and occurred exclusively among

ocrelizumab-treated patients. Maintaining a high index of suspicion for disseminated disease in high-risk patients might expedite earlier diagnosis and improve outcomes. Ongoing surveillance and broader optimization of enterovirus and parechovirus detection assays remain essential for comprehensive public health tracking.

Acknowledgments

We thank Hoffman-La Roche Pharmaceuticals for providing aggregate numbers of patients receiving ≥1 doses of ocrelizumab in Alberta Province. We obtained written permission from Hoffman-La Roche Pharmaceuticals to include those numbers in this manuscript (personal communication).

The deidentified datasets used or analyzed during the current study are available from the corresponding author upon reasonable request.

About the Author

Dr. Kanji is an infectious diseases consultant and medical microbiologist at Alberta Precision Laboratories, University of Alberta, and University of Calgary in Alberta, Canada. His research interests include public health virology, viral zoonoses, and clinical infection control.

References

1. Bodilsen J, Mens H, Midgley S, Brandt CT, Petersen PT, Larsen L, et al.; Danish Study Group of Infections of the Brain (DASGIB). Enterovirus meningitis in adults: a prospective nationwide population-based cohort study. Neurology. 2021;97:e454–63. https://doi.org/10.1212/WNL.0000000000012294
2. Bodilsen J, Storgaard M, Larsen L, Wiese L, Helweg-Larsen J, Lebech AM, et al.; DASGIB study group. Infectious meningitis and encephalitis in adults in Denmark: a prospective nationwide observational cohort study (DASGIB). Clin Microbiol Infect. 2018;24:1102.e1–5. https://doi.org/10.1016/j.cmi.2018.01.016
3. Petersen PT, Bodilsen J, Jepsen MPG, Larsen L, Storgaard M, Hansen BR, et al.; Danish Study Group of Infections of the Brain (DASGIB). Clinical features and prognostic factors in adults with viral meningitis. Brain. 2023;146:3816–25. https://doi.org/10.1093/brain/awad089
4. Ueda Y, Kobayashi H, Fujiwara H, Hagiya H, Hashida R, Kubota S, et al. A fatal case of enterovirus A71-induced meningoencephalitis following allogenic hematopoietic stem cell transplantation. J Infect Chemother. 2025;31:102630. https://doi.org/10.1016/j.jiac.2025.102630
5. Smith WG. Coxsackie B myopericarditis in adults. Am Heart J. 1970;80:34–46. https://doi.org/10.1016/0002-8703(70)90035-9
6. Lin GL, McGinley JP, Drysdale SB, Pollard AJ. Epidemiology and immune pathogenesis of viral sepsis. Front Immunol. 2018;9:2147. https://doi.org/10.3389/fimmu.2018.02147
7. Tavakoli NP, Wang H, Nattanmai S, Dupuis M, Fusco H, Hull R. Detection and typing of enteroviruses from CSF specimens from patients diagnosed with meningitis/encephalitis. J Clin Virol. 2008;43:207–11. https://doi.org/10.1016/j.jcv.2008.06.016
8. Edwin JJ, Domingo FR, Booth TF, Mersereau T, Skowronski DM, Chambers C, et al. Surveillance summary of hospitalized pediatric enterovirus D68 cases in Canada, September 2014. Can Commun Dis Rep. 2015;41:2–8. https://doi.org/10.14745/ccdr.v41is1a01
9. Chaggar G, Waldner D, Scozzafava J, Harrison R, Kashmere J, Jassal R, et al. Teaching neuroimage: severe enterovirus encephalitis as a complication of ocrelizumab treatment for multiple sclerosis. Neurology. 2025;104:e213585. https://doi.org/10.1212/WNL.0000000000213585
10. Deézsi-Magyar N, Zsidei G, Kiss N, Novák B, Mezősi-Csaplár M, Tarcsai KR, et al. Evaluating enterovirus diversity among symptomatic patients in Hungary during and after easing the COVID-19 lockdown. Virol J. 2025;22:204. https://doi.org/10.1186/s12985-025-02835-2
11. Łuczyńska A, Beyrer K, Holle I, Baillot A, Monazahian M, Dreesman J, et al. Evaluation of 17 years of MERIN (meningitis and encephalitis register in Lower Saxony, Germany) surveillance system: participants acceptability survey, completeness and timeliness of data. BMC Health Serv Res. 2024;24:59. https://doi.org/10.1186/s12913-023-10482-y
12. Brouwer L, Wolthers KC, Pajkrt D. Parechovirus A prevalence in adults in The Netherlands. Arch Virol. 2020;165:963–6. https://doi.org/10.1007/s00705-020-04547-0
13. Mizuta K, Yamakawa T, Nagasawa H, Itagaki T, Katsushima F, Katsushima Y, et al. Epidemic myalgia associated with human parechovirus type 3 infection among adults occurs during an outbreak among children: findings from Yamagata, Japan, in 2011. J Clin Virol. 2013;58:188–93. https://doi.org/10.1016/j.jcv.2013.05.019
14. Mardekian SK, Fortuna D, Nix A, Bhatti T, Wiley CA, Flanders A, et al. Severe human parechovirus type 3 myocarditis and encephalitis in an adolescent with hypogammaglobulinemia. Int J Infect Dis. 2015;36:6–8. https://doi.org/10.1016/j.ijid.2015.05.008
15. George G, Restivo L, Freire Jijon D, Robinson JL, Fonseca K, Pabbaraju K, et al. Emergence of a new pathogen: a retrospective study of HPeV-5 central nervous system disease in Alberta, Canada. Viruses. 2024;16:1684. https://doi.org/10.3390/v16111684
16. Chimunda T, Subramanian R, Smith J, Mahony A. First reported case of human parechovirus encephalitis in an adult patient complicated by refractory status epilepticus. IDCases. 2018;15:e00475. https://doi.org/10.1016/j.idcr.2018.e00475
17. Dunn JJ. Enteroviruses and parechoviruses. Microbiol Spectr. 2016;4. https://doi.org/10.1128/microbiolspec.DMIH2-0006-2015
18. Cassidy H, van Leer-Buter C, Niesters HGM. Enterovirus infections in solid organ transplant recipients: a clinical comparison from a regional university hospital in the Netherlands. Microbiol Spectr. 2022;10:e0221521. https://doi.org/10.1128/spectrum.02215-21
19. Martin de Frémont G, Chabrolles H, Mirand A, L'Honneur AS, Mélé N, Dunogue B, et al. Severe enterovirus infections in patients with immune-mediated inflammatory diseases receiving anti-CD20 monoclonal antibodies. RMD Open. 2024;10:e004036. https://doi.org/10.1136/rmdopen-2023-004036
20. Omland LH, Holm-Hansen C, Lebech AM, Dessau RB, Bodilsen J, Andersen NS, et al. Long-term survival, health,

social functioning, and education in patients with an enterovirus central nervous system infection, Denmark, 1997–2016. J Infect Dis. 2020;222:619–27. https://doi.org/10.1093/infdis/jiaa151
21. Banks SA, Poliakov I, Flanagan EP, Toledano M, Nathoo N. Enterovirus encephalitis in people with multiple sclerosis on ocrelizumab: insights from a multicenter case series. Neurol Neuroimmunol Neuroinflamm. 2026;13:e200534. https://doi.org/10.1212/NXI.0000000000200534
22. Stögbauer J, Schegerer V, Berger FK, Schulz-Schaeffer W, Fassbender K, Naumann J, et al. Severe coxsackie virus B5 encephalitis mimics autoimmune limbic encephalitis in a young woman under long-term B-cell depletion with ocrelizumab: a case report. Mult Scler. 2025;31:1258–61. https://doi.org/10.1177/13524585251322327
23. Starosta AD, Ehler J, Löffler B, Tannapfel A, Zipprich A, Reuken PA, et al. Echovirus serotype 11 induced sepsis in a young female patient with multiple sclerosis treated with anti-CD20 monoclonal antibody ocrelizumab. Infection. 2025; 53:1507–12. https://doi.org/10.1007/s15010-025-02479-y
24. Nel H, Merritt A, Lawson E, Porter M. Disseminated enterovirus infection treated with intravenous immunoglobulin in a patient on maintenance ocrelizumab for multiple sclerosis. BMJ Case Rep. 2025;18:e261915. https://doi.org/10.1136/bcr-2024-261915
25. Pabbaraju K, Wong S, Wong AA, Tellier R. Detection of enteroviruses and parechoviruses by a multiplex real-time RT-PCR assay. Mol Cell Probes. 2015;29:81–5. https://doi.org/10.1016/j.mcp.2015.02.001
26. Pabbaraju K, Wong S, Chan EN, Tellier R. Genetic characterization of a coxsackie A9 virus associated with aseptic meningitis in Alberta, Canada in 2010. Virol J. 2013;10:93. https://doi.org/10.1186/1743-422X-10-93
27. Coiras MT, Aguilar JC, García ML, Casas I, Pérez-Breña P. Simultaneous detection of fourteen respiratory viruses in clinical specimens by two multiplex reverse transcription nested-PCR assays. J Med Virol. 2004;72:484–95. https://doi.org/10.1002/jmv.20008
28. Honorato L, Ferreira NE, Domingues RB, Senne C, Leite FBVM, Santos MVD, et al. Evaluation of enterovirus concentration, species identification, and cerebrospinal fluid parameters in patients of different ages with aseptic meningitis in São Paulo, Brazil. J Med Virol. 2024;96:e29471. https://doi.org/10.1002/jmv.29471
29. Otani IM, Lehman HK, Jongco AM, Tsao LR, Azar AE, Tarrant TK, et al. Practical guidance for the diagnosis and management of secondary hypogammaglobulinemia: a work group report of the AAAAI Primary Immunodeficiency and Altered Immune Response Committees. J Allergy Clin Immunol. 2022;149:1525–60. https://doi.org/10.1016/j.jaci.2022.01.025
30. Salzer U, Bacchielli C, Buckridge S, Pan-Hammarström Q, Jennings S, Lougaris V, et al. Relevance of biallelic versus monoallelic *TNFRSF13B* mutations in distinguishing disease-causing from risk-increasing *TNFRSF13B* variants in antibody deficiency syndromes. Blood. 2009;113:1967–76. https://doi.org/10.1182/blood-2008-02-141937
31. Centers for Disease Control and Prevention. Enterovirus surveillance—United States, 2002–2004. MMWR Morb Mortal Wkly Rep. 2006;55:153–6.
32. de Schrijver S, Vanhulle E, Ingenbleek A, Alexakis L, Johannesen CK, Broberg EK, et al.; ENPEN Study Collaborators. Epidemiological and clinical insights into enterovirus circulation in Europe, 2018–2023: a multicenter retrospective surveillance study. J Infect Dis. 2025;232:e104–15. https://doi.org/10.1093/infdis/jiaf179
33. Alonso A, Eisele P, Ebert AD, Griebe M, Engelhardt B, Szabo K, et al. Leptomeningeal contrast enhancement and blood–CSF barrier dysfunction in aseptic meningitis. Neurol Neuroimmunol Neuroinflamm. 2015;2:e164. https://doi.org/10.1212/NXI.0000000000000164
34. Miller JM, Binnicker MJ, Campbell S, Carroll KC, Chapin KC, Gonzalez MD, et al. Guide to utilization of the microbiology laboratory for diagnosis of infectious diseases: 2024 update by the Infectious Diseases Society of America (IDSA) and the American Society for Microbiology (ASM). Clin Infect Dis. 2024;ciae104. https://doi.org/10.1093/cid/ciae104
35. Tyler KL. Emerging viral infections of the central nervous system: part 1. Arch Neurol. 2009;66:939–48. https://doi.org/10.1001/archneurol.2009.153
36. Wildenbeest JG, van den Broek PJ, Benschop KS, Koen G, Wierenga PC, Vossen AC, et al. Pleconaril revisited: clinical course of chronic enteroviral meningoencephalitis after treatment correlates with in vitro susceptibility. Antivir Ther. 2012;17:459–66. https://doi.org/10.3851/IMP1936
37. Meinhardt A, Reilly L, Kaliakatsos M, Abdel-Aziz K, Alsharidah S, Bodi I, et al. Novel antivirals for severe enterovirus infection in immunocompromised hosts; a case series. J Infect. 2024;88:106142. https://doi.org/10.1016/j.jinf.2024.106142
38. Harvala H, Broberg E, Benschop K, Berginc N, Ladhani S, Susi P, et al. Recommendations for enterovirus diagnostics and characterisation within and beyond Europe. J Clin Virol. 2018;101:11–7. https://doi.org/10.1016/j.jcv.2018.01.008

Address for correspondence: Jamil N. Kanji, Public Health Laboratory, Alberta Precision Laboratories, University of Alberta Hospital, 8440 112 St NW, Edmonton, AB T6G 2G3, Canada; email: Kanji1@ualberta.ca

Five-Biomarker Definition for Hypervirulent *Klebsiella pneumoniae* Bloodstream Infection and Abscess Complications, Japan, 2022–2024

Naoki Watanabe, Tomohisa Watari, Yoshihito Otsuka, Tomoh Matsumiya

Hypervirulent *Klebsiella pneumoniae* (hvKp) is an emerging cause of invasive infection, but clinical relevance of a 5-biomarker genotypic definition remains unclear. We analyzed 207 episodes of *K. pneumoniae* bloodstream infection at a tertiary hospital in Japan during 2022–2024. We defined hvKp by PCR detection of all 5 biomarkers: *rmpA*, *rmpA2*, *iucA*, *iroB*, and *peg-344*. Overall, hvKp accounted for 14% (28/207) of episodes. Abscess complications occurred in 61% (17/28) of hvKp episodes and 13% (23/179) of classical *K. pneumoniae* episodes. hvKp case-patients had longer median hospitalization (28 vs. 14 days) and duration of antimicrobial drug treatment (43 vs. 14 days) than those with classical *K. pneumoniae*. Most (9/10) sequence type 23 hvKp episodes involved abscesses. Short-read whole-genome sequencing detected CTX-M–type extended-spectrum β-lactamase genes in 11% (3/28) of hvKp isolates, representing 1.4% (3/207) of all *K. pneumoniae* episodes. The 5-biomarker definition delineated a clinically distinct subgroup, demonstrating its value for genomic surveillance of emerging hvKp.

Klebsiella pneumoniae is a leading cause of bloodstream infection and was linked to ≈790,000 deaths globally in 2019 (*1*). Classical *K. pneumoniae* (cKp) predominantly causes infections in patients with underlying or immunocompromising conditions. Conversely, hypervirulent *K. pneumoniae* (hvKp) can cause invasive, metastatic infections, including liver abscess, endophthalmitis, and meningitis, even in persons without underlying conditions (*2*). Reports of hvKp acquiring carbapenem-resistance genes triggered alerts from the World Health Organization and European Centre for Disease Prevention and Control, highlighting the need for reliable identification of this pathotype (*3*,*4*).

Definitions of hvKp vary across studies, but the combination of 5 genotypic biomarkers (*iucA*, *iroB*, *peg-344*, *rmpA*, and *rmpA2*) has demonstrated high diagnostic accuracy for identifying hvKp (*5*–*7*). Among *K. pneumoniae* bloodstream infections, hvKp prevalence varies across geographic settings, from 4% in the United States and Norway to 26% in Japan (*8*–*10*). However, direct comparisons across studies are complicated by variations in hvKp definitions. Moreover, epidemiologic and clinical data specifically on the basis of the 5-biomarker definition remain limited. Consequently, whether 5 biomarker–defined hvKp identifies a clinically and epidemiologically distinct subgroup of bloodstream infections and whether its effects differ across lineages remain unclear.

We conducted a retrospective cohort study at a tertiary hospital in Japan to compare the clinical characteristics of 5 biomarker–defined hvKp and cKp bloodstream infections. The primary aim was to determine whether 5 biomarker–defined hvKp was more frequently associated with abscess complications. Secondary aims were to estimate post–disease onset length of stay (LOS; i.e., hospitalization), total antibiotic duration, and 30-day mortality risk. We also summarized the lineage-specific genomic features of hvKp isolates and assessed convergence between hypervirulence and antimicrobial resistance.

Materials and Methods

Study Design and Data Collection

This single-center, retrospective cohort study was conducted at Kameda Medical Center, a 907-bed tertiary hospital in Kamogawa, Japan. We included consecutive patients from whom *K. pneumoniae* species

Author affiliations: Hirosaki University Graduate School of Health Sciences, Hirosaki, Japan (N. Watanabe, T. Matsumiya); Kameda Medical Center, Kamogawa, Japan (T. Watari, Y. Otsuka)

DOI: https://doi.org/10.3201/eid3211.260825

complex was isolated in ≥1 set of blood cultures during January 1, 2022–December 31, 2024. Patients with bloodstream infections had routine consultations for infectious diseases at the institution. For patients with multiple bloodstream infection episodes, we included only the first episode.

Of 290 unique episodes of *K. pneumoniae* species complex bloodstream infections identified, we excluded 2 because clinical data were insufficient or no stored isolate was available (Figure 1). We excluded 81 other episodes because species-level differentiation by PCR (*11*) identified *K. variicola* or *K. quasipneumoniae* isolates. Thus, we had a total of 207 *K. pneumoniae* isolates for analysis.

We collected clinical and microbiological data from electronic medical records and laboratory information systems and recorded patient sex according to medical records. We processed blood cultures by using the BD BACTEC FX system (Becton, Dickinson and Company, https://www.bd.com) and performed species identification by using a MALDI Biotyper (Bruker Daltonics GmbH, https://www.bruker.com) for matrix-assisted laser desorption/time-of-flight mass spectrometry. We used a Dry Plate Eiken (Eiken Chemical Co., Ltd., https://www.eiken.co.jp) to perform antimicrobial susceptibility testing by the broth microdilution method. We tested for susceptibility to the following antimicrobial agents: piperacillin, ampicillin/sulbactam, amoxicillin/clavulanate, piperacillin/tazobactam, cefazolin, ceftriaxone, cefepime, cefmetazole, imipenem, meropenem, aztreonam, gentamicin, tobramycin, amikacin, levofloxacin, ciprofloxacin, minocycline, and trimethoprim/sulfamethoxazole. We interpreted susceptibility results according to Clinical and Laboratory Standards Institute standards (*12*). This study was approved by the Research Ethics Committee of the Kameda Medical Center (approval no. 25-016) with a waiver for informed consent and an opt-out process.

Definitions

We classified isolates as hvKp or cKp according to the 5-biomarker definition and assessed antimicrobial resistance phenotypes separately. We defined hvKp as presence of all 5 genotypic biomarkers (*iucA*, *iroB*, *peg-344*, *rmpA*, and *rmpA2*), as proposed by others (*5*–*7*). We classified isolates that did not meet the 5-biomarker definition as cKp. We performed PCR-based screening by using previously published primers for *rmpA*, *rmpA2*, *iucA*, *iroB*, and *peg-344* (*5*) (Appendix Table 1, https://wwwnc.cdc.gov/EID/article/32/11/26-0825-App1.pdf). We performed screening sequentially: first, we tested for *rmpA*; then, we tested for the other markers only in *rmpA*-positive isolates. We assigned the hvKp classification retrospectively for study analyses; the classification was not available to the treating clinicians during routine care.

We defined third-generation cephalosporin resistance (3GCR) as nonsusceptibility to ceftriaxone and multidrug resistance as nonsusceptibility to ≥1 agent in ≥3 antimicrobial categories (*13*). We classified

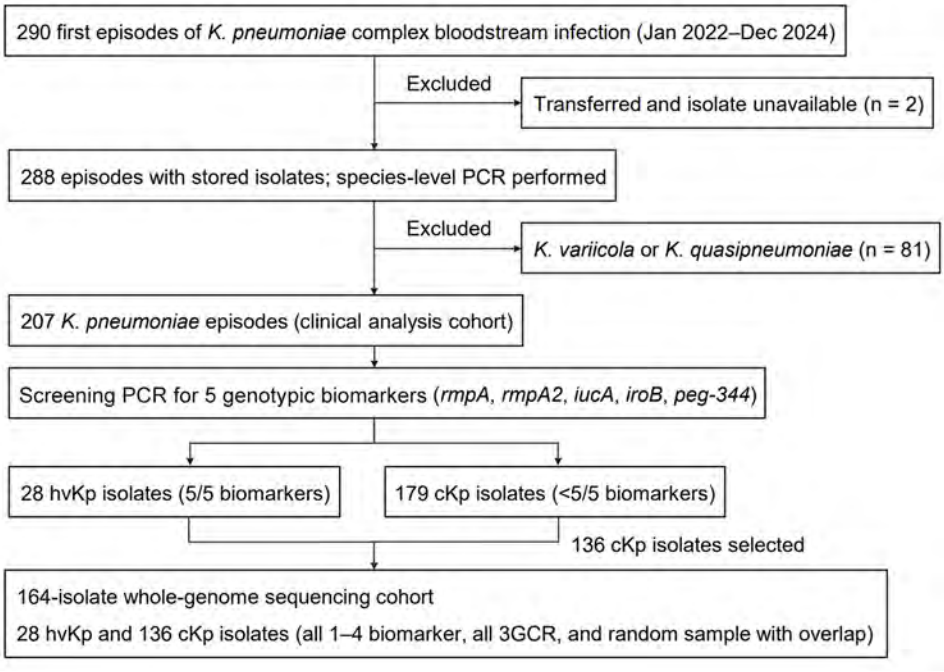

Figure 1. Flow diagram of episode inclusion in study of 5-biomarker definition for hvKp bloodstream infection and abscess complications, Japan, 2022–2024. Of 290 first episodes of *Klebsiella pneumoniae* complex bloodstream infection, 207 *K. pneumoniae* episodes were included in the clinical analysis. Whole-genome sequencing was performed on 164 isolates by using an enriched sampling strategy comprising all hvKp isolates, all isolates with 1–4 biomarkers, all 3GCR isolates, and a random sample of the cKp isolates with overlap between categories. 3GCR, third-generation cephalosporin–resistant; cKp, classical *K. pneumoniae*; hvKp, hypervirulent *K. pneumoniae*.

infection onset as community-acquired if the index blood culture was collected within 48 hours of admission without prior healthcare exposure. We classified all other episodes as healthcare-associated. We calculated Charlson comorbidity index (CCI) after excluding age points (*14*). We defined abscess complications only on the basis of imaging findings and excluded clinically suspected abscesses without imaging confirmation. We defined metastatic infection as a secondary infectious focus anatomically distinct from the presumed primary source of bloodstream infection, including abscesses and nonsuppurative manifestations, such as endophthalmitis. We defined post–disease onset LOS as the number of days from index blood culture collection to hospital discharge or transfer. We determined total antibiotic duration as the total number of days of antimicrobial therapy for a bloodstream infection episode and its complications, including oral therapy after discharge (Appendix).

Whole-Genome Sequencing

We performed whole-genome sequencing (WGS) on a subset of isolates selected to maximize representation of biomarker-positive and antimicrobial-resistant isolates within the available sequencing budget. The sequenced subset comprised 164 isolates, which included all hvKp isolates (n = 28), a random sample of cKp isolates (n = 125), additional cKp isolates selected to ensure complete representation of isolates with 1–4 positive biomarkers (n = 8), and 3GCR isolates (n = 31). Selection categories overlapped.

We performed short-read sequencing on a NovaSeq X Plus platform (Illumina, https://www.illumina.com) and used Unicycler (*15*) to perform de novo assembly. We assessed assembly quality by using QUAST and CheckM2 with predefined quality criteria (*16*,*17*).

We performed multilocus sequence typing, capsular locus typing, virulence gene profiling, and virulence scoring by using Kleborate version 3.2.4 outputs provided by Pathogenwatch (*18*,*19*). We additionally used AMRFinderPlus to evaluate β-lactam resistance determinants (*20*). We inferred a recombination-filtered core-genome single-nucleotide polymorphism (SNP) phylogeny by using Snippy (https://github.com/tseemann/snippy) to map reads to the *K. pneumoniae* NTUH-K2044 reference genome (GenBank accession no. AP006725.1), removed recombinant regions with Gubbins (*21*), and constructed a maximum-likelihood tree with IQ-TREE (*22*). We calculated pairwise SNP differences within selected lineages from the recombination-filtered core-genome SNP alignment. For hvKp isolates carrying extended-spectrum β-lactamase (ESBL) genes, we performed contig-level analysis to assess the genomic context of resistance and virulence determinants (Appendix).

Statistical Analysis

We used EZR version 1.70 (*23*) for statistical analyses. We compared continuous variables by using the Mann-Whitney U test and categorical variables by using Fisher exact tests. All tests were 2-sided, and we considered $p<0.05$ statistically significant.

We selected a priori covariates as baseline confounders on the basis of clinical relevance and constrained the number of covariates by the number of outcome events to avoid overfitting. We used multivariable logistic regression to evaluate abscess complications and adjusted for age, sex, and CCI. For 30-day mortality risk, we used Firth's penalized logistic regression, adjusted for age and CCI because the number of death events was limited relative to the number of candidate covariates (*24*).

For LOS and antibiotic duration, we fitted 2 sequential models: model A estimated the overall association of hvKp with each outcome, and model B included abscess complications to assess attenuation. We analyzed LOS as ln(LOS + 1) by using multivariable linear regression and exponentiated coefficients to report adjusted ratios with 95% CIs. We also analyzed total antibiotic duration among the treatment completers, using multivariable linear regression to analyze duration after log transformation. For both models, we used a common base adjustment set comprising age, sex, CCI, and infection acquisition category. For antibiotic duration, we also included the primary infection source because treatment duration was strongly influenced by the infectious syndrome and source-control requirements. For each outcome, we excluded episodes that had missing data from the corresponding analysis (Appendix).

As a prespecified exploratory analysis, we stratified outcomes by biomarker counts of 0, 1–4, or all 5. We descriptively summarized genomic features of the hvKp isolates, including lineage, capsule type, and virulence plasmid structure, rather than formally comparing across lineages.

Results

Patient Characteristics

Among 207 *K. pneumoniae* bloodstream infection episodes, 28 (14% [95% CI 9%–19%]) were classified as hvKp and 179 (86% [95% CI 81%–91%]) as cKp (Table 1; Appendix Table 2). The median age was similar between the 2 groups: hvKp median patient age was

Table 1. Baseline characteristics of 207 patients with hypervirulent and classical *Klebsiella pneumoniae* bloodstream infections in a study of five-biomarker definition for hvKp, Japan, 2022–2024*

Characteristics	hvKp, n = 28	cKp, n = 179	p value†
Demographic characteristics			
Median age, y (IQR)	76 (71–81)	78 (69–85)	0.64
Sex			
M	21 (75)	108 (60)	0.15
F	7 (25)	71 (40)	
Median body mass index (IQR), n = 201	21 (20–23)	20 (18–24)	0.65
Underlying conditions			
Median CCI score (IQR)	2 (1–4)	3 (2–5)	0.15
Diabetes, any	9 (32)	62 (35)	>0.99
Chronic kidney disease	3 (11)	23 (13)	>0.99
Liver disease	1 (4)	9 (5)	>0.99
Solid tumor	8 (29)	64 (36)	0.53
Healthcare exposure			
Indwelling device	12 (43)	114 (64)	0.04
Recent hospitalization	12 (43)	112 (63)	0.06
Prior antibiotic exposure	9 (32)	99 (55)	0.02
Infection characteristics			
Onset classification			0.30
Healthcare-associated	15 (54)	114 (64)	
Community-acquired	13 (46)	65 (36)	
Primary source of infection			0.03
Urinary tract	7 (25)	37 (21)	
Catheter-related	0 (0.0)	5 (3)	
Intraabdominal	13 (46)	83 (46)	
Respiratory	4 (14)	5 (3)	
Other	1 (4)	1 (<1)	
Unknown	3 (11)	48 (27)	
Microbiological characteristics			
Multidrug resistance	3 (11)	53 (30)	0.04
Polymicrobial bloodstream infection	3 (11)	42 (23)	0.15

*Values are no. (%) except as indicated. CCI, Charlson comorbidity index; cKp, classical *K. pneumoniae*; hvKp, hypervirulent *K. pneumoniae*; IQR, interquartile range.
†p values were calculated using Fisher exact test for categorical variables and Mann–Whitney U test for continuous variables and were provided for descriptive purposes.

76 (interquartile range [IQR] 71–81) years, and cKp median patient age was 78 (IQR 69–85) years. In the hvKp group, 75% (21/28) of patients were male and 25% (7/28) were female, whereas the cKp group comprised 60% (108/179) male and 40% (71/179) female patients. Patients with hvKp had fewer underlying conditions; 57% (16/28) had CCI scores ≥2 compared with 80% (143/179) of the cKp group. Patients with hvKp also less frequently had markers of healthcare exposure than the cKp group, including indwelling devices (43% [12/28] vs. 64% [114/179]) and prior antimicrobial drug use (32% [9/28] vs. 55% [99/179]).

Primary infection sources were broadly similar between the groups, although respiratory infection was more frequent in the hvKp group and unknown source was more frequently reported for the cKp group. However, respiratory infection remained uncommon, accounting for only 4% (9/207) of episodes. Polymicrobial bloodstream infection was less frequent among hvKp episodes than among cKp episodes (11% [3/28] vs. 23% [42/179]). Multidrug resistance was less common in the hvKp group than in the cKp group (11% [3/28] vs. 30% [53/179]) (Appendix Table 3). Appropriate empiric antimicrobial therapy was administered in 27 (96%) of the hvKp episodes and 151 (84%) of the cKp episodes. We compiled data and population analyses (Appendix Table 4).

Abscess Complications

Abscess complications occurred in 40 (19%) *K. pneumoniae* episodes, among which 23 (58%) were cKp and 17 (42%) were hvKp according to the 5-biomarker definition. The within-group frequency of abscess complications was 61% (95% CI 41%–79%) in hvKp episodes and 13% (95% CI 8%–19%) in cKp episodes (Table 2). Among episodes with abscess complications, polymicrobial bloodstream infection was observed in 12% (2/17) of hvKp episodes and 26% (6/23) of cKp episodes. In the multivariable logistic regression analysis, hvKp was independently associated with abscess complications (adjusted odds ratio [aOR] 10.7 [95% CI 4.4–26.2]) (Appendix Table 5).

The most common hvKp abscess site was the liver (32% [9/28], compared with 7% [12/179] in cKp infections), and hvKp also more frequently involved abscesses at other sites than cKp infections (39% [11/28] vs. 7% [12/179]). Extrahepatic sites included urogenital, intraabdominal, central nervous system,

Table 2. Clinical outcomes and adjusted associations among *Klebsiella pneumoniae* bloodstream infection patients in a study of 5-biomarker definition for hvKp bloodstream infection and abscess complications, Japan, 2022–2024*

Clinical outcome	hvKp, n = 28	cKp, n = 179	Total no.	Estimate (95% CI)†	
				Crude	Adjusted
Any abscess complication	17 (61)	23 (13)	207 (100)	10.5 (4.4–25.2)	10.7 (4.4–26.2)
Liver abscess	9 (32)	12 (7)	207 (100)	–	–
Other abscess sites‡	11 (39)	12 (7)	207 (100)	–	–
Metastatic infection	4 (14)	1 (<1)	207 (100)	–	–
Median postonset hospitalization, d (IQR)§#	28 (14–42)	14 (11–18)	206 (99.5)	1.6 (1.2–2.2)	Model A, 1.6 (1.2–2.2) Model B, 1.1 (0.8–1.5)
Median antibiotic duration, d (IQR)#††	43 (16–67)	14 (14–18)	168 (81)	2.1 (1.6–2.7)	Model A, 2.1 (1.6–2.8) Model B, 1.2 (1.0–1.5)
30-d mortality rate, deaths/no.	4/27 (15)	34/170 (20)	197 (95)	0.8 (0.2–2.1)	0.9 (0.3–2.4)

*Data are no. (%) or median (IQR) unless otherwise indicated. Adjusted estimate is shown only for prespecified primary, secondary, and supportive outcomes. Liver abscess, other abscess sites, and metastatic infection are presented descriptively and were not modeled separately. cKp, classical *K. pneumoniae*; hvKp, hypervirulent *K. pneumoniae*; IQR, interquartile range.
†Estimates are odds ratios for abscess complications and 30-day mortality, and ratios for length of hospitalization and antibiotic duration. Adjusted estimates for abscess complication were derived from multivariable logistic regression adjusted for age, sex, and Charlson comorbidity index (CCI); for post–disease onset length of stay, from multivariable linear regression of ln(length of stay + 1) adjusted for age, sex, CCI, and infection acquisition category; for total antibiotic duration, from multivariable linear regression of log-transformed duration among treatment completers adjusted for age, sex, CCI, infection acquisition category, and primary infection source; and for 30-d mortality, from Firth penalized logistic regression adjusted for age and CCI.
‡Other abscess sites included pelvic or intra-abdominal abscess, lung abscess or necrotizing pneumonia, prostatic abscess, endophthalmitis, central nervous system abscess, and musculoskeletal or soft tissue infection; episodes may have had >1 site.
§Post–disease onset length of stay was defined as days from index blood culture collection to hospital discharge or interhospital transfer. If hospitalization continued for reasons judged unrelated to the bloodstream infection, follow-up was censored at the end of the bloodstream infection-directed therapy. Episodes ending in in-hospital death were included, with length of stay calculated up to the date of death.
#Model A indicates the base-adjusted model and model B indicates the model additionally adjusted for the development of an abscess complication.
††Total antibiotic duration was analyzed among treatment completers.

pulmonary, musculoskeletal, and ocular locations, some of which exclusively occurred in hvKp (Appendix Table 2). We identified metastatic infection in 14% (4/28) of hvKp and <1% (1/179) of cKp episodes. Abscess complication rates rose with the number of biomarkers, occurring in 12% (21/171) of the 0-marker group, 25% (2/8) of the 1–4-marker group, and 61% (17/28) of the 5-marker group (Figure 2; Appendix Table 6).

LOS, Antibiotic Duration, and 30-Day Mortality Risk

Among 207 episodes, 206 (28 hvKp and 178 cKp) had post–disease onset LOS data available. LOS was longer for the hvKp group (median 28 [IQR 14–42] days) than for the cKp group (14 [IQR 11–18] days). For antibiotic duration, we excluded 39 episodes, primarily because of patient death before treatment completion. Among the 168 (24 hvKp and 144 cKp) patients who completed treatment, the total antibiotic

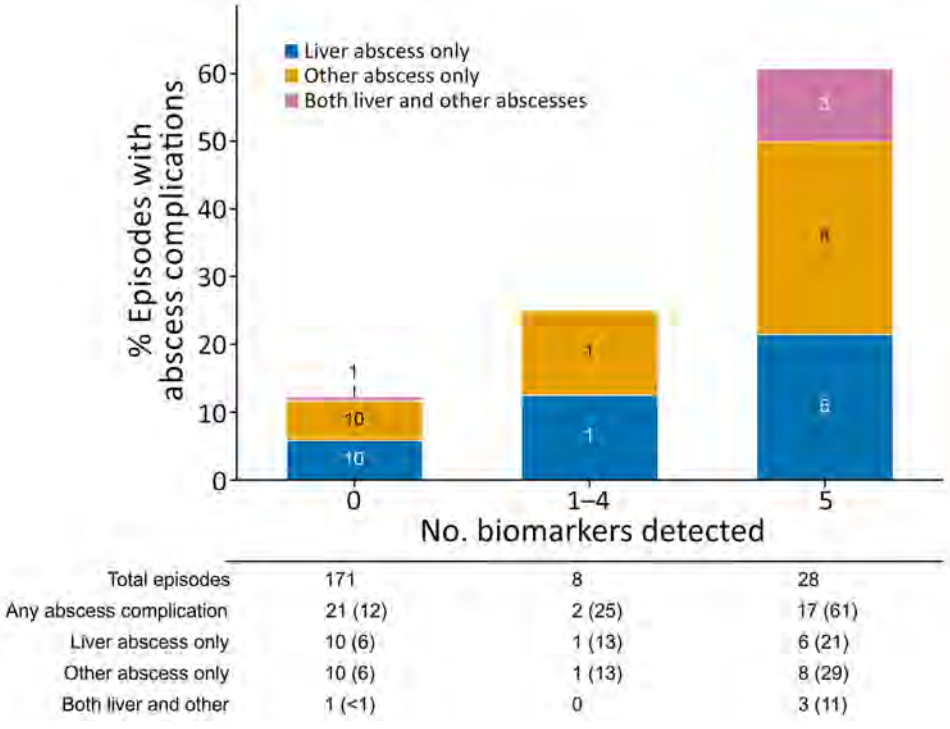

Figure 2. Abscess complications among 207 episodes of *Klebsiella pneumoniae* bloodstream infection by biomarker group in study of hypervirulent *K. pneumoniae*, Japan, 2022–2024. Stacked bars show mutually exclusive categories of liver abscess only, nonhepatic abscess only, and both liver and nonhepatic abscesses. Bar height represents the percentage of episodes with any abscess complication; numbers within colored bar segments indicate case counts. Case counts and percentages are provided below each bar.

duration was longer in the hvKp group (median 43 [IQR 16–67] days) than in the cKp group (median 14 [IQR 14–18] days). In the adjusted analyses, hvKp was associated with longer LOS (adjusted ratio 1.6 [95% CI 1.2–2.2]) and antibiotic duration (adjusted ratio 2.1 [95% CI 1.6–2.8]) (Appendix Tables 7, 8). Those associations were attenuated after additional adjustment for abscess complication (LOS adjusted ratio 1.1 [95% CI 0.8–1.5]; antibiotic duration adjusted ratio 1.2 [95% CI 1.0–1.5]). The prespecified threshold analyses of prolonged antibiotic duration aligned with those findings (Appendix Table 9).

The 30-day mortality rate was 15% (95% CI 4%–34%) in the hvKp group and 20% (95% CI 14%–27%) in the cKp group; we excluded episodes with unknown vital status. In the adjusted analyses, the aOR was 0.9 (95% CI 0.3–2.4) for 30-day mortality associated with hvKp (Appendix Table 10). Intensive care unit admission rates were 18% (5/28) in the hvKp group and 14% (25/179) in the cKp group. Vasopressor use was 25% (7/28) in the hvKp group and 28% (51/179) in the cKp group. Mechanical ventilation was more frequent in the hvKp group (14% [4/28]) compared with the cKp group (3% [5/179]); nonetheless, we did not perform an adjusted analysis on those categories because so few events were recorded.

Genomic Characteristics and Lineage-Specific Findings

We performed WGS on 164 isolates, including 28 hvKp and 136 cKp isolates. All assemblies met predefined quality criteria. Patient clinical characteristics were similar between those with randomly sampled cKp isolates (n = 125) and those cKp isolates not included in the random sample (n = 54), except for the distribution of primary infection sources (Appendix Tables 11, 12). Kleborate virulence scores, based on key virulence loci (*19*), were ≥3 in all 28 sequenced hvKp isolates: 7 had a score of 3; 6 had a score of 4; and 15 had a score of 5. Among sequenced cKp isolates, 98% (133/136) had scores of 0–2, whereas 3 had a score of 4 despite not meeting the 5-biomarker definition.

We analyzed sequence type (ST) and capsule synthesis locus (K-locus [KL]) distributions among isolates (Appendix Tables 13, 14). Among hvKp isolates, predominant lineages were ST23/KL1 (36%, 10/28) and ST65/KL2 (29%, 8/28) (Figure 3), within which pairwise SNP differences ranged from 36 to 359 among the 10 ST23/KL1 isolates and from 132 to 432 among the 8 ST65/KL2 isolates (Appendix Figure). Other hvKp lineages included ST412/KL57 accounting for 14% (4/28) and ST86/KL2 accounting for 7% (2/28) of hvKp isolates. Randomly sampled cKp isolates comprised 75 sequence types, most commonly ST37 (8%, 10/125) and ST45 (7%, 9/125). Among the 3GCR isolates, 3 lineages predominated: ST307/KL102 (26%, 8/31), ST37/KL15 (23%, 7/31), and ST353/KL110 (23%, 7/31).

STs commonly associated with hvKp were uncommon among 136 sequenced cKp isolates; ST23/KL1 and ST65/KL2 were each detected in 1 isolate, and ST86 was not detected. Both ST23/KL1 and ST65/KL2 cKp isolates were in the 1–4 biomarker group and carried 3 of the 5 biomarkers, *rmpA*, *iroB*, and *peg-344*.

Abscess complication rates among hvKp episodes differed by lineage (Table 3): 9/10 (90%) in ST23/KL1, 5/8 (63%) in ST65/KL2, and 1/4 (25%) in ST412/KL57. We also observed genomic differences across hvKp lineages. ST23/KL1 isolates uniformly carried intact *K. pneumoniae* virulence plasmid 1 (KpVP-1) and yersiniabactin, whereas most (88%, 7/8) ST65/KL2 isolates had KpVP-1 truncation.

We identified ESBL genes in 11% (3/28) of hvKp episodes, representing 1.4% (3/207) of all *K. pneumoniae* bloodstream infection episodes. Two episodes involved ST412/KL57 isolates harboring $bla_{\text{CTX-M-15}}$; those isolates differed by 23 recombination-filtered core-genome SNPs and were isolated in 2023 and 2024. The third episode involved an ST893/KL20 isolate carrying $bla_{\text{CTX-M-55}}$. All 3 convergence episodes were healthcare-associated, and none resulted in death. In all 3 isolates, the $bla_{\text{CTX-M}}$ gene was located on a contig assigned to a putative plasmid cluster, separate from the contigs carrying virulence-associated sequences (Appendix). We did not detect any carbapenemase genes among the 164 sequenced isolates.

Discussion

In this retrospective cohort of 207 *K. pneumoniae* bloodstream infection episodes, we identified 28 (14%) hvKp episodes by using the 5-biomarker definition. Those episodes were characterized by frequent abscess complications and prolonged hospitalization and antibiotic treatment. WGS revealed genomic heterogeneity within hvKp and lineage-specific differences in abscess frequency.

The 14% prevalence of hvKp in this cohort was lower than that reported from Japan (*10*) but was higher than that reported in the United States and Norway (*9*,*25*). Those differences likely reflect both the epidemiologic setting and variability in hvKp definitions across studies. Broader definitions on the basis of a subset of biomarkers might classify isolates in the 1–4-marker group as hvKp, thereby yielding

higher prevalence estimates than the 5-marker definition used in this study. In this cohort, abscess complication rates rose across biomarker strata, from 12% in the 0-marker group to 25% in the 1–4-marker group and 61% in the 5-marker group. That gradient aligns with studies reporting that requiring all 5 biomarkers provides greater accuracy for identifying hvKp than lower thresholds (*6*). Therefore, isolates positive for 1–4 markers might be better considered an intermediate group rather than definitively considered hvKp.

The 5-biomarker definition identified an abscess-prone subgroup of *K. pneumoniae* bloodstream infections. However, 58% of abscess complications occurred in cKp episodes. That finding underscores that the 5-biomarker definition identifies a subgroup at increased risk for abscess complications rather than a criterion intended to capture all abscess complications. Although the observed 30-day mortality risk was not higher in hvKp than cKp episodes, that difference should not be interpreted as evidence that hvKp imposes no clinically meaningful burden. Rather, the burden was reflected in longer hospitalization and antibiotic treatment. The discrepancy with prior reports of increased early hvKp mortality (*26*) might be explained by differences in infection–source composition. In our cohort, respiratory infections,

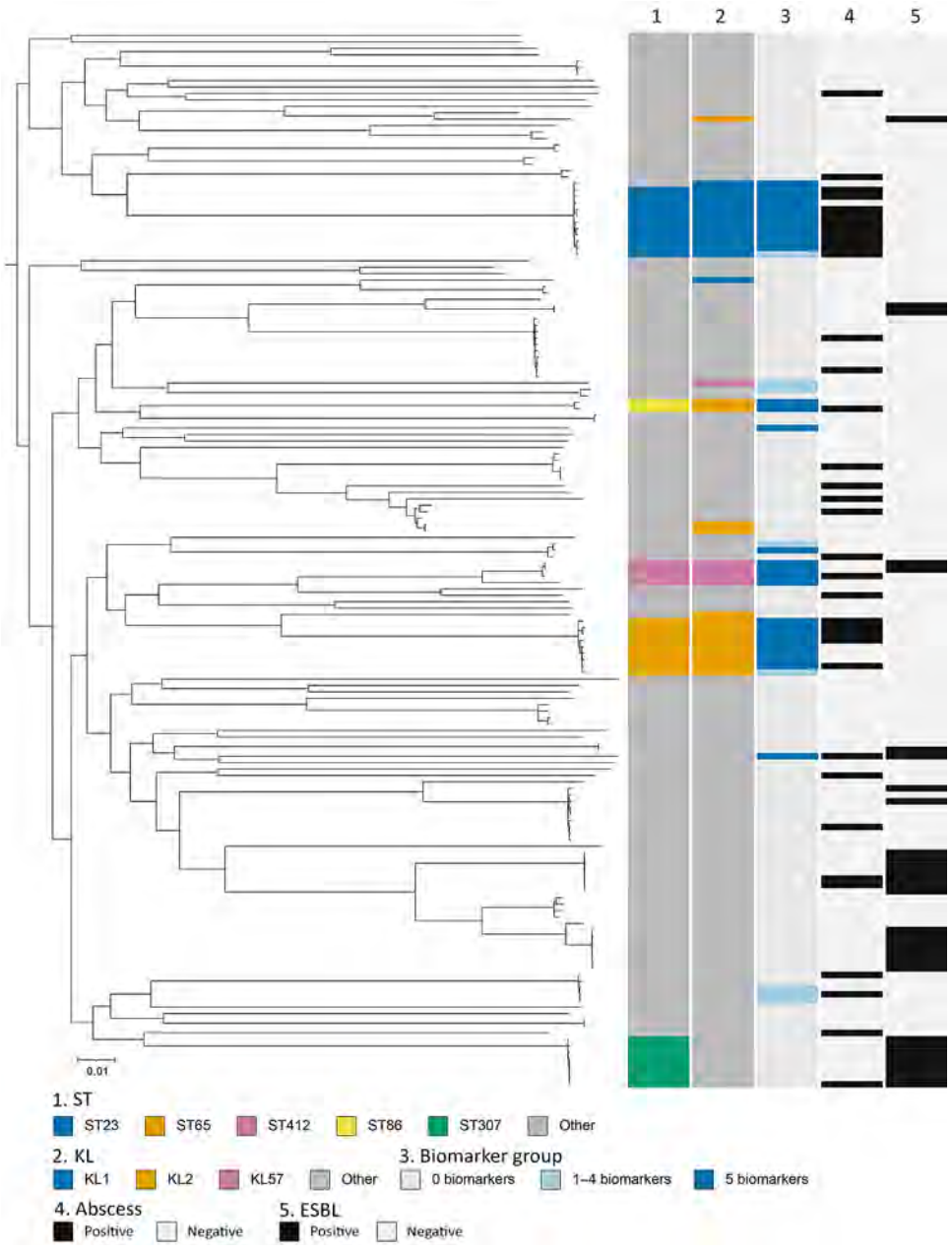

Figure 3. Maximum-likelihood phylogeny of 164 isolates from study of 5-biomarker definition for hypervirulent *Klebsiella pneumoniae* bloodstream infection and abscess complications, Japan, 2022–2024. The tree was inferred from a recombination-filtered core genome single-nucleotide polymorphism alignment. Annotation tracks indicate the ST, KL capsule type, biomarker group, abscess complication, and ESBL status. Scale bar indicates nucleotide substitutions per site. ESBL, extended-spectrum β-lactamase; KL, K-locus; ST, sequence type.

Table 3. Lineage-specific genomic and clinical features of hypervirulent *Klebsiella pneumoniae* isolates from cases of bloodstream infection and abscess complications, Japan, 2022–2024*

Lineage	No. isolates	K-locus	KpVP-1 intact	ybt-positive	ESBL-positive	HAI	Abscess
ST23	10	KL1	10 (100)	10 (100)	0	2 (20)	9 (90)
ST65	8	KL2	1 (13)	3 (38)	0	5 (63)	5 (63)
ST412	4	KL57	2 (50)	2 (50)	2 (50)	3 (75)	1 (25)
ST86	2	KL2	2 (100)	2 (100)	0	1 (50)	1 (50)
Other†	4	KL1, KL20, KL54	4 (100)	4 (100)	1 (25)	4 (100)	1 (25)

*Values are no. (%) except as indicated. ESBL, extended-spectrum β-lactamase; HAI, healthcare-associated infection; KpVP-1, *K. pneumoniae* virulence plasmid 1; ST, sequence type; ybt, yersiniabactin locus.
†Other lineages included ST268 (n = 1), ST29 (n = 1), ST893 (n = 1), and a single-locus variant of ST23 (n = 1).

previously associated with poor outcomes in *K. pneumoniae* bloodstream infection (*8*), accounted for only 4% of episodes. Mortality rates for hvKp might depend on clinical setting and source distribution, whereas abscess-associated treatment burden might occur even in the absence of higher mortality rates.

The clinical and public health challenges posed by *K. pneumoniae* bloodstream infections vary with the local prevalence of hvKp. In a cohort from the United States, where hvKp is rare, resistance to the initial prescribed antibiotic was an independent predictor of in-hospital death (*8*). In our analysis, antimicrobial resistance remained a concern for cKp, which accounted for 86% of episodes and had a higher multidrug-resistance rate than hvKp. Conversely, hvKp isolates were generally susceptible to standard empiric agents but were associated with abscess complications and prolonged care. Those findings suggest that management priorities could differ between subgroups: cKp warrants attention to antimicrobial resistance, whereas hvKp might warrant careful evaluation for abscess complications and source control. Thus, awareness of local epidemiology could help align management strategies with the dominant clinical burden of *K. pneumoniae* bloodstream infection.

Beyond the clinical burden of hvKp bloodstream infection, clinically accessible diagnostic tests and ongoing genomic surveillance remain priorities. Currently, the 5-biomarker PCR for hvKp is a research tool, and no commercial assay is available for routine clinical use (*5*,*7*). Although such assays could be developed on existing PCR platforms (*27*), they have not yet been validated in clinical laboratories (*7*). Distinguishing hvKp from cKp could enable abscess evaluation and source control. Another concern is the genomic convergence of hypervirulence and antimicrobial resistance (*3*). A US multicenter study found that 0.7% of carbapenem-resistant *K. pneumoniae* isolates harbored a virulence plasmid (*28*). Although we did not identify carbapenemase-producing isolates in our cohort, 11% (3/28) of hvKp episodes were ESBL-producing, corresponding to 1.4% (3/207) of all *K. pneumoniae* bloodstream infection episodes studied. In all 3 ESBL-producing hvKp isolates, $bla_{\text{CTX-M}}$ genes were carried on plasmid contigs separate from the virulence-associated sequences, suggesting independent acquisition. Collectively, those findings support the need for clinically accessible hvKp diagnostic tools and continued genomic surveillance to monitor the convergence of hypervirulence and antimicrobial resistance.

The first limitation of this study is that the retrospective design at a single tertiary hospital might limit the generalizability of our findings. Second, abscess imaging was performed at the discretion of the treating clinicians without a standardized study protocol, and imaging-frequency data were unavailable. Because hvKp episodes might more frequently have features prompting cross-sectional imaging, differential ascertainment of abscess complications cannot be excluded and could have contributed to the observed intergroup differences in abscess rates. Nevertheless, the large effect size and descriptive gradient in abscess frequency across biomarker strata suggest that ascertainment bias alone is unlikely to fully account for the observed association. Third, the number of hvKp episodes was small, limiting the statistical power of some comparisons, including 30-day mortality rate. Fourth, WGS was performed on 164 of 207 isolates. The clinical characteristics were similar between randomly sampled cKp isolates and those not included in the random sample; however, residual selection bias cannot be ruled out. Despite those limitations, the consecutive case design in a tertiary care setting with routine infectious diseases consultation might have enabled characterization of the clinical burden of abscesses in this cohort.

In conclusion, we identified 5-biomarker–defined hvKp as a clinically and epidemiologically distinct subgroup of *K. pneumoniae* bloodstream infection characterized by frequent abscess complications and prolonged care in a tertiary-care cohort in Japan. The clinical burden differed between groups, with abscess-prone disease in hvKp and greater antimicrobial resistance in cKp. Those findings suggest that clinical management should be informed by local epidemiology and support the need for continued surveillance of hvKp and cKp in bloodstream infections.

This article was preprinted at https://doi.org/10.64898/2026.04.10.26350004.

The clinical data underlying this article are not publicly available because of privacy and ethics restrictions related to the institutional review board approval and opt-out process for this retrospective study. WGS data are available in DDBJ/GenBank under BioProject accession no. PRJDB40619.

This work was supported by the Morinomiyako Medical Research Foundation (grant no. 2025-01-014 to N.W.) and the Kurozumi Medical Foundation grant to N.W. The funders had no role in the design of the study; the collection, analysis, or interpretation of data; or the decision to submit the manuscript for publication.

During preparation of the manuscript, the authors used ChatGPT-5.5 (OpenAI, https://chatgpt.com) to assist with English-language drafting and sentence-level editing of author-written text. The tool was not used for data analysis, data interpretation, figure generation, or drawing scientific conclusions. All output was reviewed and edited by the authors, who take full responsibility for the final content.

About the Author

Dr. Watanabe is a lecturer in the Department of Bioscience and Laboratory Medicine at Hirosaki University Graduate School of Health Sciences, Hirosaki, Japan. His research interests include diagnostic microbiology, bloodstream infections, and antimicrobial resistance.

References

1. GBD 2019 Antimicrobial Resistance Collaborators. Global mortality associated with 33 bacterial pathogens in 2019: a systematic analysis for the Global Burden of Disease Study 2019. Lancet. 2022;400:2221–48. https://doi.org/10.1016/S0140-6736(22)02185-7
2. Russo TA, Marr CM. Hypervirulent *Klebsiella pneumoniae.* Clin Microbiol Rev. 2019;32:e00001-19. https://doi.org/10.1128/CMR.00001-19
3. World Health Organization. Antimicrobial resistance, hypervirulent *Klebsiella pneumoniae*—global situation. 2024 Jul 31 [cited 2024 Aug 3]. https://www.who.int/emergencies/disease-outbreak-news/item/2024-DON527
4. European Centre for Disease Prevention and Control. Rapid risk assessment—emergence of hypervirulent *Klebsiella pneumoniae* ST23 carrying carbapenemase genes in EU/EEA countries—first update. 2024 Feb 14 [cited 2026 Mar 13]. https://www.ecdc.europa.eu/en/publications-data/risk-assessment-emergence-hypervirulent-Klebsiella-pneumoniae-eu-eea
5. Russo TA, Olson R, Fang CT, Stoesser N, Miller M, MacDonald U, et al. Identification of biomarkers for differentiation of hypervirulent *Klebsiella pneumoniae* from classical *K. pneumoniae.* J Clin Microbiol. 2018;56:e00776-18. https://doi.org/10.1128/JCM.00776-18
6. Russo TA, Alvarado CL, Davies CJ, Drayer ZJ, Carlino-MacDonald U, Hutson A, et al. Differentiation of hypervirulent and classical *Klebsiella pneumoniae* with acquired drug resistance. MBio. 2024;15:e0286723. https://doi.org/10.1128/mbio.02867-23
7. Russo TA, Lebreton F, McGann PT. A step forward in hypervirulent *Klebsiella pneumoniae* diagnostics. Emerg Infect Dis. 2025;31:1–3. https://doi.org/10.3201/eid3101.241516
8. Roach DJ, Sridhar S, Oliver E, Rao SR, Slater DM, Hwang W, et al. Clinical and genomic characterization of a cohort of patients with *Klebsiella pneumoniae* bloodstream infection. Clin Infect Dis. 2024;78:31–9. https://doi.org/10.1093/cid/ciad507
9. Fostervold A, Raffelsberger N, Hetland MAK, Bakksjø R, Bernhoff E, Samuelsen Ø, et al.; Assoc. on behalf of The Norwegian Study Group on Klebsiella pneumoniae. Risk of death in *Klebsiella pneumoniae* bloodstream infections is associated with specific phylogenetic lineages. J Infect. 2024;88:106155. https://doi.org/10.1016/j.jinf.2024.106155
10. Harada S, Aoki K, Yamamoto S, Ishii Y, Sekiya N, Kurai H, et al. Clinical and molecular characteristics of *Klebsiella pneumoniae* isolates causing bloodstream infections in Japan: occurrence of hypervirulent infections in health care. J Clin Microbiol. 2019;57:e01206-19. https://doi.org/10.1128/JCM.01206-19
11. Barrios-Camacho H, Silva-Sánchez J, Cercas-Ayala E, Lozano-Aguirre L, Duran-Bedolla J, Aguilar-Vera A, et al. PCR system for the correct differentiation of the main bacterial species of the *Klebsiella pneumoniae* complex. Arch Microbiol. 2022;204:73. https://doi.org/10.1007/s00203-021-02668-x
12. Clinical and Laboratory Standards Institute. Performance standards for antimicrobial susceptibility testing, 34th edition (M100-S34). Wayne (PA): The Institute; 2024.
13. Magiorakos AP, Srinivasan A, Carey RB, Carmeli Y, Falagas ME, Giske CG, et al. Multidrug-resistant, extensively drug-resistant and pandrug-resistant bacteria: an international expert proposal for interim standard definitions for acquired resistance. Clin Microbiol Infect. 2012;18:268–81. https://doi.org/10.1111/j.1469-0691.2011.03570.x
14. Charlson ME, Pompei P, Ales KL, MacKenzie CR. A new method of classifying prognostic comorbidity in longitudinal studies: development and validation. J Chronic Dis. 1987;40:373–83. https://doi.org/10.1016/0021-9681(87)90171-8
15. Wick RR, Judd LM, Gorrie CL, Holt KE. Unicycler: Resolving bacterial genome assemblies from short and long sequencing reads. PLOS Comput Biol. 2017;13:e1005595. https://doi.org/10.1371/journal.pcbi.1005595
16. Gurevich A, Saveliev V, Vyahhi N, Tesler G. QUAST: quality assessment tool for genome assemblies. Bioinformatics. 2013;29:1072–5. https://doi.org/10.1093/bioinformatics/btt086
17. Chklovski A, Parks DH, Woodcroft BJ, Tyson GW. CheckM2: a rapid, scalable and accurate tool for assessing microbial genome quality using machine learning. Nat Methods. 2023;20:1203–12. https://doi.org/10.1038/s41592-023-01940-w
18. Argimón S, David S, Underwood A, Abrudan M, Wheeler NE, Kekre M, et al.; NIHR Global Health Research Unit on Genomic Surveillance of Antimicrobial Resistance. Rapid genomic characterization and global surveillance of *Klebsiella* using Pathogenwatch. Clin Infect Dis. 2021;73:S325–35. https://doi.org/10.1093/cid/ciab784
19. Lam MMC, Wick RR, Watts SC, Cerdeira LT, Wyres KL, Holt KE. A genomic surveillance framework and genotyping

tool for *Klebsiella pneumoniae* and its related species complex. Nat Commun. 2021;12:4188. https://doi.org/10.1038/s41467-021-24448-3
20. Feldgarden M, Brover V, Gonzalez-Escalona N, Frye JG, Haendiges J, Haft DH, et al. AMRFinderPlus and the Reference Gene Catalog facilitate examination of the genomic links among antimicrobial resistance, stress response, and virulence. Sci Rep. 2021;11:12728. https://doi.org/10.1038/s41598-021-91456-0
21. Croucher NJ, Page AJ, Connor TR, Delaney AJ, Keane JA, Bentley SD, et al. Rapid phylogenetic analysis of large samples of recombinant bacterial whole genome sequences using Gubbins. Nucleic Acids Res. 2015;43:e15. https://doi.org/10.1093/nar/gku1196
22. Wong TKF, Ly-Trong N, Ren H, Demotte P, Baños H, Roger AJ, et al. IQ-TREE 3: phylogenomic inference software using complex evolutionary models. Mol Biol Evol. 2026;43:msag117. https://doi.org/10.1093/molbev/msag117
23. Kanda Y. Investigation of the freely available easy-to-use software 'EZR' for medical statistics. Bone Marrow Transplant. 2013;48:452–8. https://doi.org/10.1038/bmt.2012.244
24. Firth D. Bias reduction of maximum likelihood estimates. Biometrika. 1993;80:27–38. https://doi.org/10.1093/biomet/80.1.27
25. Kochan TJ, Nozick SH, Medernach RL, Cheung BH, Gatesy SWM, Lebrun-Corbin M, et al. Genomic surveillance for multidrug-resistant or hypervirulent *Klebsiella pneumoniae* among United States bloodstream isolates. BMC Infect Dis. 2022;22:603. https://doi.org/10.1186/s12879-022-07558-1
26. Tang Y, Du P, Du C, Yang P, Shen N, Russo TA, et al. Genomically defined hypervirulent *Klebsiella pneumoniae* contributed to early-onset increased mortality. Nat Commun. 2025;16:2096. https://doi.org/10.1038/s41467-025-57379-4
27. Yu F, Lv J, Niu S, Du H, Tang YW, Pitout JDD, et al. Multiplex PCR analysis for rapid detection of *Klebsiella pneumoniae* carbapenem-resistant (sequence type 258 [ST258] and ST11) and hypervirulent (ST23, ST65, ST86, and ST375) strains. J Clin Microbiol. 2018;56:e00731-18. https://doi.org/10.1128/JCM.00731-18
28. Jiang J, Long T, Porter AR, Lovey A, Lee A, Jacob JT, et al. Carbapenem-resistant, virulence plasmid–harboring *Klebsiella pneumoniae*, United States. Emerg Infect Dis. 2025;31:761–71. https://doi.org/10.3201/eid3104.241396

Address for correspondence: Naoki Watanabe, Hirosaki University Graduate School of Health Sciences, 036-8564, 66-1 Honcho, Hirosaki, Aomori, Japan; email: naoki.watanabe.ids@hirosaki-u.ac.jp

EID Podcast A Worm's Eye View

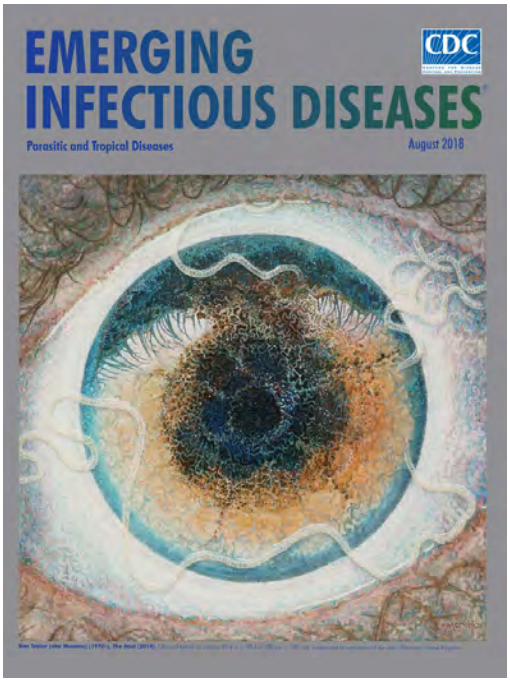

Seeing a several-centimeters-long worm traversing the conjunctiva of an eye is often the moment when many people realize they are infected with *Loa loa*, commonly called the African eyeworm, a parasitic nematode that migrates throughout the subcutaneous and connective tissues of infected persons. Infection with this worm is called loiasis and is typically diagnosed either by the worm's appearance in the eye or by a history of localized Calabar swellings, named for the coastal Nigerian town where that symptom was initially observed among infected persons. Endemic to a large region of the western and central African rainforests, the *Loa loa* microfilariae are passed to humans primarily from bites by flies from two species of the genus *Chrysops*, *C. silacea* and *C. dimidiate*. The more than 29 million people who live in affected areas of Central and West Africa are potentially at risk of loiasis.

Ben Taylor, cover artist for the August 2018 issue of EID, discusses how his personal experience with the *Loa loa* parasite influenced this painting.

Visit our website to listen: https://tools.cdc.gov/medialibrary/index.aspx#/media/id/392605

EMERGING INFECTIOUS DISEASES

Pediatric Deaths during Measles Outbreak, Jerusalem, Israel, 2025–2026

Zohar Mor, Hanna Shoob, Irinia Sokolov, Efrat Bucris, Chen Stein-Zamir, Ariel Tenenbaum, Orli Megged,[1] Oren Gordon[1]

Of 1,289 measles case-patients during April 2025–March 2026 in Jerusalem, Israel, 11 children died, a measles-specific mortality rate of 1.1 deaths/100,000 population. The measles-specific mortality rate among children <5 years of age was 7.7 deaths/100,000 population but 80.1 deaths/100,000 population in 6 neighborhoods populated by ultraorthodox Jews, a 47% measles-attributed death fraction.

In the United States, 2–3 deaths occur for every 1,000 reported measles cases (https://www.cdc.gov/surv-manual/php/table-of-contents/chapter-7-measles.html), a case-fatality rate (CFR) of 0.2%–0.3%. Overall, measles CFR is 0.3%–5.3% in low- and middle-income countries (*1*). The measles-specific mortality rate (MSMR) ranges from 0.04 deaths/100,000 population in Europe to 2.2 deaths/100,000 population in Africa (*2*). Immunosuppressed persons, malnourished persons, and children <5 years of age are at higher risk for death from measles (*3*).

The previous outbreak in Israel occurred during 2018–2019, during which 4,290 cases were reported (*4*). Of those cases, a total of 1,415 (33.0%) were in persons living in the city of Jerusalem (*5*,*6*), and 2 fatalities were reported (CFR 0.14%; MSMR 0.2 deaths/100,000 Jerusalem population). Jerusalem is the largest city in Israel, having a population of ≈1 million in 2025 (10.2% of the population of Israel), comprising ≈600,000 (62%) Jewish and ≈400,000 (38%) Arab persons (*7*). Of the Jewish population, ≈50.0% (≈300,000) were ultraorthodox religious Jews.

Coverage with the first measles, mumps, and rubella (MMR) and measles, mumps, rubella, and varicella (MMRV) vaccines among children 1–6 years of age in Jerusalem has decreased from 94.7% in 2019 to 78.3% in 2024 and is the lowest in Israel (https://datadashboard.health.gov.il/portal/dashboard/serviceQuality). Substantial geographic and ethnocultural differences exist across the city; coverage in April 2025 ranged from 99.4% among East Jerusalem Arab children to ≈55.0% in 6 designated neighborhoods (the 6 neighborhoods) in central Jerusalem, which has a population of ≈67,500, mostly ultraorthodox Jews.

We describe measles disease and death in Jerusalem during April 2025–March 2026. We also identify contributing factors to the unexpectedly elevated mortality rate.

The Study

We determined measles diagnosis by using reverse transcription PCR of pharyngeal or urine specimens or by a combination of clinical symptoms and epidemiologic linkage to another measles case (https://www.gov.il/BlobFolder/policy/epi-92335924/he/files_regulation_epidemiology_epi-92335924.pdf). We sequenced samples by using Sanger or next-generation sequencing at the Ministry of Health's Central Virology Laboratory. We conducted epidemiologic investigations on all cases to identify the source of exposure and define close contacts.

We calculated acute-phase measles mortality rates for all cases reported to surveillance teams during the 2025–2026 outbreak, expressing results as CFR and by MSMR because not all incident cases were reported. We calculated CFR by dividing

Author affiliations: Ministry of Health, Jerusalem, Israel (Z. Mor, H. Shoob, I. Sokolov); Ashkelon Academic College, Ashkelon, Israel (Z. Mor); Ministry of Health Virology Laboratory, Tel Hashomer, Israel (E. Bucris); Hebrew University of Jerusalem Faculty of Medicine, Jerusalem (C. Stein-Zamir, A. Tenenbaum, O. Megged, O. Gordon); Hadassah Ein Karem Medical Center, Jerusalem (A. Tenenbaum, O. Gordon); Shaare Zedek Medical Center, Jerusalem (O. Megged)

DOI: https://doi.org/10.3201/eid3211.261397

[1]These authors contributed equally to this article.

measles-related deaths by all reported measles cases in a designated area, and calculated MSMR by dividing measles-related deaths by the total population in the designated area (Appendix, https://wwwnc.cdc.gov/EID/article/32/11/26-1397-App1.pdf).

During April 2025–March 2026, a total of 1,289 measles cases (129.2 cases/100,000 Jerusalem population) were reported in Jerusalem, comprising 36.1% of the total 3,574 cases reported in Israel (36.6 cases/100,000 Israel population). The median age of case-patients in Jerusalem was 3.1 (interquartile range [IQR] 1.5–5.4) years. Of all case-patients, 70.7% (912/1,289) were children <5 years of age. Median household size was 6 (IQR 5–8) persons, and 870 (95.4%) were unvaccinated for measles, whereas 42 (4.6%) received a vaccine single-dose. Most (885/1,289 [68.7%]) case-patients resided in the 6 neighborhoods, home to 6.8% of Jerusalem's <5-year-old population, but 71.9% of <5-year-old case-patients in Jerusalem were reported in the 6 neighborhoods.

Of all 1,289 case-patients in Jerusalem, 11 died (64.7% of the 17 total deaths reported in Israel), yielding a CFR of 0.85% and an MSMR of 1.1 deaths/100,000 population (Table 1, Figure). The MSMR among children <5 years of age was 7.7 deaths/100,000 population in Jerusalem compared with 0.5 deaths/100,000 population in the rest of Israel. The MSMR among children <5 years of age in the 6 neighborhoods was 80.1 deaths/100,000 population, and the measles-attributed mortality fraction in that area compared with all-cause deaths during the previous year was 47%.

The median age of children who died was 1.4 (IQR 1.1–2.5) years; 8 (72.7%) were boys and 3 (27.3%) were girls (Table 2). Ten of the children were otherwise healthy; 9 of those were <3 years of age, had not received any vaccinations, and were not registered in the mother-and-child health clinics. One 7-year-old child who died had known truncus arteriosus and was vaccinated with a single MMRV dose at 1 year of age, but did not receive the second dose.

Analysis of the N450 region of the measles genome confirmed that 2 available samples from deceased children belonged to genotype B3. Those sequences matched the B3-named strain MVs/Quetta.PAK/44.20 (distinct sequence identifier 6418), which circulated in previous measles outbreaks in Europe (*8*,*9*).

The median household size of case-patients who died was 7 (IQR 6–11) persons, and 1–3 other family members reportedly had measles. Reverse transcription PCR–based diagnosis was confirmed in 9 (81.8%) children who died (Table 3), whereas 2 had clinical signs of measles and epidemiologic links. The median time from the first measles symptom (fever or rash) to emergency department (ED) visit was 8 (IQR 6–14) days, and death was reported within 15 (IQR 9–24) days. Six children were dead on arrival at the ED, and 5 children were hospitalized for a median of 21 (IQR 11–32) days; of those, 3 were treated with extracorporeal membrane oxygenation. Eight (72.7%) case-patients had radiologic findings indicative of pneumonia on chest radiograph at admission, and 6 case-patients had positive blood cultures

One limitation of our study is the uncertainty about the actual number of measles cases in Jerusalem. A back-calculation based on the 11 observed measles death in Jerusalem and CFR estimates of 0.1%–0.3% in developed countries (https://www.ecdc.europa.

Table 1. Age-specific number of measles cases, number of measles-specific deaths, and case-fatality rates during measles outbreak, Jerusalem, Israel, April 2025–March 2026*

Characteristics	Jerusalem	Six neighborhoods in central Jerusalem
Total population, no.	997,870	67,530
No. reported cases of measles (measles cases/100,000 population)		
All reported measles cases	1,289 (129.2)	885 (1,310)
0–1 y	193 (825)	118 (5,254)
<5 y	912 (780)	656 (5,842)
5–9 y	272 (251)	193 (2,234)
<10 y	1,184 (525.4)	849 (4,273)
No. reported measles deaths (measles-specific deaths/100,000 population)		
All reported measles cases	11 (1.1)	11 (16.3)
0–1 y	1 (4.3)	1 (44.5)
<5 y	9 (7.7)	9 (80.1)
5–9 y	2 (1.8)	2 (23.1)
<10 y	11 (4.9)	11 (55.3)
Case-fatality rate, %		
All reported measles cases	0.85	1.2
0–1 y	0.5	0.85
<5 y	1.0	1.4
5–9 y	0.7	1.0
<10 y	0.9	1.3

*Age groups may overlap.

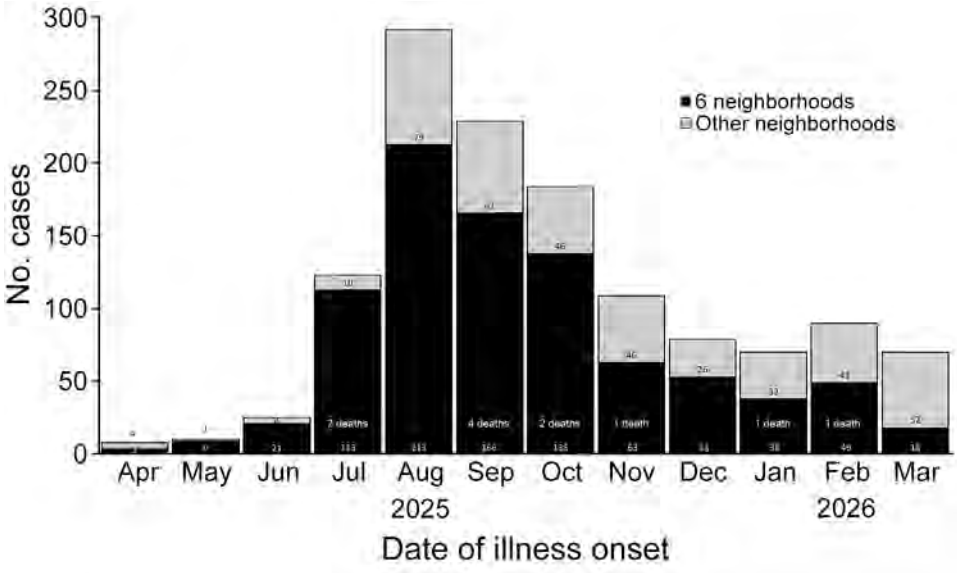

Figure. Number of reported measles cases and deaths, by month of illness onset, during measles outbreak, Jerusalem, Israel, April 2025–March 2026. Number of deaths per area and month are included.

eu/sites/default/files/documents/MEAS-AER-2024-Report.pdf; https://www.cdc.gov/surv-manual/php/table-of-contents/chapter-7-measles.html) suggest that the actual number of measles cases might have been substantially higher than the number reported in Jerusalem. Because of the possible underascertainment, we added an MSMR calculation, which is more stable and population-based. In addition, we only calculated acute measles deaths, not long-term mortality rates.

Conclusions

The reported 2025–2026 measles disease rate in Jerusalem was 129.2 cases/100,000 population, which was 15 times higher than in the rest of Israel. CFR was 0.85% in Jerusalem and 0.26% in the rest of Israel, higher than the 0.1% reported in Europe (https://www.ecdc.europa.eu/sites/default/files/documents/MEAS-AER-2024-Report.pdf; https://measles-rubella-monthly.ecdc.europa.eu) and 0.2%–0.3% in the United States (https://www.cdc.gov/measles/data-research/index.html). The high MSMR among children <5 years of age also might reflect the overwhelming effect of the outbreak, which caused 80.1 deaths/100,000 children in the 6 neighborhoods in Jerusalem.

Prevention through vaccination is the mainstay in controlling measles outbreaks. Given the measles first-vaccine coverage of 55% in the 6 neighborhoods at the beginning of the outbreak, combined with MMR vaccine efficacy of 95% at 12 months (*3*), an estimated 47.7% of infants in each birth cohort were unprotected against measles. The young age of the unvaccinated measles case-patients, in addition to overcrowding and the presence of other sick household members, increased domestic measles transmission because of higher in-house viral inoculum and repeated exposures (*10*). In response, the Ministry of Health recommended MMR vaccine in Jerusalem at 6 months because maternal antibodies wane over time (*3*).

Table 2. Demographic and other characteristics of children who died during measles outbreak, Jerusalem, Israel, April 2025–March 2026*

Case	Age, y/sex	No. measles vaccine doses	No. household members	Other vaccinations	No. ill household members	Days from first symptom to ED visit	Days from first symptom to death
1	2.4/M	0	10	None	2	9	27†
2	0.9/F	0	4	None	2	1	59†
3	1.3/M	0	7	None	1	8	38
4	1.3/M	0	12	None	1	15	15‡
5	1.4/M	0	14	None	1	19	19‡
6	1.9/M	0	6	None	2	7	7‡
7	2.5/F	0	10	None	1	4	15†
8	7.1/M	1	7	Partial	2	14	14‡
9	1.1/M	0	11	None	2	8	15
10	1.1/M	0	5	None	3	9	9‡
11	6.5/F	0	7	Partial	2	7	7‡

*ED, emergency department.
†Patient received extracorporeal membrane oxygenation.
‡Patient dead on arrival at ED.

Table 3. Laboratory and clinical characteristics of children who died during measles outbreak, Jerusalem, Israel, April 2025–March 2026*

Case	Measles RT-PCR result	Fever	Rash	Cough	Conjunctivitis	Koplik spots	Pneumonia on chest x-ray	Blood culture findings	Respiratory aspirate or pleural fluid culture findings
1	+	Y	Y	N	N	N	Y	*Staphylococcus pneumoniae*	–
2	+	Y	Y		Y	Y	Y	–	–
3	+	Y	Y	Y	Y	Y	Y	–	–
4	NA	Y	Y	Y	N	N	Y	MSSA	–
5	NA	Y	Y	Y	N	N	Y	*S. pyogenes*	*S. pyogenes*
6	+	Y	Y	Y	N	N	N	MSSA and *Haemophilus influenzae* (non–B)	–
7	+	Y	Y	Y	Y	Y	Y	–	MSSA and *S. pyogenes*
8	+	Y	Y		N	N	N	–	–
9	+	Y	Y	Y	Y	Y	Y	–	MSSA
10	+	Y	Y	N	N	N	N	*S. pneumoniae*	–
11	+	Y	Y	N	N	N	Y	*S. pettenkoferi*	–

*MSSA, methicillin-susceptible *Staphylococcus aureus*; NA, not available; RT-PCR, reverse transcription PCR; +, positive; –, negative.

The late appearance in the ED of patients with fatal cases (i.e., 6/11 case-patients were dead upon arrival), might reflect avoidance of healthcare utilization in ultraorthodox communities because of distinct cultural, religious, and social considerations and insularity from government and secular media (*5*). A possible mistrust of government institutions might contribute to vaccine hesitancy, alongside frustration with isolation and coerced measures imposed during the COVID-19 pandemic and skepticism about MMR/MMRV vaccination.

Some parents reported they first consulted community mediators when the child's condition deteriorated. Those mediators were known in the community for their medical backgrounds, having served as medical orderlies or midwives. The mediators used pulse oximeters to monitor the ill children, and some suggested vitamin A supplements or provided intravenous fluids before seeking conventional medical support, which might explain delayed referral to healthcare facilities. Underutilization of the healthcare system and low vaccination coverage underscore trust gaps between the ultraorthodox community and the public healthcare system, reflecting an intricate interplay of cultural, socioeconomic, and informational influences (*11*). A similar community response was demonstrated during COVID-19; prevalence of disease and death were much higher among ultraorthodox Jews in Israel compared with the overall population of Israel, but vaccine coverage remained low (*12*) among ultraorthodox Jewish persons in Israel and in other ultraorthodox Jewish communities elsewhere (*13*).

Additional factors contributing to the low level of trust and undervaccination might include a high spiritual locus of control. Persons with pronounced spiritual beliefs might be less inclined to vaccinate because of a belief in divine control over health outcomes, as found in a recent study in Israel (*14*).

Ultraorthodox communities comprise diverse subgroups, each guided by its own religious leadership and differing in their sources of influence, attitudes toward the community and external institutions, and relationships with wider society, all of which affect attitudes and behaviors toward vaccines and immunizations (*12*). Although rabbinical endorsement is essential to support a timely vaccination schedule, some indications suggest that the community is becoming less obedient to religious authority. The decrease in the influence of central religious authority, parallel with individual decision-making, is an opportunity to establish direct channels of communication between religious persons and healthcare providers to deliver direct health messages to ultraorthodox persons.

Secondary infection attributable to immune suppression and immune amnesia might have contributed to severe outcomes (*10*). Longer follow-up on children recovering from measles might identify additional cases of measles illness and death. That explanation is supported by the large number of case-patients who had bacteremia among all fatal cases (6 of the 11 children who died), whereas 2 were infected with vaccine-preventable pathogens.

In summary, we observed high MSMR and measles prevalence in Jerusalem during 2025–2026, mainly among unvaccinated children <5 years of age from ultraorthodox Jewish families. The 11 childhood deaths, including 6 in children who died before hospital arrival, represent a serious public health event in a city with advanced medical and vaccination services but where vaccination gaps exist. Although the previous 2018–2019 outbreak was successfully controlled, measles vaccine coverage has declined, partly

because of changes in community behavior and the post–COVID-19 social climate. Outbreak vaccination efforts need to be followed by continuous maintenance of routine coverage. Culturally tailored interventions, developed in partnership with community leaders, are needed to strengthen trust in healthcare providers and vaccines, promote earlier healthcare-seeking among parents to enable timely recognition and medical assessment, reduce the risk for delayed diagnosis, and prevent clinical deterioration (*14*).

About the Author

Prof. Mor is a senior public health physician who heads the Jerusalem Department of Health at the Ministry of Health and the Program of Public Health at the Ashkelon Academic College. His primary research interests include infectious diseases in special populations.

References

1. Sbarra AN, Mosser JF, Jit M, Ferrari M, Ramshaw RE, O'Connor P, et al. Estimating national-level measles case-fatality ratios in low-income and middle-income countries: an updated systematic review and modelling study. Lancet Glob Health. 2023;11:e516–24. https://doi.org/10.1016/S2214-109X(23)00043-8
2. Antoni S, Ferrari MJ, Wimmer A, Nedelec Y, Steulet C, Gacic-Dobo M, et al. Progress towards measles elimination—worldwide, 2000–2024. Weekly epidemiological record. 2025 Nov 28 [cited 2026 Jul 10]. https://iris.who.int/server/api/core/bitstreams/8c65dd54-ee98-4438-938c-e7114851f870/content
3. Do LAH, Mulholland K. Measles 2025. N Engl J Med. 2025;393:2447–58. https://doi.org/10.1056/NEJMra2504516
4. Anis E, Haas EJ, Indenbaum V, Singer SR, Warshavsky B, Rishpon S, et al. A prolonged, nationwide measles outbreak despite very high vaccination coverage in Israel, 2018-19. J Infect. 2021;83:678–85. https://doi.org/10.1016/j.jinf.2021.09.025
5. Stein-Zamir C, Abramson N, Shoob H. Large measles outbreak in orthodox Jewish communities—Jerusalem District, Israel, 2018–2019. MMWR Morb Mortal Wkly Rep. 2020;69:562–3. https://doi.org/10.15585/mmwr.mm6918a3
6. Stein-Zamir C, Shoob H, Abramson D. Measles clinical presentation, hospitalization and vaccination status among children in a community-wide outbreak. Vaccine. 2023;41:2764–8. https://doi.org/10.1016/j.vaccine.2023.03.043
7. Jerusalem Institute for Policy Research. Jerusalem statistical yearbook 2026. 2026 [cited 2026 Jun 27]. https://jerusaleminstitute.org.il/en/yearbook/#/4372/31934
8. Bucris E, Zuckerman NS, Levin T, Kanaaneh Y, Erster O, Indenbaum V, et al.; National Measles Working Group; National Measles Working Group. Genomic and epidemiologic insights into ongoing measles outbreak, Israel, 2025–2026. Emerg Infect Dis. 2026;32:1678–82. https://doi.org/10.3201/eid3209.260625
9. Cassini A, Cobuccio L, Glampedakis E, Cherpillod P, Crisinel PA, Pérez-Rodríguez FJ, et al. Adapting response to a measles outbreak in a context of high vaccination and breakthrough cases: an example from Vaud, Switzerland, January to March 2024. Euro Surveill. 2024;29:2400275. https://doi.org/10.2807/1560-7917.ES.2024.29.22.2400275
10. Jacobson A, Spitzer S, Gorelik Y, Edelstein M. Barriers and enablers to vaccination in the ultra-orthodox Jewish population: a systematic review. Front Public Health. 2023;11:1244368. https://doi.org/10.3389/fpubh.2023.1244368
11. Spitz A, Siman-Tov M, Shapiro E. The complex issue of trust of Israel's Jewish religious community in health care and religious institutions involved in addressing the COVID-19 pandemic. J Relig Health. 2026;65:573–93. https://doi.org/10.1007/s10943-025-02436-x
12. Berger Lipsky T, Gabbay E. Sociocultural and religious perspectives toward the COVID-19 pandemic in the Haredi Jewish community. J Relig Health. 2023;62:389–407. https://doi.org/10.1007/s10943-022-01667-6
13. Gendler Y, Ofri L, Videl H. Understanding factors contributing to vaccination underutilization among Jewish ultra-orthodox communities in Israel: a cross-sectional study. Vaccine. 2025;47:126711. https://doi.org/10.1016/j.vaccine.2025.126711
14. Kasstan B. "If a rabbi did say 'you have to vaccinate,' we wouldn't": Unveiling the secular logics of religious exemption and opposition to vaccination. Soc Sci Med. 2021;280:114052. https://doi.org/10.1016/j.socscimed.2021.114052

Address for correspondence: Zohar Mor, Jerusalem Department of Health, 86 Jaffa Rd, Jerusalem 9137001, Israel; email: zmor100@gmail.com

Serologic Assessment of Public Health Action Needed for Trachoma, Coastal Ecuador, 2021–2024

Everlyn Kamau, Lesly Simbaña, Stuart Torres, Nikolina Walas, Gretchen Cooley, Chabier Coleman, E. Brook Goodhew, Diana L. Martin, Hadley Burroughs, Manuel Calvopiña, William Cevallos, Sandra Vivero, Victoria Nipaz, Josefina Coloma, Gwenyth O. Lee, Gabriel Trueba, Joseph N.S. Eisenberg, Karen Levy, Benjamin F. Arnold

We evaluated the probability of needing public health actions against trachoma in Esmeraldas Province, Ecuador, by estimating seroconversion rates of *Chlamydia trachomatis* plasma gene protein 3 IgG in children. Seroconversion rates suggest high probability of the need for public health interventions in rural communities and motivate further assessment.

Trachoma is a blinding eye disease caused by infection with ocular strains of *Chlamydia trachomatis*; trachoma has been declared a public health concern by the World Health Organization and targeted for elimination by 2030 (*1*). Public health interventions for trachoma include surgery for trichiasis, mass administration of antimicrobial drugs, and programs to support facial cleanliness and environmental improvement (*2*).

IgGs against the plasma gene protein 3 (Pgp3) of *C. trachomatis* are sensitive markers of past infections, making them suitable for monitoring populations after mass administration of antimicrobial drugs (*3*). Pgp3 antibodies can be used to measure trachoma transmission intensity in population-based surveys (*4*). A global analysis of trachoma was used to develop methods that use the Pgp3 IgG seroconversion rate (SCR) to estimate the probability of needing public health actions (*5*).

The highest prevalence of trachoma is found in sub-Saharan Africa (*2*). Trachoma also remains a public health concern in remote areas of South America; elimination efforts by the Pan American Health Organization are ongoing (*6*). Little is known about trachoma in Ecuador. We recently identified high levels of incident seroconversion of Pgp3 antibodies within a birth cohort in Esmeraldas Province of coastal Ecuador (L. Simbaña et al., unpub. data, https://doi.org/10.64898/2026.02.16.26346420). Here, we describe augmenting those birth cohort samples by including samples from older children living in villages within the same region and estimated Pgp3 antibody SCRs. We compared those data with global SCR distributions to estimate the probability of needing public health actions against trachoma.

The Study

We included samples from 2 studies. The ECoMiD longitudinal birth cohort study in Esmeraldas Province enrolled pregnant mothers during 2019–2022 along an urban–rural gradient that included Esmeraldas city (urban), Borbón (commercial center for the region), 4 communities accessible by road, and 4 communities accessible via the Santiago and Onzole Rivers (Appendix Figure, https://wwwnc.cdc.gov/EID/article/32/11/26-1024-App1.pdf) (*7*). Dried blood spots were collected during 2021–2024, when children were 6, 9, 12, 18, and 24 months of age (L. Simbaña et al., unpub. data). We also included serum samples collected from community-based, annual serologic surveillance of arbovirus transmission in Borbón; 5 other communities, 4 of which overlapped with

Author affiliations: University of California, San Francisco, California, USA (E. Kamau, N. Walas, H. Burroughs, B.F. Arnold); Universidad de San Francisco de Quito, Quito, Ecuador (L. Simbaña, S. Torres, V. Nipaz, G. Trueba); Centers for Disease Control and Prevention, Atlanta, Georgia, USA (G. Cooley, C. Coleman, E.B. Goodhew, D.L. Martin); Universidad de las Americas, Quito (M. Calvopiña); Universidad Central del Ecuador, Quito (W. Cevallos, S. Vivero); University of California, Berkeley, California, USA (J. Coloma); Rutgers University, New Brunswick, New Jersey, USA (G.O. Lee); University of Michigan, Ann Arbor, Michigan, USA (J.N.S. Eisenberg); University of Washington, Seattle, Washington, USA (K. Levy)

DOI: https://doi.org/10.3201/eid3211.261024

the ECoMiD study areas (Maldonado, Colon Eloy, Timbiré, Santo Domingo); and Santa Maria, along the Cayapas River (*8*). Annual surveys were conducted during August–October and used age-stratified sampling, which oversampled 2–14-year-old children.

We tested samples from 2–15-year-old children collected during the 2021 and 2022 surveys for Pgp3 IgG by using the Luminex platform (https://www.luminexcorp.com) at Universidad San Francisco de Quito (L. Simbaña et al., unpub. data). We combined data from both cohorts and stratified the communities into 2 groups, Borbón (799 samples) and rural villages (2,002 samples). We excluded birth cohort samples from Esmeraldas city (n = 355) because the city was not included in the arbovirus surveillance study. We summarized details of study setting, sample testing, and statistical analysis (Appendix).

We used SCRs to assess the probability of whether *C. trachomatis* transmission was at a level that warranted public health action (*5*). For the Borbón and rural village groups, we estimated SCRs by using a catalytic model and a constant force of infection (Appendix). We then estimated the probability (*P*) of populations falling into either action needed or action not needed categories (*5*) by using the equation $P(\text{Category}\,|\,\text{SCR}) = P(\text{SCR}\,|\,\text{Category}) \times P(\text{Category})$. The action needed category identifies populations likely to experience disease sequelae and blindness from trachoma without intervention; the action not needed category identifies populations unlikely to have transmission intense enough to justify population-level interventions. We calculated the likelihood $P(\text{Category}\,|\,\text{SCR})$ as the empirical probability of SCR estimates from Ecuador relative to SCRs in a global trachoma serology dataset derived from well-characterized populations (*9*) (Appendix). We considered the serologic survey in coastal Ecuador to be the baseline and used an uninformative prior of category $P(\text{Category}) = 0.5$ (*5*). For each group, we also calculated the probability that the SCR was above or below specific thresholds to measure confidence levels. We used SCR thresholds of 2 and 4 per 100 person-years because those thresholds aligned with regions of high confidence (>90% probability) for action not needed (SCR $\leq$2) versus action needed (SCR $\geq$4) (*5*).

We analyzed a total of 2,801 dried blood spots from 1,243 children 0–15 years of age for Pgp3 IgG. The sample numbers were larger for younger children because of greater sample contributions from the birth cohort; fewer samples were obtained from 3–5-year-old children (Figure 1, panel A). Pgp3 IgG seroprevalence rose earlier and to a higher level in rural villages than in Borbón; IgG levels in both groups converged in children 13 years of age (Figure 1, panel B). Overall, Pgp3 IgG seroprevalence was 7.0% (95% CI 5.3%–9.0%; 56/799) in Borbón and ranged from 0% (95% CI 0%–9.3%) in Colon de Onzole to 31% (95% CI 19.1%–44.8%; 17/55) in Zancudo (Figure 1, panel C). Among 401 children (790 samples) who were 1–5 years of age, the SCRs per 100 person-years were 4.6 (95% CI 3.5–6.2) overall, 1.9 (95% CI 0.7–5.5) in Borbón, and 5.7 (95% CI 4.2–7.7) in rural villages per 100 person-years.

When compared with SCR distributions from 34 global trachoma surveys, the probability that public health action was needed was 99.3% for the rural villages and 32.0% for Borbón (Figure 2, panel A). The probability that SCR was $\leq$2/100 person-years [i.e., $P(\text{SCR} \leq 2)$], which represented high confidence for no public health action needed, was 0% for the rural

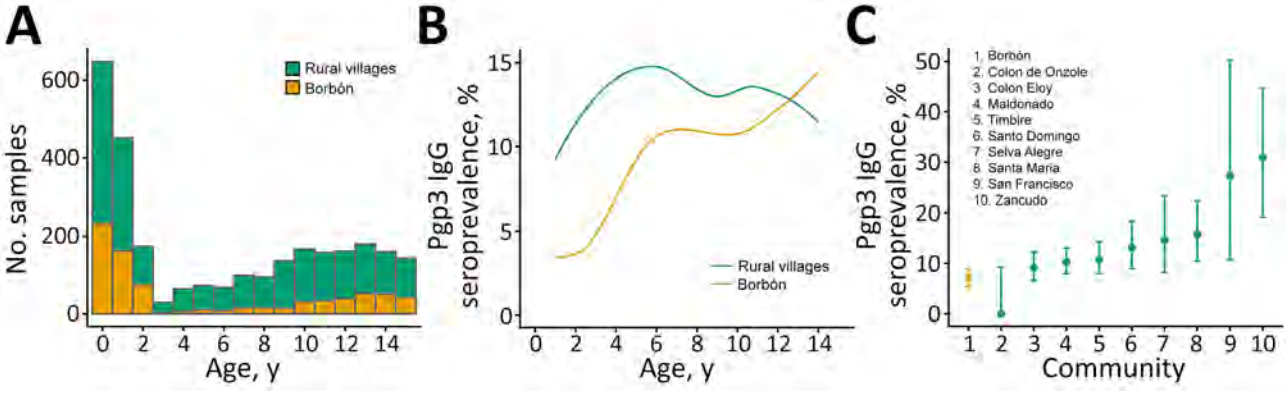

Figure 1. Seroprevalence of *Chlamydia trachomatis* Pgp3 IgG in rural areas and Borbón (commercial center) in Esmeraldas Province in study of serologic assessment of public health action needed for trachoma, coastal Ecuador, 2021–2024. A) Number of samples according to age and community type. A total of 2,801 samples were collected from 1,243 children who were 0–15 years of age; 790 samples were from 401 children 1–5 years of age. B) Seroprevalence according to age and community type estimated by using locally weighted regression, trimmed to 1–14 years of age to reduce edge effects. C) Seroprevalence among all children who were 0–15 years of age in BorbÓn and 9 rural villages. Error bars indicate 95% CIs. Pgp3, plasma gene protein 3.

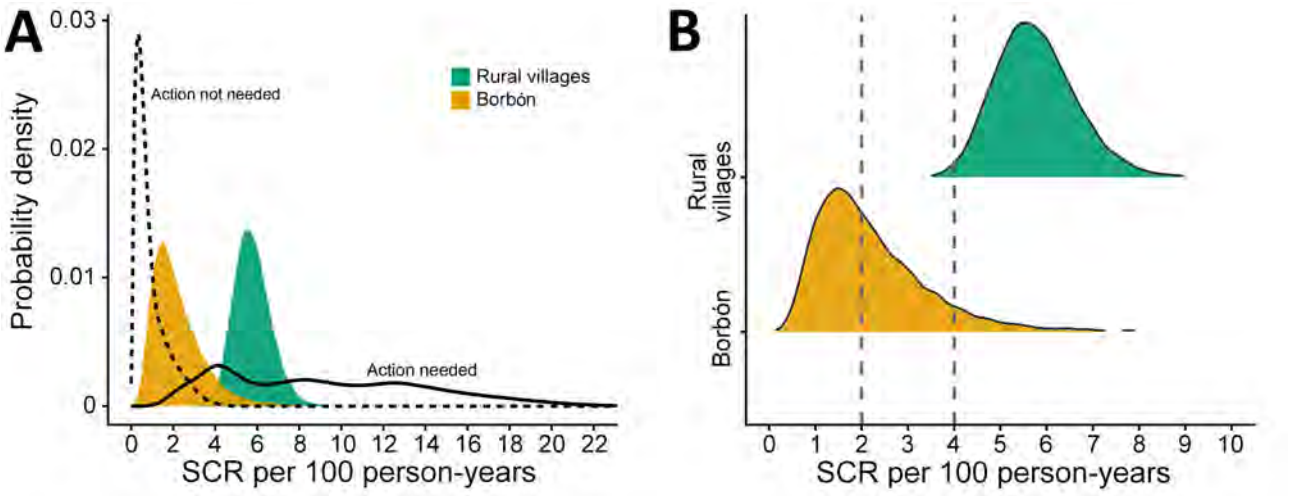

Figure 2. Model-based probability estimates of SCRs for IgGs against *Chlamydia trachomatis* plasma gene protein 3 in study of serologic assessment of public health action needed for trachoma, coastal Ecuador, 2021–2024. Estimates compared data from Esmeraldas Province in Ecuador and global trachoma serology distributions (*5*). A) Probability density of SCRs for Borbón (commercial center) and 9 rural villages estimated for children who were 1–5 years of age. We superimposed those data with pooled SCR distributions from populations classified as public health action not needed (dashed line) and public health action needed (solid line), according to public health responses for trachoma control in a global analysis across a range of disease endemicity (*5*). B) Ridgeline plot of SCR probability densities for Borbón and rural villages from panel A compared with illustrative thresholds of 2 and 4/100 person-years (vertical dashed lines). We identified SCR ≤2 as a region of >90% probability that public health action is not needed, whereas SCR ≥4 is a region of ≥90% probability that public health action is needed. Intermediate ranges of SCR that are >2 and <4 per 100 person-years could motivate additional testing (e.g., PCR testing for infection or consideration for further monitoring depending on programmatic context [*5*]). SCR, seroconversion rate.

villages and 52.4% for Borbón (Figure 2, panel B). Conversely, the probability that SCR was ≥4 [i.e., *P*(SCR ≥4)] was 91.3% for the rural villages and 8.8% for Borbón (Figure 2, panel B).

Conclusions

Pgp3 IgG SCRs in children from rural villages within the Santiago River basin of Ecuador suggest a high probability that public health action is needed for trachoma when compared with global SCR distributions (*9*). SCR estimates in rural villages fall within the range observed in districts with high levels of ongoing transmission that require interventions (*5*) and are consistent with estimates within disease-endemic districts of Ethiopia considered to have persistent, active trachoma (*10*).

Trachoma elimination efforts in the Americas include planned trachoma surveys in Ecuador; priority surveillance is within the Amazon basin (*11*). Our findings suggest that Esmeraldas Province should be considered as well. Although the World Health Organization has not yet set Pgp3 IgG SCR thresholds for stopping or starting interventions, we used SCRs of ≤2 and ≥4 as regions of high confidence to determine action not needed versus action needed. Additional monitoring of SCRs in Borbón is warranted, because the 95% CI of the SCR spanned the intermediate range of 2–4 cases/100 person-years.

The first limitation of our study is that we did not use a population-based probability sampling strategy that had many sampling clusters, as is commonly recommended for trachoma surveillance (*12*–*14*). Therefore, children who were 3–5 years of age might have been underrepresented, particularly in Borbón. Second, we did not characterize blood samples according to clinical signs of trachoma or ocular *C. trachomatis* infection. A natural next step would be to conduct standardized baseline surveys (*12*–*14*) to ascertain the presence of active trachoma and provide reference points to measure trachoma elimination progress.

Our analysis provides a generalizable example of using existing serosurveys to inform public health decision-making to support trachoma elimination. Pgp3 IgG SCRs can be used to identify communities at risk for persistent or reemerging trachoma transmission in the Americas, particularly in rural communities with limited access to safe water, sanitation, and hygiene.

Acknowledgments

We thank Anthony Solomon for his comments on a draft of this paper.

Institutional review boards (IRBs) at the University of Washington (approval no. STUDY00014270), Emory University (approval no. IRB00101202), University of California, San Francisco (approval no. 21-33932),

University of Michigan (approval no. HUM00140967), Universidad San Francisco de Quito (approval nos. 2017-159M and 2018−022M), and Ministry of Health of Ecuador (approval no. MSPCURI000253-4) reviewed and approved the study protocol. Caregivers provided informed consent, and field staff obtained consent and assent before each sample collection.

Replication files are available through Zenodo (https://zenodo.org/records/22926086). Because of the small population within the study region, the University of California, San Francisco, IRB determined that individual-level data that included the age of the child (essential for the analysis), even if deidentified, would be considered potentially identifiable. Please contact the corresponding author regarding possible access to data used for this analysis, pending approval from the University of California, San Francisco, IRB.

This work was supported by the National Institute of Allergy and Infectious Diseases at the National Institutes of Health (grant nos. R01AI137679, R01AI162867, R01AI158884, R01AI132372, and U01AI151788).

Contributions: B.F.A. provided supervision, conducted project administration, and secured funding. E.K. and B.F.A. conceptualized the research goals, developed the methods, validated results, conducted the formal analysis, prepared figures, and wrote the original manuscript draft. L.S., S.T., N.W., and B.F.A. conducted data curation. All authors contributed to manuscript review and editing and approved the manuscript.

About the Author

Dr. Kamau is a researcher at the University of California, San Francisco, California, USA. Her primary research interests are epidemiology and surveillance of infectious diseases of public health concern.

References

1. World Health Organization. Validation of elimination of trachoma as a public health problem. 2016 [cited 2026 Jun 3]. https://www.who.int/publications/i/item/who-htm-ntd-2016.8
2. Solomon AW, Burton MJ, Gower EW, Harding-Esch EM, Oldenburg CE, Taylor HR, et al. Trachoma. Nat Rev Dis Primers. 2022;8:32. https://doi.org/10.1038/s41572-022-00359-5
3. Martin DL, Bid R, Sandi F, Goodhew EB, Massae PA, Lasway A, et al. Serology for trachoma surveillance after cessation of mass drug administration. PLoS Negl Trop Dis. 2015;9:e0003555. https://doi.org/10.1371/journal.pntd.0003555
4. Tedijanto C, Solomon AW, Martin DL, Nash SD, Keenan JD, Lietman TM, et al. Monitoring transmission intensity of trachoma with serology. Nat Commun. 2023;14:3269. https://doi.org/10.1038/s41467-023-38940-5
5. Kamau E, Ante-Testard PA, Gwyn S, Blumberg S, Abdalla Z, Aiemjoy K, et al. Characterizing trachoma elimination using serology. Nat Commun. 2025;16:5545. https://doi.org/10.1038/s41467-025-60581-z
6. Pan American Health Organization. Initiative for the elimination of trachoma in the Americas [cited 2025 Dec 10]. https://www.paho.org/en/initiative-elimination-trachoma-americas
7. Lee GO, Eisenberg JNS, Uruchima J, Vasco G, Smith SM, Van Engen A, et al. Gut microbiome, enteric infections and child growth across a rural–urban gradient: protocol for the ECoMiD prospective cohort study. BMJ Open. 2021;11:e046241. https://doi.org/10.1136/bmjopen-2020-046241
8. Andrade P, Sosa-Moreno A, Vivero S, Nipaz V, Lee GO, Cevallos W, et al. The impact of Zika emergence in remote communities in northwestern Ecuador. J Infect Dis. 2024;230:e1058–66. https://doi.org/10.1093/infdis/jiae384
9. Kamau E, Ante-Testard PA, Colado J, Nash SD, Martin DL, Arnold BF, et al. Data resource profile: global trachoma serology data repository. Int J Epidemiol. 2025;54:dyaf183. https://doi.org/10.1093/ije/dyaf183
10. Nash SD, Astale T, Nute AW, Bethea D, Chernet A, Sata E, et al. Population-based prevalence of *Chlamydia trachomatis* infection and antibodies in four districts with varying levels of trachoma endemicity in Amhara, Ethiopia. Am J Trop Med Hyg. 2021;104:207–15. https://doi.org/10.4269/ajtmh.20-0777
11. Pan American Health Organization. Ecuador: partnership to eliminate trachoma as a public health problem [cited 2025 Dec 10]. https://www.paho.org/sites/default/files/2024-03/2024-cde-paho-canada-trachoma-public-health-ecuador.pdf
12. World Health Organization. Design parameters for population-based trachoma prevalence surveys. 2018 [cited 2026 Jun 3]. https://www.who.int/publications/i/item/who-htm-ntd-pct-2018.07
13. Harding-Esch EM, Burgert-Brucker CR, Jimenez C, Bakhtiari A, Willis R, Bejiga MD, et al. Tropical data: approach and methodology as applied to trachoma prevalence surveys. Ophthalmic Epidemiol. 2023;30:544–60. https://doi.org/10.1080/09286586.2023.2249546
14. Kamau E, Gass K, Harding-Esch E, Díaz MIS, Ante-Testard PA, Kello A, et al. Design considerations for incorporating serological monitoring into trachoma prevalence surveys. Am J Epidemiol. 2026 Oct 1 [Epub ahead of print]. https://doi.org/10.1093/aje/kwag245

Address for correspondence: Benjamin F. Arnold, F.I. Proctor Foundation, University of California, 490 Illinois St, San Francisco, CA 94158, USA; email: ben.arnold@ucsf.edu

Serologic Testing for Middle East Respiratory Syndrome Coronavirus and SARS-CoV-2 Cross-Reactive Immune Responses, the Netherlands

Merel R. te Marvelde, Anna Z. Mykytyn, Matthijs P. Raadsen, Alexandre H.J. Bouffier, Sivana Baptista Varela, Rory D. de Vries, Corine H. GeurtsvanKessel, Bart L. Haagmans

Cross-reactive SARS-CoV-2–specific antibodies could compromise the specificity of MERS-CoV serology, potentially leading to misclassification of infection history. SARS-CoV-2 exposure induced MERS-CoV antibodies primarily targeting the conserved S2 domain, with occasional neutralizing capacity. Combining MERS-CoV S1 binding with neutralization, however, limited the influence of SARS-CoV-2–induced cross-reactivity on MERS-CoV serology.

Since its discovery in 2012, Middle East respiratory syndrome coronavirus (MERS-CoV) has caused small outbreaks in humans with case-fatality rates of ≈30%–40% (*1*,*2*). Primary cases typically result from direct contact with infected dromedary camels, but the virus can cause large outbreaks in healthcare settings (*2*). No licensed MERS-CoV vaccines are available, whereas COVID-19 vaccines were rapidly developed when SARS-CoV-2 emerged in 2019 (*3*,*4*). Serologic detection of MERS-CoV cases is essential for identifying previously undetected infections during outbreaks and surveillance among high-risk populations, providing insights into MERS-CoV epidemiology in settings where molecular testing is unavailable or incomplete (*5*,*6*). However, cross-reactivity induced by SARS-CoV-2 infection or vaccination could hamper detection of MERS-CoV–specific antibodies.

The spike protein, the most immunogenic protein of coronaviruses, is used in mRNA- and vector-based vaccines and shares 58% similarity between SARS-CoV-2 and MERS-CoV (*7*). Several studies have demonstrated the presence of cross-binding antibodies after SARS-CoV-2 infection (*7*–*10*), sometimes with MERS-CoV neutralizing capacity (*11*–*13*). Such cross-reactivity can be difficult to distinguish from MERS-CoV–induced immune responses. World Health Organization (WHO) guidance for laboratory testing of MERS-CoV, published in 2018, states that a positive screening assay (e.g., ELISA) in combination with a positive result for neutralization indicates past MERS-CoV infection (https://iris.who.int/server/api/core/bitstreams/38aebc9e-4604-4640-9f7c-99e58d92d34a/content). No effect of SARS-CoV-2–induced cross-reactivity on those recommendations has been reported, but such effect would be critical for determining the specificity of MERS-CoV serology. We investigated the influence of different types of SARS-CoV-2 exposures on antibody cross-reactivity to MERS-CoV and consequences for MERS-CoV serology.

The Study

We tested serum samples from persons in the Netherlands with different SARS-CoV-2 exposures (Appendix Table 1, https://wwwnc.cdc.gov/EID/article/32/11/26-0690-App1.pdf). Samples were obtained from patients with mild symptomatic COVID-19 infection (no hospital admission) and severe COVID-19 infection (admission to the intensive care unit), before COVID-19 vaccines were available. In addition, we included serum samples from persons who had received multiple COVID-19 vaccines; most had also experienced breakthrough COVID-19 infection (Appendix Table 2). The time of serum collection after SARS-CoV-2 exposure differed: 28 (interquartile range [IQR] 27–28) days after vaccination for the

Author affiliation: Erasmus Medical Center, Rotterdam, the Netherlands

DOI: https://doi.org/10.3201/eid3211.260690

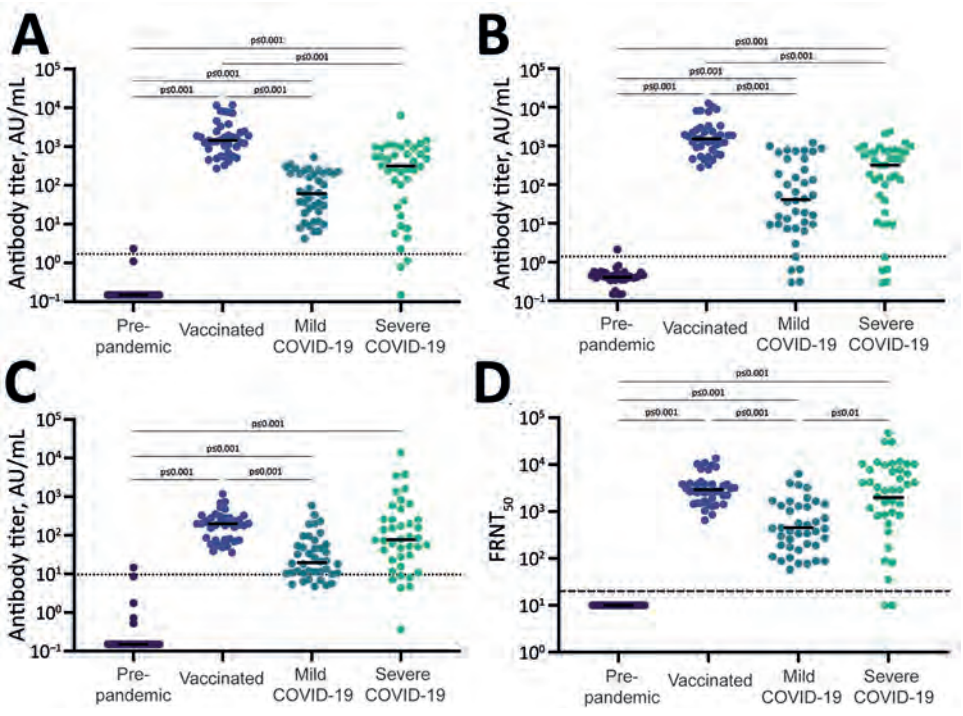

Figure 1. SARS-CoV-2 binding and neutralizing antibody titers after different SARS-CoV-2 exposures from study of serologic testing for Middle East respiratory syndrome coronavirus and SARS-CoV-2 cross-reactive immune responses, the Netherlands. Prepandemic serum samples were collected during 2015–2018, serum samples from persons vaccinated against COVID-19 were collected in 2023, and serum samples for persons with mild and severe COVID-19 were collected in 2020. A–C) Binding IgG to SARS-CoV-2 full spike (A), SARS-CoV-2 S1 (B), and SARS-CoV-2 S2 (C) were measured by in-house ELISA. Horizontal bars indicate medians; dotted lines indicate the cutoff for positivity on the basis of prepandemic samples. D) Neutralizing antibody titers were determined by focus reduction neutralization test by using SARS-CoV-2 D614G. Horizontal bars indicate geometric mean titer; dashed line indicates the lower limit of detection. We used a nonparametric Kruskal-Wallis test followed by a Dunn multiple comparisons test to evaluate the statistical significance between groups. $FRNT_{50}$, 50% focus reduction neutralization test.

vaccinated group, 59 (IQR 41–69.75) days after symptom onset for the mild COVID-19 group, and 1 (IQR 0–1) day after intensive care unit admission for the severe COVID-19 group. Because the cohorts were established in the Netherlands, we assumed participants had not been exposed to MERS-CoV.

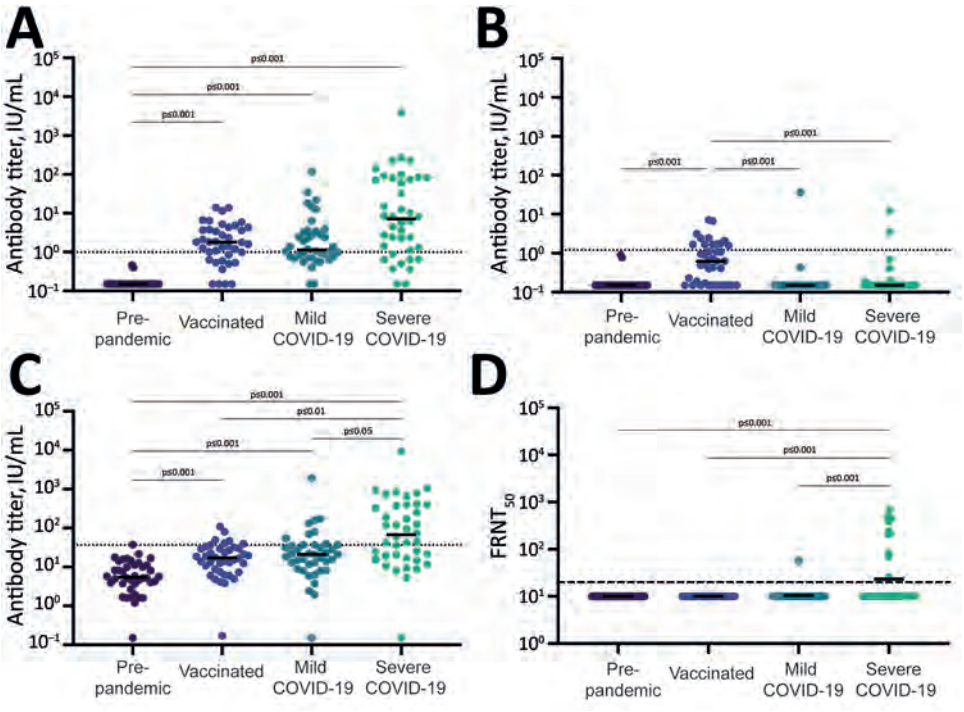

Figure 2. MERS-CoV binding and neutralizing antibodies after different SARS-CoV-2 exposures from study of serologic testing for Middle East respiratory syndrome coronavirus and SARS-CoV-2 cross-reactive immune responses, the Netherlands. Prepandemic serum samples were collected during 2015–2018, serum samples from persons vaccinated against COVID-19 were collected in 2023, and serum samples for persons with mild and severe COVID-19 were collected in 2020. A–C) Binding IgG to MERS-CoV full spike (A), MERS-CoV S1 (B), and MERS-CoV S2 (C) were measured by in-house ELISA. Horizontal bars indicate medians; dotted lines indicate the cutoff for positivity based on prepandemic samples. D) Neutralizing antibody titers were determined by focus reduction neutralization test. Horizontal bars indicate geometric mean titer; dashed line indicates the lower limit of detection. We used a nonparametric Kruskal-Wallis test followed by a Dunn multiple comparisons test to evaluate the statistical significance between groups. $FRNT_{50}$, 50% focus reduction neutralization test.

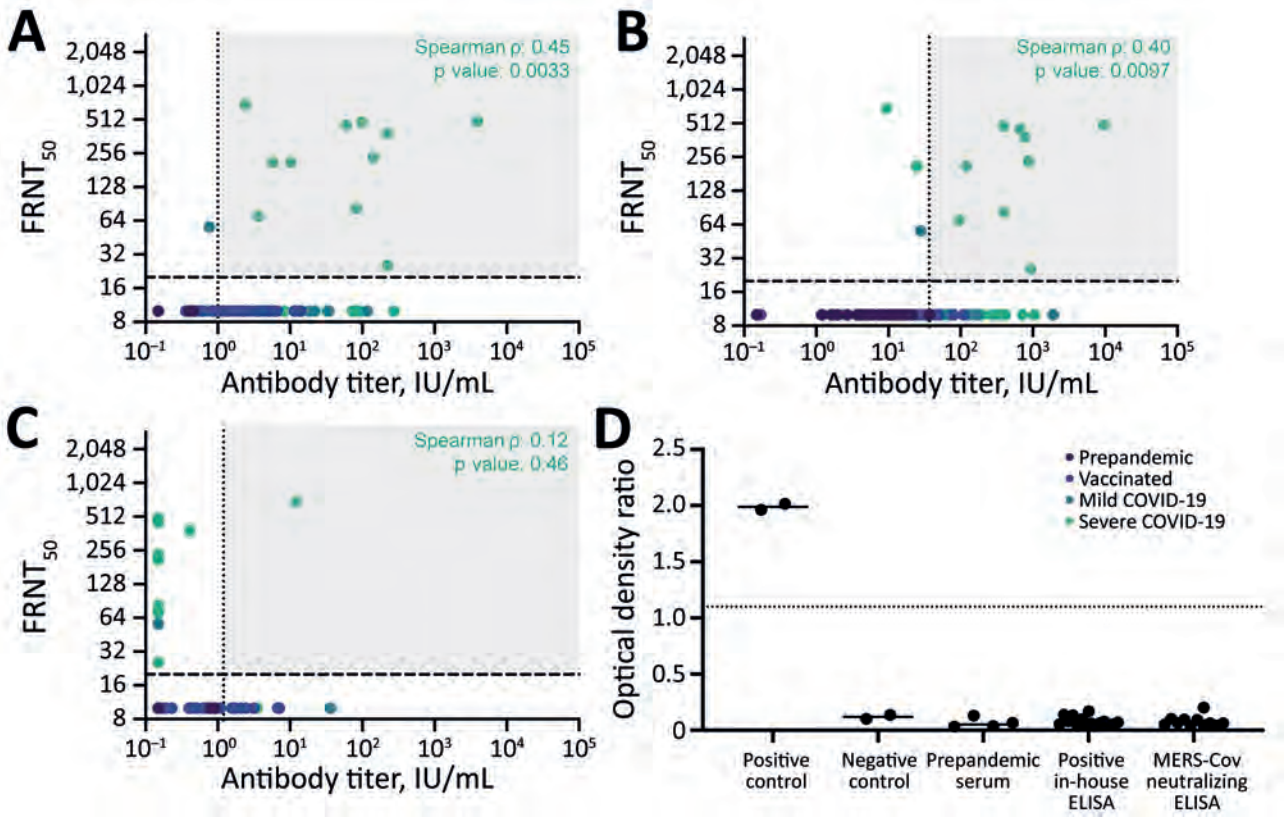

Figure 3. Correlation plot of MERS-CoV neutralization and MERS-CoV binding IgG levels from study of serologic testing for Middle East respiratory syndrome coronavirus and SARS-CoV-2 cross-reactive immune responses, the Netherlands. Prepandemic serum samples were collected during 2015–2018, serum samples from persons vaccinated against COVID-19 were collected in 2023, and serum samples for persons with mild and severe COVID-19 were collected in 2020. A–C) Serum samples from all groups were visualized showing the MERS-CoV neutralization titer and binding antibodies to MERS-CoV full spike (A), MERS-CoV S2 (B), and MERS-CoV S1 (C). For persons with severe COVID-19, the correlation between MERS-CoV neutralization and binding was determined by the Spearman rank-order correlation coefficient (ρ). Dashed horizontal lines indicate the lower limit of detection of the focus reduction neutralization test; vertical dotted lines indicate cutoff for positivity based on prepandemic samples for in-house ELISAs. Gray shading indicates double-positive samples capable of neutralizing MERS-CoV and binding to MERS-CoV spike in the in-house ELISA. D) A subset of prepandemic control serum samples (n = 4), serum samples positive on the in-house MERS-CoV S1 ELISA (n = 15), and MERS-CoV neutralizing serum samples (n = 11) tested on a commercial ELISA routinely used in MERS-CoV diagnostic testing according to manufacturer's protocol. Assay controls provided by the manufacturer are shown. The optical density ratio depicts the optical density value of the sample divided by the calibrator. The dotted line indicates the recommended cutoff for positivity by the manufacturer (ratio ≥1.1). $FRNT_{50}$, 50% focus reduction neutralization test.

We measured SARS-CoV-2–binding IgG by in-house ELISA using full spike protein and the S1 and S2 subunits to determine SARS-CoV-2–specific immune responses in exposed persons. The pattern of binding antibodies was similar across groups for all antigens; serum from vaccinees with multiple SARS-CoV-2 exposures contained the highest levels of binding antibodies, followed by serum collected after severe and mild infection (Figure 1, panels A–C). The negative control prepandemic serum showed limited binding to SARS-CoV-2. To assess the functionality of the antibodies, we conducted a focus reduction neutralization test (FRNT) using SARS-CoV-2 with the spike mutation D614G. Neutralizing titers were again highest in vaccinated persons, followed by those with severe COVID-19 and mild COVID-19 (Figure 1, panel D).

Next, we assessed cross-reactivity by evaluating MERS-CoV immune responses in the SARS-CoV-2–exposed groups. The antibody binding patterns for MERS-CoV were different than for SARS-CoV-2 (Figure 2, panels A–C). All SARS-CoV-2 exposed groups included serum that could bind MERS-CoV full spike, but binding was highest after severe COVID-19 (median 7.1 [IQR 1.2–78.3] IU/mL), followed by after vaccination (median 1.8 [IQR 0.7–4.2] IU/mL) and mild COVID-19 (median 1.1 [IQR 0.7–3.4] IU/mL). Cross-reactivity was mostly mediated by binding

to MERS-CoV S2; MERS-CoV S1 binding was low but observed in several serum samples. The severe COVID-19 group had the highest MERS-CoV S2 binding antibody levels (median 67.0 [IQR 17.5–390.0] IU/mL) compared with the mild COVID-19 group (median 21.0 [IQR 9.6–36.9] IU/mL) and the vaccinated group (median 17.1 [IQR 7.9–30.1] IU/mL). The prepandemic group also showed some S2 binding (median 5.4 [IQR 3.7–11.2] IU/mL), possibly indicating cross-reactivity with other coronaviruses. We further assessed the MERS-CoV neutralizing capacity of the serum samples in accordance with the WHO recommendations for MERS-CoV serology. Of note, a subset of 11 patients from the severe COVID-19 group had detectable antibodies capable of MERS-CoV neutralization (Figure 2, panel D). One sample from the mild COVID-19 group partially neutralized MERS-CoV. Neutralizing antibody titers were 26–694.

To test the WHO-recommended 2-tier approach combining ELISA screening with a neutralization assay, we investigated the correlation between MERS-CoV neutralization and binding antibodies for all samples from persons who had severe COVID-19. MERS-CoV neutralizing antibody levels correlated with full spike binding (Figure 3, panel A); some serum samples were double-positive for binding and neutralization. Binding to full spike was most likely because of S2 binding (Figure 3, panel B). Those results indicate that MERS-CoV full spike–based and S2-based assays are likely to have limited specificity to detect past MERS-CoV infection because of cross-reactivity. However, MERS-CoV S1 binding was not correlated with neutralization (Figure 3, panel C) and only 1 sample from the SARS-CoV-2–exposed cohorts was double-positive, demonstrating that combining MERS-CoV S1 binding with neutralization minimizes the influence of SARS-CoV-2–induced cross-reactivity. SARS-CoV-2 binding and neutralization were not correlated with MERS-CoV neutralization (Appendix Figure 2), indicating that the level of the SARS-CoV-2 antibody response does not explain the potency of MERS-CoV neutralization.

Although MERS-CoV neutralization and MERS-CoV S1 binding were not correlated, several serum samples showed low-level binding to MERS-CoV S1. We tested serum samples that were positive by in-house ELISA and samples could neutralize MERS-CoV by commercial MERS-CoV S1 ELISA (Euroimmun, https://www.euroimmun.com). All samples were below the ratio for positivity (Figure 3, panel D), indicating that the commercial ELISA is less sensitive but more specific than the in-house ELISA to detect MERS-CoV–binding antibodies indicative of past MERS-CoV infection. Thus, the influence of SARS-CoV-2–induced cross-reactivity can be minimized by the combination of a MERS-CoV S1 ELISA with a neutralization assay or by using a commercial ELISA with a higher cutoff.

Conclusions

We investigated antibody cross-reactivity between SARS-CoV-2 and MERS-CoV and effects on MERS-CoV serology. MERS-CoV–reactive antibodies after SARS-CoV-2 exposure are common in vaccinated and naturally infected persons (*7*–*10*), likely because the viruses have genetically similar spike proteins, mainly in S2 (*7*). Consequently, we found cross-reactivity primarily consists of binding to MERS-CoV full spike and S2, consistent with previous findings (*8*,*12*). The functionality of cross-reactive antibodies differed on the basis of SARS-CoV-2 exposure type. MERS-CoV neutralizing antibodies were detected in samples from persons with severe COVID-19 but not from vaccinated persons who were exposed to SARS-CoV-2 multiple times. Severe COVID-19 infection might expose the immune system to higher antigen loads and a different spike conformation than vaccination with prefusion stabilized spike, potentially promoting antibody responses to conserved S2 epitopes that might contribute to greater cross-reactivity with other coronaviruses (*14*).

The WHO MERS-CoV serology guidelines recommend confirming ELISA results with neutralization assays but do not specify antigens to be used or consider SARS-CoV-2–induced cross-reactivity. We found that combining MERS-CoV S1 ELISA with neutralization minimizes double-positive tests, decreasing the occurrence of false-positive results. Although we did find low levels of binding to MERS-CoV S1 using an in-house ELISA, we found no correlation between MERS-CoV neutralization and S1 binding. The samples tested negative in a commercial MERS-CoV S1 ELISA, suggesting that a high cutoff increases specificity but reduces sensitivity compared with the in-house ELISA. A higher cutoff could be applied to the MERS-CoV S1 binding assay, as in the commercial ELISA, but that approach reduces sensitivity, potentially failing to identify true MERS-CoV–positive cases with low S1 responses. The nucleocapsid protein is sometimes used in MERS-CoV serology (*15*), but SARS-CoV-2 infection can induce antibodies that bind to the MERS-CoV nucleocapsid, making that antigen less suitable for MERS-CoV serology (*9*).

In conclusion, to minimize the influence of SARS-CoV-2–induced cross-reactive antibody responses, serologic testing for MERS-CoV should combine MERS-CoV S1 binding with a neutralization assay.

That process would enable more accurate tracking of true MERS-CoV seroprevalence, enhancing surveillance and response efforts.

Acknowledgments

We thank all participants and coworkers involved in the CIUM, SWITCH-ON, CONCOVID, and COVA study.

Parts of this study were funded by the Netherlands Organization for Health Research and Development (ZonMw) (grant agreement no. 10430072110008) and by the Dutch Ministry of Health, Welfare and Sport.

B.L.H. is listed as an inventor on MERS coronavirus patents (nos. US10781426B2 and US12599668B2). All other authors declare no competing interests.

Microsoft Copilot (https://www.microsoft.com) was used to correct grammar and improve readability of the manuscript.

About the Author

Ms. te Marvelde is a PhD candidate in the Department of Viroscience at the Erasmus Medical Center in Rotterdam, the Netherlands. Her research focuses on cross-reactive immune responses following COVID-19 vaccination.

References

1. Zaki AM, van Boheemen S, Bestebroer TM, Osterhaus AD, Fouchier RA. Isolation of a novel coronavirus from a man with pneumonia in Saudi Arabia. N Engl J Med. 2012;367:1814–20. https://doi.org/10.1056/NEJMoa1211721
2. Mackay IM, Arden KE. MERS coronavirus: diagnostics, epidemiology and transmission. Virol J. 2015;12:222. https://doi.org/10.1186/s12985-015-0439-5
3. Zhou P, Yang X-L, Wang X-G, Hu B, Zhang L, Zhang W, et al. A pneumonia outbreak associated with a new coronavirus of probable bat origin. Nature. 2020;579:270–3. https://doi.org/10.1038/s41586-020-2012-7
4. Creech CB, Walker SC, Samuels RJ. SARS-CoV-2 Vaccines. JAMA. 2021;325:1318–20. https://doi.org/10.1001/jama.2021.3199
5. Khudhair A, Killerby ME, Al Mulla M, Abou Elkheir K, Ternanni W, Bandar Z, et al. Risk factors for MERS-CoV seropositivity among animal market and slaughterhouse workers, Abu Dhabi, United Arab Emirates, 2014–2017. Emerg Infect Dis. 2019;25:927–35. https://doi.org/10.3201/eid2505.181728
6. Killerby ME, Biggs HM, Midgley CM, Gerber SI, Watson JT. Middle East respiratory syndrome coronavirus transmission. Emerg Infect Dis. 2020;26:191–8. https://doi.org/10.3201/eid2602.190697
7. Hicks J, Klumpp-Thomas C, Kalish H, Shunmugavel A, Mehalko J, Denson JP, et al. Serologic cross-reactivity of SARS-CoV-2 with endemic and seasonal betacoronaviruses. J Clin Immunol. 2021;41:906–13. https://doi.org/10.1007/s10875-021-00997-6
8. Grobben M, van der Straten K, Brouwer PJ, Brinkkemper M, Maisonnasse P, Dereuddre-Bosquet N, et al.; Amsterdam UMC COVID-19 S3/HCW study group. Cross-reactive antibodies after SARS-CoV-2 infection and vaccination. eLife. 2021;10:e70330. https://doi.org/10.7554/eLife.70330
9. Lee RSH, Cheng SMS, Zhao J, Tsoi AYS, Lau KKM, Chan CHC, et al. Cross-reactive antibody responses to coronaviruses elicited by SARS-CoV-2 infection or vaccination. Influenza Other Respir Viruses. 2024;18:e13309. https://doi.org/10.1111/irv.13309
10. Ju B, Zhang Q, Ge J, Wang R, Sun J, Ge X, et al. Human neutralizing antibodies elicited by SARS-CoV-2 infection. Nature. 2020;584:115–9. https://doi.org/10.1038/s41586-020-2380-z
11. Sun S, He J, Liu L, Zhu Y, Zhang Q, Qiu Y, et al. Anti-S2 antibodies responsible for the SARS-CoV-2 infection -induced serological cross-reactivity against MERS-CoV and MERS-related coronaviruses. Front Immunol. 2025;16:1541269. https://doi.org/10.3389/fimmu.2025.1541269
12. Peng Y, Liu Y, Hu Y, Chang F, Wu Q, Yang J, et al. Monoclonal antibodies constructed from COVID-19 convalescent memory B cells exhibit potent binding activity to MERS-CoV spike S2 subunit and other human coronaviruses. Front Immunol. 2022;13:1056272. https://doi.org/10.3389/fimmu.2022.1056272
13. Zhang J, Wu Q, Liu Z, Wang Q, Wu J, Hu Y, et al. Spike-specific circulating T follicular helper cell and cross-neutralizing antibody responses in COVID-19-convalescent individuals. Nat Microbiol. 2021;6:51–8. https://doi.org/10.1038/s41564-020-00824-5
14. Crowley AR, Natarajan H, Hederman AP, Bobak CA, Weiner JA, Wieland-Alter W, et al. Boosting of cross-reactive antibodies to endemic coronaviruses by SARS-CoV-2 infection but not vaccination with stabilized spike. eLife. 2022;11:e75228. https://doi.org/10.7554/eLife.75228
15. Trivedi S, Miao C, Al-Abdallat MM, Haddadin A, Alqasrawi S, Iblan I, et al. Inclusion of MERS-spike protein ELISA in algorithm to determine serologic evidence of MERS-CoV infection. J Med Virol. 2018;90:367–71. https://doi.org/10.1002/jmv.24948

Address for correspondence: Bart L. Haagmans, Erasmus Medical Center, Dr. Molewaterplein 40, 3015GD Rotterdam, the Netherlands; email: b.haagmans@erasmusmc.nl

Differentiating Avian and Seasonal Influenza Viruses in Wastewater by Digital PCR

Valentina Paracchini, Mauro Petrillo, Francisco Mayo Leon, Gerhard Buttinger, Sabrina Marciano, Marika Crimaudo, Calogero Terregino, Carolina Veneri, Giuseppina La Rosa, Elisabetta Suffredini, Clementina Cocuzza, Bernd M. Gawlik, Tobias Wiesenthal, Ursula Vincent, Valentina Panzarin, Antonio Marchini

Highly pathogenic avian influenza A(H5Nx) viruses, particularly clade 2.3.4.4b, pose substantial global health risks. We combined and piloted 2 duplex reverse transcription digital PCRs to discriminate between avian and seasonal influenza viruses in wastewater. This approach enabled rapid, strain-specific detection to reduce ambiguity in environmental surveillance for influenza viruses.

Highly pathogenic avian influenza (HPAI) A(H5Nx) viruses, particularly clade 2.3.4.4b, continue to circulate widely among wild and domestic birds, with recurrent spillover into mammalian species and sporadic infections in humans. The extensive geographic distribution and persistent circulation of clade 2.3.4.4b, together with its predominance among HPAI A(H5) viruses currently circulating in Europe, support its continued relevance for animal and public health surveillance (*1*–*4*).

Wastewater and environmental surveillance (WES) provides a population-level complement to clinical, veterinary, and wildlife surveillance and is increasingly integrated into the monitoring framework in Europe (*5*). WES has been widely used for SARS-CoV-2 and has also been applied to influenza A and B viruses (*6*,*7*).

WES typically relies on PCR-based methods to detect and quantify pathogens. Similar to other pathogens, influenza RNA concentrations in wastewater might vary according to shedding patterns, sewer inputs, matrix characteristics, and the relative contributions of human and animal sources (*6*). Differences in laboratory methods and reporting further complicates interpretation, underscoring the necessity of considering assay sensitivity and specificity when comparing results across studies (*8*).

The matrix gene is the preferred molecular target for the screening of influenza A viruses (*9*) because it is conserved across seasonal human and animal influenza strains, but broad reactivity limits strain discrimination in mixed environmental samples. For instance, the influenza A component of the Centers for Disease Control and Prevention (CDC) influenza SARS-CoV-2 (Flu SC2) multiplex reverse transcription PCR (RT-PCR), developed for clinical respiratory specimens (10) and adapted for digital RT-PCR (dRT-PCR) analysis of wastewater samples (*11*), can detect both seasonal human and avian influenza A signals (*12*).

Several wastewater assays were designed to detect H5 viruses (*13*–*15*). Those assays are useful for broad H5 virus screening but might require further characterization to distinguish between HPAI H5N1 clade 2.3.4.4b, another H5 lineage, or low pathogenicity avian influenza. A clade-specific assay can provide additional epidemiologic resolution and help prioritize follow-up across animal and human surveillance.

We previously developed the European Commission's Joint Research Centre (JRC) RT-PCRs targeting the hemagglutinin (HA) and matrix protein (MP) genes. The JRC-HA assay targets a conserved HA region in HPAI H5N1 clade 2.3.4.4b and the JRC-MP assay targets the conserved matrix gene for broader detection of influenza A (*12*) (Appendix, http://wwwnc.cdc.gov/EID/article/32/11/26-1234-App1.pdf). We evaluated a dual-duplex dRT-PCR approach

Author affiliations: European Commission, Joint Research Centre, Geel, Belgium (V. Paracchini, F.M. Leon, G. Buttinger, U. Vincent); Seidor Italy Srl., Milan, Italy (M. Petrillo); Istituto Zooprofilattico Sperimentale delle Venezie, Legnaro, Italy (S. Marciano, M. Crimaudo, C. Terregino, V. Panzarin); Istituto Superiore di Sanità, Rome, Italy (C. Veneri, G. La Rosa, E. Suffredini); University of Milano-Bicocca, Monza, Italy (C. Cocuzza); European Commission, Joint Research Centre, Ispra, Italy (B.M. Gawlik, T. Wiesenthal, A. Marchini)

DOI: https://doi.org/10.3201/eid3211.261234

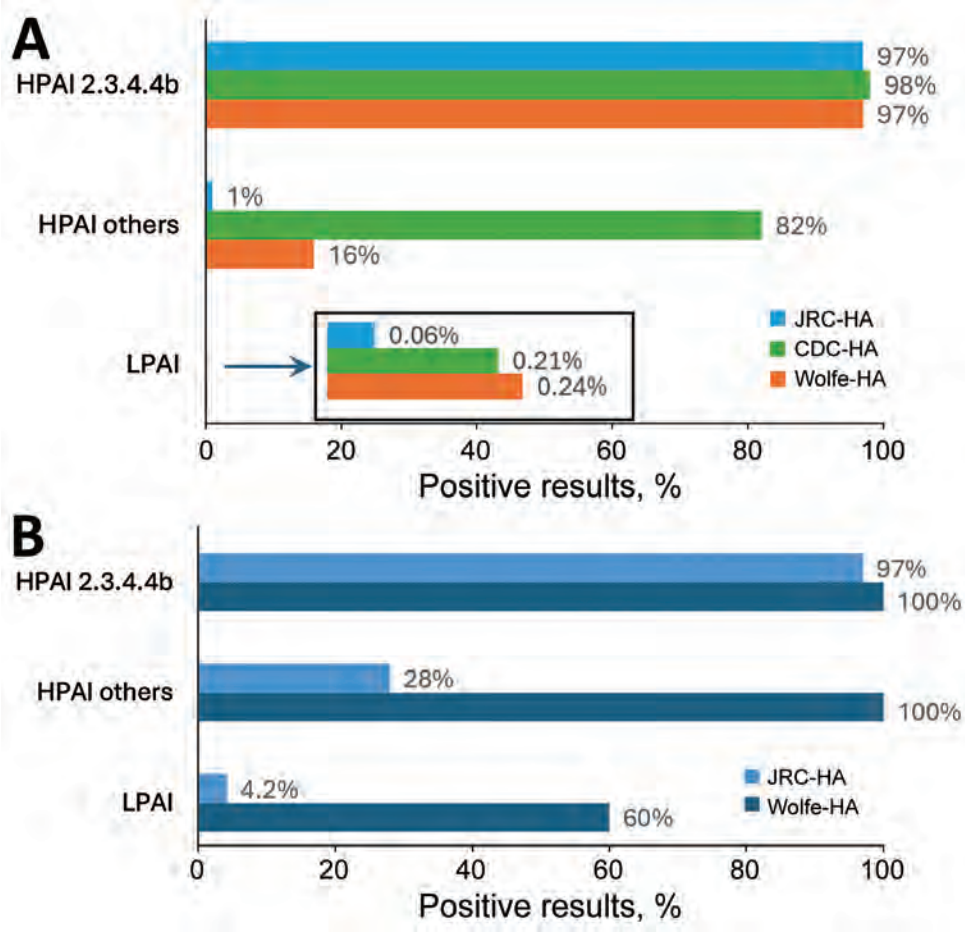

Figure 1. In silico comparative analysis of wastewater assays used to detect avian and seasonal influenza viruses in wastewater. A) Predicted detection of HA gene sequences from LPAI viruses, HPAI viruses other than clade 2.3.4.4b, and HPAI clade 2.3.4.4b viruses by the Wolfe-HA (*13*), CDC-HA (*14*,*15*), and JRC-HA (*12*) assays. Bars indicate the percentage of sequences predicted to yield positive results. Inset box represents enlarged results for LPAI. B) Predicted detection of MP gene sequences from LPAI viruses, HPAI viruses other than clade 2.3.4.4b, and HPAI clade 2.3.4.4b viruses by the Wolfe-MP (*13*), and JRC-MP (*12*) assays. Bars indicate the percentage of sequences predicted to yield positive results. CDC, Centers for Disease Control and Prevention; HPAI, highly pathogenic avian influenza; HA, hemagglutinin; JRC, Joint Research Centre; LPAI, low pathogenicity avian influenza; MP, matrix protein.

combining the CDC influenza A and B assay components with the JRC-HA and JRC-MP assay to discriminate between avian and seasonal human influenza viruses in wastewater.

The Study

We first performed a comparative in silico analysis of the publicly available primer and probe sequences from 2 H5 assays (*13*–*15*), and the JRC-HA and JRC-MP assays (*12*) (Figure 1). The predicted detection of HPAI H5 clade 2.3.4.4b was broadly comparable across the assays, but the JRC-HA assay revealed greater discrimination against non-2.3.4.4b HPAI clades (Figure 1, panel A). The JRC-HA and JRC-MP assays had the lowest predicted cross-reactivity with low pathogenicity avian influenza H5 annotated sequences (Figure 1, panels A, B).

Then, we evaluated the JRC-HA and JRC-MP duplex assay by using HPAI H5N1 clade 2.3.4.4b viruses collected from wild birds and poultry in northern Italy during October–December 2025 (Appendix Table 4). Sequence alignment revealed high conservation across the primer and probe binding regions for both assays, indicating that recent viral evolution had not substantially affected assay inclusivity. Nevertheless, we identified 2 substitutions within the JRC-HA probe-binding region in 3 samples (Appendix Figure 1). In silico PCR predicted amplification (data not shown), and both quantitative RT-PCR and dRT-PCR detected influenza A in all 10 samples, including samples with low viral concentrations (Figure 2, panels A, B). For samples H, I, and J, lowering the JRC-HA/JRC-MP dRT-PCR annealing temperature from 60°C to 56.4°C improved partition separation (Appendix Figure 2). At the revised annealing temperature, in silico analysis indicated that stable primer-dimer formation was unlikely, and assay specificity was not affected (Figure 2, panels C–F). The limit of detection was 5 copies/reaction, consistent with previous results (*12*). The CDC influenza B assay failed to detect the target in any of the 10 samples analyzed, whereas the CDC influenza A assay detected the target in all 10 samples with comparable performance to that of the JRC-HA and JRC-MP assays (Figure 2, panels A, B). Such broad detection is useful for confirming the presence of

influenza virus; however, it does not permit discrimination between avian and seasonal human influenza A viruses in mixed specimens such as wastewater samples collected during periods of seasonal influenza circulation.

To improve discrimination between avian and seasonal human influenza in wastewater samples, we evaluated the influenza A and B components of the CDC Flu SC2 multiplex assay together with the JRC-HA and JRC-MP duplex assay. We performed the 2 duplex assays separately, according to the conditions described previously (*12*) (Appendix). Because HPAI H5N1 clade 2.3.4.4b–positive wastewater samples were unavailable, we added defined amounts of avian and seasonal human influenza A RNA to RNA extracts from influenza-negative wastewater samples (Figure 3). We evaluated the 2 duplex assays under 3 simulated co-circulation scenarios.

In the first scenario, we added only HPAI H5N1 clade 2.3.4.4b RNA to the wastewater samples. The JRC-HA, JRC-MP, and CDC influenza A assays produced comparable viral RNA copy numbers, indicating detection near the analytical limits of the JRC assays (Figure 3, panel A). For the second scenario, we combined low concentrations (10 or 20 copies/μL) of HPAI H5N1 clade 2.3.4.4b RNA and seasonal influenza A RNA (35 copies/μL) to simulate periods of low seasonal influenza activity or low avian influenza prevalence. The JRC-HA and JRC-MP assays selectively detected HPAI H5N1 clade 2.3.4.4b RNA, whereas the CDC influenza A assay detected both avian and seasonal human influenza A RNA without distinction (Figure 3, panel B).

In the third scenario, we added low concentrations (10 or 20 copies/μL) of HPAI H5N1 clade 2.3.4.4b RNA to a high concentration (3,500 copies/μL) of seasonal influenza A background, representing a possible early stage of HPAI detection during peak seasonal influenza activity. The JRC-HA assay detected HPAI H5N1 RNA without cross-reactivity, whereas the JRC-MP detected both avian and seasonal human influenza A RNA, but yielded lower copy number estimates than the CDC influenza A assay (Figure 3, panel C). Together, our results suggest that JRC-HA identifies and discriminates HPAI H5N1 clade 2.3.4.4b, whereas JRC-MP provided complementary detection but might lack specificity during high seasonal influenza A circulation.

Conclusions

We propose the complementary use of CDC Flu SC2 and JRC-HA and JRC-MP duplex assays in a dual-duplex approach (Figure 4). The influenza A

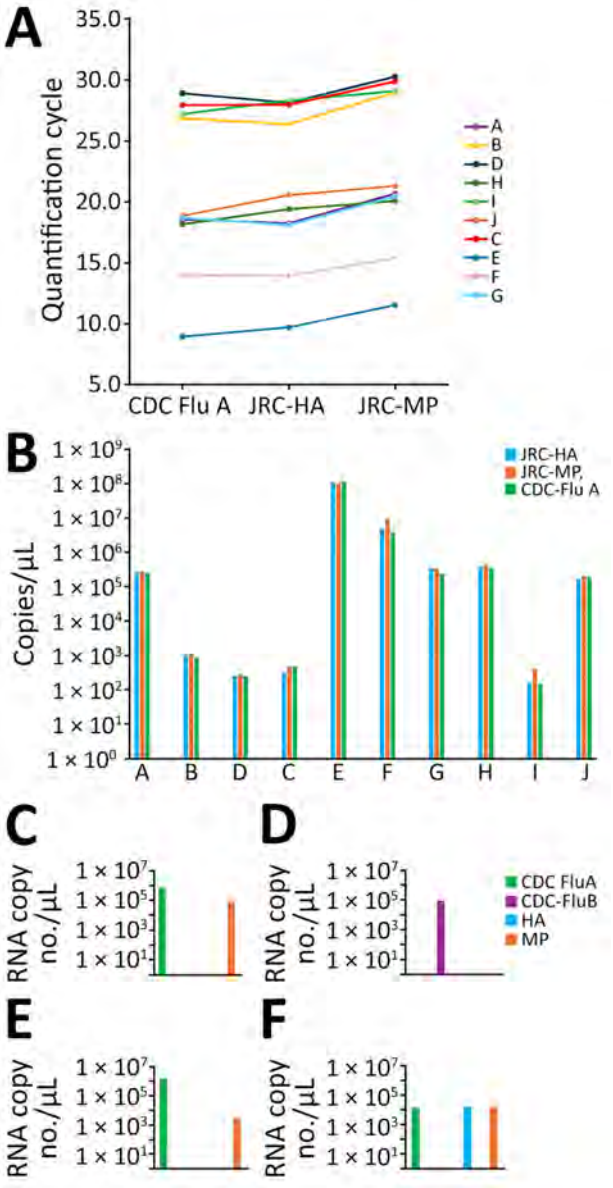

Figure 2. Analytical evaluation of JRC-HA and JRC-MP RT-PCRs against recent highly pathogenic avian influenza (HPAI) H5N1 clade 2.3.4.4b isolates for differentiating avian and human influenza A viruses from wastewater samples. A) Quantification cycle values for 10 HPAI H5N1 clade 2.3.4.4b clinical samples from Italy measured by using the JRC-HA, JRC-MP, and CDC influenza A quantitative reverse transcription PCRs. B) Viral RNA copy number estimates for 10 HPAI H5N1 clade 2.3.4.4b clinical samples from Italy measured by using the JRC-HA, JRC-MP, and CDC influenza A reverse transcription digital PCR assays. C–F) Verification of assay specificity of the JRC-HA and JRC-MP duplex assay at the annealing temperature of 56.4°C. Assay specificity was evaluated in digital PCR, compared with the influenza A and B components of the CDC influenza SARS-CoV-2 multiplex assay, by measuring the RNA copy numbers per microliter for influenza A(H1N1) (C), influenza B (D), influenza A(H3N2) synthetic RNAs (from Twist Bioscience, https://www.twistbioscience.com) (E), and HPAI H5N1 clade 2.3.4.4b RNA isolated from an infected animal (F). CDC, Centers for Disease Control and Prevention; HA, hemagglutinin; JRC, Joint Research Centre; MP, matrix protein.

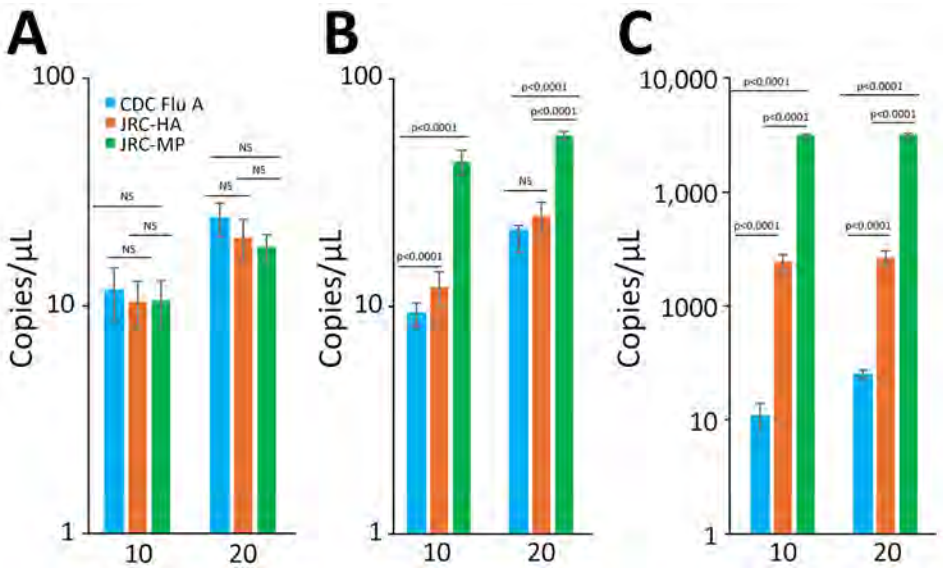

Figure 3. Detection of influenza A and highly pathogenic avian influenza (HPAI) A(H5N1) in simulated wastewater samples by using reverse transcription digital PCR. A) Copy numbers of influenza A virus in wastewater samples negative for both avian and human influenza A spiked with 10 or 20 copies/µL of HPAI H5N1 clade 2.3.4.4b virus. B) Copy number of influenza A virus in wastewater samples negative for both avian and human influenza A spiked with 10 or 20 copies/µL of HPAI H5N1 clade 2.3.4.4b virus and 35 copies/µL of human influenza A virus. C) Copy number of influenza A virus in wastewater samples negative for both avian and human influenza A spiked with 10 or 20 copies/µL of HPAI H5N1 clade 2.3.4.4b virus and 3,500 copies/µL of human influenza A virus. Error bars indicate the mean value ± SD. Statistical significance was determined by using t-test. CDC, Centers for Disease Control and Prevention; HA, hemagglutinin; JRC, Joint Research Centre; MP, matrix protein; NS, not significant;.

and B components of the CDC Flu SC2 multiplex assay are useful for routine communitywide surveillance of influenza A and B, ensuring continuity of the current public health reporting system. The JRC-HA and JRC-MP duplex assay, after the CDC Flu SC2 duplex, is used to specifically identify the

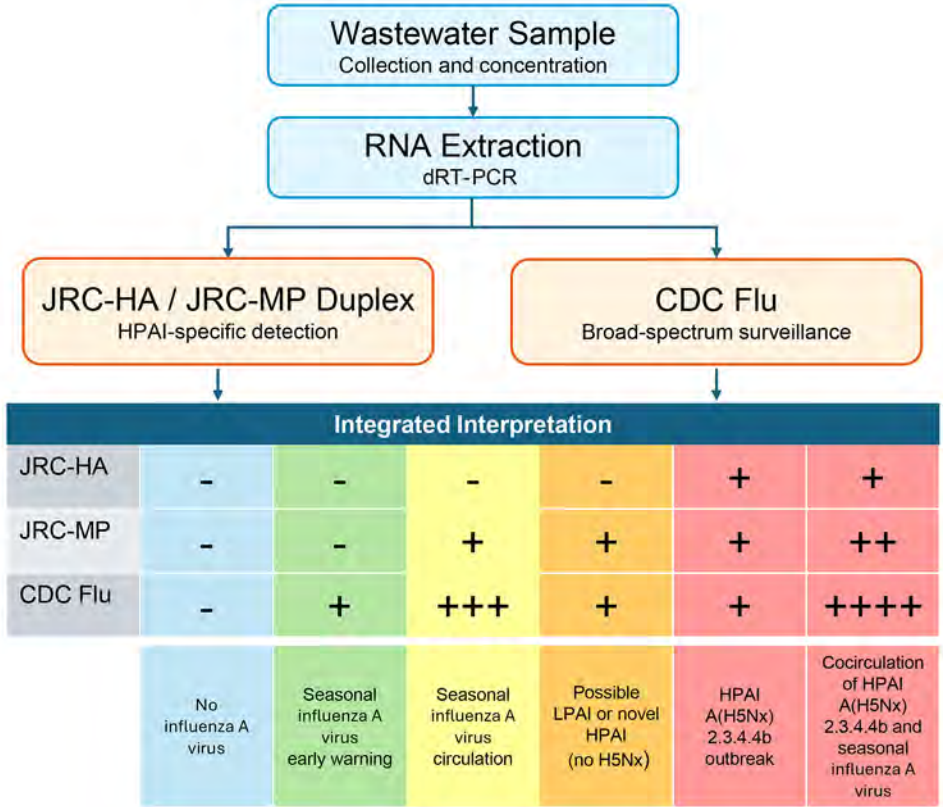

Figure 4. Interpretation of dual duplex dRT-PCR results for differentiating avian and seasonal influenza A viruses in wastewater. Extracted RNA from wastewater samples is analyzed by using the JRC-HA and JRC-MP duplex assay for detection of HPAI A(H5Nx) clade 2.3.4.4b viruses and the influenza A and B components of the CDC influenza and SARS-CoV-2 multiplex assay for broad influenza A virus surveillance. Results from both assays are then integrated to classify wastewater detections according to the presence, absence, and relative signal intensity of assay targets. Detection patterns are interpreted as indicating no influenza A virus detected, seasonal influenza A early warning, seasonal influenza A circulation, possible LPAI or non–clade 2.3.4.4b HPAI virus, HPAI A(H5Nx) clade 2.3.4.4b circulation, or co-circulation of HPAI A(H5Nx) clade 2.3.4.4b and seasonal influenza A viruses. Minus signs (−) indicate no target detection; increasing numbers of plus signs (+ to ++++) indicate increasing relative assay signal. CDC, Centers for Disease Control and Prevention; HA, hemagglutinin; HPAI, highly pathogenic avian influenza; JRC, Joint Research Centre hemagglutinin; LPAI, low pathogenicity avian influenza; MP, matrix protein; RT-dPCR, reverse transcription digital PCR.

occurrence of HPAI H5N1 clade 2.3.4.4b virus in a population, providing an early-warning capability that is effective in the presence of seasonal influenza backgrounds.

We evaluated our dual duplex dRT-PCR by using animal-derived viral material and spiked wastewater RNA extracts, rather than confirmed HPAI-positive wastewater samples. Further field evaluation will be useful to assess performance under naturally occurring conditions and in different wastewater matrices. Because influenza viruses evolve rapidly, periodic sequence-based evaluations, followed by experimental validation and assay updates when necessary, will be required to maintain assay performance as new H5 clades emerge.

A clade-specific wastewater result would not by itself determine a different public health response from a broad H5-positive result. However, it could reduce ambiguity, prioritize confirmatory testing, and enable integration of wastewater findings with veterinary, wildlife, domestic animal, and human surveillance data.

This article was preprinted at https://doi.org/10.5281/zenodo.19054950.

Acknowledgments

We thank Renaud Seigneuric, Simona Tavazzi, Aisha Sauer, Patricia Urban-Lopez, Gabriele Leoni, Maddalena Querci, Els Vanlancker, and Ciarán Nicholl for their support. We also thank Alessio Bortolami, Alice Fusaro, and Bianca Zecchin and the Istituti Zooprofilattici Sperimentali network for providing animal samples and sequences. In addition, we thank those involved in generating and sharing sequence data via the GISAID initiative (https://www.gisaid.org).

This project received partial financial support from the European Commission, through a Directorate-General for Health Emergency Preparedness and Response grant (grant no. GLOWASENSE - JRC_COMPT_37000) and within the framework of the activities foreseen by the European Union Reference Laboratory for Avian Influenza and Newcastle Disease.

About the Author

Dr. Paracchini is employed as scientific officer at the European Commission's Joint Research Centre in Geel, Belgium. Her research interests include working on the development of novel assays and reference materials for enhanced pathogen surveillance such as SARS-CoV-2, avian influenza, and antimicrobial resistance.

References

1. European Food Safety Authority, European Union Reference Laboratory for Avian Influenza, Ducatez M, Fusaro A, Gonzales JL, Kuiken T, et al. Unprecedented high level of highly pathogenic avian influenza in wild birds in Europe during the 2025 autumn migration. EFSA J. 2025;23:e9811.
2. Peacock TP, Moncla L, Dudas G, VanInsberghe D, Sukhova K, Lloyd-Smith JO, et al. The global H5N1 influenza panzootic in mammals. Nature. 2025;637:304–13. https://doi.org/10.1038/s41586-024-08054-z
3. Rolfes MA, Kniss K, Kirby MK, Garg S, Reinhart K, Davis CT, et al. Human infections with highly pathogenic avian influenza A(H5N1) viruses in the United States from March 2024 to May 2025. Nat Med. 2025;31:3889–98. https://doi.org/10.1038/s41591-025-03905-2
4. Cohen J. Bird flu antibodies found in cow in the Netherlands, a first outside of U.S. Science. 2026 Jan 24 [cited 2026 Feb 14]. https://doi.org/10.1126/science.zu49l21
5. European Commission. Commission staff working document. SWD (2025) 393 final. 2025 [cited 2026 Aug 28]. https://eur-lex.europa.eu/legal-content/EN/TXT/?uri=celex:52025SC0393
6. Diamond MB, Keshaviah A, Bento AI, Conroy-Ben O, Driver EM, Ensor KB, et al. Wastewater surveillance of pathogens can inform public health responses. Nat Med. 2022;28:1992–5. https://doi.org/10.1038/s41591-022-01940-x
7. Viviani L, Vecchio R, Pariani E, Sandri L, Binda S, Ammoni E, et al. Wastewater-based epidemiology of influenza viruses: a systematic review. Sci Total Environ. 2025; 986:179706. https://doi.org/10.1016/j.scitotenv.2025.179706
8. Honein MA, Olsen SJ, Jernigan DB, Daskalakis DC. Challenges and opportunities for wastewater monitoring of influenza viruses during the multistate outbreak of highly pathogenic avian influenza A(H5N1) virus in dairy cattle and poultry. Am J Public Health. 2024;114:1309–12. https://doi.org/10.2105/AJPH.2024.307860
9. World Health Organization. WHO information for the molecular detection of influenza viruses. 2020 [cited 2026 Feb 14]. https://cdn.who.int/media/docs/default-source/influenza/global-influenza-surveillance-and-response-system/related-documents/protocols_influenza_virus_detection_jan_2020.pdf
10. Shu B, Kirby MK, Davis WG, Warnes C, Liddell J, Liu J, et al. Multiplex real-time reverse transcription PCR for influenza A virus, influenza B virus, and severe acute respiratory syndrome coronavirus 2. Emerg Infect Dis. 2021;27:1821–30. https://doi.org/10.3201/eid2707.210462
11. Mancini P, Brandtner D, Veneri C, Bonanno Ferraro G, Iaconelli M, Puzelli S, et al.; Evaluation of trends in influenza A and B viruses in wastewater and human surveillance data: insights from the 2022–2023 season in Italy. Food Environ Virol. 2024;17:6. https://doi.org/10.1007/s12560-024-09622-2
12. Buttinger G, Petrillo M, Valastro V, Marciano S, Crimaudo M, D'Amico V, et al. Novel (d)PCR assays for influenza A(H5Nx) viruses clade 2.3.4.4b surveillance. Euro Surveill. 2025;30:2500183. https://doi.org/10.2807/1560-7917.ES.2025.30.33.2500183
13. Wolfe MK, Duong D, Shelden B, Chan EMG, Chan-Herur V, Hilton S, et al. Detection of hemagglutinin H5 influenza A virus sequence in municipal wastewater solids at wastewater treatment plants with increases in influenza A in spring, 2024. Environ Sci Technol Lett. 2024;11:526–32. https://doi.org/10.1021/acs.estlett.4c00331
14. Centers for Disease Control and Prevention. National wastewater surveillance system analytics data set, year(s), as compiled from data provided through national

wastewater surveillance system in the rapid response research and surveillance branch (R3SB) [cited 2026 Aug 14]. https://data.cdc.gov/Public-Health-Surveillance/CDC-Wastewater-Data-for-Avian-Influenza-A-H5-/mtpu-urpp

15. Centers for Disease Control and Prevention. Singleplex digital PCR testing of influenza A, H1pdm09, H3, and H5 from wastewater (Version 1) instructions for use. 2024 [cited 2026 Aug 28] https://stacks.stanford.edu/file/jd535xb1898/LB-177Rev00D%20-%20Singleplex%20Digital%20PCR%20Testing%20of%20Influenza%20A%2C%20H1pdm09%2C%20H3%2C%20and%20H5%20from%20Wastewater%20-%20Instructions%20for%20Use.pdf

Address for correspondence: Antonio Marchini, European Commission Joint Research Centre, via E. Fermi 2749, 21027 Ispra (VA), Italy; email: antonio.marchini@ec.europa.eu

The Public Health Image Library

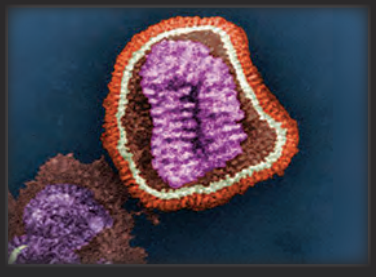
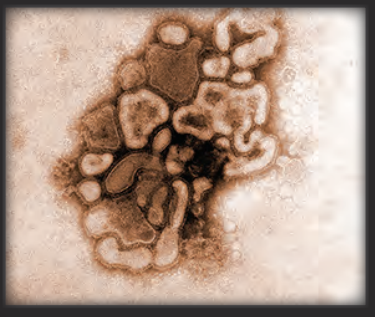
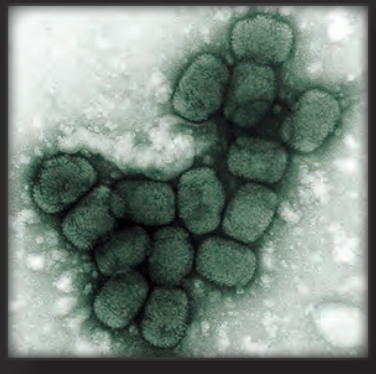

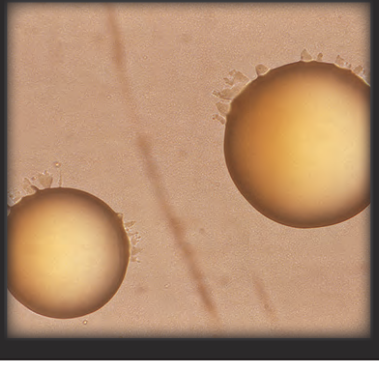
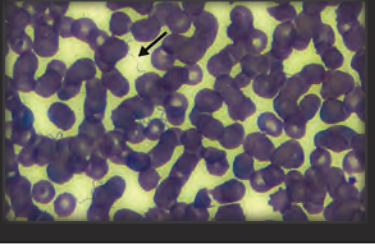

The Public Health Image Library (PHIL), Centers for Disease Control and Prevention, contains thousands of public health–related images, including high-resolution (print quality) photographs, illustrations, and videos.

PHIL collections illustrate current events and articles, supply visual content for health promotion brochures, document the effects of disease, and enhance instructional media.

PHIL images, accessible to PC and Macintosh users, are in the public domain and available without charge.

Visit PHIL at: https://phil.cdc.gov/

Dirofilaria asiatica Infection and Asymptomatic Microfilaremia, Sri Lanka, 2025

Dilini Mataraarachchi, Iroshini Abeysekara, Harsha Narammalage, Thulangi Siriwardana, Nayana Gunathilaka, Murali Vallipuranathan, Prasanga Serasinghe, Lakmini Liyanage, Nilanka Perera, Guwani Liyanage, Shalindra Ranasinghe, Nilmini Chandrasena

We report 2 cases of asymptomatic *Dirofilaria* microfilaremia in humans in Sri Lanka, detected during night blood surveillance for lymphatic filariasis in 2025. Partial sequence of microfilarial cytochrome c oxidase 1 gene revealed that both infections were caused by the novel species *D. asiatica*, originally described in Hong Kong as *Candidatus* D. honkongensis.

Dirofilariasis is an emerging mosquitoborne zoonosis caused by nematodes of the family Onchocercidae, genus *Dirofilaria* (*1*). Two main species are of relevance in veterinary and clinical practice, *Dirofilaria immitis* (dog heartworm) and *D. repens*. *D. immitis* worms have a wider distribution (Americas, Africa, Europe, and Australasia) and cause potentially life-threatening cardiopulmonary dirofilariasis in canids and felids and pulmonary lesions in accidental human infections. *D. repens* worms are limited to the Old World and cause subcutaneous and ocular dirofilariasis in canines, felines, and in accidental human infections.

A novel *D. asiatica* nematode species (formerly *Candidatus* Dirofilaria honkongensis) of canine origin was reported in Hong Kong in 2012 and subsequently in other countries in the region; it is gaining prominence as a zoonosis with diverse manifestations including cervical lymphadenopathy, abdominal subcutaneous masses, and subconjunctival nodules (*2*). Stray dogs and putative vector mosquitoes of genera *Aedes*, *Culex*, *Mansonia*, and *Armigeres* are abundant in Sri Lanka. Surveys in Sri Lanka have documented the presence of *D. asiatica* worms among 27.9% of canines with isolation of adult *D. asiatica* worms in subcutaneous nodules, scrota, and spermatic cords (*3*).

Adult filarial worms and their larval stages were historically identified on the basis of morphology and morphometry (*4*,*5*). However, differentiation of taxa was challenging because of morphologic similarities and the paucity of specific identification features. Using a combined morphologic and molecular approach has enabled differentiation of morphologically similar but genetically distinct species with identification of cryptic species (*2*). Sri Lanka has the highest number of human *Dirofilaria* spp. infections in Asia (*6*).

Most *Dirofilaria* infections in humans are amicrofilaremic (*1*,*5*). The developmental cycle deviates as immature worms localize in aberrant hosts, triggering host inflammatory responses against *Dirofilaria* and *Wolbachia* (essential endosymbiont) antigens that arrest worm development or destroy them, resulting in inflammatory granulomas with indwelling immature worms (*1*). Thus, humans were regarded as dead-end hosts. However, occasional reports of microfilaremic infections have queried this theory (*7*,*8*). We report asymptomatic *D. asiatica* microfilaremia in 2 cases detected incidentally during night blood surveillance for lymphatic filariasis, in Kalutara district, in western Sri Lanka in 2025 (Figure 1).

The Study

Case 1 was in a 60-year-old mason who had a microfilaria count of 7 in a 60-μL night blood smear (NBS) in April 2025. The microfilaria was morphologically compatible with genus *Dirofilaria*. The patient was receiving treatment for diabetes mellitus and hypertension and had longstanding bilateral lower-limb

Author affiliations: Anti Filariasis Campaign, Colombo, Sri Lanka (D. Mataraarachchi, I. Abeysekara, H. Narammalage, M. Vallipuranathan, P. Serasinghe, L. Liyanage); University of Kelaniya, Ragama, Sri Lanka (T. Siriwardana, N. Gunathilaka, N. Chandrasena); Colombo South Teaching Hospital, Colombo (N. Perera, G. Liyanage); University of Sri Jayewardenepura, Nugegoda, Sri Lanka (N. Perera, G. Liyanage, S. Ranasinghe)

DOI: https://doi.org/10.3201/eid3211.260015

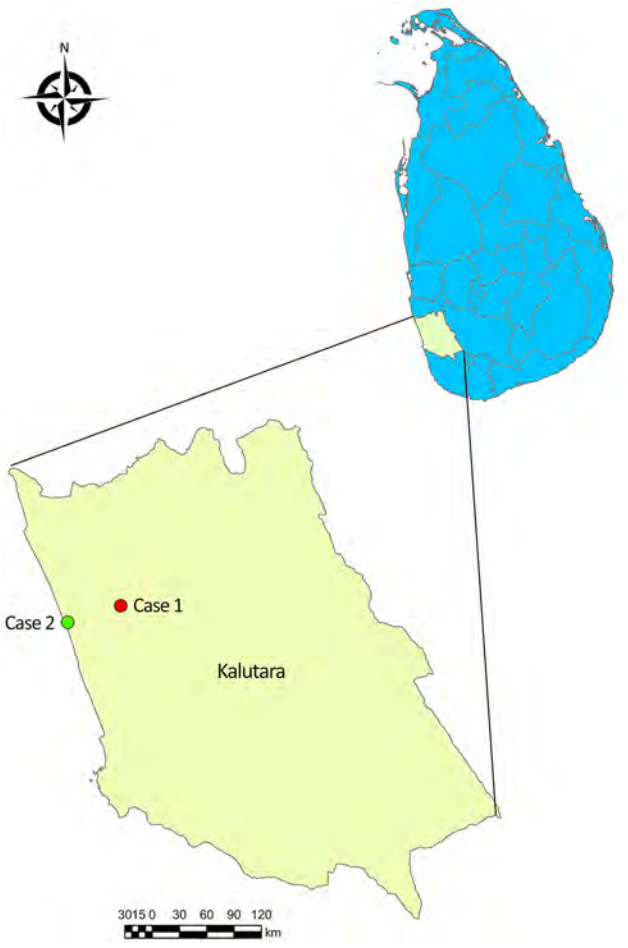

Figure 1. Locations of *Dirofilaria asiatica* microfilaremia cases in study of *Dirofilaria* infection and asymptomatic microfilaremia, Sri Lanka, 2025. Close-up view shows Kalutara district in western Sri Lanka. Cases were detected from night blood smear specimens.

swelling with no identifiable cause and a few palpable inguinal lymph nodes. Other physical examination results were unremarkable. Abdominal ultrasonography and ophthalmology screening results were unremarkable. After obtaining 5 mL of venous blood, we administered diethylcarbamazine (6 mg/kg/d for 12 d) and albendazole (400 mg). His microfilaremia was cleared at 5 weeks posttreatment.

Case 2 was in a 14-year-old boy who had a microfilaria count of 3/60 µL NBS in June 2025. The microfilaria was morphologically compatible with genus *Dirofilaria*. The patient had an occasional dry cough without diurnal variation. Hematology revealed eosinophilia of 568/µL (10.5%). Chest and abdominal imaging and echocardiography were unremarkable. He received doxycycline (100 mg 2×/d for 5 d) and albendazole (400 mg 2×/d for 5 d). Persistence of microfilaremia (1/60µL) at 1 month posttreatment necessitated a repeat course of treatment. His microfilaremia was cleared at 3 months posttreatment.

Giemsa-stained NBSs from both case-patients at 1,000× magnification revealed microfilaria with morphology compatible with *D. repens* and *D. asiatica* worms (*2*). (Table; Figure 2). We performed molecular speciation to establish species identity. We extracted genomic DNA from venous blood of both patients using the QIAGEN Tissue Kit (QIAGEN, https://www.qiagen.com). We amplified mitochondrial cytochrome c oxidase subunit I (COI) gene using the primer pair COIfilF/COIfilR, designed from conserved nematode regions (*9*). We sequenced purified amplicons (QIAquick PCR Purification Kit; QIAGEN) bidirectionally by Sanger sequencing (SeqStudio Genetic Analyzer; Thermo Fisher Scientific, https://www.thermofisher.com) and deposited the resulting sequences in GenBank (accession nos. PZ359659 [AFC615] and PZ359660 [AFC621]). We edited chromatograms manually in BioEdit version 7.2.5 (https://www.updatestar.com) and queried against the National Center for Biotechnology Information nucleotide database using BLASTn (https://blast.ncbi.nlm.nih.gov/Blast.cgi) for homology assessment. We performed multiple sequence alignment using ClustalW in BioEdit. Both isolates were consistently identified as *Dirofilaria asiatica*; BLAST results showed near-complete

Table. Characteristics of *Dirofilaria* microfilariae detected in study of *Dirofilaria asiatica* infection and asymptomatic microfilaremia, compared with those of reference strains, Sri Lanka, 2025*

Morphology	Microfilaria in this study	*D. repens* microfilaria†	*D. asiatica* microfilaria‡
Sheath	Absent	Absent	Absent
Mean total body length, µm	349	369 ±10	300.3
Mean width, µm	8	8.87±0.5	5.7
Cephalic space			
Mean length, µm	2.5	2.96 ± 1.18	3.27
Location	Round anterior end	Round anterior end	Not specified
No. nuclei	2–3	2 nuclei	2–3 nuclei
Tail	Tapering, curved, free of nuclei	Tapering, curved, free of nuclei	Tapering, curved, free of nuclei

*Specimens in this study were human blood smears stained with 10% Giemsa; we observed a mean of 10 microfilariae per specimen. Characteristics were obtained using Olympus microscope (original magnification ×1,000) and cell analysis software ScopeImage version 9.0 (https://www.bioimager.com).
†Magnis et al. (*5*).
‡Colella et al. (*2*) Specimens were stained with 0.1% methylene blue.

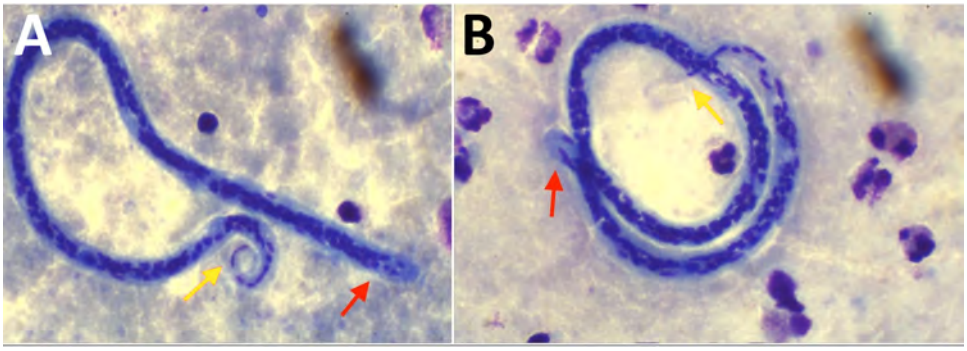

Figure 2. Microfilaria detected in Giemsa-stained thick blood smears from case-patients 1 (A) and 2 (B) in study of *Dirofilaria* infection and asymptomatic microfilaremia, Sri Lanka, 2025. Red arrows indicate the anterior end (cephalic space) with 2–3 distinct nuclei; yellow arrows indicate the tails free of any nuclei. Original magnification ×1,000.

query coverage (≈100%) and high percentage identity (>99%) to reference *D. asiatica* sequences, confirming species-level identification.

We constructed a maximum-likelihood phylogenetic tree in MEGA version 11 (*10*), using the best-fit substitution model selected by Bayesian Information Criterion (Figure 3). We assessed branch support using 1,000 bootstrap replicates and genetic distances estimated under the Kimura 2-parameter model. The resulting tree resolved 6 well-defined major clades, corresponding to *D. asiatica*, *D. repens*, *D. immitis*, *D. ursi*, *Onchocerca* sp., and *Onchocercidae* sp.; the deepest nodes separating the clades were supported at 10%–23%. Both study isolates, AFC615 and AFC621, clustered firmly within the *D. asiatica* clade alongside reference sequences also obtained from GenBank (accession nos. PV523839, PV523835, PV523843, and PV523842). Isolate AFC615 grouped closely with

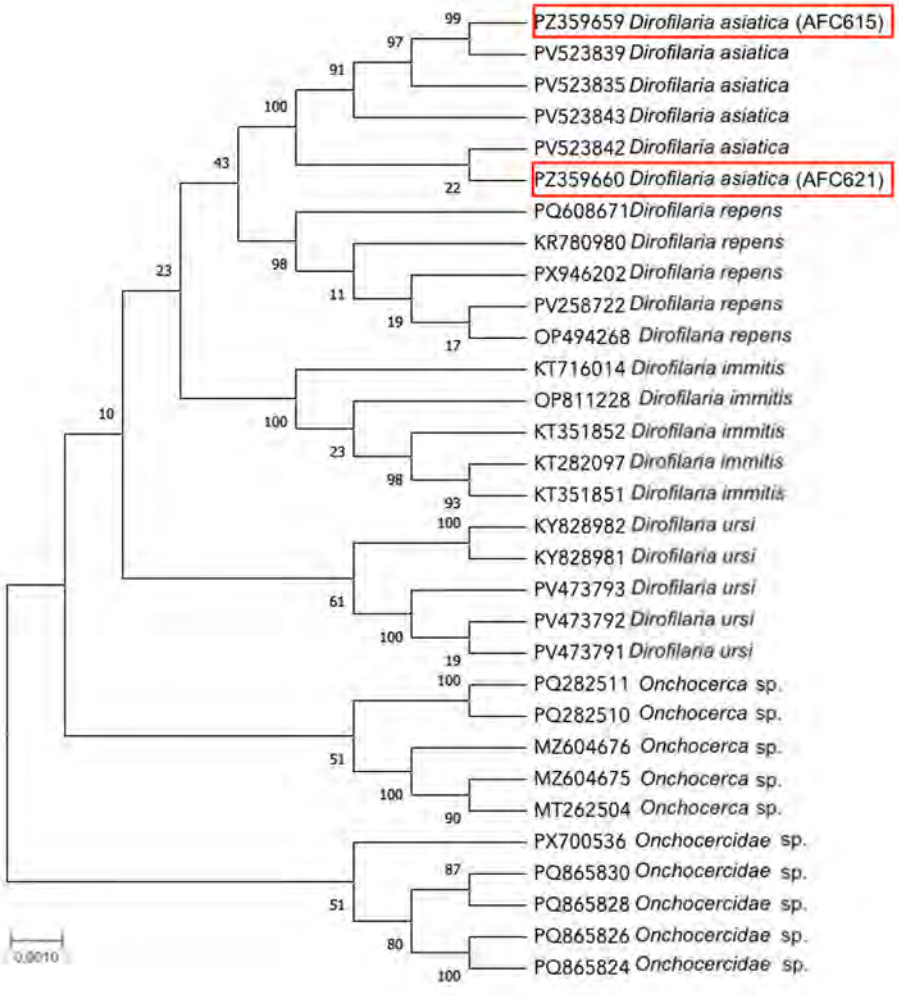

Figure 3. Maximum-likelihood phylogenetic tree generated in study of *Dirofilaria asiatica* infection and asymptomatic microfilaremia, Sri Lanka, 2025. Tree includes partial mitochondrial *cox1* gene sequences from 2 *D. asiatica* isolates in this study (red boxes) and curated reference sequences representing *D. asiatica*, *D. repens*, *D. immitis*, and *D. ursi*; we included *Onchocerca* sp. and *Onchocercidae* sp. as non-*Dirofilaria* outgroups. We constructed the tree in MEGA version 11 (www.megasoftware.net) under the Kimura 2-parameter substitution model, selected as the best-fit model by Bayesian Information Criterion. Node support was assessed using 1,000 bootstrap replicates; numbers at nodes indicate bootstrap values ≥50%. GenBank accession numbers are provided. Scale bar represents nucleotide substitutions per site.

PV523839 and PV523835; bootstrap support was 99% at the terminal node and 97% and 91% at the supporting internal nodes. Isolate AFC621 formed a pair with reference sequence PV523842; the pair nested within the broader *D. asiatica* clade at 43% support. The clustering we observed was fully consistent with the BLASTn results, confirming both isolates as genuine *D. asiatica*.

Overall, the phylogenetic tree demonstrated clear separation of the 6 major clades (*D. asiatica*, *D. repens*, *D. immitis*, *D. ursi*, *Onchocerca* sp., and *Onchocercidae* sp.), with both study isolates aligning unambiguously within the *D. asiatica* lineage. The range of bootstrap support observed within this clade (22%–99%) reflects a degree of intraspecific genetic variation among *D. asiatica* sequences from different geographic sources, while clearly resolving both Sri Lanka isolates as *D. asiatica* (Figure 3).

Human *Dirofilaria* infections have been reported in Sri Lanka over many decades (*6*), although not specifically microfilaremia caused by *D. asiatica* filarial worms. Case-patient 1, who had underlying conditions, was probably immunodeficient to some extent, enabling the maturation of *D. asiatica* larvae into adults, whereas case-patient 2 may have had multiple exposure events.

A literature review revealed use of 3 treatment regimens with no preference of one over the other (*11*). The first 2 regimens were diethylcarbamazine/albendazole combination therapy or doxycycline/albendazole combination therapy targeting the endosymbiont *Wolbachia*. The third regimen was ivermectin (200 μg/kg/d for 4 d) and doxycycline (100 mg 2×/d for 7 d) (*12*). We used the diethylcarbamazine/albendazole and doxycycline/albendazole regimens because ivermectin was not registered for human use in Sri Lanka at the time of treatment. Although both treatment regimens achieved clearance of microfilaremia, the viability of adult worms remains uncertain; attempts to locate adult worms were unsuccessful. Thus, we deliberated recommendations for annual follow-up by blood screening for 5 years.

Conclusions

Our report establishes the presence of accidental *D. asiatica* infections among humans in Sri Lanka who were asymptomatic with microfilaremia. Further investigations will support the establishment of dirofilariasis as a zoonotic public health problem. We recommend routine administration of antifilarial drugs to dogs and cats, control of mosquitoes, and raising awareness of dirofilariasis.

Acknowledgments

We gratefully acknowledge the technical support provided in obtaining the morphometry of microfilariae by Hemantha Sudusinghe. We also thank the medical registrars K.C.T. Wijayawardana and L.U.S. Seneviratna for assisting with medical screening of cases. We appreciate the valuable guidance provided by reviewers in the preparation of the manuscript.

Author contributions: D.M. initiated the study. D.M., I.A., M.V., P.S., and L.L. collected the data and samples for further studies. G.L. and N.P. were involved in case management. N.C. and S.R. guided the investigations. N.G. and T.S. performed molecular analysis. I.A., N.C., T.S., and S.R. drafted the report. All authors provided critical feedback and granted final approval.

About the Author

Dr. Mataraarachchi was the acting consultant community physician attached to the Anti Filaria Campaign, Colombo, at the time of case detection. She is the regional epidemiologist, Matara, Regional Director of Health Services, Matara, Sri Lanka.

References

1. Simón F, Siles-Lucas M, Morchón R, González-Miguel J, Mellado I, Carretón E, et al. Human and animal dirofilariasis: the emergence of a zoonotic mosaic. Clin Microbiol Rev. 2012;25:507–44. https://doi.org/10.1128/CMR.00012-12
2. Colella V, Young ND, Manzanell R, Atapattu U, Sumanam SB, Huggins LG, et al. *Dirofilaria asiatica* sp. nov. (Spirurida: Onchocercidae)—defined using a combined morphological-molecular approach. Int J Parasitol. 2025;55:461–74. https://doi.org/10.1016/j.ijpara.2025.04.006
3. Atapattu U, Koehler AV, Huggins LG, Wiethoelter A, Traub RJ, Colella V. Dogs are reservoir hosts of the zoonotic *Dirofilaria* sp. 'hongkongensis' and potentially of *Brugia* sp. Sri Lanka genotype in Sri Lanka. One Health. 2023;17:100625. https://doi.org/10.1016/j.onehlt.2023.100625
4. Pampiglione S, Rivasi F. Human dirofilariasis due to *Dirofilaria* (*Nochtiella*) *repens*: an update of world literature from 1995 to 2000. Parassitologia. 2000;42:231–54.
5. Magnis J, Lorentz S, Guardone L, Grimm F, Magi M, Naucke TJ, et al. Morphometric analyses of canine blood microfilariae isolated by the Knott's test enables *Dirofilaria immitis* and *D. repens* species-specific and *Acanthocheilonema* (syn. *Dipetalonema*) genus-specific diagnosis. Parasit Vectors. 2013;6:48. https://doi.org/10.1186/1756-3305-6-48
6. Balendran T, Yatawara L, Wickramasinghe S. Human dirofilariasis caused by *Dirofilaria repens* in Sri Lanka from 1962 to 2020. Acta Parasitol. 2022;67:628–39. https://doi.org/10.1007/s11686-022-00543-3
7. Poppert S, Hodapp M, Krueger A, Hegasy G, Niesen WD, Kern WV, et al. *Dirofilaria repens* infection and concomitant meningoencephalitis. Emerg Infect Dis. 2009;15:1844–6. https://doi.org/10.3201/eid1511.090936
8. Frenzen FS, Loewe I, Müller G, Schoenlebe J, Tappe D, Teichmann D. *Dirofilaria repens* infection of the eye with

concomitant microfilaremia in a traveller. J Travel Med. 2021;28:taaa119. https://doi.org/10.1093/jtm/taaa119
9. Casiraghi M, Anderson TJ, Bandi C, Bazzocchi C, Genchi C. A phylogenetic analysis of filarial nematodes: comparison with the phylogeny of *Wolbachia* endosymbionts. Parasitology. 2001;122:93–103. https://doi.org/10.1017/S0031182000007149
10. Tamura K, Stecher G, Kumar S. MEGA11: Molecular Evolutionary Genetics Analysis version 11. Mol Biol E vol. 2021;38:3022–7. https://doi.org/10.1093/molbev/msab120
11. Valčiukaitė-Žilinskienė R, Zablockienė B, Zablockis R. Dirofilariasis presenting as pleural effusion: a rare case report with unusual manifestations and treatment modalities. BMC Pulm Med. 2024;24:340. https://doi.org/10.1186/s12890-024-03154-y
12. Biasizzo H, Šoba B, Ilovski F, Harlander M, Lukin M, Blatnik O, et al. Severe and rare case of human *Dirofilaria repens* infection with pleural and subcutaneous manifestations, Slovenia. Emerg Infect Dis. 2022;28:2504–7. https://doi.org/10.3201/eid2812.221366

Address for correspondence: Nilmini Chandrasena, Department of Parasitology, Faculty of Medicine, University of Kelaniya, Thalagolla Rd, Ragama, Sri Lanka; email: nilmini@kln.ac.lk

October 2026

Vaccine-Preventable Diseases

- Reassortment of Highly Pathogenic Avian Influenza as a Driver for Zoonotic Spillover, Asia
- Early Action Review of Detection, Notification, and Response Timeliness during Cross-Border Bundibugyo Virus Disease Outbreak, Uganda, 2026
- Meta-analysis of Maternal and Fetal Outcomes of Crimean-Congo Hemorrhagic Fever during Pregnancy
- Detection of *Anaplasma capra* in Patients with Suspected Crimean-Congo Hemorrhagic Fever, Turkey, 2022
- Systematic Review and Meta-analysis of Group B *Streptococcus* Rectovaginal Colonization Rates and Serotype Distribution among Pregnant Women, Asia-Pacific Region, 2014–2025
- Human Myiasis Resulting from Reemergence of *Cochliomyia hominivorax* Screwworm, Mexico, 2025–2026
- Meta-analysis of Asymptomatic Monkeypox Virus Prevalence in Nonendemic Regions, 2022–2024
- Emergence of Rabies in Cape Fur Seals, South Africa

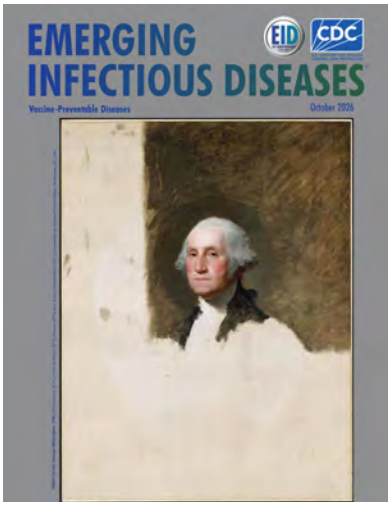

- Multiple Introductions and Cross-Sector Transmission of *Salmonella enterica* Serovar Infantis Carrying $bla_{CTX-M-65}$ Gene, South Korea, 2022–2024
- Molecular Epidemiology and Evolution of Swine Influenza A Viruses, Vietnam, 2020–2024
- Genomic Epidemiology of *Salmonella enterica* Serovar Hadar Strain Linked to Poultry-Associated Salmonellosis Outbreaks, United States
- Persistent *Bartonella quintana* Infection in Macaques at Primate Research Institute, Japan
- Detection of Influenza D Virus using Reverse Transcription Loop-Mediated Isothermal Amplification
- Multisectoral Emergence of Multidrug-Resistant *Campylobacter coli* Sequence Type 10042 Lineage, Europe, 2018–2025
- Experimental Highly Pathogenic Avian Influenza A(H5N1) Clade 2.3.4.4b Virus Infection in Alpacas, 2026
- Wastewater Surveillance to Track Resurgent Measles Outbreak, Ontario, Canada, 2025
- Variolation Techniques, Medical Explanations, and Dissemination in Late Imperial China
- Fatal Infection with Dengue Virus and Avian Orthoavulavirus 1 in Traveler Returning from Saudi Arabia to France, 2025
- Characteristics and Superspreading Potential of Andes Virus Person-to-Person Transmission
- Monkeypox Virus in Healthcare Settings, Sierra Leone, June 2025
- Clinical Characterization of Invasive Meningococcal Disease Epidemic, Uzbekistan, 2026

EMERGING INFECTIOUS DISEASES®

To revisit the October 2026 issue, go to:
https://wwwnc.cdc.gov/eid/articles/issue/32/10/table-of-contents

Persistent Microfilaremia Caused by *Dirofilaria asiatica* Infection in 2-Year Old Child, Sri Lanka, 2024

Ushani Atapattu, Indeewarie E. Gunaratna,[1] Lucas G. Huggins,[1] Murali Vallipuranathan, Lakmini Liyanage, Harsha K. Narammalage, Nipuni Shilpeswarage, Udayi B. Gunawardana, S.T.A. Prasanga Serasinghe, Vito Colella

Filarial nematodes cause significant illness worldwide, including lymphatic and subcutaneous filariases in tropical regions. *Dirofilaria asiatica* is a recently described canine filarioid increasingly implicated in zoonotic human infections. Here, we report a patent infection in a child in Sri Lanka who had persistent microfilaraemia after 2 rounds of diethylcarbamazine treatment.

Filarial worms can cause significant disease and profoundly affect quality of life for both humans and animals. Key human-infecting species encompass those causing lymphatic filariasis (*Wuchereria bancrofti* and *Brugia* spp.) and subcutaneous and ocular filariases (*Onchocerca volvulus* and *Loa loa*) (*1*). Despite considerable progress in controlling those parasitic diseases, the World Health Organization (WHO) estimates that >650 million persons remain at risk for lymphatic filariasis (*1*). As research into filarial worm control continues, the role that zoonotic species might play in hampering elimination efforts has become more prominent.

In Sri Lanka, *Dirofilaria asiatica* (formerly known as the *Dirofilaria* Hong Kong genotype) and the *Brugia* Sri Lanka genotype are recognized as 2 zoonotic filarial worms that primarily infect dogs, typically subclinically, and can be transmitted to humans (*2*,*3*). Although knowledge of *D. asiatica* infection in humans is still in its infancy, it has been associated with subcutaneous and subconjunctival nodules and potentially life-threatening anaphylaxis during surgical worm excision (*4*). Furthermore, nodules caused by *D. asiatica* worms can mimic serious conditions (*5*) such as breast tumors (*6*) or testicular torsion, complicating its diagnosis (*7*). Sri Lanka has reported the highest number of human subcutaneous infections caused by *Dirofilaria* spp. worms; those accounted for >50% of subcutaneous nodules in pediatric surgical patients (*8*). The increasing number of reported human cases of *D. asiatica* infection in the region might reflect its important role as a cause of canine subcutaneous dirofilariasis in the Asia-Pacific, potentially increasing opportunities for zoonotic transmission (*3*,*5*,*9*,*10*). Nonetheless, humans are considered dead-end hosts for *Dirofilaria* spp. worms; cases of microfilaremia are rarely observed (*11*).

We report on a case of *Dirofilaria* spp. infection in a child identified by the Anti-Filariasis Campaign, part of a national postvalidation surveillance program in lymphatic filariasis–endemic districts in Sri Lanka. The Ethics Review Committee of the Postgraduate Institute of Medicine, University of Colombo, Sri Lanka, approved molecular confirmation of positive samples for the program (ID no. ERC/PGIM/2023/133). We obtained informed consent from adults, and parental assent for children, as described previously (*3*).

The Study

In April 2024, a 2-year-old girl with trisomy 21 from Kalutara District, Sri Lanka, was confirmed to have microfilaremia caused by an unidentified filarial parasite

Author affiliations: The University of Melbourne, Melbourne, Victoria, Australia (U. Atapattu, L.G. Huggins, V. Colella); Government of Sri Lanka Ministry of Health, Colombo, Sri Lanka (I.E. Gunaratna, M. Vallipuranathan, L. Liyanage, H.K. Narammalage, N. Shilpeswarage, U.B. Gunawardana, S.T.A.P. Serasinghe); Government of Sri Lanka Regional Director of Health Services, Kalutara, Sri Lanka (H.K. Narammalage, U.B. Gunawardana, S.T.A.P. Serasinghe)

DOI: https://doi.org/10.3201/eid3211.260739

[1]These authors contributed equally to this article.

during routine night blood smear surveillance conducted as part of an ongoing campaign. Methylene blue staining revealed unsheathed microfilariae with a rounded anterior end, 1–2 cephalic nuclei, and a curved tail (Figure), consistent with *Dirofilaria* spp. (*2*). We observed no clinical signs of lymphatic filariasis. We collected a whole-blood sample and administered oral diethylcarbamazine (3 mg/kg/d for 12 d). One month posttreatment, night blood smear showed persistent microfilaremia, prompting a second course of diethylcarbamazine. The patient did not return for care after the second treatment. Attempts to contact the family were unsuccessful until a year later; we then initiated follow-up testing. Microscopy remained positive for microfilariae with morphology consistent with *Dirofilaria* spp., but results for both *Brugia* Test Plus (BT+) (Drugs & Diagnostics for Tropical Diseases, https://www.ddtd.org) and STANDARD Q Filariasis Antigen test (SD Biosensor, https://www.sdbiosensor.com) were negative. Eight days later, we initiated a third 12-day course of diethylcarbamazine (6 mg/kg/d) with albendazole (400 mg). Four weeks after treatment, in July 2025, a thick blood smear specimen tested negative for microfilariae.

We performed molecular characterization on whole blood from the patient, initially collected in 2024, at the University of Melbourne (Melbourne, VIC, Australia). We extracted DNA using the DNeasy Blood and Tissue Kit (QIAGEN, https://www.qiagen.com) and analyzed it using a prevalidated nanopore-based metabarcoding assay capable of detecting all filarial worm species through selective amplification and sequencing of the mitochondrial cytochrome c oxidase 1 (*cox-1*) gene (*12*). We used a second nanopore-based metabarcoding assay targeting the nuclear 18S ribosomal RNA (rRNA) gene, internal transcribed spacer (ITS) 1 and ITS-2 regions, and 28S rRNA gene to characterize the blood microfilariae (*2*) (Appendix, https://wwwnc.cdc.gov/EID/article/32/11/26-0739-App1.pdf)). Both assays identified *D. asiatica* worms as the cause of the infection. We identified no other filarial worm infection. We deposited the generated sequences into GenBank (accession nos. PZ167699 and PZ168005).

Conclusions

We document a confirmed case of persistent patent *D. asiatica* infection in a human. Microfilariae were observed in the patient's blood over a period of >1 year. Of interest, a small number of human microfilaremia cases have been reported for the closely related filarial species *D. repens*; therefore, its occurrence with *D. asiatica* infection may not be entirely unexpected (*11*). A potential contributing factor could be the patient's underlying trisomy 21, which impairs both innate and adaptive immunity (*13*); those immunologic vulnerabilities might have enabled the reproductive maturation of *D. asiatica* worms in this young patient.

Figure. *Dirofilaria asiatica* microfilaria isolated from a 2-year-old girl from Kalutara District, Sri Lanka, stained with methylene blue. The microfilaria has a rounded anterior end with 2 cephalic nuclei (visible at lower right) and a curved tail. Original magnification ×1,000.

The ability of *D. asiatica* worms to produce patent infections has public health implications beyond individual cases. In filariasis-endemic settings, the morphologic similarity of *Dirofilaria* microfilariae to those of other known pathogens could complicate microscopy-based surveillance, particularly where species identification relies on field-level morphologic assessment.

This report further highlights the need for surveillance programs to adopt more versatile and species-discriminating diagnostic platforms. For example, recent postvalidation surveillance in Sri Lanka detected *Brugia*-like microfilaremia in 52 persons, including 17 case-patients in Kalutara District; molecular characterization using nanopore metabarcoding of available cases identified *Brugia* SL genotype but found no filarial coinfections (*2*). Such improvements are critical given that the transmission dynamics of *D. asiatica* and *Brugia* SL genotype differ from anthroponotic species; specifically, those species are maintained in canine (*3*,*10*) and potentially feline reservoir hosts. Hence, the control of zoonotic filarial worms such as *D. asiatica* and *Brugia* SL genotype might not be adequately addressed through conventional elimination strategies. For example, despite its benefits in reducing lymphatic filariasis, mass drug administration (MDA) is unlikely to reduce zoonotic transmission of *D. asiatica* worms, particularly given

their high (≈33%) prevalence in dogs in the southern and western regions of Sri Lanka (*10*). Moreover, molecular detections of *D. asiatica* worms in dogs have increased across Asia, indicating a broader distribution than previously assumed (*9*,*10*). Emerging evidence suggests that many human dirofilariasis cases in the Asia-Pacific region previously attributed to *D. repens* infection might have actually been caused by *D. asiatica* infection, a misattribution potentially resulting from previous limitations in diagnostic tools and reference data (*2*). In the case we describe, imaging, including ultrasonography, to locate adult worms, could not be performed because we could not reestablish contact with the patient and her family.

Persistent microfilaremia after repeated courses of diethylcarbamazine might reflect treatment failure or reinfection, suggesting inconsistent efficacy against *D. asiatica* and the need for improved therapeutic regimens for zoonotic filarial infections. No established treatment protocols exist for human dirofilariasis with microfilaremia; reported therapeutic approaches, including ivermectin and anti-*Wolbachia* therapy with doxycycline, are largely based on experience with *D. repens* infections rather than controlled studies (*14*). Furthermore, the use of ivermectin in very young children is limited because its safety and effectiveness have not been established in children weighing <15 kg (*15*).

Our findings demonstrate the ability of *D. asiatica* worms to cause microfilaremia in humans; the clinical implications of patent *D. asiatica* infection remain unknown. This study underscores critical gaps in diagnostic and therapeutic strategies for lymphatic filariasis surveillance and control in regions where cryptic and zoonotic filarial species cocirculate, supporting the need for integrated One Health approaches. Species-specific diagnostic tools within filariasis surveillance will enable accurate detection, which in turn will provide a clearer understanding of the distribution and prevalence of patent zoonotic filarial infections in endemic regions.

About the Author

Dr. Atapattu is a research assistant at the University of Melbourne, Australia. Her research is focused on the development of control strategies for zoonotic vectorborne diseases.

References

1. World Health Organization. Lymphatic filariasis. 2026 [cited 2026 Mar 2]. https://www.who.int/news-room/fact-sheets/detail/lymphatic-filariasis
2. Colella V, Young ND, Manzanell R, Atapattu U, Sumanam SB, Huggins LG, et al. *Dirofilaria asiatica* sp. nov. (Spirurida: Onchocercidae)—defined using a combined morphological-molecular approach. Int J Parasitol. 2025;55:461–74. https://doi.org/10.1016/j.ijpara.2025.04.006
3. Gunaratna IE, Huggins LG, Atapattu U, Liyanage L, Shilpeswarage N, Vallipuranathan M, et al. Emergence of a novel zoonotic brugian filarial infection during post-validation surveillance for lymphatic filariasis in Sri Lanka. Lancet Reg Health Southeast Asia. 2026;46:100735. https://doi.org/10.1016/j.lansea.2026.100735
4. Luk BWC, Cheung CN, Chan YF. Anaphylaxis after surgical excision of subcutaneous infection with parasitic *Dirofilaria*: a case report. Hong Kong Med J. 2021;27:297–9. https://doi.org/10.12809/hkmj208675
5. Kumar A, Sreedhar A, Biswas L, Prabhat S, Suresh P, Asokan A, et al. *Candidatus* Dirofilaria hongkongensis infections in humans during 2005 to 2020, in Kerala, India. Am J Trop Med Hyg. 2021;104:2046–9. https://doi.org/10.4269/ajtmh.20-1521
6. Schroeder J, Rothe C, Hoerauf A, Kroidl I, Pfarr K, Hübner MP. First case of *Dirofilaria hongkongensis* infection in Germany presenting as a breast tumour. J Travel Med. 2023;30:taad121. https://doi.org/10.1093/jtm/taad121
7. Wijekoon N, Antony D, Muhunthan T, Samarasinghe M. Dirofilariasis causing pediatric acute scrotum: a case series and review of the literature. J Indian Assoc Pediatr Surg. 2024;29:356–9. https://doi.org/10.4103/jiaps.jiaps_268_23
8. Wijekoon N, Antony D, Muhunthan T, Samarasinghe M. Dirofilarial nodule as a differential diagnosis for subcutaneous lumps in children. Pediatr Surg Int. 2022;39:55. https://doi.org/10.1007/s00383-022-05348-z
9. Huggins LG, Atapattu U, Khieu V, Traub R, Colella V. Genetic characterization of zoonotic *Dirofilaria asiatica* in Cambodian dogs through nanopore metabarcoding. Microbiol Spectr. 2025;13:e01990-25. https://doi.org/10.1128/spectrum.01990-25
10. Atapattu U, Koehler AV, Huggins LG, Wiethoelter A, Traub RJ, Colella V. Dogs are reservoir hosts of the zoonotic *Dirofilaria* sp. 'hongkongensis' and potentially of *Brugia* sp. Sri Lanka genotype in Sri Lanka. One Health. 2023;17:100625. https://doi.org/10.1016/j.onehlt.2023.100625
11. Simón F, Siles-Lucas M, Morchón R, González-Miguel J, Mellado I, Carretón E, et al. Human and animal dirofilariasis: the emergence of a zoonotic mosaic. Clin Microbiol Rev. 2012;25:507–44. https://doi.org/10.1128/CMR.00012-12
12. Huggins LG, Atapattu U, Young ND, Traub RJ, Colella V. Development and validation of a long-read metabarcoding platform for the detection of filarial worm pathogens of animals and humans. BMC Microbiol. 2024;24:28. https://doi.org/10.1186/s12866-023-03159-3
13. Ram G, Chinen J. Infections and immunodeficiency in Down syndrome. Clin Exp Immunol. 2011;164:9–16. https://doi.org/10.1111/j.1365-2249.2011.04335.x
14. Tasić-Otasevic S, Golubović M, Trichei S, Zdravkovic D, Jordan R, Gabrielli S. Microfilaremic *Dirofilaria repens* infection in patient from Serbia. Emerg Infect Dis. 2023;29:2548–50. https://doi.org/10.3201/eid2912.230796
15. World Health Organization. WHO guideline on preventive chemotherapy for public health control of strongyloidiasis. Geneva: World Health Organization; 2024.

Address for correspondence: Vito Colella, Melbourne Veterinary School, The University of Melbourne, Grattan St, Parkville, Melbourne, VIC, 3010, Australia; email: vito.colella@unimelb.edu.au

Fatal *Rickettsia parkeri* Rickettsiosis in Immunocompromised Pediatric Patient, Georgia, USA, 2025

Stephanie Bellman,[1] Thomas G. Fox,[1] Sunil S. Raikar, Daniel John Bergsagel, Meredith Steuer, Kiran B. Hebbar, Jennifer Kasten-Metz, Sandor E. Karpathy, Christopher D. Paddock, Kristy O. Murray

We describe a fatal *Rickettsia parkeri* rickettsiosis case in a 3-year-old boy in Georgia, USA, receiving chemotherapy for B-cell acute lymphoblastic leukemia, hospitalized with febrile neutropenia. Plasma microbial cell-free DNA sequencing confirmed the diagnosis. This report highlights the need to maintain suspicion for tickborne diseases in immunocompromised hosts in some settings.

Rickettsia parkeri rickettsiosis is a mild to moderately severe spotted fever rickettsiosis (SFR) characterized by fever, myalgias, headache, rash, and, commonly, an eschar at the site of tick attachment (*1*). Since 2020, nearly 5,000 cases of SFR have been reported in the United States, including infections with *R. parkeri* (*2*). A systematic review of 77 *R. parkeri* rickettsiosis cases found that only 9% (16% in confirmed cases) required hospitalization and only 7% (3% in confirmed cases) occurred in children (*3*). Doxycycline is the treatment of choice for all rickettsial infections. We describe a fatal case of *R. parkeri* infection in an immunocompromised child in Georgia, USA.

The Study

A 3-year-old boy from southwestern Georgia receiving chemotherapy for high-risk B-cell acute lymphoblastic leukemia was admitted to the hospital in late July 2025 with febrile neutropenia. At admission, he had profound neutropenia and thrombocytopenia (leukocyte count 110/μL, absolute neutrophil count 20/μL, platelets 19,000/μL). He was on the second month of delayed intensification chemotherapy as part of a high-risk B-cell acute lymphoblastic leukemia regimen and had received cyclophosphamide, cytarabine, and 6-thioguanine 2 weeks before admission. His examination was unremarkable except for 2 pink papulonodules with central eschars on the left upper extremity (Figure 1, panel A). He was started on empiric cefepime therapy after blood cultures were obtained.

On the second and third day of hospitalization, a rash developed that began with small pink macules on the upper back and arms (Figure 1, panel B). Over the next 3 days, the rash progressed to numerous pink macules, some with overlying vesicles involving the bilateral upper and lower extremities, face, and trunk. Upon further questioning, his parents reported that the lesions on his left arm had been present for about 1 month before hospitalization and had been draining clear fluid. They attributed those lesions to suspected insect bites because he frequently played in the grass around their suburban home, but they did not recall seeing any insects.

He remained febrile despite cefepime therapy and had persistent pancytopenia and unmeasurable lymphocyte count; blood culture results were negative. Micafungin and acyclovir were initiated to target potential disseminated infection with *Candida* or herpes viruses. PCR testing for herpes simplex virus and varicella zoster virus from an unroofed vesicle returned negative results. Computed tomography with intravenous contrast of the lungs showed minimal ground glass opacities; abdominal ultrasound revealed hepatomegaly, trace ascites, and thickened and inflamed small bowel loops consistent with neutropenic enteritis.

On hospital day 7, he developed hypotension and respiratory failure and was transferred to the intensive care unit, requiring bilevel positive airway pressure.

Author affiliations: Children's Healthcare of Atlanta, Atlanta, Georgia, USA (S. Bellman, T.G. Fox, S.S. Raikar, D.J. Bergsagel, M. Steuer, K.B. Hebbar, K.O. Murray); Emory University School of Medicine, Atlanta (S. Bellman, T.G. Fox, S.S. Raikar, D.J. Bergsagel, M. Steuer, K.B. Hebbar, K.O. Murray); Centers for Disease Control and Prevention, Atlanta (J. Kasten-Metz, S.E. Karpathy, C.D. Paddock)

DOI: https://doi.org/10.3201/eid3211.261174

[1]These first authors contributed equally to this article.

Figure 1. Photographs of rash from study of fatal *Rickettsia parkeri* rickettsiosis in immunocompromised pediatric patient, Georgia, USA, 2025. A) Eschar on left upper extremity; B) rash on patient's torso.

Antimicrobial treatment was changed to meropenem, vancomycin, amphotericin B, isavuconazole, and doxycycline. He continued to have hemodynamic deterioration and worsening hypoxia. During intubation, he suffered a 20-minute cardiac arrest requiring chest compressions before return of spontaneous circulation, but unfortunately he later developed fixed and dilated pupils. The decision was made to withdraw life-sustaining therapies, and he died on hospital day 8. The next day, a sample submitted on hospital day 7 for plasma microbial cell-free DNA sequencing (Karius, https://kariusdx.com) returned positive results for *R. parkeri* (8,374 molecules/100 nL).

Confirmatory laboratory testing was performed by the Centers for Disease Control and Prevention (Atlanta, GA, USA). DNA was extracted from the residual plasma specimen and was found positive by real-time PCR targeting a 96-bp segment of the *omp*B gene specific for *R. parkeri* (*4*). Formalin-fixed, paraffin-embedded sections of the skin biopsy specimen were stained by an immunoalkaline phosphatase technique for multiple species of spotted fever group *Rickettsia*, including *R. parkeri*, yielding abundant staining for rickettsiae and rickettsial antigens in the lumina and endothelium of vessels and extension into adjacent dermal tissue (Figure 2) (*1*).

Conclusions

In this article, we describe a fatal case of *R. parkeri* rickettsiosis in a young, immunocompromised child.

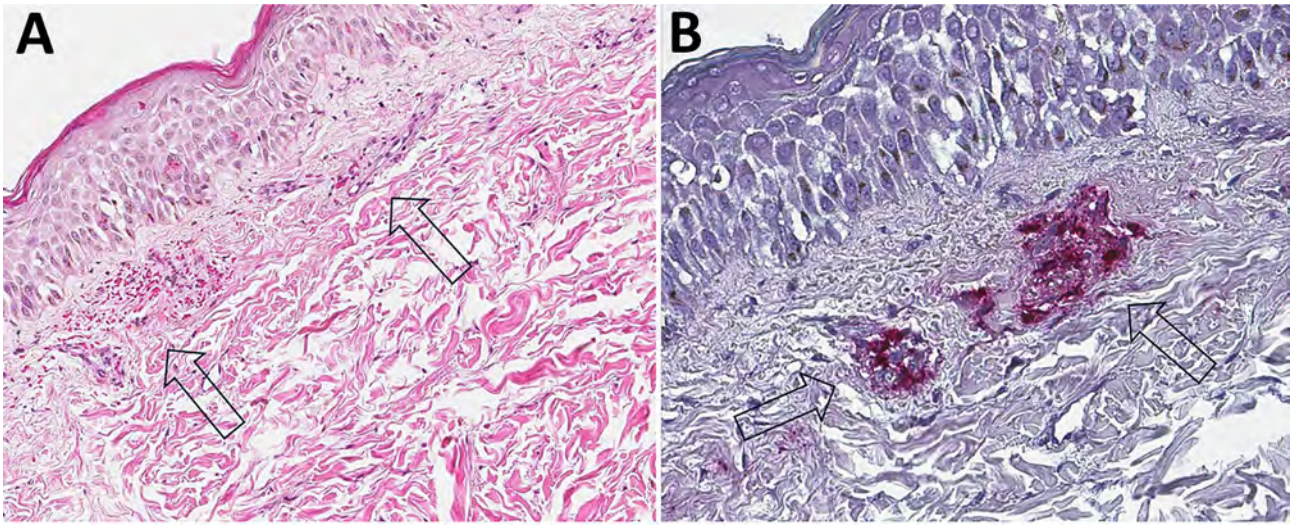

Figure 2. Immunohistochemistry and skin pathology from study of fatal *Rickettsia parkeri* rickettsiosis in immunocompromised pediatric patient, Georgia, USA, 2025. A) Punch biopsy specimen obtained from a rash lesion of the lower extremity of the patient demonstrating mild superficial dermal edema and small perivascular hemorrhages (arrows) without distinct inflammatory cell infiltrates. Hematoxylin and eosin stain; original magnification ×62.5. B) Immunohistochemical staining using an antibody reactive with spotted fever group *Rickettsia* spp., including *Rickettsia parkeri*, shows abundant staining of rickettsiae and rickettsial antigens in the lumens of the vessels, with invasion through the endothelium into the surrounding tissue (arrows). Immunoalkaline phosphatase with naphthol fast red and hematoxylin counterstain; original magnification ×62.5.

There is 1 known case of *R. parkeri* infection in an immunocompromised patient: a kidney transplant recipient who developed a moderately severe *R. parkeri* infection shortly after transplantation characterized by fever, diffuse rash, arthralgias, elevated inflammatory markers, and mildly elevated transaminases, which resolved after treatment with doxycycline (*5*).

Multiple factors contributed to the delay in recognition of SFR in this patient. *R. parkeri* infection is more commonly diagnosed in adults >40 years of age (*2*,*6*). In addition, hospital admission for febrile neutropenia is common during the stage of chemotherapy this child was receiving. A comprehensive study of >600 children with acute lymphoblastic leukemia showed that 72.9% of patients receiving high-risk delayed intensification were hospitalized at least once (*7*). The initial antibiotic for febrile neutropenia is typically chosen to target gram-negative bacteria, with a fourth-generation cephalosporin (e.g., cefepime) administered according to institutional guidelines (*8*). Persistent fevers and clinical deterioration led to the expansion of antibiotic treatment, covering gram-positive bacteria and fungal pathogens, a common strategy used in febrile neutropenia without confirmatory infectious results. Unfortunately, given the treatment phase and the reason for admission, recognizing a tickborne rickettsial infection was challenging. Clinicians might not consider those infections in patients with common syndromes like febrile neutropenia. Advanced diagnostic tools, such as unbiased cell-free DNA sequencing (e.g., Karius Spectrum), can expand our ability to detect fastidious or difficult to diagnose pathogens (*9*). Such tools have been increasingly used to detect rickettsial species (*5*,*10*,*11*), although the outsourcing of the test takes additional time to obtain a result, which can delay pathogen-targeted treatment.

Although a history of presumed insect bites was reported, no tick or insect was ever visualized on the child. Diagnosis of tickborne infection is often difficult without known tick exposure. *R. parkeri* is transmitted by the Gulf Coast tick, *Amblyomma maculatum*, the range for which includes the part of southwestern Georgia where this patient lived (*12*). Adult ticks are most active during July and August near the Gulf Coast (*13*), coinciding with the timing of this case.

The manifestation of *R. parkeri* rickettsiosis in this immune-suppressed patient was atypical for multiple reasons and contributed to the unusual severity of disease. The rash associated with *R. parkeri* consists typically of scattered pink macules with overlying vesicles (*1*). This patient's rash was more extensive than what is typically reported, including facial lesions. Furthermore, real-time PCR conducted at Centers for Disease Control and Prevention detected a high concentration of *R. parkeri* rickettsia in the plasma, and pathology examination found a high concentration of rickettsial antigen stain in and around dermal vessels. In vitro studies of rickettsial infection have demonstrated the importance of CD4 and CD8 T-cells, especially highlighting the necessity of CD8 T-cells in successfully eliminating the pathogen (*14*). The patient we describe had profound lymphopenia from his underlying leukemia and chemotherapy, which likely contributed to increased disease severity. In addition, a study in mice infected with *R. parkeri* demonstrated lethality with high inoculation dose (*15*), indicating that, whereas the infection is typically mild, high pathogen concentrations could be linked to death. On the basis of this case and the previous report in a kidney transplant patient (*5*), *R. parkeri* rickettsiosis represents a larger threat to immunocomprimised patients than previously thought.

This case highlights a rare but potentially serious tickborne infection in immunocompromised hosts and the importance of recognizing SFR in patients not typically considered at high risk. Clinicians should consider *R. parkeri* rickettsiosis in patients seeking care for fevers and eschar lesions who reside in or travel to areas where *A. maculatum* ticks exist, particularly during summer months.

Acknowledgments

We thank Kirsten Williams for her guidance.

About the Author

Dr. Bellman is a physician-scientist in training and postdoctoral researcher at Emory University and Children's Healthcare of Atlanta. Her main interests include understanding the ecology and epidemiology of emerging infectious diseases, vectorborne diseases, and improving diagnostics for neglected tropical diseases. Dr. Fox is an associate professor of pediatrics at Emory University and a pediatric infectious diseases physician at Children's Healthcare of Atlanta. His work focuses on infections in immunocompromised patients, antimicrobial and diagnostic stewardship, and medical education.

References

1. Paddock CD, Finley RW, Wright CS, Robinson HN, Schrodt BJ, Lane CC, et al. *Rickettsia parkeri* rickettsiosis and its clinical distinction from Rocky Mountain spotted fever. Clin Infect Dis. 2008;47:1188–96. https://doi.org/10.1086/592254
2. Centers for Disease Control and Prevention. Data and statistics on spotted fever rickettsiosis [cited 2026 Apr 21]. https://www.cdc.gov/rocky-mountain-spotted-fever/data-research/facts-stats/index.html

3. Silva-Ramos CR, Hidalgo M, Faccini-Martínez ÁA. Clinical, epidemiological, and laboratory features of *Rickettsia parkeri* rickettsiosis: a systematic review. Ticks Tick Borne Dis. 2021;12:101734.
4. Jiang J, Stromdahl EY, Richards AL. Detection of *Rickettsia parkeri* and *Candidatus* Rickettsia andeanae in *Amblyomma maculatum* Gulf Coast ticks collected from humans in the United States. Vector Borne Zoonotic Dis. 2012;12:175–82. https://doi.org/10.1089/vbz.2011.0614
5. Phadke GM, Gajurel K, Kasten J, DeLeon-Carnes M, Ramos C, Karpathy SE, et al. *Rickettsia parkeri* rickettsiosis in kidney transplant recipient, North Carolina, USA, 2023. Emerg Infect Dis. 2024;30:1459–62. https://doi.org/10.3201/eid3007.240217
6. Biggs HM, Behravesh CB, Bradley KK, Dahlgren FS, Drexler NA, Dumler JS, et al. Diagnosis and management of tickborne rickettsial diseases: Rocky Mountain spotted fever and other spotted fever group rickettsioses, ehrlichioses, and anaplasmosis—United States. MMWR Recomm Rep. 2016;65:1–44. https://doi.org/10.15585/mmwr.rr6502a1
7. Bassal M, Silva M, Patel S, Gibson PJ, Breakey VR, Athale U, et al. Phase-specific risks of outpatient visits, emergency visits, and hospitalizations during Children's Oncology Group-based treatment for childhood acute lymphoblastic leukemia: a population-based study. Pediatr Blood Cancer. 2021;68:e29141. https://doi.org/10.1002/pbc.29141
8. Lehrnbecher T, Robinson PD, Ammann RA, Fisher B, Patel P, Phillips R, et al. Guideline for the management of fever and neutropenia in pediatric patients with cancer and hematopoietic cell transplantation recipients: 2023 update. J Clin Oncol. 2023;41:1774–85. https://doi.org/10.1200/JCO.22.02224
9. Park SY, Chang EJ, Ledeboer N, Messacar K, Lindner MS, Venkatasubrahmanyam S, et al. Plasma microbial cell-free DNA sequencing from over 15,000 patients identified a broad spectrum of pathogens. J Clin Microbiol. 2023;61:e0185522. https://doi.org/10.1128/jcm.01855-22
10. Chiang L, Ramchandar N, Aramkul J, Fireizen Y, Beatty ME, Monroe M, et al. Rocky Mountain spotted fever in children along the US–Mexico Border, 2017–2023. Emerg Infect Dis. 2024;30:2288–93. https://doi.org/10.3201/eid3011.231760
11. Centeno FH, Lasco T, Ahmed AA, Al Mohajer M. Characteristics of *Rickettsia typhi* infections detected with next-generation sequencing of microbial cell-free deoxyribonucleic acid in a tertiary care hospital. Open Forum Infect Dis. 2021;8:ofab147. https://doi.org/10.1093/ofid/ofab147
12. Goddard J, Norment BR. Notes on the geographical distribution of the Gulf Coast tick, *Amblyomma maculatum* (Koch) [Acari:Ixodidae]. Entomol News. 1983;94:103–4.
13. Goddard J, Paddock CD. Observations on distribution and seasonal activity of the Gulf Coast tick in Mississippi. J Med Entomol. 2005;42:176–9. https://doi.org/10.1093/jmedent/42.2.176
14. Walker DH, Dumler JS. The role of CD8 T lymphocytes in rickettsial infections. Semin Immunopathol. 2015;37:289–99. https://doi.org/10.1007/s00281-015-0480-x
15. Londoño AF, Mendell NL, Walker DH, Bouyer DH. A biosafety level-2 dose-dependent lethal mouse model of spotted fever rickettsiosis: *Rickettsia parkeri* Atlantic Rainforest strain. PLoS Negl Trop Dis. 2019;13:e0007054. https://doi.org/10.1371/journal.pntd.0007054

Address for correspondence: Kristy Murray, Department of Pediatrics, Emory University School of Medicine, 2015 Uppergate Dr, Atlanta, GA 30322, USA; email: kristy.murray@emory.edu

EID Podcast

Telework during Epidemic Respiratory Illness

The COVID-19 pandemic has caused us to reevaluate what "work" should look like. Across the world, people have converted closets to offices, kitchen tables to desks, and curtains to videoconference backgrounds. Many employees wondered if these changes will become a new normal.

During outbreaks of influenza, coronaviruses, and other respiratory diseases, telework is a tool to promote social distancing and prevent the spread of disease. As more people telework, employers are considering the ramifications of remote work on employees' use of sick days, paid leave, and attendance.

In this EID podcast, Dr. Faruque Ahmed, an epidemiologist at CDC, discusses the economic impact of telework.

Visit our website to listen:
https://go.usa.gov/xfcmN

EMERGING INFECTIOUS DISEASES®

Transmission Dynamics of Dengue Virus, Ceará State, Brazil, 2010–2025

Shirlene T.S. de Lima,[1] Ingra M. Claro,[1] Xinyi Hua,[1] Livia Sacchetto, Ronaldo de Jesus, Leda M. Simões Mello, Júlia Forato, Erika R. Manuli, Cailin McDonald, Maria Eduarda T. de Lima, Clarissa P.M. Ferraz, Larissa M.F. Duarte, Vânia A.F. Viana, Mariana Araújo Costa, Antônio Carlos Firmino, Jayra J.P.A. Abrantes, Ludmila O.C. Sena, Débora Bezerra Silva, Sônia M.S. Macedo, Ester C. Sabino, Rodrigo F. do Carmo, Julio Croda, José Luiz Proenca-Modena, William M. de Souza

We evaluated the transmission dynamics of dengue virus (DENV) during 2010–2025 in Ceará State, Brazil. Ceará has been a dengue hyperendemic region, where all 4 DENV serotypes co-circulate, predominantly DENV-1 and DENV-2, and where DENV-3 was recently reintroduced. Our findings provide an epidemiologic baseline for postlicensure dengue vaccine evaluation.

Dengue virus (DENV) is an arbovirus estimated to cause >390 million infections annually worldwide, leading to >10,000 deaths in >125 countries (*1*,*2*). DENV (Flaviviridae family) is transmitted to humans primarily by *Aedes aegypti* and *Ae. albopictus* mosquitoes (*3*) and comprises 4 genetically and antigenically distinct serotypes (DENV-1–4) (*4*). DENV infection can be categorized as dengue without warning signs, dengue with warning signs, and severe dengue, which can include death (*5*). No specific antiviral treatment is available for dengue. As of August 2026, Dengvaxia (Sanofi Pasteur, https://www.sanofi.us), Qdenga TAK-003 (Takeda, https://www.takeda.com), and Butantan-DV (Instituto Butantan, https://en.butantan.gov.br) are 3 licensed vaccines to prevent dengue; however, Dengvaxia use remains limited because of safety concerns (*6*,*7*). Brazil remains one of the most affected countries by dengue and has annual epidemics, widespread vector distribution, and co-circulation of all 4 DENV serotypes (*8*). We integrate epidemiologic and genomic methods to investigate DENV transmission dynamics during 2010–2025 in Ceará, a hyperendemic state in Brazil.

The Study

We obtained national epidemiologic data on laboratory-confirmed dengue cases during January 2010–January 2025 from Brazil's Ministry of Health. We obtained additional epidemiologic data from the Central Laboratory of Public Health of Ceará for dengue cases reported during July 2014–June 2025. We used the MiSeq platform (Illumina, https://www.illumina.com) to sequence residual quantitative reverse transcription PCR–positive DENV serum samples collected from case-patients with DENV-1–3 serotypes during February 2024–July 2025. We assigned DENV lineages by using the DENV typing tool (*9*), followed by phylogenetic reconstruction. We also performed time-series, spatial mapping, and

Author affiliations: University of Kentucky, Lexington, Kentucky, USA (S.T.S. de Lima, I.M. Claro, X. Hua, C. McDonald, W.M. de Souza); Universidade Estadual de Campinas, Campinas, Brazil (S.T.S. de Lima, L. Sacchetto, J. Forato, J.L. Proenca-Modena); Laboratório Central de Saúde Pública do Ceará, Fortaleza, Brazil (S.T.S. de Lima, C.P.M. Ferraz, L.M.F. Duarte, V.A.F. Viana, A.C. Firmino, D.B. Silva, S.M.S. Macedo); Universidade Federal de Minas Gerais, Belo Horizonte, Brazil (R. de Jesus, L.M. Simões Mello); Universidade de São Paulo, São Paulo, Brazil (E.R. Manuli, E.C. Sabino); Universidade Municipal de São Caetano do Sul, São Caetano do Sul, Brazil (E.R. Manuli); Universidade de Fortaleza, Fortaleza (M.E.T. de Lima); Laboratório Central de Saúde Pública do Acre, Rio Branco, Brazil (M.A. Costa); Laboratório Central de Saúde Pública do Rio Grande do Norte, Natal, Brazil (J.J.P.A. Abrantes); Laboratório Central de Saúde Pública do Sergipe, Aracaju, Brazil (L.O.C. Sena); Universidade Federal do Vale do São Francisco, Petrolina, Brazil (R.F. do Carmo); FIOCRUZ, Campo Grande, Brazil (J. Croda)

DOI: https://doi.org/10.3201/eid3211.260609

[1]These authors contributed equally to this article.

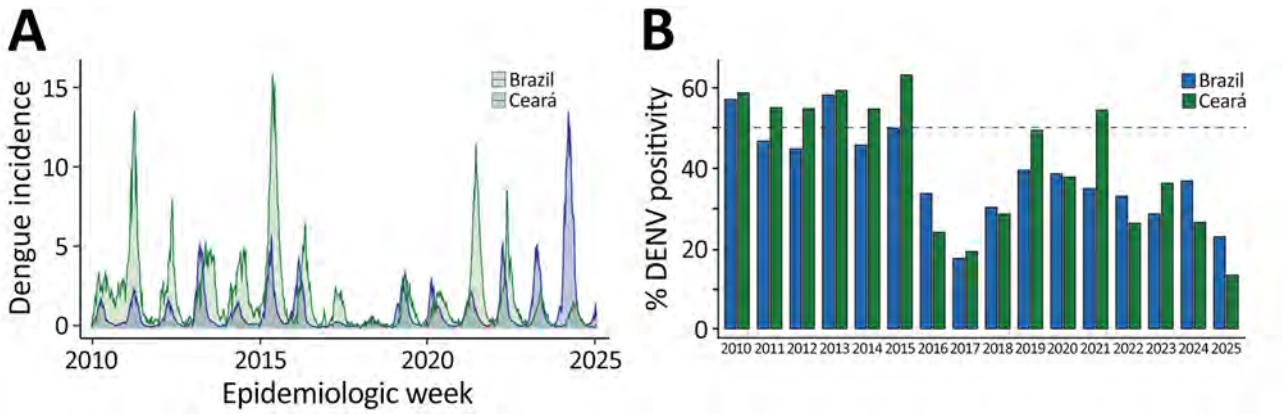

Figure 1. Dengue incidence and DENV test positivity from study of DENV transmission dynamics, Ceará State, Brazil, 2010–2025. A) Weekly incidence of laboratory-confirmed dengue cases/100,000 inhabitants at the national (Brazil) and state (Ceará) levels, from epidemiologic week 1 of 2010 (January 3–9) through epidemiologic week 4 of 2025 (January 20–26). B) Annual DENV test positivity rate (%) in Brazil and Ceará. Dashed line indicates 50% positivity. DENV, dengue virus.

demographic analyses (Appendix, https://wwwnc.cdc.gov/EID/article/32/11/26-0609-App1.pdf).

During January 3, 2010–January 25, 2025, Brazil reported 1,657,046 laboratory-confirmed dengue cases across 98.9% (5,509/5,570) of municipalities in all 26 states and the Federal District. We identified 13 major epidemic waves at the national level; annual incidence varied from 4.0 to 190.4 cases/100,000 persons tested, and the largest epidemic occurred in 2024 (Figure 1, panel A). National DENV testing positivity rate ranged from 18.2% (19,460/106,901 persons tested) to 57.1% (146,649/256,981 inhabitants) during those 15 years (Figure 1, panel B). In Ceará, a total of 131,961 laboratory-confirmed cases were reported, corresponding to a cumulative incidence of 1,500 cases/100,000 inhabitants. Ceará epidemic peaks coincided with national trends but frequently reached higher incidence and positivity rates (Figure 1).

By 2026, dengue had been reported in all 184 municipalities in Ceará; cumulative incidences range from 41.4 to 8,566 cases/100,000 inhabitants (Appendix). Nationally, dengue epidemics occurred mainly during February–June and peaked during March–April (peak monthly incidence mean 10.4 cases/100,000 inhabitants). In contrast, in Ceará, epidemics occurred during March–August, typically peaking in May (incidence mean 18.4 cases/100,000 inhabitants) (Appendix). Sex- and age-stratified analyses revealed a female-to-male ratio of 1.6 and higher incidence among female persons nationally (2-way

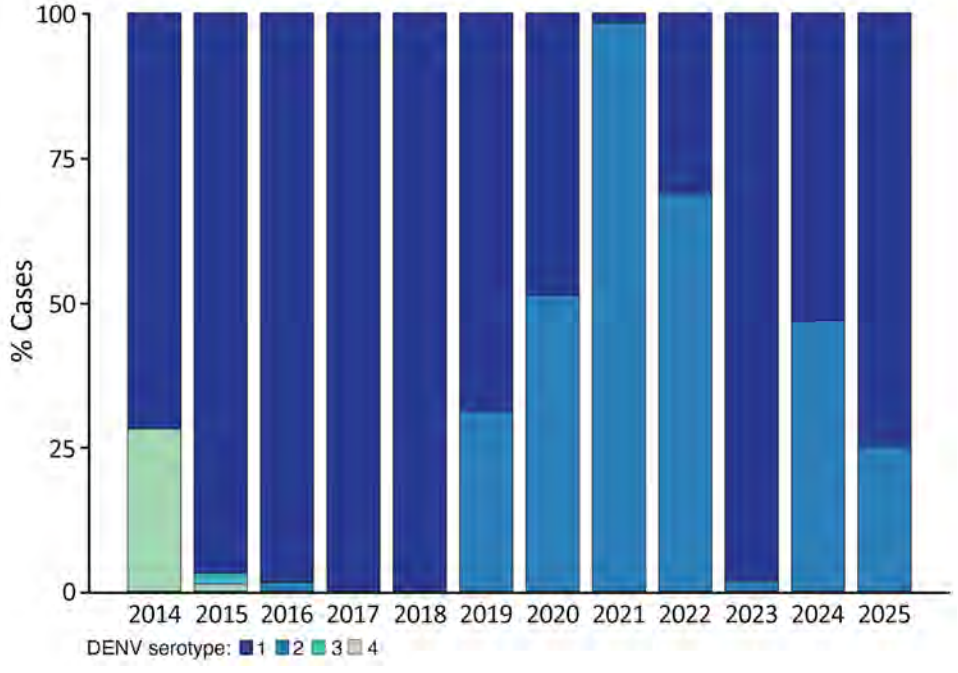

Figure 2. Annual percentage of dengue cases attributed to DENV serotypes 1, 2, 3, or 4 from study of DENV transmission dynamics, Ceará State, Brazil, 2014–2025. DENV, dengue virus.

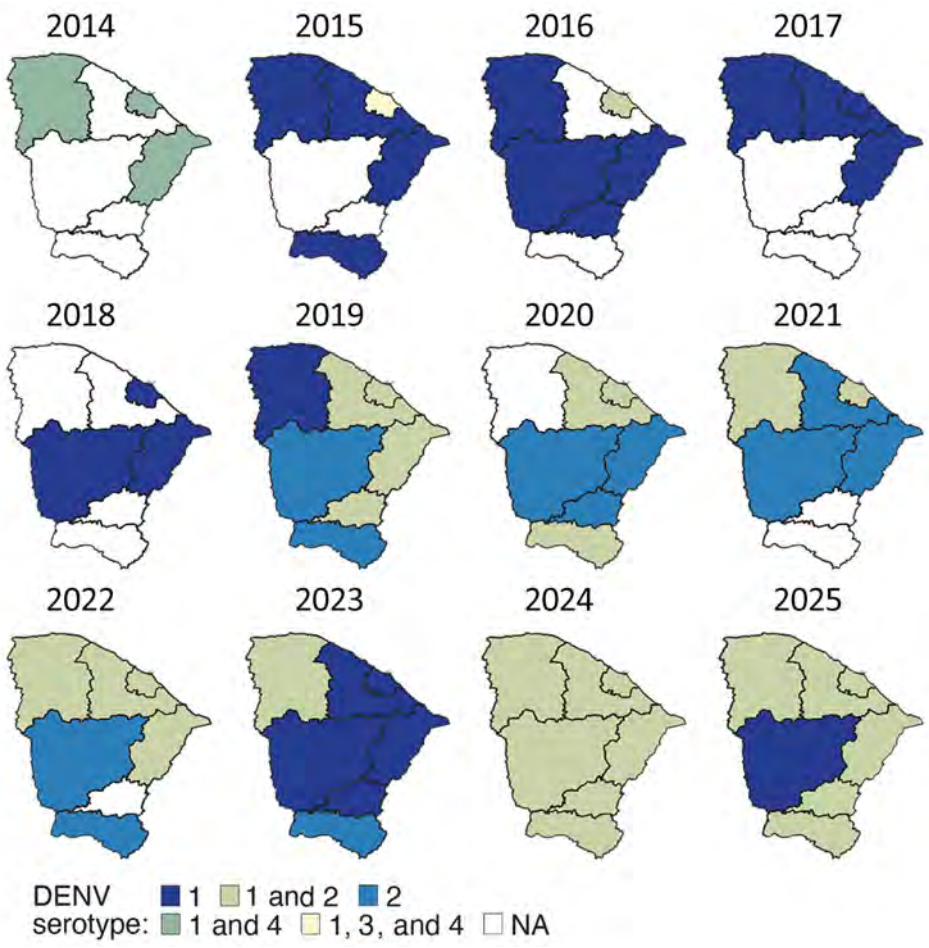

Figure 3. Annual distribution of DENV serotypes across the mesoregions from study of DENV transmission dynamics, Ceará State, Brazil, 2014–2025. DENV, dengue virus.

ANOVA test, p<0.05) and in Ceará (p<0.01) (Appendix). The cumulative incidence in Ceará was higher in persons 10–39 years of age than in persons ≥70 years of age (p<0.05) (Appendix).

We investigated the circulation of DENV serotypes in Ceará during July 2014–June 2025. DENV-1 was the predominant DENV serotype during 2014–2019 and again during 2023–2025 (Figures 2, 3). Fortaleza, the capital and most populous city in Ceará, reported co-circulation of DENV-1, DENV-3, and DENV-4 in 2015. DENV-2 reemerged in 2019, leading to its near-complete replacement of other DENV serotypes in 2021 and 2022 (Figures 2, 3). To assess current genetic diversity in Ceará, we sequenced 243 DENV genomes from cases reported during February 2024–July 2025 across 45 municipalities (Figure 4; Appendix). Cycle threshold values ranged from 10.6 to 33.0. We recovered complete or partial DENV genomes for 218 of the 243 samples (coverage 14.4%–99.2%; mean depth 16–9,877 per nucleotide) (Appendix). Among those genomes, we classified 82.6% (180/218) with >70% coverage into the following genotypes: DENV-1 V_D1.1 (n = 1), DENV-1 V_E1 (n = 111), DENV-2 II_F1.1.2 (n = 61), DENV-2 II_F1.1.5 (n = 2), DENV-2 III_C1.1 (n = 2), and DENV-3 III_B3.2 (n = 3) (*9*). We included those newly generated DENV genome sequences in maximum-likelihood phylogenetic analyses along with global DENV genome references (Appendix).

Phylogenetic analysis showed that the recent epidemic in Ceará (2024–2025) was mainly caused by DENV-1 lineage V_E1 (61.6% [n = 111 cases]). DENV lineages identified in Ceará were distributed across multiple well-supported subclades with genomes from southeast (São Paulo), central-west (Federal District, Goiás, and Mato Grosso do Sul), and northeast (Alagoas) of Brazil and from Florida (USA) and Uruguay. Lineage II_F1.1.2 (94%) predominated among DENV-2 cases, and clustered with DENV genomes from southeast and northeast Brazil and the United States (*10*). Conversely, DENV-2 II_F1.1.5 genomes grouped with sequences from France (2023–2024) and the Dominican Republic (2024), suggesting a recent international introduction. Detection of DENV-3 genomes from Ceará was consistent with a reintroduction because no local detections have occurred since 2015. Those genomes belonged to lineage III_B3.2 and

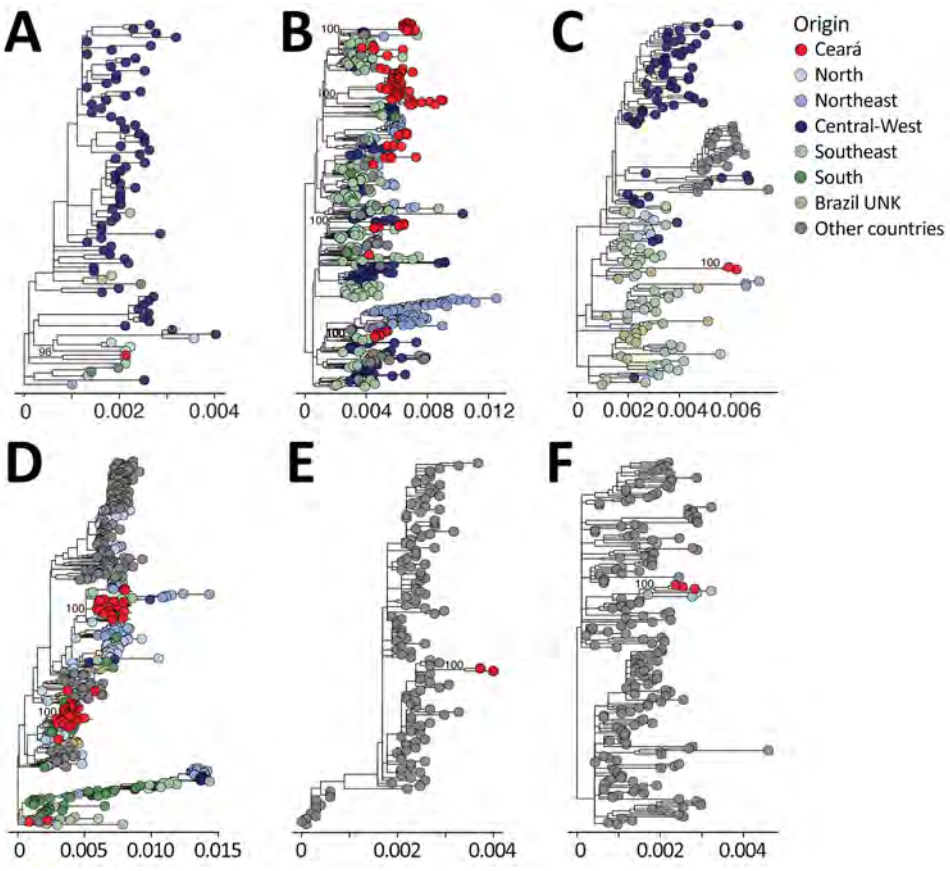

Figure 4. Maximum-likelihood phylogenetic trees of DENV lineages detected from study of DENV transmission dynamics, Ceará State, Brazil, February 2024–July 2025. A) DENV-1 lineage V_D1.1; B) DENV-1 lineage V_E1; C) DENV-2 lineage III_C1.1; D) DENV-2 lineage II_F1.1.2; E) DENV-2 lineage II_F1.1.5; F) DENV-3 lineage III_B3.2. A total of 180 DENV genomes generated in this study from Ceará were analyzed alongside publicly available global references. Final datasets comprised DENV-1 lineage V_D1.1 (n = 218), DENV-1 lineage V_E1 (n = 791), DENV-2 lineage II_F1.1.2 (n = 499), DENV-2 lineage II_F1.1.5 (n = 133), DENV-2 lineage III_C1.1 (n = 366), and DENV-3 lineage III_B3.2 (n = 734). Tips are colored by region or state of origin. Red dots indicate newly generated DENV sequences in this study. Phylogenies are midpoint-rooted for clarity. Scale bars represent substitutions per nucleotide site. Bootstrap support values (1,000 replicates) are shown at key nodes. Complete phylogenies for each lineage and GenBank accession numbers for all sequences used are provided (Appendix, https://wwwnc.cdc.gov/EID/article/32/11/26-0609-App1.pdf). DENV, dengue virus; UNK, unknown region of Brazil.

formed a well-supported clade (bootstrap 100%) with sequences from São Paulo (2024–2025) and Florida (2023) within a lineage widely circulating across the Americas, including in Cuba, the Dominican Republic, French Guiana, and Peru (Figure 4).

This study provides a 15-year overview of dengue transmission in Ceará, a dengue hyperendemic state. Our epidemiologic analyses demonstrate that dengue occurred in all 184 municipalities of Ceará and that multiple DENV epidemics reached higher incidence and testing positivity rates than national trends. Epidemic peaks typically occurred ≈1 month later and lasted longer in Ceará than the national average, which might be explained by extended periods of high temperature and humidity (*11*), supporting near year-round vector abundance and sustained DENV transmission (*3*).

We identified heterogeneous circulation of all 4 DENV serotypes and identified 6 distinct viral lineages across 3 serotypes (DENV-1, DENV-2, and DENV-3) sustained by multiple national and international introductions. We also documented the reintroduction of DENV-3, confirmed by its detection in July 2025, which could increase the risk for severe outcomes in the coming years through sequential infections and antibody-dependent enhancement after a decade of co-circulation of DENV-1 and DENV-2 (*12*). Moreover, our phylogenetic analyses showed that DENV-3 lineage III_B3.2 genomes clustered with DENV sequences detected during 2024–2025 in São Paulo State. That finding suggests a recent introduction of DENV-3 into Ceará through domestic routes, after its dissemination and sustained circulation across different regions of Brazil, rather than importation from the Caribbean and the Americas (*13*,*14*).

One limitation of our study is its reliance on variable healthcare-seeking behaviors, which might not capture the full extent of dengue cases, including asymptomatic cases. In addition, on the basis of our epidemiological data, we cannot distinguish between primary and secondary DENV infections. Moreover, we acknowledge that some dengue cases diagnosed by IgM detection might reflect cross-reactivity with Zika virus, which emerged in Brazil in 2015 (*15*). Furthermore, our genomic data are limited to 2024–2025, which, together with the

scarcity of DENV genomic data from Ceará in public genomic databases, prevents elucidation of the spatial and temporal dynamics of DENV lineages in Ceará before 2024.

Conclusions

In summary, our study described the long-term dengue transmission dynamics in Ceará, Brazil, during 2010–2025 and substantially increased the DENV genomic data from this hyperendemic region. Such genomic data enable identification of circulating and emerging DENV lineages, elucidating the spatiotemporal evolution and shifts in DENV patterns. Our findings will guide public health management and future efforts to implement dengue immunization programs using Qdenga TAK-003 and Butantan-DV in Brazil. Co-circulation of all DENV serotypes, and the current predominance of DENV-1 and DENV-2, highlight the necessity for continued serotype-specific surveillance to further monitor vaccine effectiveness.

W.M.d.S. was supported by Wellcome Trust–Digital Technology Development award (Climate Sensitive Infectious Disease Modelling; grant no. 226075/Z/22/Z) and National Institutes of Health National Institute of Allergy and Infectious Diseases (grant no. 1R01AI200941-01). J.L.P.M. is supported by the São Paulo Research Foundation (grant nos. 2022/10442-0 and 26/04488-8) and the National Council for Scientific and Technological Development (grant no. 309971/2023-3). L.S. and J.F. are supported by the São Paulo Research Foundation (grant no. 25/18991-0).

About the Author

Dr. de Lima is a researcher at the University of Campinas (Campinas, Brazil) and the University of Kentucky (Lexington, Kentucky, USA). Her research interests include epidemiologic surveillance of arboviruses and emerging RNA viruses.

References

1. Messina JP, Brady OJ, Golding N, Kraemer MUG, Wint GRW, Ray SE, et al. The current and future global distribution and population at risk of dengue. Nat Microbiol. 2019;4:1508–15. https://doi.org/10.1038/s41564-019-0476-8
2. Lim A, Shearer FM, Sewalk K, Pigott DM, Clarke J, Ghouse A, et al. The overlapping global distribution of dengue, chikungunya, Zika and yellow fever. Nat Commun. 2025;16:3418. https://doi.org/10.1038/s41467-025-58609-5
3. Liu Z, Zhang Q, Li L, He J, Guo J, Wang Z, et al. The effect of temperature on dengue virus transmission by *Aedes* mosquitoes. Front Cell Infect Microbiol. 2023;13:1242173. https://doi.org/10.3389/fcimb.2023.1242173
4. Bäck AT, Lundkvist A. Dengue viruses—an overview. Infect Ecol Epidemiol. 2013;3:3. https://doi.org/10.3402/iee.v3i0.19839
5. World Health Organization. Dengue: guidelines for diagnosis, treatment, prevention and control. 2009 Apr 21 [cited 2026 Sep 10]. https://www.who.int/publications/i/item/9789241547871
6. Sridhar S, Luedtke A, Langevin E, Zhu M, Bonaparte M, Machabert T, et al. Effect of dengue serostatus on dengue vaccine safety and efficacy. N Engl J Med. 2018;379:327–40. https://doi.org/10.1056/NEJMoa1800820
7. Cracknell Daniels B, Ferguson NM, Dorigatti I. Efficacy, public health impact and optimal use of the Takeda dengue vaccine. Nat Med. 2025;31:2663–72. https://doi.org/10.1038/s41591-025-03771-y
8. Salles TS, da Encarnação Sá-Guimarães T, de Alvarenga ESL, Guimarães-Ribeiro V, de Meneses MDF, de Castro-Salles PF, et al. History, epidemiology and diagnostics of dengue in the American and Brazilian contexts: a review. Parasit Vectors. 2018;11:264. https://doi.org/10.1186/s13071-018-2830-8
9. Fonseca V, Libin PJK, Theys K, Faria NR, Nunes MRT, Restovic MI, et al. A computational method for the identification of dengue, Zika and chikungunya virus species and genotypes. PLoS Negl Trop Dis. 2019;13:e0007231. https://doi.org/10.1371/journal.pntd.0007231
10. Gräf T, Ferreira CDN, de Lima GB, de Lima RE, Machado LC, Campos TL, et al. Multiple introductions and country-wide spread of DENV-2 genotype II (cosmopolitan) in Brazil. Virus Evol. 2023;9:vead059. https://doi.org/10.1093/ve/vead059
11. Moura MCBM, de Oliveira JV, Pedreira RM, Tavares AM, de Souza TA, de Lima KC, et al. Spatio-temporal dynamics of *Aedes aegypti* and *Aedes albopictus* oviposition in an urban area of northeastern Brazil. Trop Med Int Health. 2020;25:1510–21. https://doi.org/10.1111/tmi.13491
12. Katzelnick LC, Gresh L, Halloran ME, Mercado JC, Kuan G, Gordon A, et al. Antibody-dependent enhancement of severe dengue disease in humans. Science. 2017;358:929–32. https://doi.org/10.1126/science.aan6836
13. Pereira JS, Slavov SN, Brcko IC, Ribeiro G, de Souza VC, Ribeiro IS, et al. Unravelling dengue serotype 3 transmission in Brazil: evidence for multiple introductions of the 3III_B.3.2 lineage. Virus Evol. 2025;11:veaf034. https://doi.org/10.1093/ve/veaf034
14. Sacchetto L, Bernardi V, Brancini ML, Marques BC, Negri A, Vasilakis N, et al. Early insights of dengue virus serotype 3 (DENV-3) re-emergence in São Paulo, Brazil. J Clin Virol. 2025;176:105763. https://doi.org/10.1016/j.jcv.2025.105763
15. Katzelnick LC, Zambrana JV, Elizondo D, Collado D, Garcia N, Arguello S, et al. Dengue and Zika virus infections in children elicit cross-reactive protective and enhancing antibodies that persist long term. Sci Transl Med. 2021;13:eabg9478. https://doi.org/10.1126/scitranslmed.abg9478

Address for correspondence: William M. de Souza, University of Kentucky, Microbiology, Immunology and Molecular Genetics, 760 Elizabeth St, Lexington, Kentucky 40508, USA; email: wmdesouza@uky.edu

Post–COVID-19 Expansion of *Streptococcus pyogenes* Lineages Causing Toxic Shock Syndrome, Japan, 2023–2024

Tadayoshi Ikebe, Hitoshi Otsuka, Mari Sasaki, Takahiro Yamaguchi, Yoshimi Date, Yu Kazawa, Kazuki Saito, Kaho Ikeda, Rumi Okuno, Yukihiro Akeda; The Working Group for Beta-Hemolytic Streptococci in Japan[1]

We analyzed 919 *Streptococcus pyogenes* isolates from laboratory-confirmed streptococcal toxic shock syndrome cases in Japan during 2023–2024. Post–COVID-19 resurgence was driven by expansion of $M1_{UK}$ (49.8%) and emerging $M1_{13SNPs}$ (37.4%) lineages, replacing ancestral $M1_{global}$. $M1_{13SNPs}$ were associated with younger patient age and higher death rates in unadjusted analyses.

Streptococcal toxic shock syndrome (STSS) is a rapidly progressive, life-threatening invasive disease primarily caused by group A *Streptococcus* (*Streptococcus pyogenes*) bacteria (*1*,*2*). After relaxation of nonpharmaceutical interventions for COVID-19 in Japan, resurgence in STSS was observed, coinciding with reports of M1UK lineage expansion (3). We conducted a nationwide molecular epidemiologic study to clarify the contribution of emm1 sublineages to this increase.

The Study

This laboratory-based study analyzed *S. pyogenes* isolates from laboratory-confirmed STSS cases reported across Japan during January 1, 2023–December 31, 2024. STSS is notifiable under Infectious Disease Control Law; surveillance is coordinated by the National Institute of Infectious Diseases (NIID; Tokyo, Japan) with prefectural public health institutes and sentinel hospitals. We applied US Centers for Disease Control and Prevention criteria: isolation of group A *Streptococcus* from a normally sterile site plus clinical shock with multiorgan involvement (*4*).

A total of 919 isolates were collected from 1,477 reported STSS cases, 186 isolates in 2023 and 733 in 2024. Coverage was 62.2% overall, 45.9% in 2023, and 68.4% in 2024. Specimens from routine care were submitted to 7 regional reference laboratories (Fukushima, Tokyo, Kanagawa, Toyama, Osaka, Yamaguchi, and Oita) and NIID. Species identification was performed using API 20 Strep (bioMérieux, https://www.biomerieux.com), and Lancefield group determination used latex agglutination kits (Iwaki Corporation, https://www.iwaki-kk.co.jp). The NIID Ethics Review Board approved this public health surveillance under Article 15 of the Infectious Disease Law; individual consent was waived.

We performed *emm* genotyping by PCR and sequencing of the 5′ region using primers emm-1/emm-2 and sequencing primer emmseq2 with 180-bp sequences matched to the CDC emm database (*5*). We assessed *speA* and *speC* genes by primers described previously (*6*). Among the *emm1* isolates, we identified $M1_{UK}$, $M1_{23SNPs}$, $M1_{13SNPs}$, and $M1_{global}$ lineages using allele-specific PCR targeting single-nucleotide polymorphisms (SNPs) in *rofA*, *gldA*, and *pstB* (*7*).

To investigate the differences between the $M1_{UK}$ strain and the $M1_{13SNPs}$ strain, we amplified the

Author affiliations: National Institute of Infectious Diseases, Tokyo, Japan (T. Ikebe, Y. Akeda); Yamaguchi Prefectural Institute of Public Health and Environment, Yamaguchi, Japan (H. Otsuka); Oita Prefectural Institute of Health and Environment, Oita, Japan (M. Sasaki); Osaka Institute of Public Health, Osaka, Japan (T. Yamaguchi); Kanagawa Prefectural Institute of Public Health, Kanagawa, Japan (Y. Date); Fukushima Prefectural Institute of Public Health, Fukushima, Japan (Y. Kazawa); Toyama Institute of Health, Toyama, Japan (K. Saito, K. Ikeda); Tokyo Metropolitan Institute of Public Health, Tokyo (R. Okuno)

DOI: https://doi.org/10.3201/eid3211.260336

[1]Additional members of this group who contributed data are listed at the end of this article.

upstream region of the *speA* gene using the M1UK forward (cctagtctatacagccaaaaagc) primer and the M1UK reverse (gcattgatggagctggtggg) primer and sequenced them using the M1UKseq1 (tatacagccaaaaagcgagg) primer. We confirmed that mutations observed in the $M1_{UK}$ strain were not present in all the strains obtained as $M1_{13SNPs}$, which was consistent with the results of allele-specific PCR targeting SNPs in *rofA*, *gldA*, and *ptsB*. We conducted statistical analyses in Ekuseru-Toukei version 4.10 (Social Survey Research Information Co., Ltd, https://bellcurve.jp) using *t* test for age and Fisher exact test for deaths; we considered $p<0.05$ significant.

Among 919 STSS isolates, we identified 31 *emm* types, including 2 untypeable strains with signal sequence deletions (Appendix Table 1, https://wwwnc.cdc.gov/EID/article/32/11/26-0336-App1.pdf). Type *emm1* predominated (470/919, 51.1%), followed by *emm12* (12.3%), *emm89* (11.5%), *emm49* (7.9%), and *emm81* (5.8%), accounting for >85% of isolates overall (Appendix Figure 1, panel A). After adjusting for collection rates (Appendix Table 2), *emm1* increased markedly in 2024 (Appendix Figure 1, panel B). National surveillance data showed *emm1*-associated STSS declined during 2020–2022 but rose after mask policy relaxation (March 13, 2023), reaching 60–80 cases/month during January–June 2024 (*8*,*9*). Most other types (*emm89*, *emm81*, *emm49*) remained stable, whereas *emm12* also increased (Figure 1).

Among 470 *emm1* isolates, we identified $M1_{UK}$ (234 [49.8%]), $M1_{13SNPs}$ (176 [37.4%]), and $M1_{global}$ (60 [12.8%]) lineages. Compared with 2019 ($M1_{global}$ >60%; $M1_{UK}$ 24%; $M1_{13SNPs}$ 12%), 2023–2024 showed replacement: $M1_{UK}$ increased from 44% to 51% and $M1_{13SNPs}$ from 29% to 39%, but $M1_{global}$ decreased from 26% to 11% (Appendix Figure 2). Each lineage rose after mask relaxation (Figure 2).

Among the 470 *emm1* isolates, 458 (97.4%) were *speA* positive: 283 (60.2%) *speA*-only, 175 (37.2%) both *speA* and *speC*, and 8 (1.7%), *speC*-only. Four (0.9 %) were positive but for neither *speA* nor *speC*. $M1_{UK}$ mainly carried *speA*-only (202 [86.3%]), $M1_{13SNPs}$ harbored both genes (143 [81.3%]), and $M1_{global}$ was predominantly *speA*-only (55 [90.2%]) (Appendix Table 3).

$M1_{13SNPs}$ infections occurred in younger patients (average age 58.3 years; interquartile range [IQR] 43–75 years) and were associated with higher risk

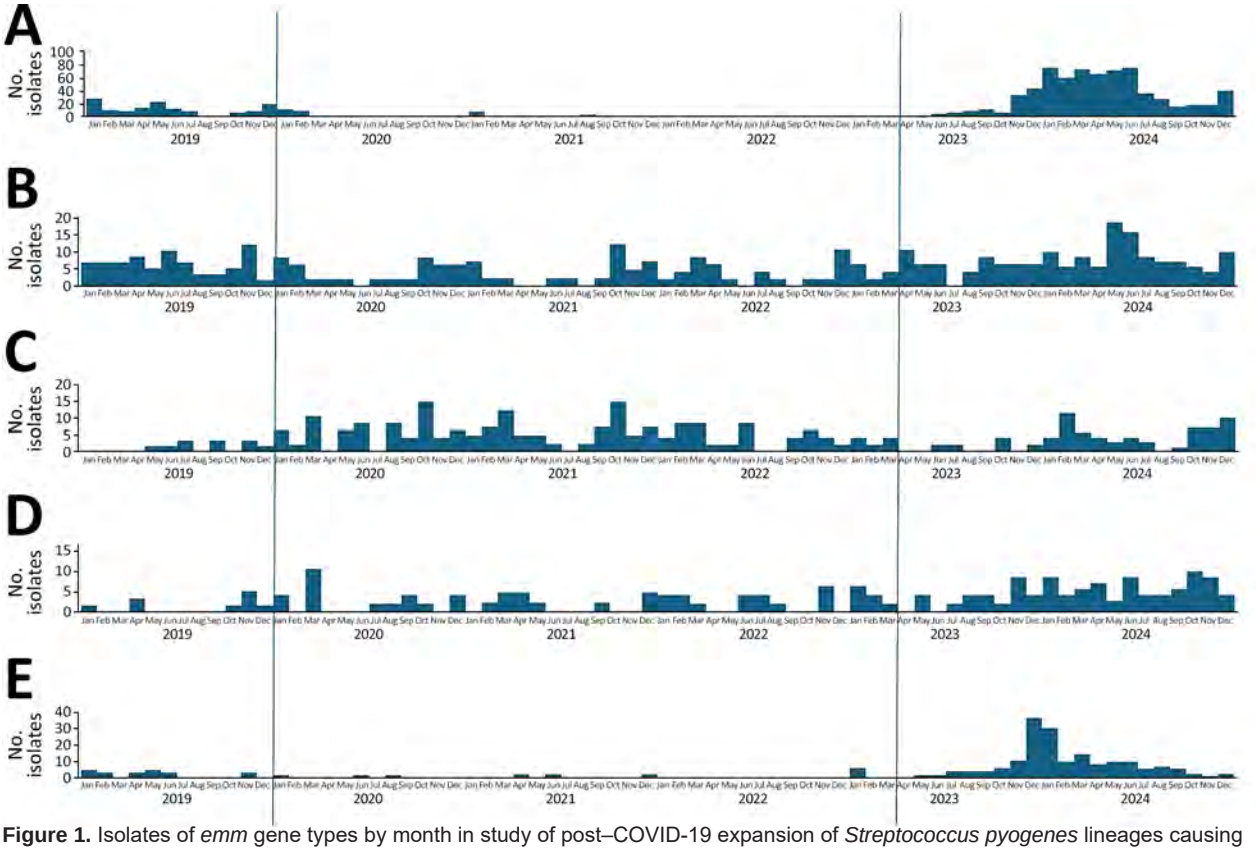

Figure 1. Isolates of *emm* gene types by month in study of post–COVID-19 expansion of *Streptococcus pyogenes* lineages causing toxic shock syndrome, Japan, 2023–2024. y-axis indicates the number of calculated 100% isolates of each *emm* type: A) *emm1*; B) *emm89*; C) *emm81*; D) *emm49*; E) *emm12*. Vertical lines separate pre–COVID-19, COVID-19, and post–COVID-19 periods.

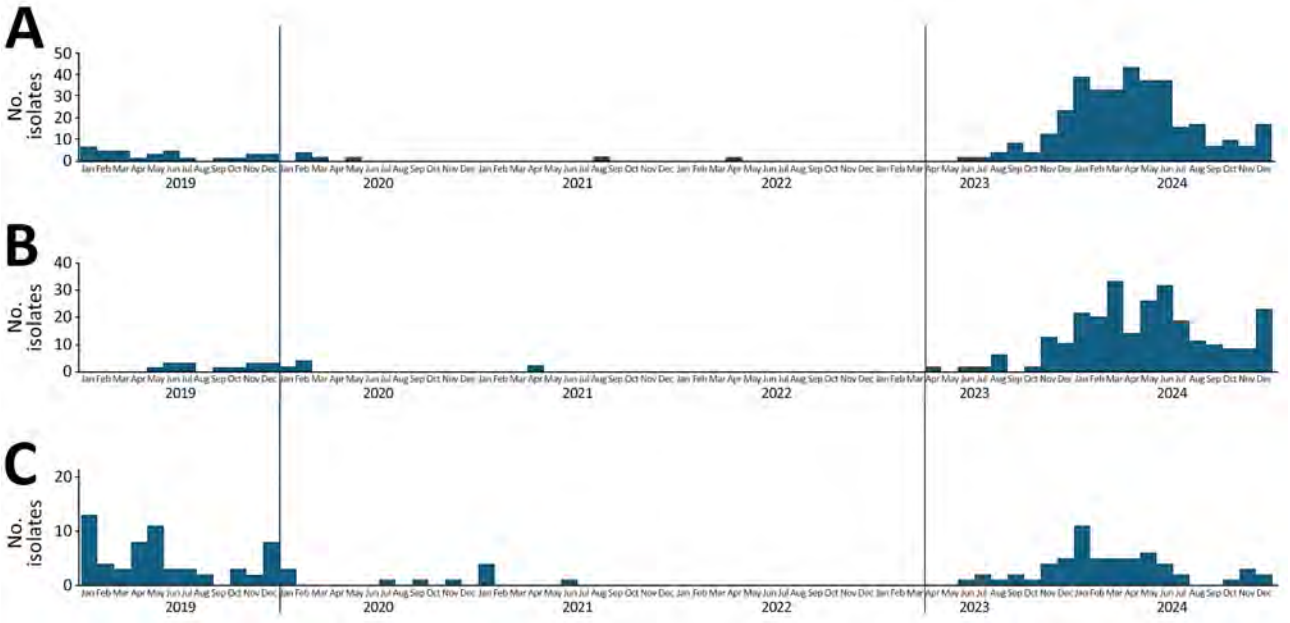

Figure 2. Isolates of M1 lineages by month in study of post–COVID-19 expansion of *Streptococcus pyogenes* lineages causing toxic shock syndrome, Japan, 2023–2024. y-axis indicates the number of calculated 100% isolates of each lineage: A) $M1_{UK}$; B) $M1_{13SNPs}$; C) $M1_{global}$. Vertical lines separate pre–COVID-19, COVID-19, and post–COVID-19 periods.

for death (mortality rate 31.3%) than non-*emm1* cases isolated during the same period, in which the average age was 62.7 (IQR 50–78) years and mortality rate 23.2%. $M1_{UK}$ also affected younger patients (average age 54.9 [IQR 41–69] years) but showed comparable mortality rate (20.5%), whereas $M1_{global}$ showed no significant differences in either age (average age 58.9 [IQR 46–72] years) or mortality rate (20.0%) (Table 1).

$M1_{13SNPs}$ infections are associated with younger patients and higher mortality rate. Because age is a major determinant of STSS outcomes, we assessed the association between age and mortality to confirm that the observed differences in mortality were not influenced by age. Although we observed no significant differences in sex or age distribution between cases of STSS caused by $M1_{13SNPs}$ and those caused non-*emm1* strains (Table 2), mortality was significantly higher in patients with $M1_{13SNPs}$ infections (31.3% vs. 23.2%; odds ratio [OR] 1.51 [95% CI 1.02–2.22]). Age-stratified analysis further revealed significantly higher mortality in the $M1_{13SNPs}$ group among patients 25–39 years of age (OR 5.00 [95% CI 1.29–19.3]) and 70–84 years of age (OR 2.24 [95% CI 1.14–4.41]).

Conclusions

Nationwide surveillance links Japan's post–COVID-19 STSS resurgence to expansion of *emm1 S. pyogenes*, driven by replacement of $M1_{global}$ with $M1_{UK}$ and $M1_{13SNPs}$ lineages. That pattern parallels $M1_{UK}$ increases reported in Europe (*9*,*10*) and highlights the emergence of $M1_{13SNPs}$, which was associated with higher mortality than were non-*emm1* strains, as well as diversity in *speA*/*speC* profiles and a younger age distribution.

The temporal association with relaxation of nonpharmaceutical interventions suggests increased opportunities for transmission in school and community settings. Clinical heterogeneity observed among *emm1* sublineages underscores the value of lineage-level molecular surveillance for risk assessment.

Limitations of our study included 62% coverage of reported cases, restriction to STSS cases,

Table 1. Clinical outcomes by lineage in study of post–COVID-19 expansion of *Streptococcus pyogenes* causing toxic shock syndrome, Japan, 2023–2024*

Lineage	No. cases	Average age (IQR), y	p value†	No. (%) deaths	p value†
$M1_{UK}$	234	54.6 (41–69)	<0.0001	48 (20.5)	0.4403
$M1_{13SNPs}$	176	58.5 (43–75)	0.0391	55 (31.3)	0.0412
$M1_{global}$	60	58.9 (46–72)	0.1158	12 (20.0)	0.7431
Non-*emm1*	449	62.7 (50–78)	Referent	104 (23.2)	Referent

*IQR, interquartile range.
†By Fisher exact test, significant at p<0.05 comparison with non-*emm1*. p values are unadjusted and should be interpreted with caution because they do not account for potential confounding factors such as underlying conditions, disease severity, or differences in initial treatment.

Table 2. Characteristics of patients with toxic shock syndrome by the causative strain of *Streptococcus pyogenes*, Japan, 2023–2024*

Characteristic	No. (%) $M1_{13SNPs}$	No. (%) with non-*emm1*	Crude RR (95% CI)	Crude OR (95% CI)	p value†
No. patients	176	449			
Sex					
M	94 (53.4)	273 (60.8)	Referent	Referent	
F	82 (46.6)	176 (39.2)	1.09 (0.98–1.21)	1.35 (0.95–1.92)	0.1040
Age group, y					
0–24	12 (6.8)	17 (3.8)	1.03 (0.99–1.08)	1.86 (0.87–3.98)	0.1368
25–39	22 (12.5)	39 (8.7)	1.04 (0.98–1.11)	1.50 (0.86–2.61)	0.1768
40–54	37 (21.0)	83 (18.5)	1.03 (0.85–1.13)	1.17 (0.76–1.81)	0.4985
55–69	43 (24.4)	118 (26.3)	0.98 (1.88–1.08)	0.91 (0.61–1.36)	0.6847
70–84	48 (27.3)	134 (29.8)	0.96 (0.87–1.08)	0.88 (0.60–1.30)	0.5579
≥85	14 (8.0)	58 (12.9)	0.85 (0.89–1.00)	0.58 (0.32–1.07)	0.0944
Deaths					
All ages	55 (31.3)	104 (23.2)	1.12 (1.00–1.25)	1.51 (1.02–2.22)	0.0412
0–24	0 (0)	1 (5.9)	0.94 (0.84–1.06)	0	1.0000
25–39	8 (36.4)	4 (10.3)	1.41 (1.01–1.97)	5.00 (1.29–19.3)	0.0202
40–54	4 (10.8)	19 (22.9)	0.86 (0.74–1.02)	0.41 (0.13–1.30)	0.1395
55–69	13 (30.2)	22 (18.6)	1.17 (0.94–1.44)	1.89 (0.85–4.20)	0.1326
70–84	23 (47.9)	39 (29.1)	1.36 (1.01–1.82)	2.24 (1.14–4.41)	0.0217
≥85	7 (50.0)	19 (32.8)	1.34 (0.77–2.33)	2.05 (0.63–6.70)	0.3525

*RR and OR between $M1_{13SNPs}$ and non-*emm1* are derived from univariate logistic regression analysis. OR and p values are unadjusted and should be interpreted with caution because they do not account for potential confounding factors such as underlying comorbidities, disease severity, or differences in initial treatment. OR, odds ratio; RR, risk ratio.
†By Fisher exact test.

limited study periods, and incomplete clinical data use that required us to perform unadjusted analyses. Although infection with $M1_{13SNPs}$ was associated with higher mortality, that finding should be interpreted cautiously because it might be affected by unmeasured confounding factors such as underlying conditions, treatment differences, or disease severity. Our results should therefore be considered exploratory and do not establish an independent effect of the $M1_{13SNPs}$ lineage on clinical outcomes.

Nonetheless, application of standardized national methods to 919 isolates provided evidence of rapid lineage replacement. We recommend continued molecular surveillance needed to monitor $M1_{UK}$ and $M1_{13SNPs}$ globally, identify emerging variants, and inform public health responses to future *S. pyogenes* epidemics.

Other members of the Working Group for Beta-Hemolytic Streptococci in Japan: Rin Satoh, Yui Kawabata (Hokkaido Institute of Public Health); Yusei Sekiya (Akita Prefectural Research Center for Public Health and Environment); Takuya Yamanaka (Iwate Prefectural Research Institute for Environmental Sciences and Public Health); Mayu Suzuki (Yamagata Prefectural Institute of Public Health); Satoko Yamaya (Miyagi Prefectural Institute of Public Health and Environment); Naomi Kogure (Niigata Prefectural Institute of Public Health and Environmental Sciences); Ryoya Akiyama (Niigata City Institute of Public Health and Environment); Yumi Uchitani (Tokyo Metropolitan Institute of Public Health); Yumi Tamura (Sagamihara City Institute of Public Health); Kentaro Tomari (Saitama City Institute of Health Science and Research); Daichi Sakamoto (Saitama Prefectural Institute of Public Health); Yoshiho Takahashi (Shizuoka City Institute of Environmental Sciences and Public Health); Takahiro Shimoda (Gunma Prefectural Institute of Public Health and Environmental Sciences); Akira Wakatsuki (Utsunomiya City Institute of Public Health and Environment); Asami Sekikawa (Tochigi Prefectural Institute of Public Health and Environmental Science); Akio Nagano (Chiba City Institute of Health and Environment); Emiri Nishizato, Yusuke Yodotani (Kawasaki City Institute for Public Health); Natsuko Kawabata, Yuko Matsumoto, Takako Katakura (Yokosuka City Institute of Public Health); Takako Nakayama, Mitsuru Kishizawa (Chiba Prefectural Institute of Public Health); Yurie Uchiyama (Nagano Environmental Conservation Research Institute); Marino Oichi (Mie Prefecture Health and Environment Research Institute); Sachiko Nakamura (Ishikawa Prefectural Institute of Public Health and Environmental Science); Mio Nishide (Kanazawa City Environmental Sanitation Testing Center); Noriko Saito (Aichi Prefectural Institute of Public Health); Koji Yokoyama, Shiho Tajima (Fukui Prefectural Institute of Public Health and Environmental Science); Tomohiro Yamaguchi (Gifu Prefectural Research Institute for Health and Environmental Sciences); Chiho Furuta (Gifu Municipal Institute of Public Health); Masaki Anraku (Osaka Institute of Public Health); Shinya Okita, Hidenobu Shimizu (Kyoto City Institute of Health and Environmental Sciences); Kenji Konaka, Yoshiyuki Kawahara (Kyoto Prefectural Institute of Public Health and Environment); Naoaki Iwasaki (Sakai City Institute of Public Health); Mayako Koide (Shiga Prefectural Institute of Public Health); Noriko Nakanishi, Shoko Komatsu (Kobe Institute of Health); Miyuki Saeki, Yui Tsukiyama (Nara Prefecture Institute of Health); Kento Tarao, Shoko

Hirata (Amagasaki City Institute of Public Health); Haruka Takeshita (Himeji City Institute of Environment and Health); Maho Ikebata (Hyogo Prefectural Institute of Public Health Science); Akira Kuwata (Wakayama Prefectural Research Center of Environment and Public Health); Takakiyo Ikebata (Wakayama City Institute of Public Health); Momoho Onda (Tottori Prefectural Institute of Public Health and Environmental Science); Jun Kawase, Yuta Kawakami (Shimane Prefectural Institute of Public Health and Environmental Science); Hisahiro Kawai (Okayama Prefectural Institute for Environmental Science and Public Health); Takahiro Hiratsuka, Keiko Ishii (Hiroshima Prefectural Technology Research Institute, Public Health and Environment Center); Hiromi Tsukiji (Hiroshima City Institute of Public Health); Chizuko Kimura, Shintarou Hirai (Ehime Prefectural Institute of Public Health and Environmental Science); Atsuko Kageyama, Masami Uchida (Kochi Prefectural Public Health and Environmental Science Research Institute); Chiharu Katamune (Fukuoka Institute of Health and Environmental Sciences); Yuri Abe (Fukuoka City Institute of Health and Environment); Etsuko Nakamura (Kitakyushu City Institute of Health and Environmental Sciences); Yumiko Amari (Saga Prefectural Institute of Public Health and Pharmaceutical Research); Yuji Migita (Nagasaki Prefectural Institute of Environment and Public Health); Emi Ogawa (Miyazaki Prefectural Institute for Public Health and Environment); Tsuyoshi Kudeken (Okinawa Prefectural Institute of Health and Environment). Aomori Prefectural Institute of Health, Sendai City Public Health Institute, Kagawa Prefectural Research Institute for Environmental Science and Public Health, and Tokushima Prefectural Public Health Pharmaceutical and Environmental Sciences Center are also represented in the Working Group.

This work was supported by the Ministry of Health, Labour and Welfare of Japan (grant no. 25HA2001).

About the Author

Dr. Ikebe is a microbiologist at the National Institute of Infectious Diseases in Tokyo, Japan. His research interests include the microbiology of β-hemolytic streptococci.

References

1. Brouwer S, Rivera-Hernandez T, Curren BF, Harbison-Price N, De Oliveira DMP, Jespersen MG, et al. Pathogenesis, epidemiology and control of group A *Streptococcus* infection. Nat Rev Microbiol. 2023;21:431–47. https://doi.org/10.1038/s41579-023-00865-7
2. Stevens DL, Bryant AE. Severe group A streptococcal infections. In: Ferretti JJ, Stevens DL, Fischetti VA, eds. *Streptococcus pyogenes*: basic biology to clinical manifestations. 2nd ed. Oklahoma City (OK): University of Oklahoma Health Sciences Center; 2022. p. 583–604.
3. Japan Institute for Health Security, National Institute of Infectious Diseases. Risk assessment for streptococcal toxic shock syndrome (STSS) in Japan. 2024 [cited 2026 Feb 12]. https://id-info.jihs.go.jp/en/risk-assessment/streptococcal-toxic-shock-syndrome/240701_NIID_STSS_2_Eng.pdf
4. Centers for Disease Control and Prevention. Case definition: streptococcal toxic shock syndrome [cited 2026 Feb 12]. https://www.cdc.gov/group-a-strep/hcp/clinical-guidance/streptococcal-toxic-shock-syndrome.html
5. Beall B, Facklam R, Thompson T. Sequencing *emm*-specific PCR products for routine and accurate typing of group A streptococci. J Clin Microbiol. 1996;34:953–8. https://doi.org/10.1128/jcm.34.4.953-958.1996
6. Ikebe T, Murayama S, Saitoh K, Yamai S, Suzuki R, Isobe J, et al.; Working Group for Streptococci in Japan. Surveillance of severe invasive group-G streptococcal infections and molecular typing of the isolates in Japan. Epidemiol Infect. 2004;132:145–9. https://doi.org/10.1017/S0950268803001262
7. Zhi X, Li HK, Li H, Loboda Z, Charles S, Vieira A, et al. Emerging invasive group A *Streptococcus* $M1_{UK}$ lineage detected by allele-specific PCR, England, 2020. Emerg Infect Dis. 2023;29:1007–10. https://doi.org/10.3201/eid2905.221887
8. Ikebe T, Okuno R, Uchitani Y, Yamaguchi T, Isobe J, Maenishi E, et al.; Working Group for Beta-Hemolytic Streptococci in Japan. Epidemiological shifts in and impact of COVID-19 on streptococcal toxic shock syndrome in Japan: a genotypic analysis of group A *Streptococcus* isolates. Int J Infect Dis. 2024;142:106954. https://doi.org/10.1016/j.ijid.2024.01.021
9. Vieira A, Wan Y, Ryan Y, Li HK, Guy RL, Papangeli M, et al. Rapid expansion and international spread of $M1_{UK}$ in the post-pandemic UK upsurge of *Streptococcus pyogenes*. Nat Commun. 2024;15:3916. https://doi.org/10.1038/s41467-024-47929-7
10. Vesty A, Ren X, Sharma P, Lorenz N, Proft T, Hardaker A, et al. The emergence and impact of the $M1_{UK}$ lineage on invasive group A *Streptococcus* disease in Aotearoa New Zealand. Open Forum Infect Dis. 2024;11:ofae457. https://doi.org/10.1093/ofid/ofae457

Address for correspondence: Tadayoshi Ikebe, Department of Bacteriology I, National Institute of Infectious Diseases, Japan Institute for Health Security, 1-23-1 Toyama, Shinjuku-ku, Tokyo 162-8640, Japan; email: ikebe.t@jihs.go.jp

Middle East Respiratory Syndrome Coronavirus in Camels, Kazakhstan, 2025

Aidyn Kydyrmanov,[1] Yermukhammet Kassymbekov, Sardor Nuralibekov, Temirlan Sabyrzhan, Yelizaveta Khan, Marat Kumar, Aigerim Abdimadiyeva, Kobey Karamendin[1]

In 2025, a respiratory disease outbreak occurred among camels in Kazakhstan. We detected Middle East respiratory syndrome coronavirus by using quantitative reverse transcription PCR in 38 symptomatic camels, demonstrating active circulation in Central Asia. Our findings highlight the need for enhanced surveillance to assess zoonotic transmission risk.

Middle East respiratory syndrome coronavirus (MERS-CoV) is a zoonotic betacoronavirus primarily found in dromedary camels and capable of causing severe respiratory disease in humans (*1*–*3*). MERS-CoV circulates widely in camel populations in the Arabian Peninsula and Africa (*4*), whereas data from Central Asia remain limited. In Kazakhstan, serologic investigations conducted in 2015 found no evidence of MERS-CoV infection in camelids (*5*). A study published in 2022, detected antibodies reactive to MERS or MERS-like coronaviruses in both Bactrian and dromedary camels, suggesting previous exposure without molecular evidence of active infection (*6*). Molecular testing of 48 asymptomatic camels sampled from the same population in 2020 was negative for MERS-CoV (*7*), and no viral RNA was detected in 13 samples collected from symptomatic camels in the same herd in 2023. In late November 2025, camel herders in the Mangystau region of Kazakhstan reported a respiratory disease outbreak affecting multiple herds. We investigated whether MERS-CoV was circulating during that outbreak.

The Study

The Mangystau region in southwestern Kazakhstan, which borders Turkmenistan and Uzbekistan, contains approximately one third of the country's camel population (Figure 1). In western Kazakhstan, camel production primarily involves extensive pastoral and seminomadic systems with seasonal animal movement, mixed dromedary–Bactrian herds, and congregation at shared grazing areas and watering points, which might enable pathogen transmission between herds.

The outbreak began in late November 2025, when temperatures were below freezing. Affected animals were predominantly dromedaries, although affected Bactrian camels were also found in mixed herds. Clinical signs included lacrimation, nasal discharge, and intermittent cough, which were observed in both juvenile and adult camels. Questionnaire data from camel breeders and veterinary practitioners, indicated similar respiratory disease in multiple areas of Mangystau region, and comparable signs were also reported by camel breeders in Turkistan region.

During December 1–18, 2025, we collected nasopharyngeal swab samples from 38 symptomatic camels from multiple MERS-CoV–positive herds or households in different settlements within the rural district. That sampling accounted for ≈1.2% of the 3,190 camels registered in the affected rural district.

We extracted viral RNA from the nasal swab samples and evaluated for MERS-CoV RNA by using 1-step quantitative reverse transcription PCR (qRT-PCR) targeting the upstream envelope (upE) and open reading frame (ORF) 1a (*8*,*9*). All 38 samples tested positive for MERS-CoV RNA with both assays (Table). Cycle threshold (Ct) values for upE ranged from 23.14–33.09 (median 29.31), and for ORF1a ranged from 14.33–31.09 (median 25.89). Approximately 4 months after the outbreak, we collected follow-up nasopharyngeal swab and serum samples from 14 camels in previously affected herds; all nasopharyngeal swabs

Authors affiliation: Research and Production Center for Microbiology and Virology, Almaty, Kazakhstan

DOI: https://doi.org/10.3201/eid3211.260394

[1]These authors contributed equally to this work and share first and last authorship.

Figure 1. Choropleth representation of camel density used in a study of Middle East respiratory syndrome coronavirus camels, Kazakhstan, 2025. Camel sampling sites and areas with anecdotal reports of symptomatic camels are shown. Colors indicate animals/100 km^2 in Kazakhstan and surrounding countries. All spatial data processing, density calculations, and map visualization were conducted by using QGIS (version 3.40.12, https://qgis.org). All spatial data were projected in by using the World Geodetic System 1984 (EPSG:4326). Map design displays geographic coordinates so that equal angular intervals of longitude and latitude are represented uniformly, despite corresponding to different ground distances, producing an elongation of the study area.

were MERS-CoV–negative by qRT-PCR. To evaluate potential causes of infection, we tested samples for influenza A and D viruses, bovine paramyxovirus, and herpesviruses by using molecular assays; all results were negative.

For molecular confirmation, we amplified partial RNA-dependent RNA polymerase gene fragments from a subset of MERS-CoV–positive samples by using pancoronavirus RT-PCR assays (*10*), and sequenced selected amplicons. We performed whole-genome sequencing for 1 representative virus and obtained complete spike gene sequences from 4 outbreak-associated viruses (*11*). Our whole-genome phylogenetic analysis placed the Kazakhstan genome within clade B5, clustering with contemporary camel-derived viruses from Saudi Arabia and Egypt (2023–2024) (Figure 2). Phylogenetic analysis of the 4 complete spike gene sequences placed the viruses from Kazakhstan within the recently described B5-2023.4 sublineage, forming a well-supported cluster with contemporary camel viruses from Saudi Arabia (Figure 3).

Comparison with recently available complete MERS-CoV genomes showed that the viruses from Kazakhstan shared spike protein substitutions P97L, G198D, and L495P with contemporary B5-2023.4 viruses, although we did not identify the L450F substitution among the publicly available genomes analyzed. Both L450F and L495P substitutions were located within the receptor-binding domain.

We performed a recombination analysis by using Recombination Detection Program version 4.101 (http://web.cbio.uct.ac.za/~darren/rdp.html), which identified 2 putative recombination events involving the Kazakhstan genome that were supported by multiple independent detection methods (Appendix 1, https://wwwnc.cdc.gov/EID/article/32/11/26-0394-App1.pdf). The inferred recombinant regions overlapped those previously reported among contemporary B5 viruses from Saudi Arabia, and 1 inferred parental lineage could not be assigned with certainty (Appendix 2, https://wwwnc.cdc.gov/EID/article/32/11/26-0394-App2.xlsx). Our findings are consistent with the recurrent within-lineage recombination previously described (*12*). However, additional complete genome sequences are required to determine the frequency and evolutionary significance of those recombination events in Central Asia.

Conclusions

We provided molecular evidence of active MERS-CoV infection in camels in Kazakhstan, extending the documented geographic range of virus circulation into Central Asia. Earlier regional investigations detected serologic reactivity without RNA confirmation (*6*), and nationwide screening conducted during 2020–2021 did not find MERS-CoV antibodies in sampled camels (*7*). The detection of MERS-CoV RNA during the 2025 outbreak suggests active infection in camel populations in Kazakhstan. That detection also likely reflects targeted sampling of acutely symptomatic animals exhibiting extensive nasal discharge and

coughing, with clinical signs occasionally linked to MERS-CoV, particularly in younger camels (*9*).

We detected MERS-CoV RNA in both juvenile and adult camels. Although viral RNA is often detected more frequently in juveniles in endemic settings, adult camels remain susceptible to infection and reinfection, with differences in detection patterns likely reflecting levels of preexisting immunity and duration of viral shedding (*13*). The occurrence of infection across multiple age groups in this outbreak is consistent with active virus transmission within affected herds. Together, those findings indicate that active MERS-CoV infection occurs in camel populations in Kazakhstan and highlight the need for expanded surveillance to better define its epidemiology.

Our whole-genome and spike gene phylogenetic analyses placed the viruses from Kazakhstan within the contemporary B5-2023.4 sublineage of MERS-CoV circulating among camels in the Arabian Peninsula. Previous studies have suggested enhanced replication and transmission fitness for some clade B MERS-CoV lineages from the Arabian Peninsula (*14*). Although the viruses from Kazakhstan clustered with contemporary Arabian B5 lineage viruses, the available genomic data do not permit inference of viral phenotype or transmissibility. Detection of a closely related lineage in a region with limited molecular evidence of active MERS-CoV circulation highlights the need for continued surveillance and genomic characterization.

Our genomic analyses revealed that most spike protein substitutions identified in the viruses from Kazakhstan have previously been reported among contemporary B5-2023.4 viruses, whereas the L450F substitution was not identified among the publicly available

Table. Results of quantitative reverse transcription PCR of nasopharyngeal swab samples positive for Middle East respiratory syndrome coronavirus, Kazakhstan, 2025*

Camel species	Age, y	Consistent clinical signs	UpE, Ct	ORF1a, Ct	RdRp, bp	Sequenced†
Dromedary	12	Nasal discharge	27.94	24.13	760	NA
Dromedary	10	Nasal discharge	30.80	26.60	760	NA
Bactrian	<1	Nasal discharge	29.37	25.29	760	NA
Bactrian	6	Nasal discharge	26.90	22.50	760	760-nt RdRp
Dromedary	4	Nasal discharge	34.30	30.13	NA	NA
Dromedary	13	Nasal discharge	33.40	29.78	NA	NA
Dromedary	10	Nasal discharge	31.65	28.25	NA	NA
Dromedary	12	Nasal discharge	27.20	22.30	760	760-nt RdRp and full spike gene
Bactrian	12	Nasal discharge	28.43	25.97	440	440-nt RdRp and full spike gene
Bactrian	8	Nasal discharge	30.60	27.00	440	440-nt RdRp
Bactrian	12	Nasal discharge	28.90	24.70	NA	NA
Dromedary	<1	Nasal discharge	23.56	20.66	760	Whole genome
Dromedary	<1	Nasal discharge	26.55	22.40	760	NA
Bactrian	7	Nasal discharge	31.19	26.41	NA	NA
Dromedary	9	Nasal discharge	28.70	25.10	NA	NA
Dromedary	10	Nasal discharge	29.05	22.22	NA	NA
Bactrian	8	Nasal discharge	32.10	28.02	NA	NA
Dromedary	10	Nasal discharge	23.82	14.33	760	Full spike gene
Dromedary	<1	Nasal discharge	33.09	30.61	760	NA
Dromedary	14	Nasal discharge	28.93	26.63	760	NA
Dromedary	6	Nasal discharge	30.40	27.10	760	NA
Dromedary	<1	Nasal discharge	29.82	26.29	NA	NA
Dromedary	12	Nasal discharge	31.20	27.29	NA	NA
Dromedary	12	Nasal discharge	33.00	29.50	NA	NA
Dromedary	10	Nasal discharge	29.13	25.97	NA	NA
Dromedary	10	Nasal discharge	29.30	25.40	NA	NA
Dromedary	10	Nasal discharge	25.99	22.73	760	NA
Dromedary	14	Nasal discharge	28.60	24.70	760	NA
Dromedary	9	Nasal discharge	23.14	31.09	NA	NA
Dromedary	8	Nasal discharge	32.80	29.32	NA	NA
Dromedary	7	Nasal discharge	30.00	27.47	NA	NA
Dromedary	13	Nasal discharge	33.50	29.59	NA	NA
Dromedary	13	Nasal discharge	31.76	30.46	NA	NA
Dromedary	8	Nasal discharge	28.80	25.10	NA	NA
Dromedary	9	Nasal discharge	26.76	24.41	NA	NA
Dromedary	3	Nasal discharge	25.22	23.25	NA	NA
Dromedary	5	Nasal discharge	29.32	25.33	NA	NA
Dromedary	7	Nasal discharge	28.40	25.72	NA	NA
Median Ct			29.31	25.89	NA	NA

*bp, base pair; Ct, cycle threshold; nt, nucleotide; NA, not applicable; ORF1a, open reading frame 1a; RdRp, RNA-dependent RNA polymerase; UpE, upstream envelope protein.
†RdRp was amplified by using pancoronavirus RT-PCR and then selected amplicons were sequenced.

Figure 2. Whole-genome phylogenetic analysis of MERS-CoV detected in camels, Kazakhstan, 2025. Complete genome sequences were aligned by using MAFFT version 7 (https://mafft.cbrc.jp/alignment/software). Maximum-likelihood phylogenetic trees were reconstructed in IQ-TREE (https://iqtree.github.io) by using the best-fit nucleotide substitution model selected by ModelFinder, and branch support was assessed with 1,000 bootstrap replicates. Black triangle indicates MERS-CoV sequence from Kazakhstan (GenBank accession no. PZ439299). Scale bar indicates nucleotide substitutions per site. MERS-CoV, Middle East respiratory syndrome coronavirus.

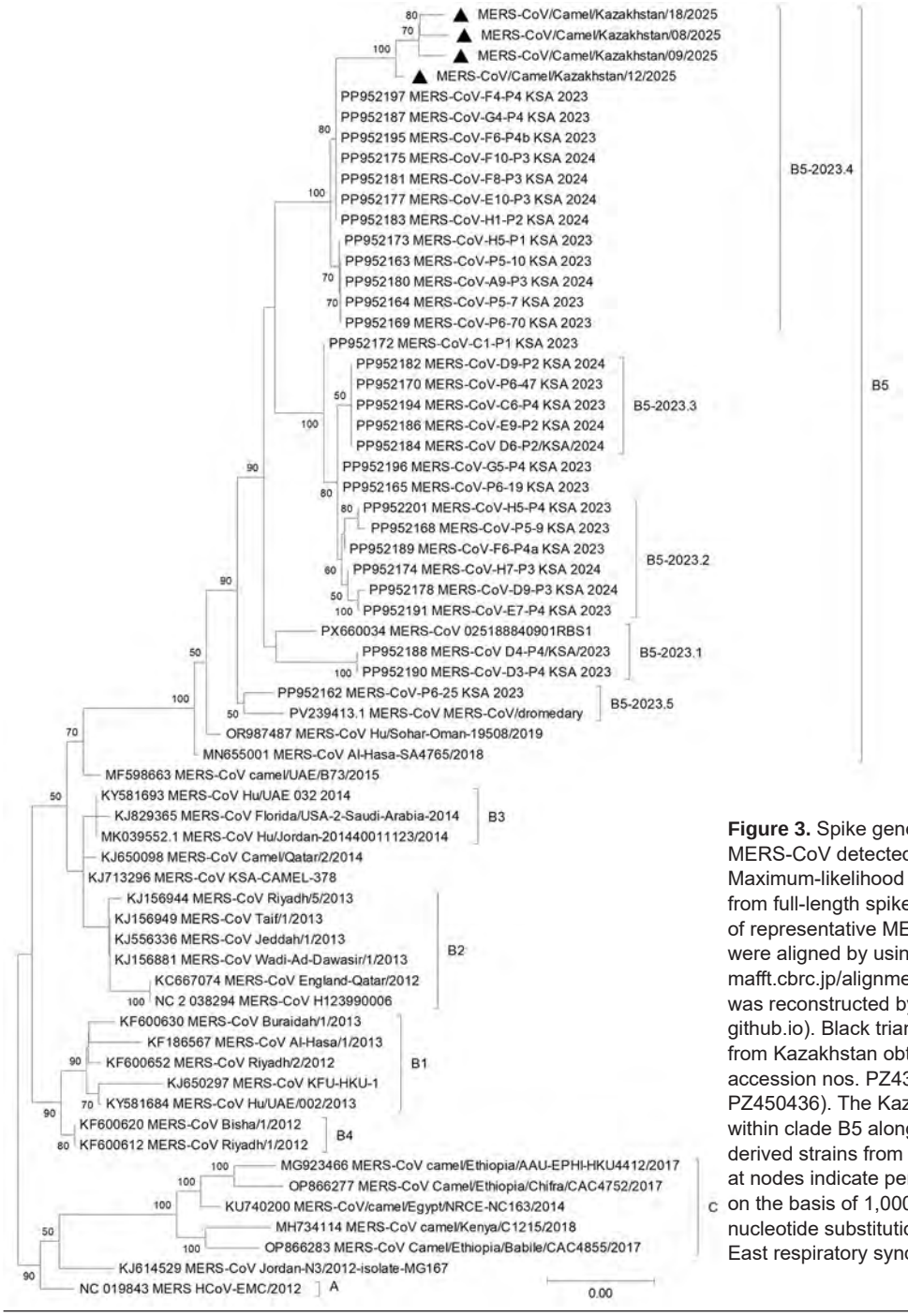

Figure 3. Spike gene phylogenetic analysis of MERS-CoV detected in camels, Kazakhstan, 2025. Maximum-likelihood phylogenetic tree inferred from full-length spike gene nucleotide sequences of representative MERS-CoV strains. Sequences were aligned by using MAFFT version 7 (https://mafft.cbrc.jp/alignment/software) and the phylogeny was reconstructed by using IQ-TREE (https://iqtree.github.io). Black triangles indicated sequences from Kazakhstan obtained in this study (GenBank accession nos. PZ439299, PZ450434, PZ450435, PZ450436). The Kazakhstan sequences clustered within clade B5 along with contemporary camel-derived strains from the Arabian Peninsula. Numbers at nodes indicate percent bootstrap support values on the basis of 1,000 replicates. Scale bar indicates nucleotide substitutions per site. MERS-CoV, Middle East respiratory syndrome coronavirus.

genomes included in our analysis. Recombination analysis suggested 2 putative recombination events. However, the biologic and evolutionary implication of those findings require further investigation.

Although the available sequence data do not permit determination of the geographic origin or directionality of virus movement, the Mangystau region lies within regional livestock movement networks connecting Central Asia with neighboring regions. Animal movement, livestock exchange, and increasing connectivity with the Arabian Peninsula might enable transboundary dissemination of zoonotic pathogens. Those findings highlight the need for coordinated surveillance and genomic monitoring of camel populations and exposed persons across Central Asia.

The outbreak occurred during winter conditions, in contrast to seasonal peaks often reported in warmer months in endemic regions (*15*). Whether climatic

conditions influence viral stability, host susceptibility, or transmission dynamics in temperate continental environments remain to be investigated.

In conclusion, detection of active viral shedding in camels within a high-density livestock region bordering several countries emphasizes the potential for zoonotic spillover. No human MERS cases were identified in connection with the 2025 camelid outbreak in Kazakhstan. However, continued molecular surveillance and expanded genomic characterization of camel MERS-CoV are needed to better define viral diversity, transmission dynamics, and potential public health risks in the region.

Acknowledgments

We thank the regional veterinary services of Mangystau, especially veterinary practitioners Sadir Otesinov and Sattar Ozgan, for their support during field investigations, and the camel owners for their cooperation in reporting suspected cases and enabling sampling.

This study was supported by the Science Committee of the Ministry of Science and Higher Education of the Republic of Kazakhstan (grant no. AP23485202).

Perplexity AI (https://www.perplexity.ai) was used to assist with searching for relevant references, while NotebookLM (https://notebook.google) was used for a preliminary review of relevant sources. ChatGPT 5.6 (OpenAI, https://chatgpt.com) and Grammarly AI (https://www.grammarly.com) were used to edit and rephrase the text to improve English language quality. All scientific content, interpretations, and final wording were reviewed and approved by the authors.

About the Author

Dr. Kydyrmanov is head of the Laboratory for Ecology of Viruses at the Research and Production Center for Microbiology and Virology in Almaty, Kazakhstan. His research focuses on molecular surveillance of emerging respiratory viruses, zoonotic transmission, and the ecology of animal viruses in Central Asia.

References

1. Zaki AM, van Boheemen S, Bestebroer TM, Osterhaus ADME, Fouchier RAM. Isolation of a novel coronavirus from a man with pneumonia in Saudi Arabia. N Engl J Med. 2012;367:1814–20. https://doi.org/10.1056/NEJMoa1211721
2. Corman VM, Ithete NL, Richards LR, Schoeman MC, Preiser W, Drosten C, et al. Rooting the phylogenetic tree of Middle East respiratory syndrome coronavirus by characterization of a conspecific virus from an African bat. J Virol. 2014; 88:11297–303. https://doi.org/10.1128/JVI.01498-14
3. World Health Organization. Disease outbreak news: Middle East respiratory syndrome coronavirus—global update [cited 2026 Feb 16]. https://www.who.int/emergencies/disease-outbreak-news/item/2025-DON591
4. Killerby ME, Biggs HM, Midgley CM, Gerber SI, Watson JT. Middle East respiratory syndrome coronavirus transmission. Emerg Infect Dis. 2020;26:191–8. https://doi.org/10.3201/eid2602.190697
5. Miguel E, Perera RA, Baubekova A, Chevalier V, Faye B, Akhmetsadykov N, et al. Absence of Middle East respiratory syndrome coronavirus in camelids, Kazakhstan, 2015. Emerg Infect Dis. 2016;22:555–7. https://doi.org/10.3201/eid2203.151284
6. Orynbayev MB, Hitch AT, Kerimbayev AA, Nissanova RK, Sultankulova KT, Rystayeva RA, et al. Serological exposure in Bactrian and dromedary camels in Kazakhstan to a MERS or MERS-like coronavirus. Transbound Emerg Dis. 2022;69:e1374–81. https://doi.org/10.1111/tbed.14468
7. Karamendin K, Seidalina A, Sabyrzhan T, Nuralibekov S, Kasymbekov Y, Suleimenova S, et al. Serological screening for Middle East respiratory syndrome coronavirus and hepatitis E virus in camels in Kazakhstan. Pathogens. 2022;11:1224. https://doi.org/10.3390/pathogens11111224
8. Corman VM, Eckerle I, Bleicker T, Zaki A, Landt O, Eschbach-Bludau M, et al. Detection of a novel human coronavirus by real-time reverse-transcription polymerase chain reaction. Euro Surveill. 2012;17:20285. https://doi.org/10.2807/ese.17.39.20285-en
9. World Organisation for Animal Health. Manual of diagnostic tests and vaccines for terrestrial animals. Middle East respiratory syndrome (infection of dromedary camels with Middle East respiratory syndrome coronavirus) [cited 2026 Feb 16]. https://www.woah.org/en/what-we-do/standards/codes-and-manuals
10. Lelli D, Papetti A, Sabelli C, Rosti E, Moreno A, Boniotti MB. Detection of coronaviruses in bats of various species in Italy. Viruses. 2013;5:2679–89. https://doi.org/10.3390/v5112679
11. Aljabr W, Alruwaili M, Penrice-Randal R, et al. Amplicon and metagenomic analysis of Middle East respiratory syndrome (MERS) coronavirus and the microbiome in patients with severe MERS. mSphere. 2021;6:e0021921. https://doi.org/10.1128/msphere.00219-21
12. Hassan AM, Mühlemann B, Al-Subhi TL, Rodon J, El-Kafrawy SA, Memish Z, et al. Ongoing evolution of Middle East respiratory syndrome coronavirus, Saudi Arabia, 2023–2024. Emerg Infect Dis. 2025;31:57–65. https://doi.org/10.3201/eid3101.241030
13. Hemida MG, Alnaeem A, Chu DKW, Perera RAPM, Chan SMB, Almathen F, et al. Longitudinal study of Middle East respiratory syndrome coronavirus infection in dromedary camel herds in Saudi Arabia, 2014–2015. Emerg Microbes Infect. 2017;6:e56. https://doi.org/10.1038/emi.2017.44
14. Rodon J, Mykytyn AZ, Te N, Okba NMA, Lamers MM, Pailler-García L, et al. Extended viral shedding of MERS-CoV clade B virus in llamas compared with African clade C strain. Emerg Infect Dis. 2023;29:585–9. https://doi.org/10.3201/eid2903.220986
15. Rabaan AA, Al-Ahmed SH, Sah R, Alqumber MA, Haque S, Patel SK, et al. MERS-CoV: epidemiology, molecular dynamics, therapeutics, and future challenges. Ann Clin Microbiol Antimicrob. 2021;20:8. https://doi.org/10.1186/s12941-020-00414-7

Address for correspondence: Aidyn Kydyrmanov, Laboratory for Ecology of Viruses, Research and Production Center for Microbiology and Virology, 105 Bogenbai Batyr St, Almaty 050010, Kazakhstan; email: aidyn.kydyrmanov@gmail.com

Alignment-Free Tool for Assemblies and Reads in Genomic Surveillance of Tuberculosis

Paula Ruiz-Rodriguez, Mireia Coscollá

Whole-genome sequencing strengthens tuberculosis surveillance, but incomplete lineage schemes can misclassify isolates. We developed Pathotypr, an alignment-free tool for assemblies and reads, using 2,145 markers derived from 26,813 genomes. Across 88,071 samples, Pathotypr improved concordance, expanded uncommon lineage coverage, and detected resistance markers, supporting molecular epidemiology and public health surveillance.

According to the World Health Organization, tuberculosis caused an estimated 1.23 million deaths in 2024 (https://www.who.int/teams/global-programme-on-tuberculosis-and-lung-health/tb-reports/global-tuberculosis-report-2025). Whole-genome sequencing can strengthen disease control by linking cases, detecting resistance, and distinguishing local transmission from repeated introduction; however, those benefits depend on results that are both rapid and comparable. The *Mycobacterium tuberculosis* complex (MTBC) currently includes 10 human-adapted lineages (L1–L10) and 4 animal-adapted clades (A1–A4), and several uncommon or recently described groups remain sparsely sampled or absent from some typing schemes (*1*–*5*). When a scheme does not represent that diversity, isolates may remain unclassified or be assigned to the nearest available label. Differences in sequencing access and reporting remain broader challenges across programs in Europe, but a shared and current lineage framework is still essential wherever genomic surveillance is used (*6*,*7*).

We developed Pathotypr as an open-source, alignment-free software that accepts assembled genomes or raw short reads and returns lineage assignments, World Health Organization–cataloged resistance-associated variants, and a closely related reference genome for downstream analysis. Assemblies can be classified from phylogenetic markers or an independent *k*-mer model, whereas reads are screened directly for lineage and resistance markers and can return ≥1 supported lineage when mixed signals are present. We evaluated those functions in independent datasets, an 88,071-sample benchmark, and 7,148 genomes from the Comprehensive Resistance Prediction for Tuberculosis: an International Consortium (CRyPTIC) dataset (Appendix, https://wwwnc.cdc.gov/EID/article/32/11/26-1074-App1.pdf).

The Study

To extract lineage phylomarkers, we obtained a maximum-likelihood phylogeny of 26,813 MTBC genomes and 609,003 polymorphic sites, which placed L1–L10 and A1–A4 within 1 evolutionary backbone and exposed the marked underrepresentation of certain lineages (Figure 1, panel A). We then mapped substitutions to branches and selected single-nucleotide polymorphisms (SNPs) on the stem branch leading to each monophyletic lineage or clade. After removing 3,039 missense variants and 454 homoplastic nonmissense variants, 2,145 of 5,638 candidates remained as lineage-defining markers. A variable overlap of lineage markers occurred with other tools, ranging from no overlap to 698 (62.8%) with TB-Profiler (https://tbdr.lshtm.ac.uk) and 1,750 (12.9%) with SNP-IT (https://github.com/samlipworth/snpit) (Appendix Table 1). Pathotypr lineage-defining markers comprised 33%–46% of total SNPs across lineages, supporting the filtering approach (Figure 1, panel B). However, the small number of genomes for L7–L10 and A1–A3 might be missing diversity not sampled to date.

Author affiliation: Institute for Integrative Systems Biology, Spanish National Research Council–University of Valencia, FISABIO Joint Research Unit “Infection and Public Health,” Paterna, Spain

DOI: http://doi.org/10.3201/eid3211.261074

Pathotypr uses 3 modules for lineage assignment (Figure 2). The Predict module assigns lineages to genome assemblies using the *k*-mer–based Random Forest algorithm generated by the Train model, and the Classify and Split-FASTQ modules assign lineages on the basis of SNP markers to assemblies (Classify) and raw sequencing reads (Split-FASTQ). First, we compared lineage assignments by Predict and Classify with the phylogenetic placement of 498 complete RefSeq genomes: Predict matched the phylogenetic lineage in all 498 genomes, and Classify assigned 497. The unassigned genome did not contain the complete marker path required for a call, which could reflect assembly gaps or errors at diagnostic marker positions. Next, Predict and Classify successfully returned the same major-lineage assignment for all 254 chromosome-level assemblies that were not used to train the Random Forest. Finally, Split-FASTQ assigned all 162 clinical read datasets to the expected lineage. Those results show the specific role of each module: Classify provides traceable SNP-based assignments, Predict offers an alternative when the marker path is incomplete, and Split-FASTQ extends the lineage framework directly to short reads (Appendix Table 2, Figure 1).

Because the reference choice for read mapping can affect genome coverage and variant calls, we developed and tested Pathotypr's fourth module, Match Ref, a lineage-aware reference selection (*8*,*9*). Across 162 clinical read sets, mapping to the reference selected by Pathotypr reduced nonfixed SNPs by a median of 89% relative to the MTBC ancestral reference and increased median coverage breadth by 0.84 percentage points (*9*) (Appendix Figure 2).

To test whether the new lineage framework could be applied to surveillance-scale datasets, we typed 88,071 UShER-TB samples (*10*; L.M. Karim et al., unpub. data,_https://www.medrxiv.org/content/10.1101/2025.07.22.25331806v1) with Pathotypr module Split-FASTQ (≈24 hours using 4 threads). To compare typing results with TB-Profiler, we excluded 1,290 genomes with multiple lineage calls from the

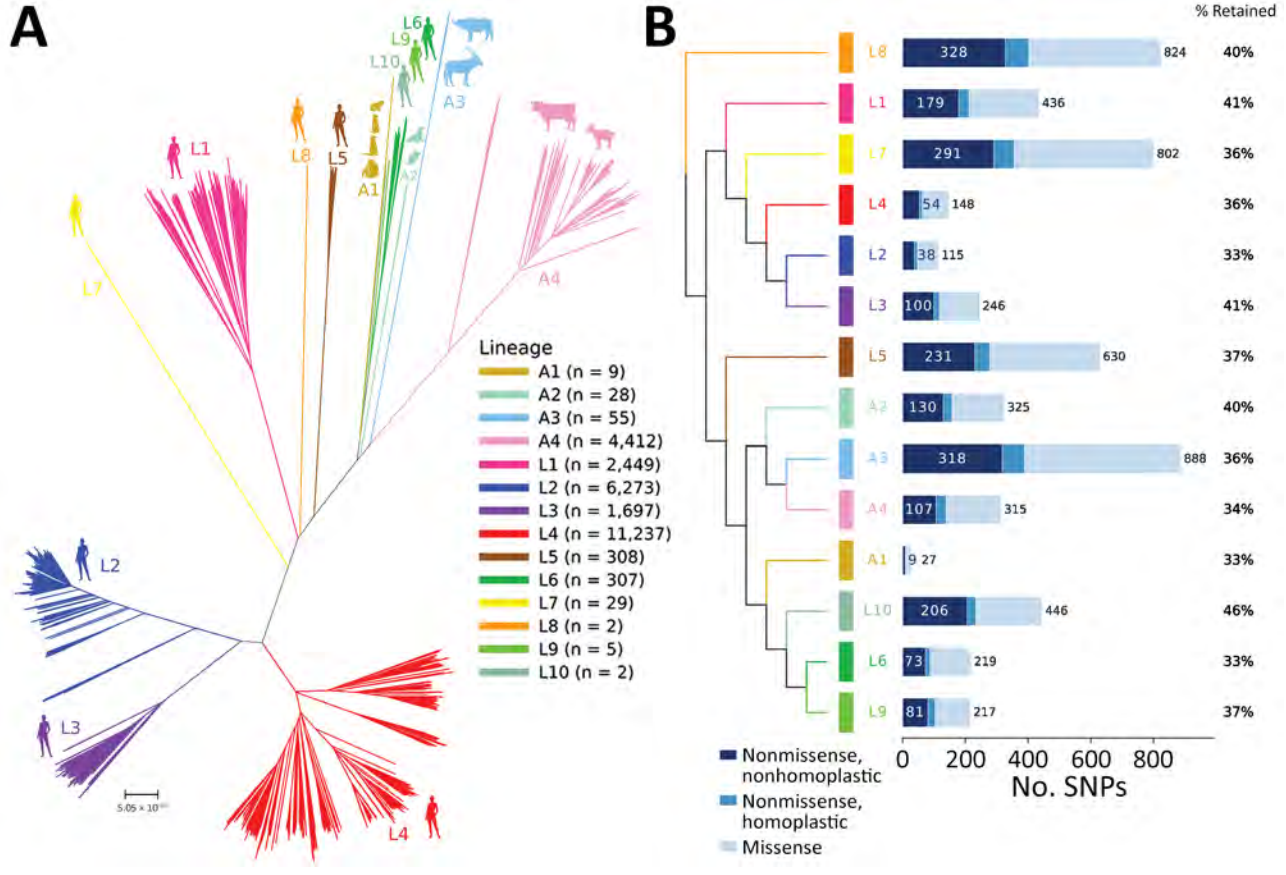

Figure 1. Development and implementation of the lineage framework for Pathotypr, an alignment-free tool for assemblies and reads in genomic surveillance of tuberculosis. A) Maximum-likelihood phylogeny of 26,813 *Mycobacterium tuberculosis* complex genomes, showing L1–L10 and A1–A4. B) Selection of 2,145 lineage-defining markers from 5,638 candidate variants after excluding missense and homoplastic variants. SNP, single-nucleotide polymorphism.

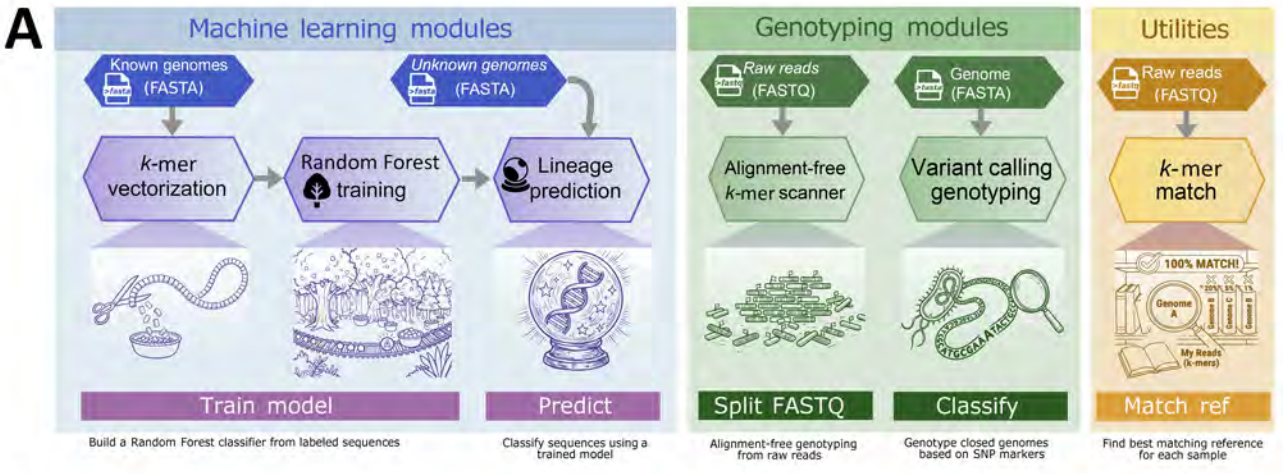

B

Module	Train	Predict	Split-FASTQ	Classify	Match
Input	Labeled FASTA assemblies	FASTA assembly and trained model	FASTQ or FASTQ.gz reads and marker database	FASTA assembly and marker database	FASTQ reads and reference FASTA database
Method	Feature-hashed 31-mers and 100-tree Random Forest	Alignment-free majority-vote classification	Direct reference/alternate k-mer counting	Diagnostic 31-bp marker matching and hierarchical path validation	Weighted k-mer containment
Primary output	Trained lineage model	Predicted lineage and confidence	Marker calls, lineage counts, mixed-lineage signals, and resistance profile	Lineage/sublineage, mixed-lineage signals and resistance-marker calls	Closest-reference assignment

Figure 2. Schematic overview of the 5 modules grouped into 3 functional categories—machine learning, genotyping, and utilities—in developing Pathotypr, an alignment-free tool for assemblies and reads in genomic surveillance of tuberculosis. A) Workflow and data flow across the 5 modules. The Train and Predict modules perform machine learning–based lineage classification; Split-FASTQ and Classify provide alignment-free genotyping from sequencing reads or genome assemblies; and Match identifies the closest reference genome using *k*-mer containment. B) Summary of the input data, analytical method, and primary output of each module. SNP, single-nucleotide polymorphism.

comparison. Although only 698 (62.8%) of the TB-Profiler lineage markers were shared with Pathotypr, both tools assigned the same major lineage to every directly comparable sample (Appendix Table 3). Pathotypr additionally identified 2 L10, 6 A1, and 23 A2 isolates that were not identified with the

Table. Comparison of *Mycobacterium tuberculosis* complex genomic analysis tools, showing main analytical approach, accepted input formats, use of alignment, lineage resolution and taxonomic coverage, drug-resistance reporting, and approximate runtime*

Tool	Reference	Method	Input	AF	Coverage	DR	Runtime†	Interface
Pathotypr	This study	k-mer + RF	FA; FQ(.gz)	Yes	L1–L10; A1–A4	Yes	≈1 s	Desktop; CLI
TB-Profiler	(*10*)	Mapping + SNP DB	FQ; BAM; VCF	No	L1–L9; A3–A4	Yes	3–10 min	Web; CLI
Mykrobe	(*11*)	de Bruijn graph	FQ	Yes	L1–L6	Yes	≈3 min	Desktop; CLI
SNP-IT	(*12*)	SNP panel	FA; VCF	No	L1–L7; animal MTBC	No	1–2 min	CLI
fastlin	(*13*)	Split k-mer	FA; FQ; BAM	Yes	L1–L9; A4	No	<5 s	CLI; binary
KvarQ	(*14*)	Targeted k-mer	FQ	Yes	L1–L7; A4	Yes	≈2 min	Desktop; CLI
MTBseq	(*15*)	Mapping + SNP panel	FQ.gz	No	Major MTBC groups	Yes	≈42 min	CLI
MAGMA	(*16*)	Mapping + cohort calling	PE-FQ	No	TB-Profiler DB	Yes	79/4 h‡	Nextflow; CLI

*AF, alignment-free; CLI, command-line interface; DR, drug-resistance prediction; FA, FASTA; FQ, FASTQ; PE, paired-end; RF, Random Forest; SNP DB, curated SNP database.
†Runtime values were obtained with different datasets, hardware, sequencing depths, and software settings and are shown only for context; they do not constitute a controlled benchmark. Only the Pathotypr runtime was measured in this study.
‡Reported for 79 samples processed in ≈4 h.

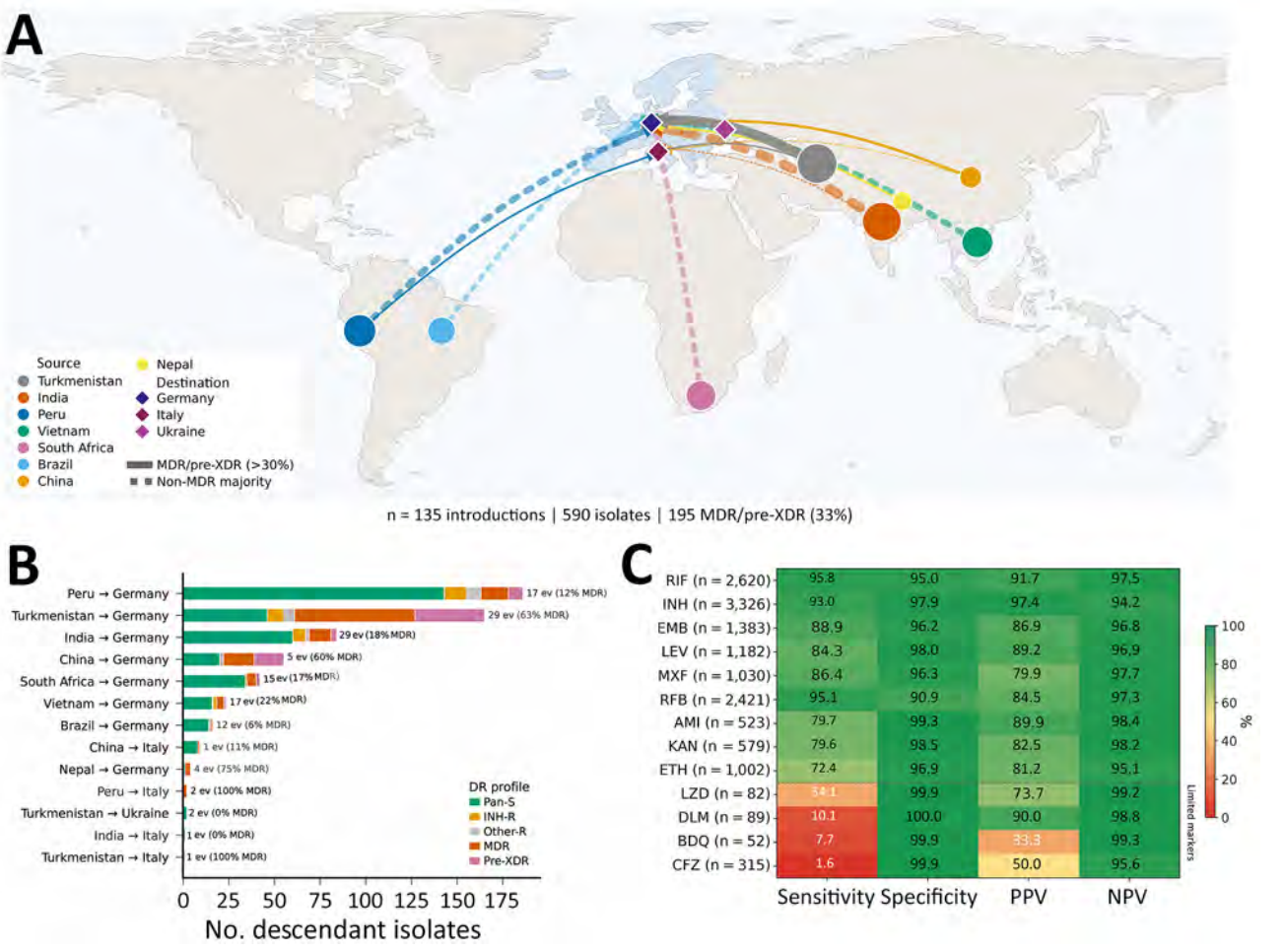

Figure 3. Resistance-informed surveillance analysis of 7,148 CRyPTIC isolates in developing Pathotypr, an alignment-free tool for assemblies and reads in genomic surveillance. A) Probable introductions from non-Europe ancestral states into Germany, Italy, and Ukraine. AMI, amikacin; B) Number and resistance profiles of descendant isolates by source–destination pair; C) Performance of WHO confidence group 1–2 resistance markers compared with phenotypic drug-susceptibility results. BDQ, bedaquiline; CFZ, clofazimine; DLM, delamanid; DR, drug resistance; EMB, ethambutol; ETH, ethionamide; EV, introduction events; INH, isoniazid; KAN, kanamycin; LEV, levofloxacin; LZD, linezolid; MDR, multidrug-resistant; MXF, moxifloxacin; NPV, negative predictive value; pan-S, pansusceptible; PPV, positive predictive value; R, resistant; RFB, rifabutin (genotypic resistance predicted from rifampin-associated variants); RIF, rifampin; XDR, extensively drug-resistant.

TB-Profiler marker set. TB-Profiler misclassified 1 L10 isolate as La1.5/*M. bovis* and left the other L10 genome and A1 and A2 genomes unassigned. Compared with 7 other MTBC genomic analysis tools, Pathotypr uniquely combined rapid *k*-mer/Random Forest classification (≈1 s), support for both FASTA and FASTQ file type inputs, drug-resistance prediction, desktop and command-line interfaces, and the broadest lineage coverage (L1–L10 and A1–A4), and still maintained sublineage resolution (Table).

Pathotypr's Split-FASTQ Classify module complements lineage assignment by reporting World Health Organization–cataloged resistance-associated variants alongside the lineage call in assemblies with different coordinates, as illustrated across the 498-genome validation phylogeny (Appendix Figure 1). For 7,148 CRyPTIC isolates, we generated categorical resistance profiles from World Health Organization confidence groups 1 and 2 and compared them with phenotypic drug-susceptibility results. Genotypic and phenotypic resistance profiles agreed for 86.4% of isolates, and severe disagreement, defined as a difference of ≥3 levels between the genotypic and phenotypic profiles, occurred in 1.4%. Multidrug-resistant or pre–extensively drug-resistant status was assigned with 93.5% sensitivity and 92.3% positive predictive value. Agreement was lowest for bedaquiline, clofazimine, delamanid, and linezolid, for which most phenotypically resistant isolates carried variants of uncertain significance or no cataloged variant (Figure 3, panel A).

We next used the 7,148-isolate CRyPTIC dataset to examine how Pathotypr–Split-FASTQ outputs could contribute to public health surveillance. Lineage assignments formed monophyletic groups in the annotated phylogeny (Appendix Figure 3), and ancestral-state reconstruction inferred 135 probable transitions from non-Europe ancestors into Germany, Italy, or Ukraine, comprising 590 descendant isolates (Figure 3, panels B and C). Among these 590 isolates, 195 (33.1%) had multidrug-resistant or pre–extensively drug-resistant genotypes, compared with 5.5% of the remaining Europe isolates in the dataset. Because CRyPTIC is enriched for drug-resistant isolates, is not population-based, and, after restriction to isolates with a documented country of origin and collection date, includes only Germany, Italy, and Ukraine as recipient countries in Europe, those proportions should not be interpreted as national estimates of importation or transmission. Rather, the analysis illustrates how standardized lineage and resistance outputs can be combined with other tools to identify cross-border clusters that merit epidemiologic follow-up (*17*).

Conclusions

The central scientific advance of this study is a phylogeny-derived lineage framework that represents the recognized diversity of the MTBC, with Pathotypr as the software system we developed to make that framework usable in genomic surveillance. This system's 2,145 markers provide a traceable and extensible basis for assigning common and uncommon, human-adapted and animal-adapted groups, and the independent *k*-mer model preserves classification when direct marker detection is incomplete. By analyzing assemblies and reads without a conventional mapping workflow, reporting multiple supported lineages in mixed samples, and selecting a closely related reference genome, Pathotypr reduces unresolved or inappropriate assignments and places resistance results within a consistent evolutionary context.

Broad lineage coverage, rapid processing, standardized resistance reporting, and lineage-aware reference selection make Pathotypr a practical route from sequence data to comparable surveillance results. Our platform's low memory requirements, desktop graphical interface, and command-line implementation make the same workflow accessible to laboratories with limited bioinformatics infrastructure while supporting automated analysis of large collections. Those features can improve reporting across laboratories, recognition of uncommon introductions, outbreak review, and prioritization of resistant cross-border clusters.

Computational analyses were performed on the Garnatxa high-performance computing cluster at the Institute for Integrative Systems Biology (Paterna, Spain), a joint research center of the University of Valencia and the Spanish National Research Council.

Pathotypr is distributed free of charge as open-source software under the GNU General Public License v3. Pathotypr source code and documentation are available from the PathoGenOmics-Lab GitHub repository (https://github.com/PathoGenOmics-Lab/pathotypr). The phylogenetic marker set is deposited in Zenodo (https://zenodo.org; https://doi.org/10.5281/zenodo.19210043). Accession-level data and supplementary datasets are available at https://doi.org/10.5281/zenodo.20630545.

This work was supported by grants PID2021-123443OB-I00 (MCIN/AEI/10.13039/501100011033; FEDER, EU "A way to make Europe") and PID2024-158536NB-I00 (MICIU/AEI/10.13039/501100011033; FEDER, EU "A way to make Europe").

The authors declare no conflicts of interest. Neither the authors nor their affiliated institutions hold any patent, ownership, royalty, or other financial interest in Pathotypr or in the methods it implements.

About the Authors

Dr. Ruiz-Rodriguez is a researcher at the Institute for Integrative Systems Biology, Spanish National Research Council–University of Valencia, working on pathogen genomics, computational analysis, and tuberculosis genomics. Dr. Coscollá is a Spanish National Research Council Senior Scientist and group leader at the Institute for Integrative Systems Biology who studies the evolution, virulence, transmission, and resistance of *Mycobacterium tuberculosis*.

References

1. Brites D, Loiseau C, Menardo F, Borrell S, Boniotti MB, Warren R, et al. A new phylogenetic framework for the animal-adapted *Mycobacterium tuberculosis* complex. Front Microbiol. 2018;9:2820. https://doi.org/10.3389/fmicb.2018.02820
2. Zwyer M, Çavusoglu C, Ghielmetti G, Pacciarini ML, Scaltriti E, Van Soolingen D, et al. A new nomenclature for the livestock-associated *Mycobacterium tuberculosis* complex based on phylogenomics. Open Res Eur. 2021;1:100. https://doi.org/10.12688/openreseurope.14029.2
3. Coscolla M, Gagneux S, Menardo F, Loiseau C, Ruiz-Rodriguez P, Borrell S, et al. Phylogenomics of *Mycobacterium africanum* reveals a new lineage and a complex evolutionary history. Microb Genom. 2021;7:000477. https://doi.org/10.1099/mgen.0.000477
4. Ngabonziza JCS, Loiseau C, Marceau M, Jouet A, Menardo F, Tzfadia O, et al. A sister lineage of the *Mycobacterium*

tuberculosis complex discovered in the African Great Lakes region. Nat Commun. 2020;11:2917. https://doi.org/10.1038/s41467-020-16626-6
5. Guyeux C, Senelle G, Le Meur A, Supply P, Gaudin C, Phelan JE, et al. Newly identified *Mycobacterium africanum* lineage 10, Central Africa. Emerg Infect Dis. 2024;30:560–3. https://doi.org/10.3201/eid3003.231466
6. Andrés M, van der Werf MJ, Ködmön C, Albrecht S, Haas W, Fiebig L; Survey study group. Molecular and genomic typing for tuberculosis surveillance: a survey study in 26 European countries. PLoS One. 2019;14:e0210080. https://doi.org/10.1371/journal.pone.0210080
7. Tagliani E, Anthony R, Kohl TA, de Neeling A, Nikolayevskyy V, Ködmön C, et al.; ECDC molecular surveillance project participants. Use of a whole genome sequencing-based approach for *Mycobacterium tuberculosis* surveillance in Europe in 2017–2019: an ECDC pilot study. Eur Respir J. 2021;57:2002272. https://doi.org/10.1183/13993003.02272-2020
8. Modlin SJ, Robinhold C, Morrissey C, Mitchell SN, Ramirez-Busby SM, Shmaya T, et al. Exact mapping of Illumina blind spots in the *Mycobacterium tuberculosis* genome reveals platform-wide and workflow-specific biases. Microb Genom. 2021;7:mgen000465. https://doi.org/10.1099/mgen.0.000465
9. Comas I, Chakravartti J, Small PM, Galagan J, Niemann S, Kremer K, et al. Human T cell epitopes of *Mycobacterium tuberculosis* are evolutionarily hyperconserved. Nat Genet. 2010;42:498–503. https://doi.org/10.1038/ng.590
10. Phelan JE, O'Sullivan DM, Machado D, Ramos J, Oppong YEA, Campino S, et al. Integrating informatics tools and portable sequencing technology for rapid d etection of resistance to anti-tuberculous drugs. Genome Med. 2019;11:41. https://doi.org/10.1186/s13073-019-0650-x
11. Hunt M, Bradley P, Lapierre SG, Heys S, Thomsit M, Hall MB, et al. Antibiotic resistance prediction for *Mycobacterium tuberculosis* from genome sequence data with Mykrobe. Wellcome Open Res. 2019;4:191. https://doi.org/10.12688/wellcomeopenres.15603.1
12. Lipworth S, Jajou R, de Neeling A, Bradley P, van der Hoek W, aphalala G, et al. SNP-IT Tool for identifying subspecies and associated lineages of *Mycobacterium tuberculosis* complex. Emerg Infect Dis. 2019;25:482–8. https://doi.org/10.3201/eid2503.180894
13. Derelle R, Lees J, Phelan J, Lalvani A, Arinaminpathy N, Chindelevitch L. fastlin: an ultra-fast program for *Mycobacterium tuberculosis* complex lineage typing. Bioinformatics. 2023; 39:btad648. https://doi.org/10.1093/bioinformatics/btad648
14. Steiner A, Stucki D, Coscolla M, Borrell S, Gagneux S. KvarQ: targeted and direct variant calling from fastq reads of bacterial genomes. BMC Genomics. 2014;15:881. https://doi.org/10.1186/1471-2164-15-881
15. Kohl TA, Utpatel C, Schleusener V, De Filippo MR, Beckert P, Cirillo DM, et al. MTBseq: a comprehensive pipeline for whole genome sequence analysis of *Mycobacterium tuberculosis* complex isolates. PeerJ. 2018;6:e5895. https://doi.org/10.7717/peerj.5895
16. Heupink TH, Verboven L, Sharma A, Rennie V, de Diego Fuertes M, Warren RM, et al. The MAGMA pipeline for comprehensive genomic analyses of clinical *Mycobacterium tuberculosis* samples. PLoS Comput Biol. 2023;19:e1011648. https://doi.org/10.1371/journal.pcbi.1011648
17. Abascal E, Pérez-Lago L, Martínez-Lirola M, Chiner-Oms Á, Herranz M, Chaoui I, et al. Whole genome sequencing-based analysis of tuberculosis (TB) in migrants: rapid tools for cross-border surveillance and to distinguish between recent transmission in the host country and new importations. Euro Surveill. 2019;24:1800005. https://doi.org/10.2807/1560-7917.ES.2019.24.4.1800005

Address for correspondence: Mireia Coscollá, Institute for Integrative Systems Biology, Carrer del Catedràtic Agustín Escardino Benlloch, 9, Paterna, Valencia 46980, Spain; email: mireia.coscolla@csic.es

Evidence of Exposure to Highly Pathogenic Avian Influenza H5 Viruses in East Greenland Polar Bears

Kayla J. Buhler, Charlene Ranadheera, Nathalie Bastien, Marcy Zirino, Emily Jenkins, Morten Tryland, Rune Dietz, Jens Søndergaard, Christian Sonne

Author affiliations: University of Inland Norway, Koppang, Norway (K.J. Buhler, M. Tryland); Cornell University, Ithaca, New York, USA (K.J. Buhler); Public Health Agency of Canada, Winnipeg, Manitoba, Canada (C. Ranadheera, N. Bastien, M. Zirino); University of Saskatchewan, Saskatoon, Saskatchewan, Canada (E. Jenkins); Aarhus University, Arctic Research Cluster, Roskilde, Denmark (R. Dietz, J. Søndergaard, C. Sonne)

DOI: https://doi.org/10.3201/eid3211.261050

We detected influenza A virus antibodies in plasma collected from East Greenland polar bears during subsistence hunts in 2024 (3/14 [21%]) and 2025 (6/14 [43%]). Four bears from 2025 had antibodies for the globally emerging highly pathogenic avian influenza virus H5 clade 2.3.4.4b, consistent with survival after exposure.

Highly pathogenic avian influenza (HPAI) is an emerging ecologic and public health threat in the Arctic (*1*). Seasonal bird migrations to Arctic nesting grounds create a hot spot for HPAI outbreaks, amplifying interspecies interactions and the risk for viral reassortment and dissemination across migratory flyways (*1*). Recent detection of HPAI in wild Arctic mammals, along with their nutritional and cultural relevance for Indigenous peoples, emphasizes a strong need for surveillance in Arctic ecosystems (*2*–*4*).

Polar bears (*Ursus maritimus*) are Arctic apex predators that face increased challenges associated with their ecologic position at the interface between marine and terrestrial ecosystems. Climate warming and the subsequent loss of sea ice leads to increased time spent on land and exposure to terrestrial pathogens through the exploitation of new food sources (*5*). Cases of deceased polar bears infected with HPAI have been reported in Alaska, USA (H5N1 in 2023), and Svalbard, Norway (H5N5 in 2026), emphasizing that these emerging viruses may pose a risk to Arctic species (*2*,*6*).

As part of an ongoing collaboration with Indigenous hunters, heart blood was collected during subsistence harvests from polar bears that appeared healthy near Scoresby Sound (Ittoqqortoormiit) in East Greenland (Appendix Figure, https://wwwnc.cdc.gov/EID/article/32/11/26-1050-App1.pdf) during the hunting season (January–May). We screened 109 plasma samples (collected during 2016–2025) for antibodies against all influenza A viruses by using a competitive ELISA (cELISA) that targets the influenza A virus (IAV) nucleoprotein (ID Screen Influenza A Antibody Competition Multi-Species; Innovative Diagnostics, https://www.innovative-diagnostics.com), according to the manufacturer's instructions. We detected no IAV antibodies before 2024. Three bears (all male) harvested during 2024 had signal-to-noise values within the positive range (≤45%) of the cELISA (21% [95% CI 8%–48%]; n = 3/14); the number increased to 6 bears (5 male, 1 female) in 2025 (43% [95% CI 21%–67%]; n = 6/14) (Appendix Table).

We conducted further screening on positive samples (n = 9) and a subset of negative samples (n = 3) by using a hemagglutination inhibition assay that used horse red blood cells (Rockland Immunochemicals, https://www.rockland.com), as described by Kayali et al. (*7*), with minor modifications. In brief, we heat-inactivated plasma at 56 °C for 30 minutes, then hem-adsorbed it and treated it with receptor-destroying enzyme. We used avian influenza viruses representative of H5 and H7 subtypes in the assay (Table). Plasma from 4 animals harvested in 2025 that were positive for IAV antibodies on the cELISA were positive (≥1:40) for antibodies to H5N1 viruses falling within clade 2.3.4.4b on the hemagglutination inhibition assay, suggesting that the animals had been exposed to an HPAI virus in this clade (Table).

We first detected IAV antibodies in East Greenland polar bears in 2024 and antibodies to the highly pathogenic H5 clade 2.3.4.4b in 2025. H5N5 and H5N1 strains were previously confirmed in sea birds (including *Uria aalge* [H5N1 in 2022], *Larus hyperboreus* [H5N5 in 2023], *Fulmarus glacialis* [H5N5 in 2023 and 2024], and *Larus marinus* [H5N5 in 2024]) from the west coast of Greenland (*8*,*9*), consistent with our findings of evidence of IAV exposure in East Greenland polar bears in 2024. Positive bears probably were exposed during the summer–fall bird migration the year before the bears were harvested, given that migratory birds are absent during the polar bear hunting season. Hunters reported no clinical signs, suggesting that bears can recover from HPAI infection. That finding is consistent with the high prevalence reported in our study and survival of the bears for months after the departure of migratory birds. Although cross-reactivity with low

Table. Antibodies detected for influenza A viruses and H5 viruses in 12 polar bears sampled in the Ittoqqortoormiit region of East Greenland during 2024–2025 and submitted to the Canada's National Microbiology Laboratory for screening*

				HI assay‡			
Bear ID	Sex	Year	cELISA†	A/British_Columbia/PHL2032/2024 (clade 2.3.4.4b H5)	A/Texas/37/2024 (clade 2.3.4.4b H5)	A/Vietnam/1203/2004 (clade 1 H5)	A/Anhui/01/13 (H7N9)
63931	M	2024	**3**	20	<20	<20	20
63938	M	2024	**8**	<20	<20	<20	<20
63942	M	2024	**32**	<20	<20	<20	<20
67552	M	2025	**10**	**40**	**40**	5	<5
67554	F	2025	**24**	20	10	<5	<5
67555	M	2025	**5**	**160**	**40**	<5	<5
67556	M	2025	**40**	20	10	<5	<5
67559	M	2025	**10**	**80**	**80**	5	<5
67563	M	2025	**31**	**160**	**160**	20	<5
67560	M	2025	98	<5	<5	<5	<5
67561	M	2025	71	10	5	<5	<5
67565	M	2025	96	<5	<5	<5	<5

*Bold font indicates a positive result. cELISA, competitive ELISA; HI, hemagglutination inhibition.
†cELISA results (ID Screen Influenza A Antibody Competition Multi-Species; Innovative Diagnostics, https://www.innovative-diagnostics.com) are represented as the signal-to-noise ratio, i.e., (optical density of the sample/average optical density of the negative controls) × 100.
‡HI assay results are represented as the endpoint dilution factor (2-fold serial dilution).

pathogenic H5 subtypes is possible, plasma from all 4 seropositive bears inhibited hemagglutination of viruses within clade 2.3.4.4b (not observed when tested against clade 1) (Table). That finding strongly supports infection with a virus from clade 2.3.4.4b, which is exclusively an HPAI lineage.

HPAI spillover to mammalian hosts typically occurs through ingestion of infected birds or through contaminated environments (*1*,*3*,*10*). Transmission to wild mammals may involve multiple mechanisms, including direct contact through mucosal or nasal secretions, scavenging dead birds or bird eggs or infected mammals, and mother-to-offspring transmission through lactation (Figure) (*10*). Further studies are needed to identify which mechanisms are relevant for polar bears, although the most likely route is by eating dead or infected birds and mammals.

Greenland links the East Atlantic and the North American Atlantic flyways (Appendix Figure), and increased surveillance in this region may provide effective early warning signs of HPAI dissemination. Our findings indicate that East Greenland polar bears have been exposed to HPAI in recent years, consistent with the timeline of prior reports of HPAI in birds along the linked migratory superhighways (*3*,*8*,*9*). This carnivore may be an ideal sentinel for emerging HPAI in Arctic ecosystems, given that polar bears opportunistically scavenge coastal nests, birds, and marine mammals as they face

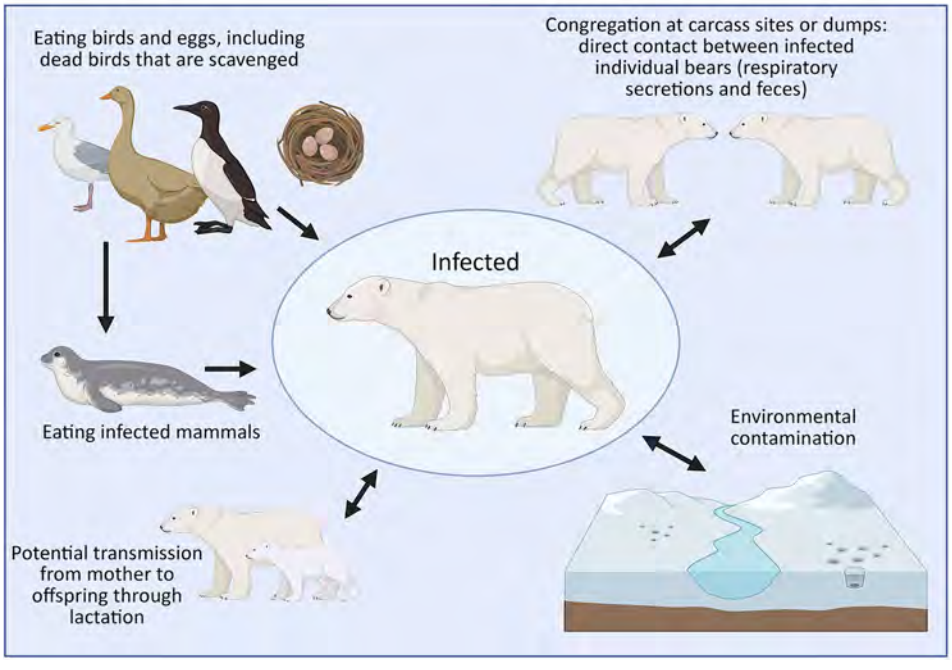

Figure. Potential mechanisms of transmission for highly pathogenic avian influenza viruses to polar bears, including direct contact through mucosal or nasal secretions, scavenging dead birds or bird eggs, eating infected mammals, and mother-to-offspring transmission through lactation. Image created by using BioRender (https://www.biorender.com).

nutritional stress associated with sea ice loss (*2*,*5*). Our study also highlights the strength of collaboration between scientists and local subsistence hunters, emphasizing the need for future research that incorporates diverse perspectives and cultural practices to effectively monitor the health of wildlife in these remote regions.

Acknowledgments

We thank the local subsistence hunters and communities in East Greenland, especially Jan Lorentzen, for ongoing collaboration and support with sample collection. We acknowledge Sandra Drewes Fabricius and Cecilie Nobel Zabel Dipo for their laboratory assistance. In addition, we thank Maria Jarque and Kim Hamonic for their assistance with sample transportation and permit acquisition.

No animal care and use committee approvals were needed because samples were collected from deceased animals from the annual legal subsistence hunting quota of 35 Greenland polar bears. Polar bear samples were collected and transported to Denmark under the International Union for Conservation of Nature's Convention on International Trade in Endangered Species of Wild Fauna and Flora permits 16GL1166991, 17GL1167116, 18GL1717224, 19GL1717365, 20GL1717427, 21GL1717628, 22GL2089580 2022, 23GL2089714, 24GL2089884, 25GL2090110, IM 1202-580/16, IM 0818-549/17, IM 0928-712/18, IM0816-496/19, DK2020-0017113-01, DK-2021-0032841-01, DK-2022-0046312-01, DK-2023-0037644-01, DK-2024-0062523-01, and DK-2025-0015153-01. Samples were transported to Norway and Canada under the International Union for Conservation of Nature's Convention on International Trade in Endangered Species of Wild Fauna and Flora permits DK-2025-0024770-01 and 26NO-0002-EX and Canadian Food Inspection Agency import permit A-2026-00277-1.

We acknowledge Denmark's Environmental Protection Agency for support through the Environmental Support for the Arctic program (Miljøstøtte til Arktis) and Cooperation for Environment in the Arctic (ZOO-PFAS grant no. 2022-86192 [awarded to C.S.], AMAP CORE BIOTA grant no. 2022-86218 [awarded to J.S.], and AMAP CORE BIOTA grant no. 2024-73867 [awarded to J.S.]). In addition, this work is funded by the European Union Horizon Europe (ArcSolution grant agreement no. 101135051), providing resources for the authors (C.S., R.D., and J.S.) to collect samples, and by the Morris Animal Foundation (grant no. D25ZO-430) and the Cornell K. Lisa Yang Center for Wildlife Health, providing early career support and funds for transportation and testing (awarded to K.J.B.).

About the Author

Dr. Buhler is a researcher at the University of Inland Norway and a postdoctoral fellow at the Cornell K. Lisa Yang Center for Wildlife Health at Cornell University. Her research interests include the epidemiology and ecology of zoonotic pathogens, using a One Health approach to investigate the transmission dynamics of pathogens in wildlife across the Arctic.

References

1. Gass JD Jr, Kellogg HK, Hill NJ, Puryear WB, Nutter FB, Runstadler JA. Epidemiology and ecology of influenza A viruses among wildlife in the Arctic. Viruses. 2022;14:1531. https://doi.org/10.3390/v14071531
2. Stimmelmayr R, Rotstein D, Torchetti MK, Gerlach R. Highly pathogenic avian influenza virus A (H5N1) clade 2.3. 4.4 b infection in free-ranging polar bear, Alaska, USA. Emerg Infect Dis. 2024;30:1660–3. https://doi.org/10.3201/eid3008.240481
3. Granstad S, Tønnessen R, Ytrehus B, Descamps S, Moe B, Strøm H, et al. Multiple introductions of highly pathogenic avian influenza viruses into the High Arctic: Svalbard and Jan Mayen, 2022–2025. J Gen Virol. 2026;107:002305. https://doi.org/10.1099/jgv.0.002305
4. Graziosi G, Lupini C, Catelli E, Carnaccini S. Highly pathogenic avian influenza (HPAI) H5 clade 2.3. 4.4 b virus infection in birds and mammals. Animals (Basel). 2024;14:1372. https://doi.org/10.3390/ani14091372
5. Pilfold NW, Richardson ES, Ellis J, Jenkins E, Scandrett WB, Hernández-Ortiz A, et al. Long-term increases in pathogen seroprevalence in polar bears (*Ursus maritimus*) influenced by climate change. Glob Change Biol. 2021;27:4481–97. https://doi.org/10.1111/gcb.15537
6. Norwegian Veterinary Institute. First detection of avian influenza in polar bears in Svalbard [in Norwegian]. 2026 May 19 [cited 2026 May 30]. https://www.vetinst.no/nyheter/forste-pavisning-av-fugleinfluensa-hos-isbjorn-pa-svalbard
7. Kayali G, Setterquist SF, Capuano AW, Myers KP, Gill JS, Gray GC. Testing human sera for antibodies against avian influenza viruses: horse RBC hemagglutination inhibition vs. microneutralization assays. J Clin Virol. 2008;43:73–8. https://doi.org/10.1016/j.jcv.2008.04.013
8. Erdelyan CNG, Kandeil A, Signore AV, Jones MEB, Vogel P, Andreev K, et al. Multiple transatlantic incursions of highly pathogenic avian influenza clade 2.3.4.4b A(H5N5) virus into North America and spillover to mammals. Cell Rep. 2024;43:114479. https://doi.org/10.1016/j.celrep.2024.114479
9. World Organisation for Animal Health. World Animal Health Information System. Events management [cited 2026 May 21]. https://wahis.woah.org/#/event-management
10. Shanta RN, Akther M, Prodhan MA, Akter SH, Annandale H, Sarker S, et al. Adaptation and outbreak of highly pathogenic avian influenza in dairy cattle: an emerging threat to humans, pets, and peridomestic animals. Pathogens. 2025;14:846. https://doi.org/10.3390/pathogens14090846

Address for correspondence: Kayla Buhler, Department of Forestry and Wildlife Management, University of Inland Norway, Anne Evenstads vei 80, 2480 Koppang, Norway; email: kayla.buhler@inn.no

Systemic *Spiroplasma turonicum* Infection Manifested as Knee Arthritis, France, 2025

Matteo Vassallo, Sabrina Manni, Eleonore Delannoy, Johanna Azulay, Aurelie Canat, Laurene Lotte, Audrey Sindt, Anne-Flore Albertini, Pascal del Giudice

Author affiliations: Unité de Recherche Clinique Cote d'Azur, Université Côte d'Azur, Nice, France (M. Vassallo); Cannes Hospital, Cannes, France (M. Vassallo, S. Manni, E. Delannoy, J. Azulay, A. Canat, L. Lotte, A. Sindt); Medipath, Mougins, France (A.-F. Albertini); Centre Hospitalier Intercommunal de Fréjus-Saint-Raphael, Frejus, France (P. del Guidice)

DOI: https://doi.org/10.3201/eid3211.261001

We report on an immunocompromised patient in southeast France who sought care for fever, knee arthritis, and skin erythema. Blood and joint samples were positive for *Spiroplasma turonicum*, an intracellular gram-negative bacterium generally found in plants, insects, and ticks. Clinicians should be aware of possible *S. turonicum* infection in immunocompromised patients.

Spiroplasma spp. are intracellular microorganisms belonging to the Mollicutes class and Spiroplasmataceae family, which also includes *Mycoplasma* spp. bacteria (*1*). *Spiroplasma* spp. bacteria require special substrates for growth in laboratory, and diagnosis often relies on use of genetic methods (*2*). Plants, insects, and ticks are known *Spiroplasma* bacteria reservoirs (*3*).

Human infections are extremely rare, and *Spiroplasma* species differ according to vectors. For instance, 2 cases of *S. ixodetis* infections in Sweden were described in immunocompromised patients after tick exposure (*4*); 1 case of human infection with *S. apis*, a species generally associated with honeybees, was described in France after the patient was stung by a hornet-like insect (*5*); and 1 case was reported in Spain of human infection with *S. turonicum*, which generally colonizes in *Haematopota* spp. horseflies (*3*,*6*). We report a case of *S. turonicum* systemic infection associated with knee arthritis in an immunocompromised patient in France. The patient gave written consent to describe her case.

In November 2025, a 61-year-old woman sought care in Cannes Hospital, in southeast France, for a 10-day history of left knee pain. Her primary underlying condition was IgA lambda multiple myeloma, diagnosed in 2017, initially treated with autograft. Since 2024, she had been receiving teclistamab, a monoclonal antibody acting as a proteasome and CD38 inhibitor.

At admission, the patient had an inflamed, painful left knee with functional impairment. Laboratory results showed elevated blood inflammatory markers, including C-reactive protein values at 83 mg/L (reference <5 mg/L), and serum protein electrophoresis revealed severe hypogammaglobulinemia (5.6 g/L, reference range 7.8–13.2 g/L), with undetectable IgA and IgM. She had inflammatory signs on the left knee, and positron emission tomography showed a hyperfixation in the popliteal region of the left leg.

A knee aspiration revealed the presence of inflammatory cells (16,800 white cells/mL, most of which were polynuclear neutrophils). We cultured knee aspirate in blood culture bottles and incubated at 35°C in a BacT/ALERT 3D system (bioMérieux, https://www.biomerieux.com); after 48 hours, the cultures flagged as positive. Gram stain of cultures showed tiny gram-negative spiral-shaped bacteria. Subcultures on blood agar plates for 48 hours showed several small zones of β-hemolysis with no macroscopic colony growth. Matrix-assisted laser desorption/time-of-flight mass spectrometry using MALDI Biotyper (Bruker Daltonics GmbH, https://www.bruker.com) failed to identify the bacterium. At the same time, blood samples drawn from the patient were cultured and showed the same gram-negative spiral-shaped bacteria.

Cytologic analysis of tissue samples collected during the arthroscopic lavage and debridement showed numerous polynuclear neutrophil cells, without any infiltration by cancer cells (Figure 1). PCR specific for *Campylobacter* spp. and *Helicobacter* spp. on the knee aspirate yielded negative results.

The patient was started on empirical carbapenems antibiotic therapy after an arthroscopic lavage and debridement of the popliteal nodular lesion. Blood inflammatory markers partially improved, but local inflammatory signs in the left knee persisted. A second arthroscopic lavage was performed 3 weeks after the first, and joint liquid analysis revealed the same inflammatory aspect; cultures were positive for gram-negative spiral-shaped bacteria but unrecognized by matrix-assisted laser desorption/time-of-flight mass spectrometry. After the surgery, the patient had several large asymptomatic annular skin erythema develop on her trunk, arms, and legs that lasted <48 hours (Figure 2).

Finally, we performed 16S rRNA gene sequencing on the joint liquid and identified the bacterium

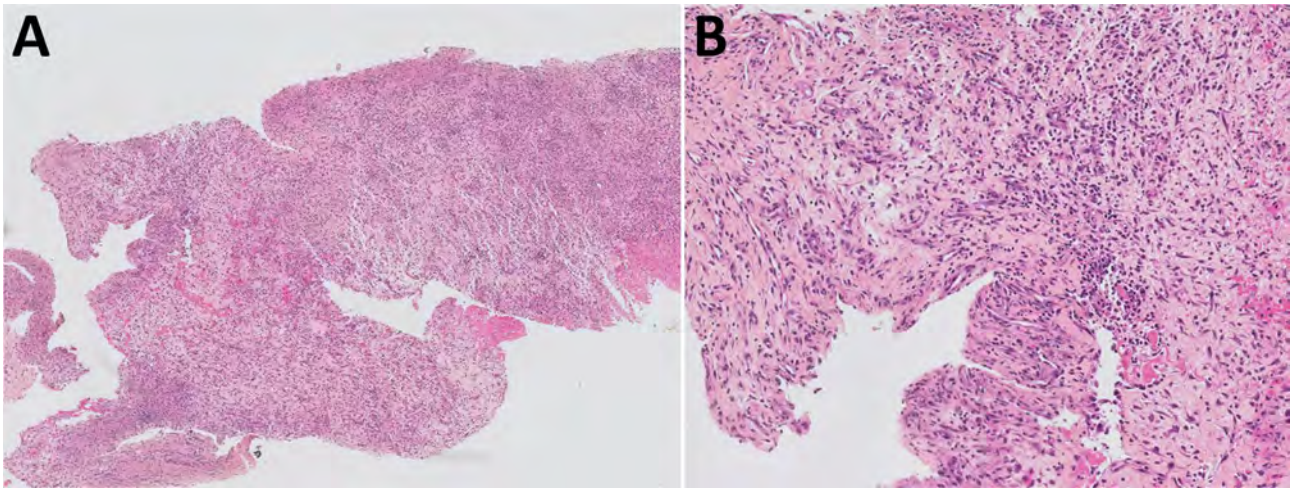

Figure 1. Histology of synovial sample of the left knee from an immunocompromised patient diagnosed with systemic *Spiroplasma turonicum* infection, France, 2025. Images show hematoxylin and eosin stain of polymorphous synovial inflammatory infiltrates. Polymorphous inflammatory granulomas are characterized by different white blood cell lineages in the knee synovial tissue. A) Original magnification ×2.5; B) original magnification ×5.

as *S. turonicum*. According to previous literature (*4*,*6*), the patient was promptly started on a dual antibiotic therapy with doxycycline and levofloxacin, after which blood markers and local inflammatory signs progressively improved.

Because horseflies generally are the main *S. turonicum* bacteria vector, we asked the patient about the possible contact with horses. She cited a short stay in the inland region of Nice, in southeast France, with a visit to a horse ranch.

After 6 days of doxycycline and levofloxacin treatment and improved blood markers, the patient was discharged home and completed a 6-week course of antibiotics. She returned for outpatient follow-up 4

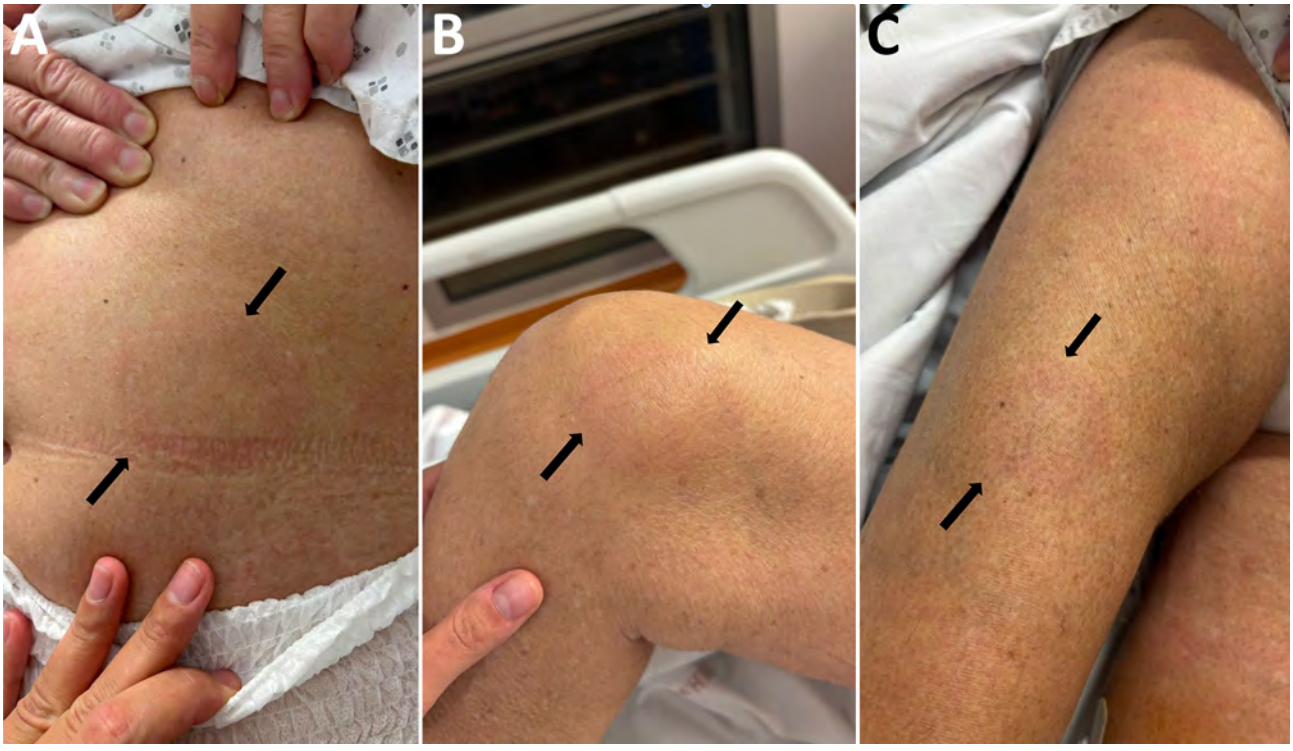

Figure 2. Skin annular erythema on an immunocompromised patient diagnosed with systemic *Spiroplasma turonicum* infection, France, 2025. After surgery, the patient had erythema (arrows) develop on the abdomen (A), knee (B), and thigh (C), which lasted <48 hours.

months after discharge; blood inflammatory markers were within reference ranges, and she had no signs of clinical relapse.

Skin manifestations, mainly as erythema multiforme, are known to be associated with *Mycoplasma pneumoniae* infections (*7*). Because *Spiroplasma* spp. and *Mycoplasma* spp. belong to the same family, we suggest that they could share the same pathophysiologic mechanisms associated with skin lesions. Moreover, arthritis due to *Spiroplasma* spp. has not previously been described, but *M. pneumoniae* has been isolated from joint fluid in some reported cases (*8*).

The patient in this case was severely immunocompromised because of multiple myeloma and the associated long-term treatment. Teclistamab targets the B-cell maturation antigen and causes a profound depletion of both malignant and normal long-lived plasma cells, resulting in prolonged hypogammaglobulinemia and a consequently substantial infectious burden (*9*,*10*).

In summary, we confirmed human *S. turonicum* infection in an immunocompromised patient with bacteremia, arthritis, and skin erythema. In severely immunosuppressed patients, clinicians and microbiologists should be aware of this very rare bacterial agent, which requires complex methods of identification and specific antibiotic treatment for resolution of infection.

Acknowledgment

We thank Moussa Hajer for editing the figures, formatting the manuscript, and submitting it for publication.

About the Author

Dr. Vassallo is an infectious diseases specialist and chief of the Department of Internal Medicine/Infectious Diseases at Cannes General Hospital, Canne, France. His research interests include HIV, viral respiratory infections, and sepsis.

References

1. Harne S, Gayathri P, Béven L. Exploring Spiroplasma biology: opportunities and challenges. Front Microbiol. 2020;11:589279. https://doi.org/10.3389/fmicb.2020.589279
2. Cisak E, Wójcik-Fatla A, Zając V, Sawczyn A, Sroka J, Dutkiewicz J. Spiroplasma—an emerging arthropod-borne pathogen? Ann Agric Environ Med. 2015;22:589–93. https://doi.org/10.5604/12321966.1185758
3. Davis RE, Shao J, Zhao Y, Gasparich GE, Gaynor BJ, Donofrio N. Complete genome sequence of Spiroplasma turonicum strain Tab4cT, a parasite of a horse fly, Haematopota sp. (Diptera: Tabanidae). Genome Announc. 2015;3:e01367–15. https://doi.org/10.1128/genomeA.01367-15
4. Eimer J, Fernström L, Rohlén L, Grankvist A, Loo K, Nyman E, et al. Spiroplasma ixodetis infections in immunocompetent and immunosuppressed patients after tick exposure, Sweden. Emerg Infect Dis. 2022;28:1681–5. https://doi.org/10.3201/eid2808.212524
5. Etienne N, Bret L, Le Brun C, Lecuyer H, Moraly J, Lanternier F, et al. Disseminated *Spiroplasma apis* infection in patient with agammaglobulinemia, France. Emerg Infect Dis. 2018;24:2382–6. https://doi.org/10.3201/eid2412.180567
6. Aquilino A, Masiá M, López P, Galiana AJ, Tovar J, Andrés M, et al. First human systemic infection caused by Spiroplasma. J Clin Microbiol. 2015;53:719–21. https://doi.org/10.1128/JCM.02841-14
7. Santos RP, Silva M, Vieira AP, Brito C. *Mycoplasma pneumoniae*–induced rash and mucositis: a recently described entity. BMJ Case Rep. 2017;2017:bcr2017220768. https://doi.org/10.1136/bcr-2017-220768
8. DermNet. Mycoplasma pneumoniae infection [cited 2026 Mar 15]. https://dermnetnz.org/topics/mycoplasma-pneumoniae-infection
9. D'Agostino M, Innorcia S, Boccadoro M, Bringhen S. Monoclonal antibodies to treat multiple myeloma: a dream come true. Int J Mol Sci. 2020;21:8192. https://doi.org/10.3390/ijms21218192
10. Huang ZY, Chen J, Zhu B, Liu XL. Infection risk associated with teclistamab in relapsed/refractory multiple myeloma: a systematic review and meta-analysis of clinical trial and real-world evidence. Front Immunol. 2026;17:1804838. https://doi.org/10.3389/fimmu.2026.1804838

Address for correspondence: Matteo Vassallo, Department of Internal Medicine/Infectious Diseases, Cannes Hospital, 15 Avenue des Broussailles, 06400 Cannes, France; email: m.vassallo@ch-cannes.fr

Sulfamethoxazole–Resistant Nocardiosis in Renal Transplant Recipient, India

Sandeep Rao Kordcal, Md Tariq Maula, Vivek Malleshappa Suguna, Adil Rashid Khan, Rahul Ranjan, Stanzin Spalkit, Aruna Nambirajan, Gagandeep Singh, Neeraj Nischal, Immaculata Xess, Manish Soneja

Authors affiliation: All India Institute of Medical Sciences, New Delhi, India

DOI: https://doi.org/10.3201/eid3211.260963

A renal transplant recipient in India receiving trimethoprim/sulfamethoxazole prophylaxis experienced fever, hemoptysis, and neurologic deficits. The diagnosis was pulmonary aspergillosis and disseminated nocardiosis caused by trimethoprim/sulfamethoxazole–resistant *Nocardia*. Antimicrobial drug therapy led to complete clinical and radiological resolution after 6 months. This case highlights a resistant breakthrough *Nocardia* pathogen in a transplant recipient.

Renal transplant recipients on lifelong immunosuppression are at increased risk for opportunistic infections. Nocardiosis affects 0.04%–3.5% of solid-organ transplant recipients; pulmonary cases disseminate in up to 44% of cases, and central nervous system involvement occurs in 20%–44% (*1*,*2*). Concurrent infection with *Nocardia* bacteria and *Aspergillus* fungus accounts for only 5%–7% of post-transplant cases (*2*). Trimethoprim/sulfamethoxazole (cotrimoxazole) has been the mainstay of treatment and prophylaxis, but the rising prevalence of trimethoprim/sulfamethoxazole–resistant *Nocardia* bacteria complicates empirical therapy and underscores the necessity of susceptibility testing for successful outcomes.

Written informed consent for publication of this case report, including clinical details and accompanying radiological and histopathological images, was obtained from the patient; personal identifiers were withheld. Formal ethics committee approval was not required for a single case report according to institutional and journal guidelines.

A 39-year-old woman who was taking tacrolimus, mycophenolate sodium, prednisolone, and trimethoprim/sulfamethoxazole prophylaxis after renal transplant had remained well for 14 months before experiencing fever, hemoptysis, anorexia, and weight loss over 45 days. High-resolution computed tomography of the chest revealed right upper lobe consolidation with pleural effusion (Figure 1, panel A); lung biopsy culture grew *Aspergillus fumigatus*, with a serum galactomannan result of 8.16 optical density index, confirming invasive pulmonary aspergillosis according to 2020 European Organization for Research and Treatment of Cancer and the Mycoses Study Group criteria (*3*). Despite the patient taking voriconazole and liposomal amphotericin B, altered sensorium and bilateral lower-limb weakness developed, leading to a higher center referral.

Physical examination revealed asymmetric upper motor neuron weakness in the lower limbs, neck stiffness, and coarse bilateral crackles. Brain imaging revealed multiple ring-enhancing supratentorial lesions with central diffusion restriction and perilesional edema (Figure 2). Repeat transbronchial lung biopsy showed suppurative inflammation with weakly acid-fast, branching, beaded filamentous bacteria when Fite stained and stained with hematoxylin and eosin (Figure 1, panels B and C). Tissue culture on Sabouraud dextrose agar grew

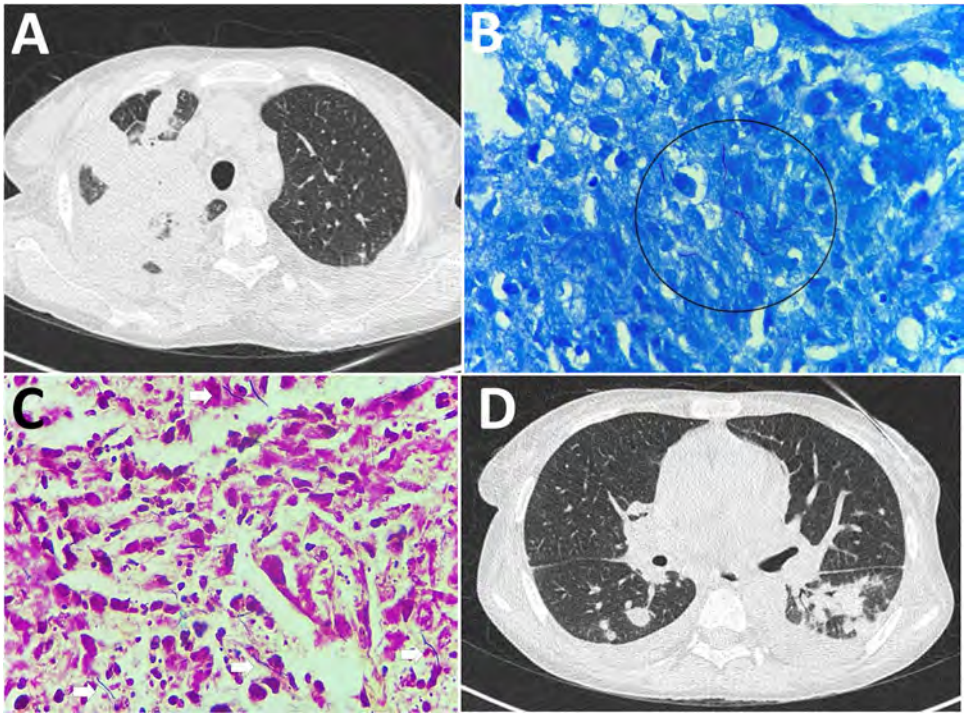

Figure 1. Histopathologic and radiologic findings in renal transplant recipient with disseminated trimethoprim/sulfamethoxazole–resistant nocardiosis, India. A) High-resolution computed tomography of the chest before treatment, showing right-upper-lobe consolidation with adjacent passive atelectasis and a left pleural effusion. B) Lung biopsy, Fite stained, showing weakly acid-fast, branching, beaded filamentous bacteria (circle). Original magnification ×1,000. C) Lung biopsy, hematoxylin and eosin stained, showing suppurative inflammation (arrows). Original magnification ×400. D) High-resolution computed tomography of the chest 6 months after treatment, showing resolution of the consolidation with residual pulmonary fibrosis.

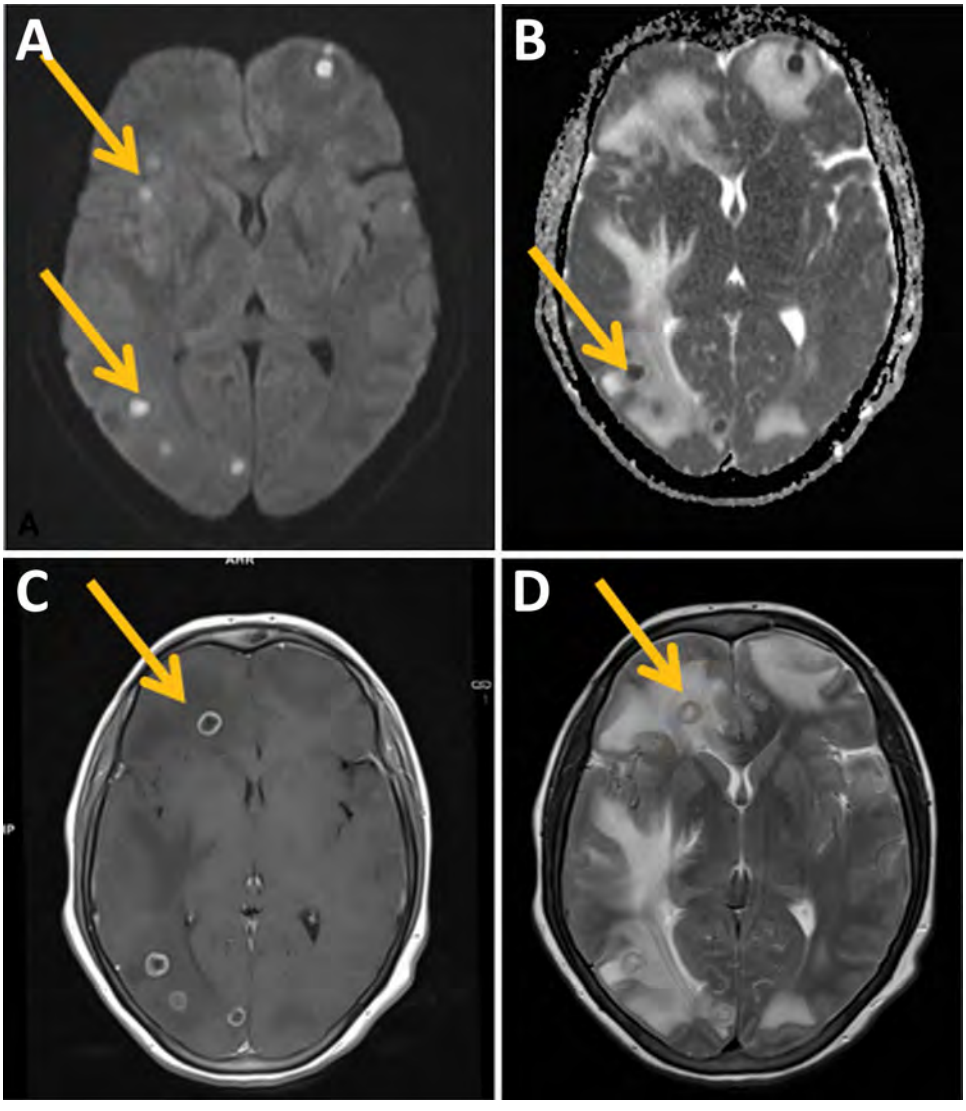

Figure 2. Brain magnetic resonance imaging in renal transplant recipient with disseminated trimethoprim/sulfamethoxazole–resistant nocardiosis, India. A) Diffusion-weighted image showing multiple foci of central diffusion restriction (arrows). B) Apparent diffusion coefficient map showing corresponding signal change (arrow). C) Axial T1-weighted postgadolinium image showing ring-enhancing supratentorial lesions (arrow). D) Axial T2-weighted image showing lesions with central hyperintensity, a hypointense rim, and perilesional edema (arrow).

dry, chalky colonies suggestive of *Nocardia* spp., although species-level identification could not be confirmed because matrix-assisted laser desorption/ionization time-of-flight mass spectrometry failed twice and 16S rRNA sequencing was unavailable. We interpreted antimicrobial susceptibility by disc diffusion on cation-adjusted Mueller–Hinton agar by using Comité de l'Antibiogramme de la Société Française de Microbiologie thresholds; the organism appeared resistant to cotrimoxazole and ciprofloxacin and susceptible to linezolid, minocycline, imipenem, and amikacin (*4*).

A diagnosis of disseminated trimethoprim/sulfamethoxazole–resistant nocardiosis with pulmonary and cerebral involvement was made. Tacrolimus and mycophenolate were withheld, low-dose prednisone was continued, and imipenem and linezolid were initiated alongside voriconazole; clinical response was noted within 1 week. After 1 month, cytopenias developed, and linezolid was switched to minocycline. Because of seizure risk, imipenem was changed to meropenem, and the patient was continued on meropenem for 3 months with minocycline. Voriconazole was stopped after 6 months. Imaging at the end of 6 months confirmed radiological resolution in both intracranial and pulmonary lesions, with preserved graft function (Figure 1, panel D). The patient continued to do well at 1-year follow-up and remains on secondary prophylaxis with minocycline.

Trimethoprim/sulfamethoxazole resistance in *Nocardia* bacteria is increasingly reported worldwide, although prevalence varies considerably with isolate source, geographic region, and the susceptibility method used. Susceptibility testing is also technically demanding and might be affected by the lack of

control strains of *Nocardia* spp. with known susceptibility patterns. One study found that 42% of United States isolates appear resistant to trimethoprim/sulfamethoxazole and 61% to sulfamethoxazole (*5*), whereas a separate study, comparing 552 isolates across 6 reference laboratories, reported only 2% resistance, attributing the difference in rates to interlaboratory variability and possible misinterpretation of trailing MIC endpoints (*6*).

Pulmonary infections remain a major cause of illness among postrenal transplant recipients, and opportunistic pathogens such as *Nocardia* bacteria frequently coexist with fungal and mycobacterial disease, with overlapping radiological and clinical features that delay diagnosis in tropical countries. Reported resistance rates among cohorts in India have been of note. In a renal-transplant series of 16 nocardiosis cases, 9 patients were receiving trimethoprim/sulfamethoxazole prophylaxis, and 4 *N. farcinica* isolates were resistant (*7*). In addition, a South India 10-year analysis reported 20.8% resistance among 48 cases (*8*), and a North India center reported nocardiosis in 12 (1.1%) renal transplant recipients, of which 60% isolates were trimethoprim/sulfamethoxazole--resistant, and 7 of 12 patients (58.3%) had breakthrough infection while receiving prophylaxis (*9*).

Brain imaging is indicated in all cases of pulmonary nocardiosis irrespective of neurologic symptom because of the 20%–44% rate of central nervous system involvement (*1*,*2*). Species-level identification remains a diagnostic challenge, because morphologic and biochemic methods are often inconclusive and the use of matrix-assisted laser desorption/ionization time-of-flight mass spectrometry might be limited (*10*). Disseminated nocardiosis carries a higher mortality rate of 64%–100% among transplant recipients (*2*). This case report underscores the potential for breakthrough nocardiosis caused by trimethoprim/sulfamethoxazole–resistant isolates despite prophylaxis and highlights the importance of antimicrobial drug susceptibility testing to guide targeted therapy and optimize clinical outcomes.

Acknowledgments

We thank the departments of medicine, radiology, microbiology, and pathology, All India Institute of Medical Sciences, New Delhi, India, for their assistance in the clinical care and diagnostic evaluation of this patient.

The data supporting the findings of this study are available from the corresponding author upon reasonable request.

Author contributions: conceptualization, investigation, and writing of the original draft, S.R.K., M.T.M., and V.M.S.; investigation and draft revision, A.R.K. and R.R.; radiologic investigation and image interpretation, S.S.; microbiologic investigation, I.X. and G.S.; histopathologic investigation, A.N.; investigation, supervision, and revision, N.N. and M.S.; review and approval of final manuscript, all authors.

About the Author

Dr. Kordcal is a clinical fellow in infectious diseases at the All India Institute of Medical Sciences, New Delhi, India. His academic and research interests include medical mycology, tuberculosis, and infections in immunocompromised hosts.

References

1. Coussement J, Lebeaux D, van Delden C, Guillot H, Freund R, Marbus S, et al.; European Study Group for Nocardia in Solid Organ Transplantation. *Nocardia* infection in solid organ transplant recipients: a multicenter European case-control study. Clin Infect Dis. 2016;63:338–45. https://doi.org/10.1093/cid/ciw241
2. Peleg AY, Husain S, Qureshi ZA, Silveira FP, Sarumi M, Shutt KA, et al. Risk factors, clinical characteristics, and outcome of *Nocardia* infection in organ transplant recipients: a matched case-control study. Clin Infect Dis. 2007;44:1307–14. https://doi.org/10.1086/514340
3. Donnelly JP, Chen SC, Kauffman CA, Steinbach WJ, Baddley JW, Verweij PE, et al. Revision and update of the consensus definitions of invasive fungal disease from the European organization for research and treatment of cancer and the mycoses study group education and research consortium. Clin Infect Dis. 2020;71:1367–76. https://doi.org/10.1093/cid/ciz1008
4. Lebeaux D, Bergeron E, Berthet J, Djadi-Prat J, Mouniée D, Boiron P, et al. Antibiotic susceptibility testing and species identification of *Nocardia* isolates: a retrospective analysis of data from a French expert laboratory, 2010–2015. Clin Microbiol Infect. 2019;25:489–95. https://doi.org/10.1016/j.cmi.2018.06.013
5. Uhde KB, Pathak S, McCullum I Jr, Jannat-Khah DP, Shadomy SV, Dykewicz CA, et al. Antimicrobial-resistant *Nocardia* isolates, United States, 1995–2004. Clin Infect Dis. 2010;51:1445–8. https://doi.org/10.1086/657399
6. Brown-Elliott BA, Biehle J, Conville PS, Cohen S, Saubolle M, Sussland D, et al. Sulfonamide resistance in isolates of *Nocardia* spp. from a US multicenter survey. J Clin Microbiol. 2012;50:670–2. https://doi.org/10.1128/JCM.06243-11
7. Bhandari G, Tiwari V, Gupta A, Bhargava V, Malik M, Gupta A, et al. Nocardiosis in renal transplantation: case series from India. Indian J Nephrol. 2023;33:456–8. https://doi.org/10.4103/ijn.ijn_205_22
8. Kudru CU, Kumar A, Chawla K, Minnamreddigari C, Siddalingaiah N, Guddattu V. A ten-year retrospective analysis of nocardiosis in a tertiary care center of South-coastal India. Infez Med. 2021;29:600–8.
9. Marak R, Abdullah, Behera M, Kaul A, Bhadauria D, Prasad N, et al. Nocardiosis in kidney transplant recipients: a tertiary care center experience. Transpl Immunol. 2024;84:102041. https://doi.org/10.1016/j.trim.2024.102041

10. Lafont E, Conan PL, Rodriguez-Nava V, Lebeaux D. Invasive nocardiosis: disease presentation, diagnosis and treatment-old questions, new answers? Infect Drug Resist. 2020;13:4601–13. https://doi.org/10.2147/IDR.S249761

Address for correspondence: Manish Soneja, Department of Medicine, Rm No. 3091, 3rd Fl, Teaching Block, All India Institute of Medical Sciences, Ansari Nagar, New Delhi 110029, India; email: manishsoneja@gmail.com

Community Transmission of Pneumonic Plague, Fenoarivobe, Madagascar, 2022

Laurence Randrianasolo, Rivo Rakotoarimisa, Soloandry Rahajandraibe, Aina Harimanana, Nantenaina Ranoelison, Mamy G. Randriamanantsoa, Berthin A. Andrianarisoa, Soanandrasana Rahelinirina, Vaoary Razafimbia, Antso Raherinandrasana, Fanjasoa Rakotomanana, Manuela A. Vololoniaina, Rindra V. Randremanana,[1] Minoarisoa Rajerison[1]

Author affiliations: Institut Pasteur, Antananarivo, Madagascar (L. Randrianasolo, A. Harimanana, N. Ranoelison, B.A. Andrianarisoa, S. Rahelinirina, F. Rakotomanana, R.V. Randremanana, M. Rajerison); Ministry of Public Health, Antananarivo (R. Rakotoarimisa, S. Rahajandraibe, M.G. Randriamanantsoa, V. Razafimbia, M.A. Vololoniaina); University of Antananarivo, Antananarivo (A. Raherinandrasana)

DOI: https://doi.org/10.3201/eid3211.260549

The results of an outbreak investigation of pneumonic plague conducted in the plague-endemic district of Fenoarivobe, Madagascar, revealed a familial cluster of plague. Transmission was aided by intrahousehold contact or gatherings and was amplified by delayed plague treatment, highlighting the need for early diagnosis and rapid initiation of appropriate therapy.

In Madagascar, where plague remains endemic, transmission typically occurs during August–April. Most cases are reported in the central highlands, which are located at an altitude above 800 m (*1*). The predominant clinical form in Madagascar is bubonic plague. However, some outbreaks of pneumonic plague occur every year (*2*). On February 18, 2022, the Bongolava Regional Health Directorate reported 8 suspected deaths of pneumonic plague from the district of Fenoarivobe. We conducted outbreak investigations (protocol study approved by the National Ethics Committee of Biomedical Research [reference no. 068 MSANP/CE] on July 29, 2011) to identify the source, reconstruct the transmission history, and contain the spread of the outbreak. We classified all cases according to the World Health Organization's international definition of plague cases (*3*).

During January 28–March 1, 2022, we identified 21 suspected plague cases (9 in persons who were alive and 12 in persons who were deceased); all deaths occurred at the community level (i.e., involving multiple households). Case-patients had a median age of 28 years (interquartile range 23–41 years); 11 (52.4%) were women and girls and 10 (47.6%) were men and boys. Twelve persons (11 with pneumonic plague and 1 with initially bubonic plague) had specimen testing at the Central Laboratory for Plague (Institut Pasteur, Antananarivo, Madagascar); 6 had PCR-confirmed plague cases (3 in living persons and 3 in deceased persons), and 1 had a probable plague case. The attack rate was 4.6% (21/45,636 inhabitants), and the overall case-fatality rate was 57.1% (12/21). The outbreak lasted 33 days.

All case-patients had respiratory symptoms, and 1 case-patient had a secondary pneumonic form resulting from neglected bubonic plague. The most common symptoms reported by case-patients were cough (81% [17/21]), chest pain (71.4% [15/21]), bloody sputum (66.7% [14/21]), and fever (61.9% [13/21]). The incubation period varied from 1 to 13 days, and the median disease duration was 3 days (interquartile range 1–9 days). The presumed index case-patient had onset of fever, headache, asthenia, and vomiting on January 28. He sought care at the health center the same day, had malaria diagnosed by rapid test, and received antimalarial treatment. On January 31, he died at home after having severe hemorrhagic symptoms. Thereafter, primary, secondary, and tertiary cases occurred (Figure 1).

Twelve case-patients reported having received antibiotics for plague, including the 9 case-patients who were still alive at the time of the outbreak investigation and 3 of 12 deceased case-patients. Antiplague treatment was administered to case-patients who sought care at health facilities starting in the fourth week of the outbreak, when health workers began to suspect the plague. Among direct contacts of

[1]These senior authors contributed equally to this article.

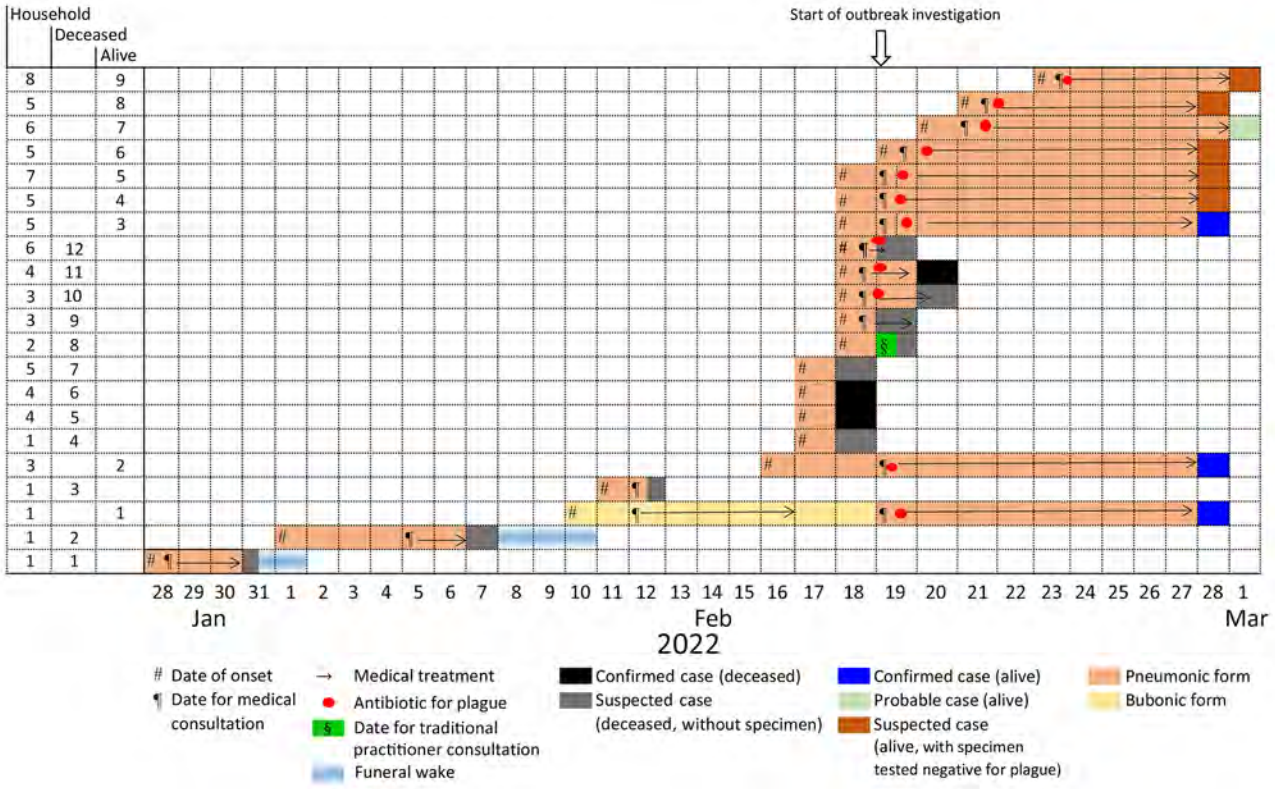

Figure 1. Timeline of events for 21 cases of pneumonic plague in the district of Fenoarivobe, Madagascar, January 28–March 1, 2022.

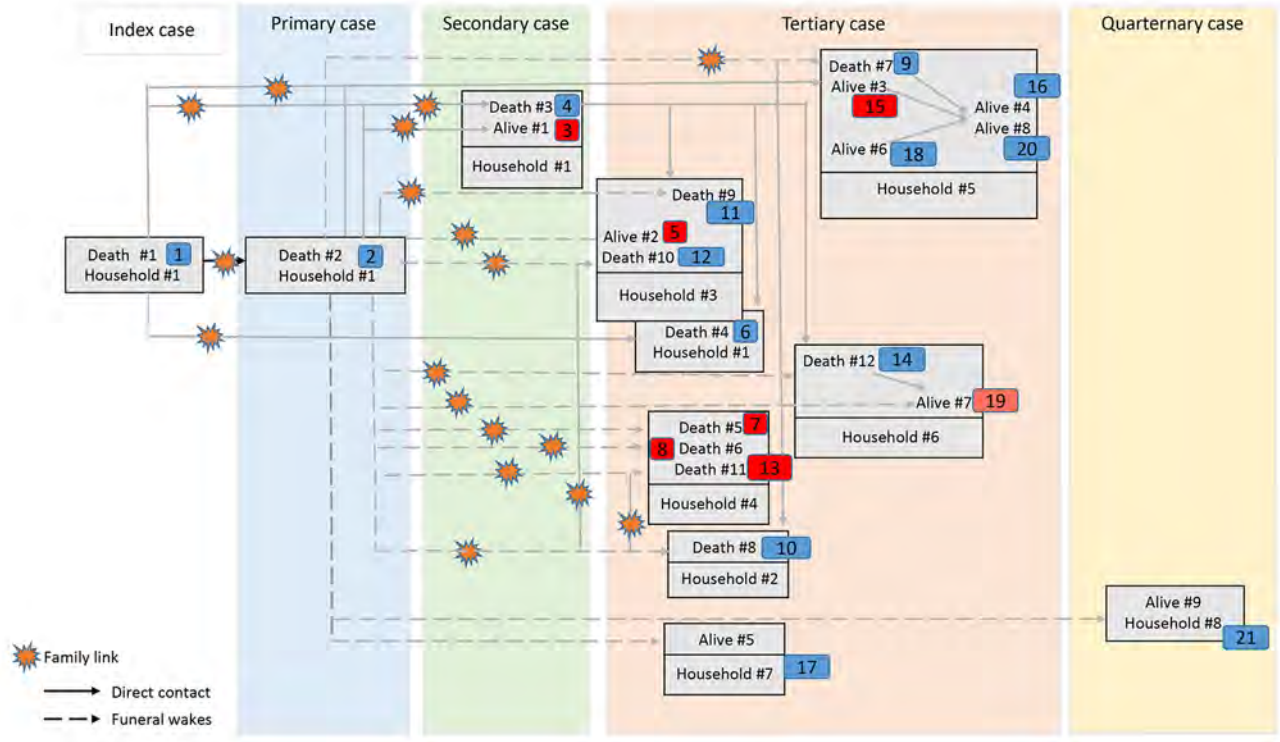

Figure 2. Reconstructed routes of transmission for 21 cases of pneumonic plague in the district of Fenoarivobe, Madagascar, January 28–March 1, 2022. The numbered boxes indicated the order in which cases of plague appeared: confirmed cases are shown in red, probable cases in reddish brown, and suspected cases or those without biological samples in blue.

case-patients, 14% (14/100) were positive for F1 IgG based on serologic testing. Identified case-patients were members of 8 households.

This outbreak investigation revealed a familial cluster with a presumed index case-patient who probably had either secondary pneumonic plague occurring after neglected bubonic plague or primary pneumonic plague with an unknown source of contamination. During the first 2 weeks, transmission primarily occurred within the index case-patient's household, where the primary case-patient was infected by direct contact. Subsequently, more widespread contact occurred at the community level (i.e., with other households) during gatherings (e.g., funerals) or after direct contact with deceased case-patients, based on the transmission routes we reconstructed (Figure 2).

Early plague treatment is curative, and the high case-fatality rate seemed to be explained by the delay in the initiation of treatment during the first 3 weeks of the outbreak because of misdiagnosis. The outbreak lasted for 1 month, and the appropriate actions to respond to the outbreak were initiated at the beginning of the fourth week, coinciding with our outbreak investigation. Pneumonic plague, like other respiratory diseases, initially manifests with nonspecific symptoms (*4*), and often no clear exposure to infected animals or fleas can be identified, which can lead to misdiagnosis and delay correct management.

This outbreak occurred in a known plague-endemic area. Our serologic results among case-patients suggested that plague continues to circulate in the environment, in the local rodent population, or both, despite the last reported human plague cases occurring 6 years before this outbreak (*5*). Our findings underscore the importance of health workers staying alert in plague-endemic areas to the possibility of reemerging cases of plague and the population to be informed about seeking medical care in case of illness (*6*,*7*).

The transmission dynamics observed in this outbreak highlight the potential for the spread of pneumonic plague, mainly within family and community clusters, particularly in remote settings. Similar patterns of family- and community-based transmission have been described in previous outbreaks in Madagascar, where social structures and caregiving customs contribute to high-risk exposure (*8*–*10*).

Identifying plague and its transmission in remote settings is challenging; therefore, rapid case detection, contact tracing, and timely implementation of preventive measures are essential. Early diagnosis and prompt treatment are important to avoid delays and associated high-fatality rates.

Acknowledgments

We thank the director of the Bongolava Regional Health Directorate, the team management of the Service de District de Santé Publique in Fenoarivobe, and the mayor of Morarano Maritampona and his colleagues for their assistance with, contribution to, and support of the field investigation. We express our warm thanks to the people of the commune of Morarano Maritampona and Firavahana, who participated in the investigation.

This work was supported by the US Agency for International Development through the Research, Innovation, Surveillance, and Evaluation (RISE) project (cooperative agreement no. 72068719CA00001).

About the Author

Dr. Randrianasolo is a public health physician at the Institut Pasteur of Madagascar. Her primary research interests include epidemiological surveillance of epidemic-prone diseases.

References

1. Chanteau S, Boisier P, Carniel E, Duchemin JB, Duplantier JM, Goodman S, et al. Atlas de la peste à Madagascar. 2006 [cited 2026 Aug 26]. https://horizon.documentation.ird.fr/exl-doc/pleins_textes/divers16-07/010035376.pdf
2. World Health Organization. Disease outbreak news: plague—Madagascar. 2021 Oct 1 [cited 2026 Aug 26]. https://www.who.int/emergencies/disease-outbreak-news/item/plague---madagascar
3. World Health Organization. Revision of the international definition of plague cases. Wkly Epidemiol Rec. 2021;24:238–40 [cited 2026 Aug 26]. https://iris.who.int/items/21e73ba6-4d85-48cb-9303-2ceab567593e
4. Salam AP, Raberahona M, Andriantsalama P, Read L, Andrianarintsiferantsoa F, Razafinambinintsoa T, et al. Factors influencing atypical clinical presentations during the 2017 Madagascar pneumonic plague outbreak: a prospective cohort study. Am J Trop Med Hyg. 2020;102:1309–15. https://doi.org/10.4269/ajtmh.19-0576
5. Andrianaivoarimanana V, Kreppel K, Elissa N, Duplantier JM, Carniel E, Rajerison M, et al. Understanding the persistence of plague foci in Madagascar. PLoS Negl Trop Dis. 2013;7:e2382. https://doi.org/10.1371/journal.pntd.0002382
6. Rakotosamimanana S, Rakotoarimanana FJ, Raharimanga V, Taglioni F, Ramamonjisoa J, Randremanana RV, et al. Influence of sociospatial determinants on knowledge, attitudes and practices related to the plague in a population living in endemic areas in the central highlands, Madagascar. BMC Public Health. 2021;21:1102. https://doi.org/10.1186/s12889-021-11101-3
7. Generis Global Legal Services. An overview of the healthcare system in Madagascar. 2024 Nov 21 [cited 2026 Aug 26]. https://generisonline.com/an-overview-of-the-healthcare-system-in-madagascar
8. Ramasindrazana B, Andrianaivoarimanana V, Rakotondramanga JM, Birdsell DN, Ratsitorahina M, Rajerison M. Pneumonic plague transmission, Moramanga, Madagascar, 2015. Emerg Infect Dis. 2017;23:521–4. https://doi.org/10.3201/eid2303.161406

9. Vogler AJ, Chan F, Nottingham R, Andersen G, Drees K, Beckstrom-Sternberg SM, et al. A decade of plague in Mahajanga, Madagascar: insights into the global maritime spread of pandemic plague. MBio. 2013;4:e00623–12. https://doi.org/10.1128/mBio.00623-12
10. Andrianaivoarimanana V, Iharisoa AL, Rahalison L, Ralimanantsoa ML, Ratsitorahina M, Rakotonanahary RJL, et al. Short- and long-term humoral immune response against *Yersinia pestis* in plague patients, Madagascar. BMC Infect Dis. 2020;20:822. https://doi.org/10.1186/s12879-020-05565-8

Address for correspondence: Rindra Vatosoa Randremanana, Epidemiology and Clinical Research Unit, Institut Pasteur de Madagascar, BP 1274, Antananarivo 101, Madagascar; email: rrandrem@pasteur.mg

September 2026

Fungal Infections

- Investigation of *Mycobacterium abscessus* Cluster in Hospital, Maryland, USA, 2024
- Epidemiology of and Risk Factors for Amebic Meningoencephalitis, Kerala, India, 2025
- Neoehrlichiosis Causing Hemolytic Anemia in Patients Treated with Rituximab, Norway, 2024–2025
- Improved Case Detection of Fleaborne Typhus by PCR Testing, Los Angeles County, California, USA, 2022–2024
- Posttuberculosis Consequences on Tuberculosis Prevention Effectiveness and Cost-effectiveness among New Immigrants, Canada
- Clustering and Source Association of Clinical and Nonclinical *Listeria monocytogenes* Isolates, New York, USA, 2000–2021
- Dual PCR–Sanger Sequencing Assay for Simultaneous *sqle*-Based Identification and Resistance Detection in *Trichophyton* Species
- Invasive *Wickerhamomyces anomalus* Infections among Injecting Drug Users, France, 2012–2024
- Pediatric Tuberculosis Care Outcomes in a Tertiary Care Center, France, 2014–2024

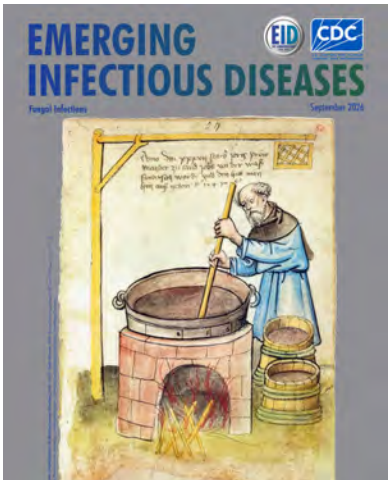

- Reemergence of Scrub Typhus Associated with *Leptotrombidium akamushi* Mites and Karp-Like *Orientia tsutsugamushi* Genotype Bacteria, Japan, 2024–2025
- Serologic Evidence of Hantavirus Exposure in Humans, Italy, 2004–2018
- Seroprevalence of Influenza A(H5N1) Virus in Domestic Cats at Epicenter of Dairy Cattle Outbreaks, California, USA, 2024–2026
- Case Report and Retrospective Review of *Acanthamoeba* Encephalitis and Chronic Lymphocytic Leukemia, United States
- Emergence of Oropouche Virus, Venezuela, 2025
- Global Spread of *Trichophyton indotineae* Tracked by Mass Spectrometry Identification Network, 2022–2025
- *Wickerhamomyces anomalus* Pseudo-Outbreak Associated with Medical Lubricating Gel, South Africa, 2023–2024
- Genetically Distinct African Swine Fever Virus Genotype II Variant in Wild Boar, Spain, 2025–2026
- Chronic Elbow Nodules Caused by *Fomitiporella* Fungus in Immunocompetent Patients, United States
- Genomic and Epidemiologic Insights into Ongoing Measles Outbreak, Israel, 2025–2026
- Pulmonary Coccidioidomycosis Linked to Shipping Containers, Taiwan, 2025
- Southern Tick–Associated Rash Illness in Pediatric Patient, New York, USA, 2025
- Powassan Virus in *Ixodes scapularis* Tick Populations, Illinois, USA, 2025
- Outbreak of Brazilian Spotted Fever, Southeastern Brazil, 2018
- Pediatric *Rickettsia massiliae* Infection, Spain, 2023

EMERGING INFECTIOUS DISEASES®

To revisit the September 2026 issue, go to:
https://wwwnc.cdc.gov/eid/articles/issue/32/9/table-of-contents

Edgar Degas (1834–1917), *Les Choristes*, 1877. Pastel on monotype. 32 cm × 27 cm (10.6 in × 12.6 in). Image © Musée d'Orsay, Paris, France. Dist. RMN-Grand Palais/Patrice Schmidt.

Choral Voices, Communal Vulnerability

Terence Chorba

On the cover of this month's issue, the oil and pastel artwork *Les Choristes* portrays a chorus of singers on stage, captured during an animated, operatic performance. The singers stand in proximity, sharing airspace as they project their voices. The creator of *Les Choristes*, Edgar Degas (1834–1917), was a pivotal figure in Impressionism, known for his depictions of ballet dancers, opera performers, and scenes of modern Parisian life. He was born in Paris into a well-to-do family, schooled in a prestigious lycée, and enrolled in the Faculty of Law at the Sorbonne. However, by age 21, he had demonstrated considerable artistic talent with technical drawings and enrolled in the École des Beaux-Arts in Paris with an intent to become a realist painter of historical scenes and settings.

Author affiliation: Centers for Disease Control and Prevention, Atlanta, Georgia, USA

DOI: https://doi.org/10.3201/eid3211.AC3211

Figure 1. Edgar Degas, *Singer with a Glove*, 1878. Pastel on canvas. 53.2 × 41 cm (20.938 in × 16.125 in). Fogg Museum, Harvard University, Cambridge, Massachusetts, USA.

Working across multiple media, including pastel, oil painting, sculpture, and printmaking, Degas eventually became fascinated by modern performance artists and the spaces in which they practiced and performed. Degas' *Les Choristes* vividly reflects his interest in the theater, an environment that is often associated with intense physical exertion, close human contact, and exposure to other conditions that are conducive to the transmission of respiratory infection.

Completed in 1877, *Les Choristes* also offers insight into Degas' artistic development and his innovative approach to representing movement and experimenting with the human form. By the mid-1870s, he had shifted his attention from historical subjects to scenes of contemporary life, especially those involving music and dance. Opera houses and ballet theaters became recurring subjects in his work, mirroring both his personal interests and the vibrant cultural life of the *Belle Époque*, the interwar years of 1871 through 1914, when Paris was renowned for cultural innovation and tremendous urban development. Although more than half of Degas' other works depict dancers, several feature solo singers either performing or rehearsing (Figures 1, 2).

Respiratory pathogens such as influenza viruses, measles virus, *Mycobacterium tuberculosis*, and SARS-CoV-2 spread through infectious respiratory particles, such as droplets and aerosols (*1*,*2*). Singing is but one of myriad group activities in which we commonly share airspace; examples of similar such activities include performing in or attending orchestral performances, being a student in the nonvirtual classroom environment, and attending theater, operatic performances, religious or political gatherings, or sporting events. In Degas' time, public singers had the added challenge of filling large theaters and opera houses with their voices in the absence of electronic amplification. Such vocal demands, combined with performances in often poorly ventilated indoor spaces, would have increased the risks of airborne disease transmission.

In the United States, singing in a group setting has been identified as an activity that could promote transmission risk for respiratory pathogens in investigations of tuberculosis outbreaks in a school choir in 1993–94 (*3*) and in a church choir in 1998 (*4*). In such settings, prolonged exposure and forceful vocalization create ideal conditions for aerosol spread (*5*). In 2008, investigation in a similar setting identified

Figure 2. Edgar Degas, *The Singer in Green*, 1884, Pastel on light blue laid paper. 60.3 × 46.4 cm (23.75 × 18.25 in). Metropolitan Museum of Art, New York, New York, USA.

multiple tuberculosis cases linked to a single source, underscoring the roles of close contact and inadequate ventilation (*6*). Early in the COVID-19 pandemic, a well-documented outbreak occurred at a choir rehearsal in Skagit Valley, Washington, USA, in 2020; in that outbreak, 52 of 61 choir participants became infected with SARS-CoV-2, and 2 of them died (*7*). All of these events have supported the hypothesis of transmission risk for respiratory pathogens in association with choral singing. Elevated risk for airborne infectious disease transmission caused by aerosols has also been reported in association with playing wind instruments (*8*), coughing, talking (*9*), and other activities in which prolonged exposures can occur in poorly ventilated and crowded environments.

In response to mounting evidence during the COVID-19 pandemic, many music ensembles, including choral groups, suspended or substantially altered practices to prevent disease transmission and outbreaks. Mitigation strategies included moving rehearsals outdoors, increasing physical distancing, shortening rehearsal times, improving ventilation, using face masks, or holding virtual rehearsals and performances to maintain musical engagement while minimizing health risks (*10*–*12*). *Les Choristes* vividly portrays the setting of an age-old challenge with which society grappled in the recent pandemic setting, namely, allowing for enjoyment of close or cloistered activities without increasing respiratory disease risk, especially during epidemics or pandemics.

The author discloses using ChatGPT (OpenAI, https://openai.com) only for locating references for this essay, not in generating content.

References

1. Asadi S, Wexler AS, Cappa CD, Barreda S, Bouvier NM, Ristenpart WD. Aerosol emission and superemission during human speech increase with voice loudness. Sci Rep. 2019;9:2348. https://doi.org/10.1038/s41598-019-38808-z
2. Fennelly KP. Particle sizes of infectious aerosols: implications for infection control. Lancet Respir Med. 2020; 8:914–24. https://doi.org/10.1016/S2213-2600(20)30323-4
3. Washko R, Robinson E, Fehrs LJ, Frieden TR. Tuberculosis transmission in a high school choir. J Sch Health. 1998;68:256–9. https://doi.org/10.1111/j.1746-1561.1998.tb06351.x
4. Mangura BT, Napolitano EC, Passannante MR, McDonald RJ, Reichman LB. *Mycobacterium tuberculosis* miniepidemic in a church gospel choir. Chest. 1998;113:234–7. https://doi.org/10.1378/chest.113.1.234
5. Loudon RG, Roberts RM. Singing and the dissemination of tuberculosis. Am Rev Respir Dis. 1968;98:297–300. https://doi.org/10.1164/arrd.1968.98.2.297
6. Mandalakas AM, Kirchner HL, Lombard C, Walzl G, Grewal HM, Gie RP, et al. Well-quantified tuberculosis exposure is a reliable surrogate measure of tuberculosis infection. Int J Tuberc Lung Dis. 2012;16:1033–9. https://doi.org/10.5588/ijtld.12.0027
7. Hamner L, Dubbel P, Capron I, Ross A, Jordan A, Lee J, et al. High SARS-CoV-2 attack rate following exposure at a choir practice—Skagit County, Washington, March 2020. MMWR Morb Mortal Wkly Rep. 2020;69:606–10. https://doi.org/10.15585/mmwr.mm6919e6
8. Firle C, Steinmetz A, Stier O, Stengel D, Ekkernkamp A. Aerosol emission from playing wind instruments and related COVID-19 infection risk during music performance. Sci Rep. 2022;12:8598. PubMed https://doi.org/10.1038/s41598-022-12529-2
9. Archer J, McCarthy LP, Symons HE, Watson NA, Orton CM, Browne WJ, et al. Comparing aerosol number and mass exhalation rates from children and adults during breathing, speaking and singing. Interface Focus. 2022;12:20210078. https://doi.org/10.1098/rsfs.2021.0078
10. Asadi S, Cappa CD, Barreda S, Wexler AS, Bouvier NM, Ristenpart WD. Efficacy of masks and face coverings in controlling outward aerosol particle emission from expiratory activities. Sci Rep. 2020;10:15665. https://doi.org/10.1038/s41598-020-72798-7
11. Vance D, Shah P, Sataloff RT. COVID-19: impact on the musician and returning to singing; a literature review. J Voice. 2023;37:292.e1–8. https://doi.org/10.1016/j.jvoice.2020.12.042
12. Daffern H, Balmer K, Brereton J. Singing together, yet apart: the experience of UK choir members and facilitators during the Covid-19 pandemic. Front Psychol. 2021;12:624474. https://doi.org/10.3389/fpsyg.2021.624474

Address for correspondence: Terence Chorba, Centers for Disease Control and Prevention, 1600 Clifton Rd NE, Mailstop H24-4, Atlanta, GA 30329-4018, USA; email: tlc2@cdc.gov

EMERGING INFECTIOUS DISEASES®

Upcoming Issue • Zoonotic Infections

- Human Breast Dirofilariasis, 1959–2025
- Management of Infant Born to Birthing Parent with Q fever (*Coxiella burnetii* Infection) in Pregnancy
- Detection of Jamestown Canyon Virus in Mosquito Populations, northeastern Illinois, USA, 2024
- Monkeypox Virus Seroprevalence among Adults Assessed at Roadside Wellness Centers along Major Transportation Corridor, Kenya, 2025
- Rat Hepatitis E Virus Circulation in Brown Rats from 8 Cities, France, 2021–2023
- Estimated Illness Linked to Animal Contact—Seven Pathogens, United States, 2019
- Identification of Zoonotic *Pteropine orthoreovirus* in *Rousettus amplexicaudatus* Fruit Bats, Indonesia
- Detection of *Mycobacterium africanum* Lineage 6 in Free-Ranging White-Nosed Coatis (*Nasua narica*), Costa Rica
- Isolation of *Orientia tsutsugamushi* from Bat-Associated Chiggers, Japan
- Controlled Cross-Sectional Study of *Leptospira* Exposure in Urban River Surfers, Munich, Germany
- Post–COVID-19 Emergence and Spread of Hypertransmissible *Cryptosporidium hominis* gp60 Subtype IfA12G1R5, Spain
- Oropouche Fever Outbreak, Havana, Cuba, June–September 2024
- Wild Mice and Shrews as Natural Reservoirs of Emerging Tickborne Yezo Virus, Hokkaido, Japan, 2023–2025
- Molecular Surveillance for Oropouche, Mayaro, West Nile, and Saint Louis Encephalitis Viruses, Northern and Northeastern Minas Gerais, Brazil, 2019–2025
- Scrub Typhus Masquerading as Typhoid Fever in Patient with Myelodysplastic Syndrome, China, 2025
- Natural Occurrence of Primate SLAM-Adapted Canine Distemper Virus, Brazil, 2018
- Detection of Infectious African Swine Fever Virus in Spray-Dried Porcine Plasma Used as a Feed Ingredient, South Korea
- Emergence of Shamonda Orthobunyavirus, Central Europe, 2026
- Using Cover Art from *Emerging Infectious Diseases* to Inspire Microbiology Education
- Serologic Evidence of Zoonotic Exposure to Porcine Deltacoronavirus with Enhanced Prevalence in Juveniles with Swine Contact, 2019–2021
- Emerging Protoparvovirus in Pigs and Wildlife, Denmark
- Detection of Heartland Virus in Lone Star Ticks Collected in South Carolina, USA, 2021–2024
- Osteomyelitis Caused by *Metamycoplasma gateae* after Cat Bite, Japan, 2026
- Serological Evidence of Avian Influenza Virus Exposure in Livestock, Egypt, 2024–2026
- Fatal Disseminated Powassan Virus Infection in an Immunosuppressed Liver Transplant Recipient, Pennsylvania, USA
- Comparative Assessment of Cross-Protection against Highly Pathogenic Avian Influenza A(H5N5) and A(H5N1) Clade 2.3.4.4b Viruses Following Influenza A(H1N1)pdm09 Infection in Ferrets
- Human Discoverterbral Infection Caused by *Camelimonas* Species, 2025
- Natural *Trichuris trichiura* infections in endemic Hydromyini rodents, Papua New Guinea, 2019–2023
- Detection of *Mycobacterium ulcerans* DNA in African Fruit Bats Despite the Disappearance of Detectable Environmental DNA from Aquatic Ecosystems, Cameroon
- Immunocompromised Patient Infected with Recurrent *Neoehrlichia mikurensis*, the Netherlands, 2024
- Lazarus and the Dogs: from Healing Symbol to Zoonotic Risk
- Mayaro Virus Emergence and Genetic Dynamics, Peru

Complete list of articles in the November issue at http://www.cdc.gov/eid/#issue-337

Earning CME Credit

Earning CME Credit

To obtain credit, you should first read the journal article. After reading the article, you should be able to answer the following, related, multiple-choice questions. To complete the questions (with a minimum 75% passing score) and earn continuing medical education (CME) credit, please go to http://www.medscape.org/journal/eid. Credit cannot be obtained for tests completed on paper, although you may use the worksheet below to keep a record of your answers.

You must be a registered user on http://www.medscape.org. If you are not registered on http://www.medscape.org, please click on the "Register" link on the right hand side of the website.

Only one answer is correct for each question. Once you successfully answer all post-test questions, you will be able to view and/or print your certificate. For questions regarding this activity, contact the accredited provider, CME@medscape.net. For technical assistance, contact CME@medscape.net. American Medical Association's Physician's Recognition Award (AMA PRA) credits are accepted in the US as evidence of participation in CME activities. For further information on this award, please go to https://www.ama-assn.org. The AMA has determined that physicians not licensed in the US who participate in this CME activity are eligible for *AMA PRA Category 1 Credits*™. Through agreements that the AMA has made with agencies in some countries, AMA PRA credit may be acceptable as evidence of participation in CME activities. If you are not licensed in the US, please complete the questions online, print the AMA PRA CME credit certificate, and present it to your national medical association for review.

Article Title:
Reducing Antibiotic Drug Use Effects on *Clostridioides difficile* Colonization in Nursing Home Residents

CME Questions

1. Which of the following variables was most associated with a higher risk for colonization with Clostridioides difficile in the current study?

A. Older age
B. Low colon microbiota diversity status at baseline
C. High colon microbiota diversity status at baseline
D. The presence of ≥3 major comorbid illnesses

2. According to the study, what was the approximate fold increase in *C. difficile* colonization prevalence per percentage-point increase in the daily proportion of nursing home residents receiving antibiotics?

A. 2- to 4-fold
B. 5- to 7-fold
C. 8- to 10-fold
D. 12- to 15-fold

3. Which of the following variables had the largest impact on the risk for transmission of *C. difficile* in the current study?

A. Longer microbiota recovery time
B. Longer duration of colonization with *C. difficile*
C. Antibiotic use rate
D. Failure to recover microbiota diversity

4. What approximate reduction in the daily percentage of nursing home residents receiving antibiotics was predicted to halve *C. difficile* colonization prevalence?

A. 4%
B. 17%
C. 36%
D. 60%Article Title